

# DSE - The HUULC

## Design of a Hydrogen-powered Unmanned Ultra Large Cargo aircraft

Thibault Clar  
Jan Dierickx  
Kenan Eken  
Max de Feber  
Myrthe Gillis

4234707  
4227611  
4104099  
4155475  
4176367

Dionisios Korovilas  
Joris Neuman  
Jennifer Stoof  
Rubén Suárez Millán  
Rob Viet

4226356  
4178106  
4230906  
4229819  
4142004

Final Report  
Design Synthesis Exercises



# Preface

This report is the product of ten weeks of close cooperation between the authors to design an aircraft which offers the speed of air cargo transport at maritime prices, thus revolutionising the transport market and combining the best of both worlds in one service.

We would like to express our deep gratitude to Dr. Ir. G. La Rocca, Dr. Ir. H.G. Vissers and Prof. C. Wang for their assistance and suggestions throughout the project.

Furthermore we would like to express our sincere appreciation to Dr. J.M.G. Heerkens and Dr. W.W.A. Beelaerts van Blokland for their feedback and enthusiasm.

We thank Prof. Dr. Ir. L.L.M. Veldhuis, Ir. J.A. Melkert, Prof. A.Rao, Ir. M.F.M. Hoogreef, S. Vitale and P. Lv, without your help and support the HUULC would not have been possible.

We are very proud to deliver our final result of the project we have embarked on ten weeks ago. It has been an interesting, educative ride with the occasional hard times but a lot of enjoyment as well.

Team HUULC  
30-06-2015

Report	Distributed to	Distributed on
Final Report version 2	Gianfranco La Rocca	30-06-2015
	Dries Visser	
	Changhui Wang	

# List of Symbols

## Greek symbols

$\eta$	shock absorber efficiency [-]
$\eta_{antenna}$	Antenna efficiency [-]
$\eta_p$	Propeller efficiency [-]
$\eta_T$	tire absorbing efficiency [-]
$\lambda$	wavelength[m]
$\Lambda_{h,l}$	Hinge line angle [rad]
$\omega$	Engine angular speed [rad/sec]
$\rho$	Air density [kg/m <sup>3</sup> ]
$\sigma$	Fracture stress [Pa]
$\sigma_{buck}$	Buckling stress [Pa]
$\sigma_y$	Direct stress in y-axis [Pa]
$\tau_y$	shear yield stress [Pa]

## Roman symbols

$\frac{\partial W_{\text{lo}}}{\partial W_{\text{pl}}}$	Payload weight growth factor [-]
$\frac{\partial W_{TQ}}{\partial W_E}$	Empty weight growth factor [-]
$\frac{L}{D}$	Lift to drag ratio [-]
$\frac{\partial W_{TQ}}{\partial \eta_p}$	Propeller efficiency growth factor [kg]
$\frac{\partial W_{TQ}}{\partial \frac{L}{D}}$	Lift to drag ratio growth factor [kg]
$\frac{\partial W_{TQ}}{\partial c_p}$	Specific fuel consumption growth factor [kg/kg/J]
$\frac{\partial W_{TQ}}{\partial E}$	Endurance growth factor [kg/s]
$\frac{\partial W_{TQ}}{\partial R}$	Range growth factor [kg/km]
$\frac{C_L}{C_D}$	Aerodynamic efficiency[-]
$a$	Lift coefficient gradient in 3-D [ $\frac{1}{rad}$ ]
$A$	Aspect ratio [-]
$a$	Empty weight regression constant [-]
$a_0$	Lift coefficient gradient in 2-D [ $\frac{1}{rad}$ ]
$A_p$	Total area of plates [m <sup>2</sup> ]
$A_s$	Stringer Inertia [m <sup>4</sup> ]
$A_s$	Stringer area [m <sup>2</sup> ]
$B$	Receiver bandwidth[Hz <sup>-1</sup> ]
$b$	Empty weight regression constant [-]

$b$	Wing span [m]
$c$	Chord [Pa]
$C_{D_0}$	Zero-lift drag coefficient [-]
$C_D$	Drag coefficient in 3-D [-]
$C_{L_{max}}$	Aircraft maximum lift coefficient [-]
$C_{l_r}$	Required lift coefficient for the rudder [-]
$C_L$	Lift coefficient in 3-D [-]
$C_l$	Lift coefficient in 2-D [-]
$C_{mac}$	Aircraft moment coefficient [-]
$c_p$	Specific Fuel Consumption [lb/hr/hp]
$D$	Antenna diameter[m]
$d$	Diameter [m]
$E$	Endurance [sec]
$E$	Young's modulus of elasticity [Pa]
$e$	Oswald factor [-]
$g$	Gravitational acceleration [m/s <sup>2</sup> ]
$G_R$	Receiver antenna gain [dBi]
$Gt$	Gigatonne [kg · 10 <sup>12</sup> ]
$h$	Wing or fuselage box height [m]
$h$	Wing or fuselage box width [m]
$h_s$	Stringer height [m]
$I_{xx}$	Inertia of wing and fuselage box about x-axis [m <sup>4</sup> ]
$I_{xz}$	Product moment of inertia of wing and fuselage box about x-z plane [m <sup>4</sup> ]
$I_{yy}$	Inertia of wing and fuselage box of y-axis [m <sup>4</sup> ]
$K$	Stringer buckling clamping constant [-]
$kt$	Kilotonne [kg · 10 <sup>6</sup> ]
$L$	Stringer effective length [m]
$l$	Wing or fuselage box length [m]
$L_{Ptotal}$	Propagation loss[dB]
$L_{req}$	Required lift[N]
$L_R$	Receiver loss [dB]
$M_{ff}$	Fuel fractions [-]
$M_{tfo}$	Fraction of trapped fuel and oil [kg]
$M_x$	Moment around x-axis [N · m]

$M_x$	Moment around z-axis [ $N \cdot m$ ]	$S_z$	Shear force in z-axis [ $N$ ]
$M_x$	Torque around y-axis [ $N \cdot m$ ]	$SNR_{available}$	Available Signal to Noise ratio [ $dB$ ]
$MAC$	Mean aerodynamic chord [ $m$ ]	$SNR_{required}$	Required Signal to Noise ratio [ $dB$ ]
$MTOW$	Maximum Take Off Weight [ $kg$ ]	$t_h$	Horizontal plate thickness [ $m$ ]
$n_{bot}$	Number of bottom stringers $[-]$	$T_{mis}$	Missing thrust [ $N$ ]
$n_{front}$	Number of front stringers $[-]$	$t_s$	Stringer thickness [ $m$ ]
$N_{gear}$	L/W; ratio of load on absorber over the landing weight $[-]$	$t_v$	Vertical plate thickness [ $m$ ]
$N_{load}$	Load factor applied $[-]$	$V$	Cruise speed [ $m/s$ ]
$n_{rear}$	Number of rear stringers $[-]$	$V_h$	Horizontal tail volume coefficient [ $Pa$ ]
$n_{top}$	Number of top stringers $[-]$	$V_s$	Stall speed [ $m/s$ ]
$P$	Power [ $W$ ]	$V_v$	Vertical tail volume coefficient [ $Pa$ ]
$p$	Pressure [ $Pa$ ]	$V_{axial}$	Propeller axial velocity [ $m/s$ ]
$P_{carrier}$	Carrier power [ $dBm$ ]	$V_{helical}$	Helical tip velocity [ $m/s$ ]
$P_{noise}$	Noise power [ $dBm$ ]	$V_{rotational}$	Propeller rotational velocity [ $m/s$ ]
$q_{torque}$	Shear flow due to torque $T_y$ [ $\frac{N}{m}$ ]	$V_{vert}$	Vertical speed [ $fps$ ]
$q_t$	Total shear flow [ $\frac{N}{m}$ ]	$W/P$	Weight to power ratio [ $N/W$ ]
$q_x$	Shear flow due to $S_x$ [ $\frac{N}{m}$ ]	$W/S$	Wing loading [ $N/m^2$ ]
$q_z$	Shear flow due to $S_z$ [ $\frac{N}{m}$ ]	$W_e$	Empty weight [ $kg$ ]
$R$	Range [ $km$ ]	$W_f$	Fuel weight [ $kg$ ]
$R$	Range [ $m$ ]	$W_{landing}$	landing weight [ $lb$ ]
$Rdata$	Datarate [ $Mbps$ ]	$W_{pay}$	Payload weight [ $kg$ ]
$Re$	Reynolds number $[-]$	$w_s$	Stringer width [ $m$ ]
$S$	Surface area [ $m^2$ ]	$W_{tfo}$	Trapped fuel and oil weight [ $kg$ ]
$S_h$	Horizontal tail surface area [ $Pa$ ]	$W_{to}$	Takeoff weight [ $kg$ ]
$S_v$	Vertical tail surface area [ $Pa$ ]	$x_h$	Distance from wing aerodynamic centre to horizontal tail aerodynamic center [ $Pa$ ]
$S_{wf}$	Wetted surface area [ $m^2$ ]	$x_v$	Distance from wing aerodynamic centre to vertical tail aerodynamic centre [ $Pa$ ]
$S_x$	Shear force in x-axis [ $N$ ]		

# Contents

Preface . . . . .	ii
<b>List of Symbols</b>	<b>iii</b>
<b>1. Introduction</b>	<b>1</b>
<b>2. Business model</b>	<b>2</b>
2.1. Positioning the HUULC within the freight transport market . . . . .	2
2.1.1. Size & growth opportunities within the freight transport market . . . . .	2
2.1.2. The SWOT analysis . . . . .	3
2.1.3. Verdict on the HUULC's market position . . . . .	3
2.2. Investigating geographic regions of operation . . . . .	4
2.3. Fleet size analysis . . . . .	5
2.4. Transportable commodity analysis . . . . .	5
2.4.1. Classification of goods by water content . . . . .	5
2.4.2. Classification of goods by biotic activity . . . . .	5
2.4.3. Classification of goods by storage climate conditions . . . . .	5
2.4.4. Limitations on commodities transportable by the HUULC . . . . .	5
<b>3. Mission and requirements analysis</b>	<b>8</b>
3.1. Mission analysis . . . . .	8
3.1.1. Functional breakdown structure . . . . .	8
3.1.2. Functional flow diagrams . . . . .	8
3.2. The N2 chart . . . . .	8
3.3. Requirements analysis . . . . .	8
3.3.1. Requirements structure . . . . .	8
3.3.2. Technical requirements . . . . .	13
3.3.3. Constraints . . . . .	13
<b>4. Network</b>	<b>18</b>
4.1. Analysis of world leading container ports . . . . .	18
4.2. Estimation of the amount of HUULCs . . . . .	18
4.3. Estimation of the amount of containers transported . . . . .	20
4.4. Hub-and-Spoke vs. Point-to-Point . . . . .	21
4.4.1. Hub-and-Spoke . . . . .	21
4.4.2. Point-to-Point . . . . .	22
4.4.3. Combination of networks . . . . .	23
4.5. Analysis of airports . . . . .	23
4.6. Assigning the network . . . . .	23
4.7. Conclusion and recommendations . . . . .	24
<b>5. Cost budget</b>	<b>25</b>
5.1. Freight rate . . . . .	25
5.2. Revenue per shipment . . . . .	26
5.3. Total Program Revenue (TPR) over entire lifespan . . . . .	26
5.4. Total Program Costs (TPC) over entire lifespan . . . . .	26
5.5. Budget . . . . .	26
<b>6. The design of the HUULC</b>	<b>29</b>
6.1. Preliminary configuration design . . . . .	29
6.1.1. Configuration trade-off . . . . .	29
6.1.2. Preliminary weight estimation . . . . .	31
6.1.3. Payload range diagram of the HUULC . . . . .	35
6.1.4. Preliminary performance constraint analysis . . . . .	36
6.1.5. Containers design . . . . .	37
6.1.6. Payload bay sizing . . . . .	39
6.1.7. Hydrogen tanks . . . . .	39
6.1.8. Conclusion and recommendations . . . . .	41
6.2. Aerodynamic model . . . . .	42
6.2.1. Airfoil design . . . . .	42

6.2.2.	Planform design . . . . .	43
6.2.3.	High lift devices . . . . .	44
6.2.4.	Conclusion and recommendations . . . . .	45
6.3.	Propulsion system selection and integration . . . . .	45
6.3.1.	General architecture . . . . .	46
6.3.1.1.	Gas turbines coupled to cryo-cooled generators & fans . . . . .	46
6.3.1.2.	Fuel cells connected to electric motors . . . . .	47
6.3.1.3.	Gas turbine directly connected to a shaft . . . . .	47
6.3.1.4.	Architecture selection . . . . .	47
6.3.2.	Engine and propeller type . . . . .	48
6.3.2.1.	Total power and required disk loading . . . . .	48
6.3.2.2.	Contra-rotating propfan technology . . . . .	48
6.3.3.	Engine number and propeller sizing . . . . .	49
6.3.3.1.	Propeller tip velocity considerations . . . . .	49
6.3.4.	Engine positioning . . . . .	50
6.3.4.1.	Longitudinal positioning . . . . .	50
6.3.4.2.	Span-wise positioning . . . . .	51
6.3.5.	Conclusion and recommendations . . . . .	51
6.4.	Structural characteristics . . . . .	52
6.4.1.	Wing sizing . . . . .	52
6.4.1.1.	Reference frame . . . . .	52
6.4.1.2.	Wing box geometry . . . . .	52
6.4.1.3.	Load discovery and modelling . . . . .	53
6.4.1.4.	Theory and assumptions . . . . .	57
6.4.1.5.	Program flow diagram . . . . .	57
6.4.1.6.	Stringer optimisation . . . . .	58
6.4.1.7.	Sizing for direct stresses . . . . .	59
6.4.1.8.	Shear stress optimisation . . . . .	60
6.4.1.9.	The iteration process . . . . .	61
6.4.2.	Fuselage sizing . . . . .	62
6.4.2.1.	Reference frame . . . . .	63
6.4.2.2.	Fuselage box geometry . . . . .	63
6.4.2.3.	Force discovery and modelling . . . . .	64
6.4.2.4.	Stringer sizing . . . . .	64
6.4.2.5.	Plates sizing . . . . .	66
6.4.2.6.	Iteration process . . . . .	66
6.4.3.	Conclusion and recommendations . . . . .	68
6.5.	Weight and balance . . . . .	69
6.5.1.	Weight breakdown . . . . .	69
6.5.2.	Weight and balance calculation . . . . .	70
6.5.3.	Conclusion and recommendations . . . . .	71
6.6.	Stability and control . . . . .	72
6.6.1.	Stability and controllability . . . . .	72
6.6.2.	Symmetric Eigenmotions . . . . .	72
6.6.3.	Asymmetric eigenmotions . . . . .	73
6.7.	Subsystems design . . . . .	75
6.7.1.	Fuel systems . . . . .	75
6.7.2.	Fuel pump and hydrogen tank to engine connection . . . . .	75
6.7.3.	Hydraulic vs. electrical systems . . . . .	75
6.7.3.1.	Normal operation . . . . .	76
6.7.3.2.	Electric power generation . . . . .	76
6.7.4.	Environmental systems . . . . .	76
6.7.5.	De-icing, anti-icing, rain removal and defog systems . . . . .	76
6.7.6.	Control surfaces and empennage sizing . . . . .	77
6.7.6.1.	Empennage configuration . . . . .	77
6.7.6.2.	Scissors plot for horizontal tail sizing . . . . .	77
6.7.6.3.	Vertical stabilizer . . . . .	78
6.7.6.4.	Empennage sizing check in case of one engine inoperative . . . . .	78
6.7.7.	Ailerons . . . . .	78
6.7.8.	Landing gear . . . . .	79
6.7.8.1.	Design process . . . . .	79
6.7.8.2.	Verification and validation . . . . .	82
6.7.8.3.	Conclusion and recommendations . . . . .	82
6.8.	Integrated design . . . . .	83
6.9.	Aircraft design riskmap . . . . .	83
6.10.	Conclusion . . . . .	85

<b>7. Unmanned operations</b>	<b>87</b>
7.1. Benefits of an unmanned cargo vehicle . . . . .	87
7.2. Implications on the design of the HUULC . . . . .	87
7.3. Ground control station . . . . .	88
7.4. Communications protocol . . . . .	88
7.5. Command and control . . . . .	88
7.5.1. Line of sight operations . . . . .	88
7.5.2. Beyond line of sight operations . . . . .	89
7.5.3. GCS and ATC towers . . . . .	89
7.6. Technical specifications and signal to noise ratio . . . . .	90
7.6.1. BLOS operations . . . . .	90
7.6.2. LOS operations . . . . .	92
7.7. Software and hardware . . . . .	93
7.7.1. Conclusion and recommendations . . . . .	94
<b>8. Airport analysis</b>	<b>95</b>
8.1. Required facilities . . . . .	95
8.2. Budget for building the airports . . . . .	96
8.3. Runway . . . . .	97
8.3.1. Load identification . . . . .	98
8.3.2. Wheels vs. weight . . . . .	98
8.3.3. Pavement type . . . . .	98
8.4. Loading and unloading architecture . . . . .	98
8.4.1. Aircraft parking formation . . . . .	99
8.4.2. Container circulation network . . . . .	99
8.4.3. Aircraft - cargo handling system interface . . . . .	100
8.5. Airport architecture . . . . .	100
8.6. Emergency procedures . . . . .	104
8.6.1. Alternate airport . . . . .	104
8.6.2. Exceeding MLW during landing . . . . .	106
8.6.2.1. Dumping fuel . . . . .	106
8.6.2.2. Flying around . . . . .	106
8.6.2.3. Dumping payload . . . . .	106
8.6.2.4. Landing with overweight . . . . .	106
8.6.3. Emergency procedures conclusion . . . . .	107
8.7. Conclusion and recommendations . . . . .	107
<b>9. Hydrogen strategy</b>	<b>108</b>
9.1. Liquid hydrogen production . . . . .	108
9.1.1. Hydrogen generation . . . . .	108
9.1.2. Hydrogen source . . . . .	109
9.1.3. Hydrogen liquefaction . . . . .	109
9.1.4. Storage & transport . . . . .	109
9.2. Renewable energy generation . . . . .	110
9.3. Hydrogen and energy generation overview . . . . .	112
9.4. Airport analysis . . . . .	112
9.4.1. Airport energy analysis . . . . .	112
9.4.2. Airport capacity analysis . . . . .	113
9.5. Fuel cost budget . . . . .	116
9.5.1. Available budget . . . . .	116
9.5.2. Freight rate sensitivity analysis . . . . .	116
9.5.3. Hydrogen strategy costs overview . . . . .	117
9.6. Advantages of hydrogen fuel as compared to kerosene . . . . .	118
9.6.1. Emissions . . . . .	118
9.6.2. Financial aspect . . . . .	118
9.7. Preliminary landscape analysis . . . . .	119
9.7.1. Onshore wind facility area . . . . .	119
9.7.2. Solar PV facility area . . . . .	119
9.7.3. Hydroelectric facility area . . . . .	119
9.7.4. Hydrogen electrolyser area . . . . .	119
9.7.5. Hydrogen liquefaction area . . . . .	119
9.7.6. Storage facility area . . . . .	119
9.7.7. Energy and hydrogen facility area per airport . . . . .	119
9.8. Strategy execution . . . . .	120

9.9. Feasibility conditions . . . . .	121
9.9.1. Energy price . . . . .	121
9.9.1.1. Solar PV energy feasibility . . . . .	121
9.9.1.2. Wind energy feasibility . . . . .	122
9.9.1.3. Hydroelectric feasibility . . . . .	123
9.9.2. Hydrogen price . . . . .	124
9.9.3. Auxiliary feasibility parameters . . . . .	124
9.9.3.1. Entry into service . . . . .	124
9.9.3.2. Operations and fuel budget . . . . .	125
9.10. Conclusion and recommendations . . . . .	125
<b>10. Cost analysis</b>	<b>126</b>
10.1. Research & development and production costs . . . . .	126
10.2. Ground support, initial spares & purchase additions . . . . .	127
10.3. Operations & maintenance . . . . .	127
10.4. System phase-out & disposal . . . . .	127
10.5. Comparing the budget and cost analysis . . . . .	128
10.6. Validation of the RAND DAPCA IV model . . . . .	128
10.7. Conclusion and recommendations . . . . .	129
<b>11. Sustainable development strategy</b>	<b>130</b>
11.1. Design and operations . . . . .	130
11.2. Production . . . . .	130
11.3. End-Of-Life . . . . .	131
<b>12. Design verification</b>	<b>132</b>
12.1. Compliance matrix . . . . .	132
12.2. Compliance analysis . . . . .	132
12.2.1. C-Leg-1 . . . . .	132
12.2.2. Tr-Ops-Flight-3 and Tr-Pl-4 . . . . .	132
12.2.3. Tr-Perf-Sust-1 and Tr-Perf-Sust-2 . . . . .	132
12.2.4. Tr-Perf-Sust-3 . . . . .	132
<b>13. Post DSE Planning</b>	<b>134</b>
13.1. Research & development . . . . .	134
13.2. Prototype manufacturing . . . . .	134
13.3. Testing & certification . . . . .	134
13.4. Production & delivery . . . . .	134
<b>14. Conclusion and recommendations</b>	<b>137</b>
<b>15. Summary</b>	<b>138</b>
<b>Bibliography</b>	<b>142</b>
<b>A. Appendix - CAD Drawings</b>	<b>143</b>

# 1. Introduction

Globalisation in the 21st century has led to a dramatic increase in demand for transportation of goods across the globe. For intercontinental distances, two modes of transportation dominate the market: maritime transport and air freight transport. Maritime transport is slow but has a low cost, while air cargo is traditionally more expensive but more reliable and much faster. This means that air cargo is used for time-sensitive and high value goods, while maritime transport is used for lower value, less time-sensitive and bulk goods. The aim of the HUULC is to alter this market with a new ultra-large aircraft. This aircraft should be able to compete with maritime freighter transport in order to obtain a portion of the market share from maritime transport. The task of Team HUULC of the Design Synthesis Exercise is to develop a feasible design for the HUULC to meet the given requirements, under the following mission statement: *“Team HUULC will design the HUULC, a freighter aircraft that will pioneer in sustainable high capacity air transport, competitive with maritime cargo shipping from 2030 onwards”*.

Sustainability is a key design driver for the HUULC project. Current long distance transport options rely on fossil fuels to provide propulsion. It is thought that the global maritime shipping industry is responsible for 3% of global carbon dioxide emissions [1]. The HUULC however, is to be powered by hydrogen fuel that does not emit any greenhouse gases. Furthermore, the hydrogen will be produced with sustainable energy sources such as wind and solar energy.

Three reports regarding this challenging task have already been written: an initial Project Plan [2], a Baseline Report [3] and a Midterm Report [4]. The Final Report is intended to be a standalone document that outlines all the design processes, design options and operational planning and costs.

This Final Report is structured as follows: firstly, the position of the HUULC in the freight transport market is analysed in Chapter 2 after which the mission is discussed and requirements are defined in Chapter 3. The network the HUULC should serve is outlined next in Chapter 4, after which Chapter 5 allocates the available budget to the different HUULC design aspects. The design is discussed in Chapter 6 starting with preliminary configuration design followed up by aerodynamic models, propulsion systems and structural characteristics. Subsequently weight & balance and stability & control are presented. The subsystems that make up the HUULC, as well as integrated design and a riskmap conclude Chapter 6. HUULC specific operational characteristics follow with Chapter 7 on unmanned operations, Chapter 8 presents the design for the airports that make up the HUULC network and Chapter 9 proposes a hydrogen strategy specified per airport. Chapter 10 discusses the costs for every aspect of the project and the sustainable development strategy describes the sustainable elements of the HUULC program in Chapter 11. The performance of the HUULC design with respect to the requirements and further planning of the project are presented in Chapter 12 and 13, respectively. The report is concluded and recommendations are given in Chapter 14 and a summary is given in Chapter 15.

## 2. Business model

As part of the operations division of the HUULC project, the market analysis was performed at the start of the project. In the Baseline Report, fundamental information was given on the freighter transport market (for both air and maritime modes), including its structure and organisation [3]. In this Final Report, key segments of this gathered information are summarised and are then applied to the project, in order to define the HUULC's business model. Four main aspects are presented in this chapter, beginning with the positioning of the HUULC within the freighter transport market in Section 2.1. An investigation is then conducted into the preferable geographical regions of operation in Section 2.2, followed by a determination of the necessary fleet size in Section 2.3. The chapter concludes with an analysis of the commodities to be transported by the HUULC in Section 2.4.

### 2.1. Positioning the HUULC within the freight transport market

Freight transport is a global business, which is characterised by an enormous, fiercely competitive market. No single project will be able to serve this vast market, regardless of how effective it may be. It is thus imperative to correctly pinpoint the position of the HUULC within the freighter transport market, in order to maximise its impact.

#### 2.1.1. Size & growth opportunities within the freight transport market

Selecting the market of operation within the global transport market requires the evaluation of two parameters: the size and projected growth of each market.

In terms of size within the total global freight transport market, air cargo accounts for about 1% of traffic by mass, whilst maritime shipping - which consist of containership, light bulk transport and heavy bulk transport - accounts for the remaining 99% [5]. The market share by mass can be seen in Figure 2.1 [5].

As was outlined in the HUULC project Baseline and Midterm Report, it is expected that the global freight transport market will see consistent yearly growth for the next 15-20 years, assuming stable economic conditions. Boeing and Airbus expect the air cargo market to grow at a constant rate of 4.7% and 4.5% respectively, per annum [5][6]. Until before the financial crisis of 2008, growth rates for containership, light bulk and heavy bulk maritime transport were 7.4%, 6.0% and 2.3% respectively and are predicted to continue at similar rates in the future [5].



Figure 2.1.: Long-haul freight transport market share by mass. [5]

### 2.1.2. The SWOT analysis

In this section a SWOT analysis for the container-ship market and for the HUULC is given in Figure 2.2a and 2.2b.



(a) SWOT analysis of the container ship market.

(b) SWOT analysis of the HUULC.

Figure 2.2.: SWOT analysis.

### 2.1.3. Verdict on the HUULC's market position

From the outlined information, air cargo's small market share (resulting from its high freight rates) does not provide favourable conditions for the introduction of an ultra large cargo aircraft, particularly when the market suffers from chronic overcapacity. Containership on the other hand, has a 14% market share by mass and has the highest growth rate of all transport modes, providing a window of opportunity for market capture through innovation.

Apart from low-value commodities, maritime containership also transports high-value goods that are typically carried by air, providing a low-cost alternative for goods that do not require the speed and reliability of air transport. By positioning the HUULC as a direct competitor to maritime containership with a freight rate comparable to maritime shipping, Group 9 hopes to win back a portion of these high-value, less time-sensitive goods from the maritime containership market on the basis of faster service and reliability. Apart from high-value products, the fast and reliable service provided by the HUULC will also be aimed at the low-value commodities typically carried by ships, in an attempt to lure them in by reducing their shipping time by a factor of 30, for the increased price factor of 2.5.

This market positioning is based on the idea that whether companies are shipping time-sensitive commodities or not, they will benefit from the speed and reliability provided by air transport over maritime transport, as long as the price is comparable to maritime transport. Faster service and greater reliability leads to less likelihood of delays in the transport chain, less unexpected costs, and greater customer satisfaction, to name a few examples, regardless of the time-sensitivity of the commodity. With large container ships carrying up to 18,000 TEU and the HUULC only carrying 0.56% of this, at 100 TEU, it is expected that at least 0.56% of containers on each shipment would benefit from this 30-fold decrease in transit time and would opt to pay the 2.5 times increase for the HUULC's service.

In parallel to competing with maritime shipping, the HUULC is still a freighter aircraft with a much lower freight rate than typical air cargo services. Moreover, many types of cargo that fit in a Unit Load Device (ULD, air cargo container) can also fit in a TEU. Hence, Group 9 expects a great interest from firms that transport their goods exclusively by air, as they will be receiving the same service for a much lower price.

To conclude, the HUULC will be positioned as a direct competitor to maritime containership, focusing to capture demand from low-value commodities and recapture demand from high-value ones, cumulatively capturing a portion of the 14% market share that containership holds. In parallel, demand from air cargo-exclusive goods is expected to arise from the high value-for-money service offered by the HUULC, capturing a portion of the 1% market share held by air cargo. In short, the maritime containership market will be the primary target market, whilst the air cargo market shall be the secondary target market of the HUULC program.

## 2.2. Investigating geographic regions of operation

With the primary and secondary target markets having been defined, it now follows to define the geographic regions of operation. The project guide provides a recommendation of focusing on operating in the Europe-Asia trade route and stipulates a requirement of a maximum range of 6,000km [7]. However, upon research, Group 9 concluded that the Europe-Asia trade route only accounts for a portion of the total containership traffic. According to the World Shipping Council (WSC), the Europe-Asia containership trade route is only second busiest, surpassed by the North America-Asia trade route. Trade route traffic values for 2013 as provided by the WSC are given in Figures 2.3 and 2.4. As can be seen, the Asia-North America trade route almost doubled the Asia-North Europe trade route in terms of number of TEUs in 2013.

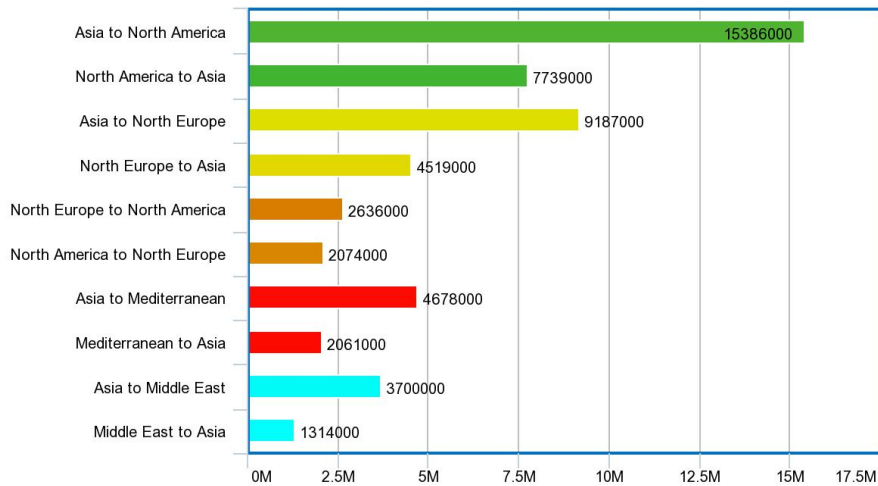


Figure 2.3.: Directional containership traffic along the main global trade routes for 2013, in number of TEU [8].

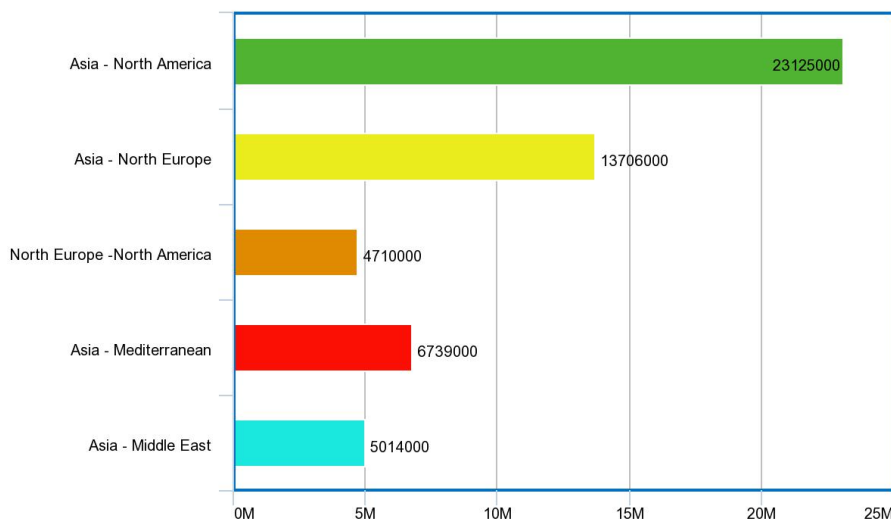


Figure 2.4.: Total containership traffic along the main global trade routes for 2013, in number of TEU [8].

For the HUULC's secondary target market - air cargo - both the Asia-North America and Asia-Europe trade routes had similar sizes in 2013, at 21.2% and 19.6% of global tonne-kilometers respectively [5]. Moreover, they both have similar projected annual growth rates of 5.4% and 5.3% respectively, in terms of tonne-kilometers, both above the global average of 4.7% [5].

It becomes clear that the Asia-North America trade route is the one with the most opportunity for the HUULC to operate, for both the primary and secondary target markets. For this reason, a feasibility study was conducted for the operation of the HUULC in the transpacific region, specifically between Shanghai and Memphis. These are two of the largest ports in the world, with the highest container throughput annually. Taking into account wind during flight, the total flight distance between the two cities is 11,941 km, which is unfeasible for this project. Hence, a stopover in Anchorage was decided, splitting the trajectory into 6,950 km from Shanghai to Anchorage and 5050 km from Anchorage to Memphis.

Furthermore, it was decided that since the network could be set up for the Asia-North America and Asia-Europe trade routes, the Europe-North America route would be easy to implement. A flight path from Terneuzen to Memphis would have a distance of 7,250 *km*, much over the maximum range of 6,000*km* set by the customer. Upon consultation with the customer, it was decided to increase the maximum range to 7,700 *km*, in order to accommodate for the Asia-North America and Europe-North America trade routes.

With this network, the HUULC will be able to serve all three of the major global trading routes, which together constitute 33% of global containership traffic.

## 2.3. Fleet size analysis

The project guide [7] proposes an estimated number of HUULCs of 110, when the freight rate is 2.5 times that of current maritime transport of \$1,150. It suggested that with this total output, a market share of 6-8% would be achieved. However, upon analysis, the team realised that due to the HUULC's low capacity with respect to ships (100 vs. up to 19,000 TEU), a market share less than 1% by mass would be achievable with 110 HUULCs. Hence, the team realised that with higher number of HUULCs produced, a higher market share would be taken. There is, however, an feasibility upper limit to the total number of HUULCs that can be produced and also the rate of production. For this reason, a number of 325 HUULCs has been chosen to be produced in total, as a compromise between gaining market share and feasible production rates.

This number has been selected by fixing the duration of this project (until approximately 2095). With this span of years, a maximum feasible production rate was set at 20 aircraft per year, based on the production rate of the Airbus A380. From these parameters, it is deduced that the number of HUULCs will total 325. This is further elaborated on in Section 4.2.

## 2.4. Transportable commodity analysis

As previously mentioned, the HUULC will carry both high-value and low-value goods that are typically carried by maritime container ships, specifically goods that are not time-sensitive. Furthermore, the HUULC will also carry time-sensitive goods, which are typically carried by cargo aircraft.

Container ships transport almost any type of commodity that fulfill two criteria: a) Fitting in the container in terms of size and mass, b) Are not (highly) time-sensitive. These commodities range from chemicals, to textiles, to machinery and autoparts, to toys and even fruits and vegetables, given they are stored in refrigerated containers (also known as reefers). High-value goods typically transported by air include fashion items, electronics and emergency deliveries.

A key requirement from the customer is TR-OPS-FLIGHT-1 which is discussed in Section 3.3: The HUULC shall not be pressurised. This requirement introduces a limitation to the commodities that can be transported by the HUULC, as the value of certain goods may deteriorate in an atmosphere other than that at sea level. The Gesamtverband der Deutschen Versicherungswirtschaft (GDV, German for German Insurance Association) has released a Container Handbook, which makes a distinction between three categorisations of goods being transported: their water content (WCC), their biotic activity (BA) and their requirements on storage climate conditions (SC). Biotic activity is defined by the GDV as: 'activities evident in products of vegetable or animal origin that during transportation exert an influence on the products themselves and/or on other animal or vegetable products' [9].

### 2.4.1. Classification of goods by water content

Four water content classes (WCC) are defined by the GDV, given in Table 2.1.

### 2.4.2. Classification of goods by biotic activity

Five biotic activity (BA) classes are defined by the GDV, given in Table 2.2.

### 2.4.3. Classification of goods by storage climate conditions

Nine storage climate condition (SC) classes are defined by the GDV, given in Table 2.3.

### 2.4.4. Limitations on commodities transportable by the HUULC

The Container Handbook provides Figure 2.4, depicting which goods fall under which WCC, BA and SC classes. Furthermore, the required container type, restrictions and storage space are given per commodity type.

Table 2.1.: Water content classes and their definitions.

<b>WCC</b>	<b>Definition</b>
WCC 0	Products containing no water, e.g. glass, porcelain, ceramic fittings, metals, plastics.
WCC 1	Products containing only a little water (water content $>0$ to $,1.5\%$ ), e.g. crystalline and pulverulent products (sugar, salt, fertilisers, citrus powder); their adsorption isotherms are characterised by discontinuities.
WCC 2	Goods with a low water content ( $WC >1.5 - ,30\%$ ), e.g. goods from, which water has been removed by natural or artificial drying, thereby, extending storage life, such as most foodstuffs and semiluxury items, also raw materials of animal origin, natural, fibers, coal, lumber, paper; their adsorption isotherms form a continuous, generally S-shaped, curve.
WCC 3	Goods with a high water content ( $WC >30\%$ ), including fruit, vegetables, meat and fish, with a water content of $>90\%$ , which have a tendency to release water vapor (water vapor release) into the storage atmosphere. This group also includes goods, such as, rafted wood or wet-salted hides (which under normal conditions belong to, WCC 2)

Table 2.2.: Biotic activity classes and their definitions [9].

<b>BA</b>	<b>Definition</b>
BA 0	Nonliving goods, goods exhibiting passive behaviour (porcelain, plastics, steel and chemical products)
BA 1	Living organisms with fully maintained intrinsic metabolism, e.g. livestock (domestic & zoo animals) and poultry.
BA 2	Living organisms, such as fruit (bananas, citrus fruits, pomaceous, fruit), vegetables (tomatoes, sweet peppers, potatoes, onions), grains, legumes, oil-bearing seeds/fruits, in which respiration processes predominate, because their supply of new nutrients has been cut off by separation from the parent plant.
BA 3	Goods in which respiration processes are suspended, but in which decomposition processes still proceed, such as meat, fish, processed grain products, dried fruits, spices, cocoa and coffee beans, tea, tobacco, expellers, fish meal, crystalline goods (sugar, salt, fertilising salts).
BA 4	Goods in which biochemical and microbial processes have stopped and, which are isolated from the external environment, e.g. sterilised and, pasteurised goods in hermetically sealed packaging (preserved foods, beverages).

Table 2.3.: Storage climate condition classes and their definitions [9].

<b>SC</b>	<b>Definition</b>
SC 0	Goods not subject to any conditions, which place no requirements on storage climate conditions
SC I	Goods which require particular ventilation conditions
SC II	Goods which require particular temperature conditions
SC III	Goods which require particular temperature and ventilation conditions
SC IV	Goods which require particular humidity/moisture and possibly ventilation conditions
SC V	Goods which require particular humidity/moisture and ventilation conditions
SC VI	Goods which require particular temperature, humidity/moisture and possibly ventilation conditions
SC VII	Goods which require particular temperature, humidity/moisture and ventilation conditions
SC VIII	Goods which require a controlled atmosphere

From Figure 2.4, all water content classes can be transported in a non-pressurised environment, as long as the humidity and temperature are regulated. For example, commodities with a high water content, such as

Table 2.4.: Classification of goods by WCC, BA and SC and requirements on transport conditions [9].

Product groups - Criteria	Ceramic products (industrial ceramics, ceramic fittings)	Crystalline goods (sugar, salt, fertilizer)	Dried fruit, spices	Shell fruit, green coffee beans	Meat, fish	Fruit, vegetables	Living animals
Packaging	unpacked, plastic film	double-layered bags (outside jute, inside plastic)	jute bags, cartons	jute bags	cartons	Jointed boxes, cartons	-
Water content class (WCC)	WCC 0	WCC 1	WCC 2	WCC 2	WCC 3	WCC 3	WCC 3
Biotic activity (BA)	BA 0	BA 3	BA 3	BA 2	BA 3	BA 2	BA 1
Storage climate conditions (SC)	not subj. to any conditions SC 0	temperature, humidity/moisture and possibly ventilation conditions SC VI			SC VI	SC VII, SC VIII	SC VII
Container type	flatrack (open container)	standard container, bulk container	Standard container	Ventilated container	low temp. refig. container	refrigerated container with fresh air supply, CA container	Livestock container
Restrictions	protection from rain and spray desirable	goods and packaging must be container dry: compliance with lower limits set for water content of goods, packaging and pallets			Compliance with cold chain	Comply with cold chain	Protect from atmospheric factors (sensitive to drafts)
Stowage space	on deck, unprotected or with tarpaulin	may be disadvantageous on deck	below deck where possible, protect from spray and heat sources		on and below deck		mostly on deck
				Ventilate intensively below deck			

fresh fruit, vegetables and fresh meat and fish, are not affected by the lack of air pressure. They do, however, deteriorate in flavour and texture when subjected to sub-zero temperatures (which freezes their water content) at high altitudes and then re-thawed when arriving at the destination. Hence, containers carrying WCC 3 goods must be temperature and humidity regulated. This can be done by using reefer containers.

In terms of biotic activity, a lack of pressure prevents BA one goods (for example, livestock) from being transported, since these commodities require near-sea level atmospheric conditions. BA 2 and BA 3 commodities, such as fresh fruit and meats, only require temperature and humidity regulation.

Other considerations must be accounted for, apart from the criteria provided in the Container Handbook. For example, sealed containers with liquids will inevitably remain pressurised. Therefore, the container must not be filled completely, to allow room for expansion due to the pressure differential. Moreover, the container must be able to structurally withstand the pressure difference. For this reason, cylindrical tanks will be used, to minimise stress concentrations arising from rectangular containers. The cylindrical tank is fitted into a frame which conforms to the rectangular TEU standard, allowing for easy stacking and management, just like any other TEU container.

## 3. Mission and requirements analysis

To ensure efficient and cost-effective operations, the functions that the HUULC has to fulfill need to be defined in advance of the design process. All mission segments of the HUULC need to be analysed to obtain a comprehensive and detailed overview, after which requirements can be specified to ensure design compliance to the mission. An analysis of the HUULC mission considering the entire lifetime is presented in Section 3.1, including a functional breakdown structure. In Section 3.2 the N2 chart is explained and how communication was performed within the team. After the N2, the requirements are defined in Section 3.3.

### 3.1. Mission analysis

The mission statement of this project is as follows: *“Team HUULC will design the HUULC, a freighter aircraft that will pioneer in sustainable high capacity air transport, competitive with maritime cargo shipping from 2030 onwards”*.

When analysing the mission, it is useful to analyse the functions of the system in two different ways. First, a Functional Breakdown Structure (FBS) is created, for function discovery. This diagram is shown and discussed in Section 3.1.1. Secondly, the chronological ordering of functions is shown in a Functional Flow Diagram (FFD). This diagram follows from the FBS and is discussed in Section 3.1.2.

#### 3.1.1. Functional breakdown structure

The FBS shows the functions the system must perform in a hierarchical manner. This hierarchic structure can be seen in the FBS on page 15. It shows that the mission consists of ten main functions. Each one of these main functions can be subdivided into a more detailed level.

#### 3.1.2. Functional flow diagrams

After the FBS has been established, the FFDs can be generated. These diagrams show the logical order of the functions that the system must perform [10]. The FFD of the transportation of the aircraft is shown in Figure 3.1. It illustrates the chronological order of assembly and transportation to the airport, for its maiden flight.

### 3.2. The N2 chart

The N2 chart can be seen in the figure on page 16. On the horizontal lines the outputs are shown and on the vertical lines the inputs. This chart was important for communicating with each other in an efficient way.

### 3.3. Requirements analysis

Requirements translate the set of design goals into parameters which the product should fulfil. In the case of the HUULC, a literature study and mission analysis were performed parallel to the requirement discovery process. The iterative process provides clear knowledge of the design challenges and the specifications the HUULC has to comply with. A discussion of the requirement's structure is provided in Section 3.3.1. For an elaborate discussion of the requirements analysis and discovery process the Baseline report should be consulted [11]. The list with both the technical requirements and constraints can be found in Section 3.3.2 and 3.3.3. Compliance of the HUULC to the requirements is evaluated in Chapter 12.

#### 3.3.1. Requirements structure

To have a clear view of all requirements and its relevance to each other, a structure has been defined. The requirements are split up into two categories, namely the technical requirements and the constraints. Technical requirements are requirements which indicate what the product has to do, while the constraints limit the number of possible design solutions. Constraints therefore limit the design freedom to meet the requirements.

Both the technical requirements and the constraints have been split into several sub-levels. Top level requirements and constraints are general, while bottom level requirements are specific. Also, the more specific a requirement becomes, the more critical it is to find a design solution to meet the criteria.

Both the requirement and constraint categories are listed in Table 3.1. The codes for each separate requirement and constraint are listed for the convenience of referencing between the table and the text. The requirements are ordered according to the different categories and can be found in Table 3.2

Table 3.1.: Legend.

Level	ID	Description	Level	ID	Description
1	C	Constraint	2	C-RES	Resources
1	TR	Technical Requirement	2	C-LEG	Legal
2	TR-COMP	Competitiveness	3	TR-PERF-CTRL	Control
2	TR-PERF	Performance	3	TR-PERF-STB	Stability
2	TR-PL	Payload	3	TR-PERF-MP	Mission Parameters
2	TR-OPS	Operations	3	TR-PERF-SUST	Sustainability
2	TR-SF	Safety	3	TR-OPS-FLIGHT	Flight Operations
2	TR-CONFIG	Configuration	3	TR-OPS-AIRPO	Airport Operations
2	TR-FUEL	Fuel	4	TR-OPS-FLIGHT-UM	Unmanned
2	C-COST	Cost	4	TR-OPS-FLIGHT-COM	Communication
2	C-TIME	Time	4	TR-OPS-AIRPO-MAIN	Maintainability

### 3.3.2. Technical requirements

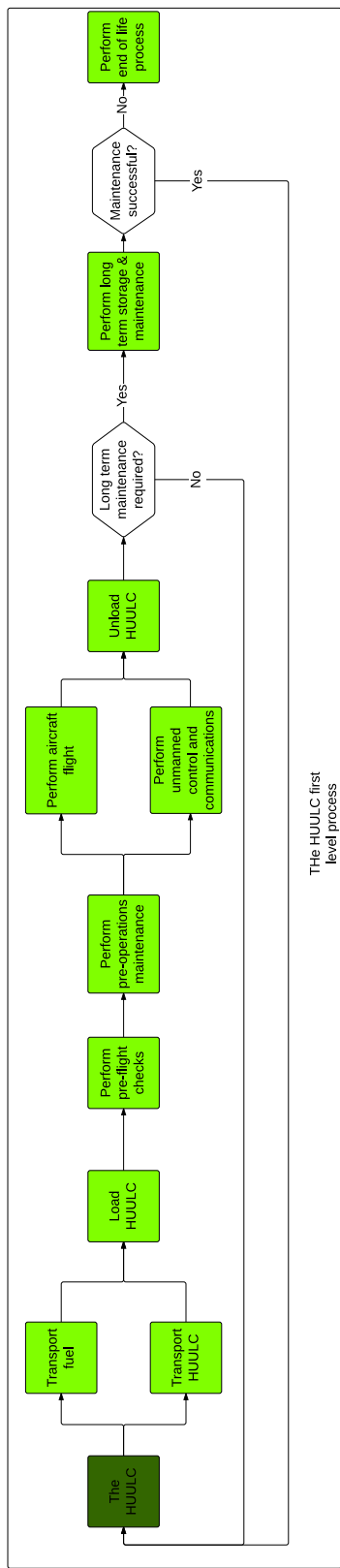
A requirement basically is a condition which must be complied with. Technical requirements are therefore technical conditions that follow from the operational needs of the aircraft, as described in Section 3.1. During the brainstorming sessions, the requirements were approached from a wide perspective and subsystem requirements were established. These requirements can be found in Table 3.2. The environmental requirements are of major importance and are discussed below.

A main design driver of the HUULC program is sustainability. For this purpose the TR-PERF-SUST requirements are defined in accordance with the team's goal to design a sustainable aircraft. Reference  $NO_x$  emissions are obtained from data of the European Conference of Ministers of Transport [12]. The  $NO_x$  goals are based upon the goals stated in Flightpath 2050 in combination with Cryoplane performance as researched by Airbus [13][14]. The noise requirements are based on Boeing 747-400 noise levels at Heathrow [15]. The 747-400 is a relatively old aircraft but the team believes, due to the expected size of the HUULC, that the noise requirements are ambitious.

### 3.3.3. Constraints

The constraints are limitations imposed on the project. The four types of constraints that are defined are:

- **Time:** Time constraints set limitations upon the deadlines and time related operations of the aircraft.
- **Legal:** Legal constraints are limitations imposed by certification authorities.
- **Cost:** Cost constraints are limitations related to the costs of the aircraft. These may include production costs and operational costs.
- **Resources:** Resource constraints impose limitations on the production and consumption of resources necessary to produce and operate the HUULC.

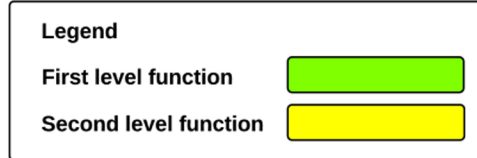
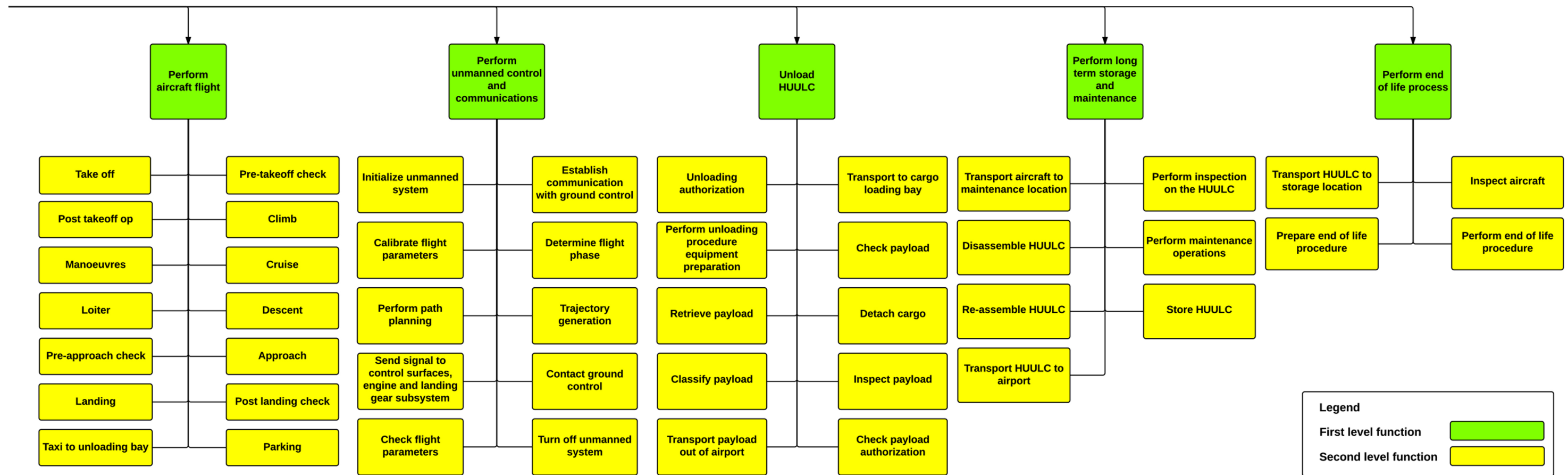
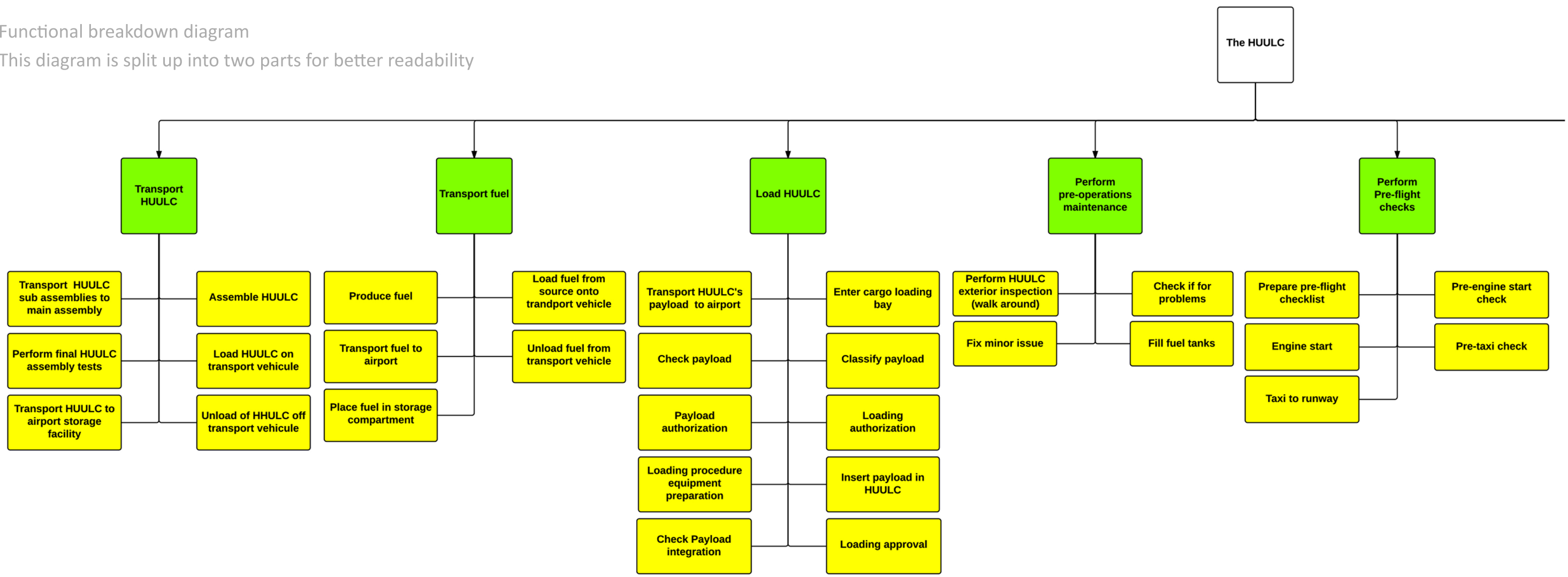


The HUULC first level process

Figure 3.1.: HUULC general (first level) process.

Functional breakdown diagram

This diagram is split up into two parts for better readability



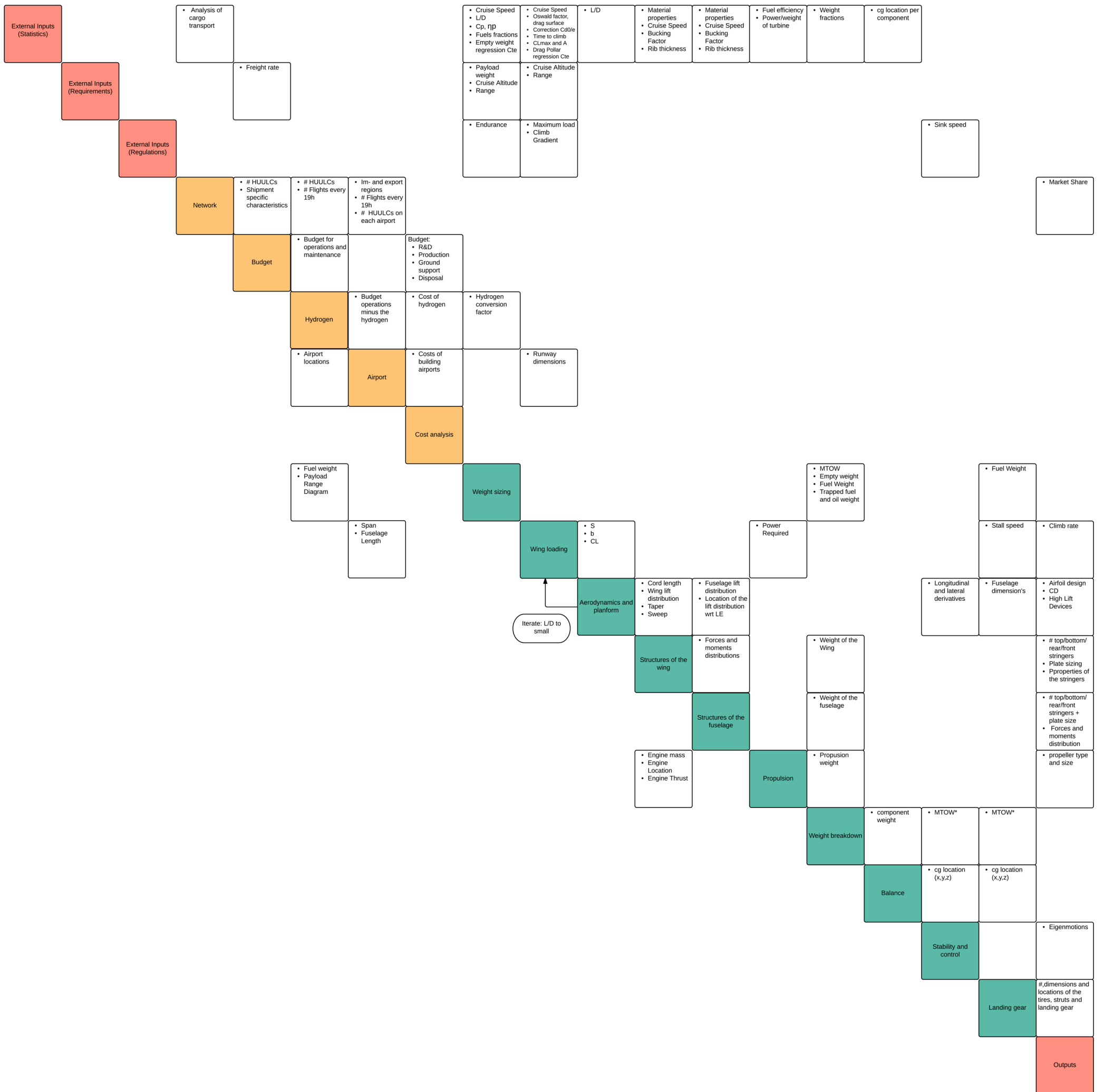


Table 3.2.: Requirements.

ID	Description
C-COST-1	The freight rate of container transport by HUULC shall not exceed 250% of the freight rate of standard container ships.
C-LEG-1	The HUULC shall meet the requirements obtained after close cooperation with certification authorities.
C-RES-1	The hydrogen production shall be sustainable.
C-RES-2	The HUULC hydrogen consumption shall not exceed the hydrogen production capacity available at time of operation.
C-TIME-1	Refueling of the HUULC shall not exceed the turnaround time stated in requirement TR-OPS-AIRPO-2.
C-TIME-2	The HUULC shall enter into service in 2030.
TR-COMP-1	The HUULC shall have a combination of cruise speed, flight trajectory, freight rate, reliability and sustainability that maximises competitiveness w.r.t. maritime transport when compared to other combinations viable at that time.
TR-COMP-2	The HUULC shall have an expected lifespan of no less than 45 years.
TR-CONFIG-1	The HUULC shall have a wing-lifting configuration.
TR-CONFIG-2	The HUULC shall not make use of the wing-in-ground effect.
TR-CONFIG-3	The HUULC shall not have a helicopter configuration.
TR-CONFIG-4	The landing gear configuration shall be compatible with the pavement's strength of the selected airfields.
TR-FUEL-1	The HUULC shall be propelled by cryogenic hydrogen.
TR-FUEL-2	The fuel tanks shall contain the required quantity of fuel to perform the design mission.
TR-FUEL-3	The fuel tanks shall allow for turnaround maintenance inspections.
TR-FUEL-4	The fuel system shall distribute the fuel to the power plants.
TR-FUEL-5	The fuel system shall be able to influence stability.
TR-OPS-AIRPO-1	The HUULC shall be able to land on selected airports (Landing gear, pavement, gate width, runway width, runway length, etc.).
TR-OPS-AIRPO-2	The turnaround time shall be less than 6 hours.
TR-OPS-AIRPO-3	The airports shall have a cargo bay capacity for 100 TEU.
TR-OPS-AIRPO-4	The airports shall be located within 25 kilometers to a renewable energy source.
TR-OPS-AIRPO-MAIN-1	The HUULC shall allow access ability for repairs.
TR-OPS-AIRPO-MAIN-2	The overall operational availability of the HUULC shall be at least 85%.
TR-OPS-FLIGHT-1	The HUULC shall not be pressurised.
TR-OPS-FLIGHT-2	The HUULC shall have no crew and no crew support systems.
TR-OPS-FLIGHT-3	The induced vibrations shall not cause the HUULC to lose structural integrity.
TR-OPS-FLIGHT-COM-1	The HUULC shall always have contact with the control centre.
TR-OPS-FLIGHT-COM-2	The communications system shall deny unauthorised control requests.
TR-OPS-FLIGHT-COM-3	The HUULC shall provide communication between ATC and ground control.
TR-OPS-FLIGHT-UN-1	The HUULC shall be flyable by at least one ground controller.
TR-PERF-CTRL-1	The HUULC shall be controllable in such a way that it can follow the predetermined flight trajectory.
TR-PERF-CTRL-2	The control system shall counteract spiral induced eigenmotions.
TR-PERF-CTRL-3	The control system shall counteract phugoid induced eigenmotions.
TR-PERF-MP-1	The HUULC shall have a cruise altitude of no lower than 5000 meters and no higher than 8000 meters.
TR-PERF-MP-2	The HUULC shall have an operating range of more than 6000 km while carrying maximum payload.
TR-PERF-STB-1	The HUULC shall be statically stable.
TR-PERF-STB-2	The HUULC shall be dynamically stable for dutch roll eigenmotion.
TR-PERF-STB-3	The HUULC shall be dynamically stable for short period eigenmotion.
TR-PERF-STB-4	The HUULC shall be dynamically stable for aperiodic roll eigenmotion.
TR-PERF-SUST-1	The HUULC shall produce no more than 104.7 dB noise during take-off at distance 4400 meters.
TR-PERF-SUST-2	The HUULC shall produce no more than 97.1 dB noise during landing at distance 4400 meters.
TR-PERF-SUST-3	The HUULC shall not produce more than 0.27 grams $NO_x$ per ton kilometer.
TR-PERF-SUST-4	The HUULC shall use no fossil fuels during flight.
TR-PL-1	The HUULC shall be able to accommodate the contents of 100 TEU lightweight containers.
TR-PL-2	The HUULC shall be able to transport a payload of 1200 metric tonnes.
TR-PL-3	The HUULC shall transport the payload without inflicting payload damage.
TR-PL-4	The induced vibrations shall not compromise the payload integrity.
TR-SF-1	The HUULC shall have a fail-safe communication system.

## 4. Network

This chapter investigates the best possible solution for the HUULC's network. In Figure 4.1 one can see the order of the process. First an analysis of the world leading container ports is done in Section 4.1. Afterwards the amount of HUULCs together with the im- and export are extrapolated from 2030 onwards in Section 4.2 and 4.3. The different types of network are discussed in Section 4.4. Next the analysis of the usable airports is done in 4.5. The team decided to analyse what it would take to built our own airport, this is done in Chapter 8. Afterwards, a trade off between enlargement of existing airports and private HUULC airports is done. With all those inputs one can assign the network which is discussed in Section 4.6. The final step is designing the airports with the amount of HUULCs, storage and hydrogen needed which again can be found in Chapter 8. The analysis of the airports will be done after the sizing of the aircraft so that the dimensions are known.

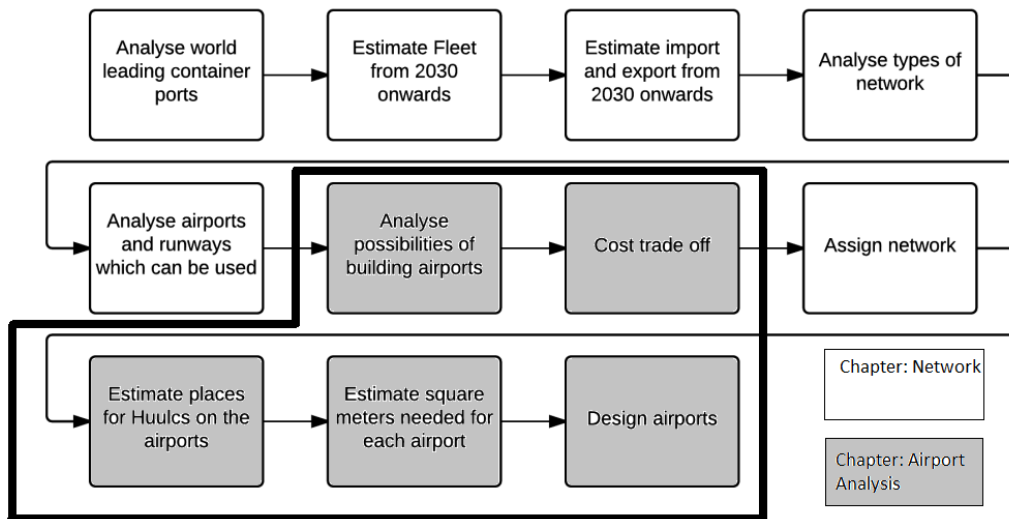


Figure 4.1.: Process of the Network of the HUULC.

### 4.1. Analysis of world leading container ports

Concerning the routes of the HUULC, a world wide network is chosen, as discussed in Chapter 2. Since air cargo only fulfils 1% of the total transport by weight, the focus of the network is on Maritime transport: containerised goods, which performs 14% of the total transport by weight [5]. Four regions have been chosen for the transportation of containerised goods by HUULC. Those four regions are the largest regions in container transport. The Yangtze River Delta Region is the busiest region followed by Western Europe. As discussed in Chapter 2, North- America - Asia will become the busiest route. In the analysis for the routes of the HUULC the busiest region in North America is chosen. This region is South-East USA as can be seen in Figure 4.2. This is because of the large amount of ports in the Gulf of Mexico and along the Mississippi River. However this region is relatively small in import and export with respect to the Yangtze River Delta Region. It is definitely interesting to look into different regions. For this project the team will only look into the four chosen regions because of time constraints. The four regions and their respective ports are given in Table 4.1.

To have an impression of the importance of containerised cargo in each region, a relative percentage is given in the table. Import and export of those four regions cover 33% of the world's transport of containerised goods. For simplicity, it is assumed the import and export values for each region are the same.

### 4.2. Estimation of the amount of HUULCs

It is assumed the HUULC has a lifetime of 45 years [16]. This value is estimated with respect to pressurised reference airplanes. It is assumed the production would start in 2030 with a delivering rate of five HUULCs a year. The amount of aircraft built per year increases up to 20 HUULCs. This value is estimated using the A380 as a reference [17]. In 2050 the HUULC's production will stop. During the last three years of the production process, the production rate will gently decrease to zero. In Figure 4.3, the number of operational HUULCs is

Table 4.1.: Import and export region examples.

Region	Cities	Relative Size
Yangtze River Delta Region	Shanghai, Ningbo-Zhoushan and Suzhou	45.69 %
Western Europe	Antwerp, Rotterdam, Amsterdam, Hamburg and Bremen	30.35 %
South-East USA	New York, Savannah, Houston and Charleston	9.79 %
United Arab Emirates	Jebel Ali Dubai and Sharjah	14.16 %

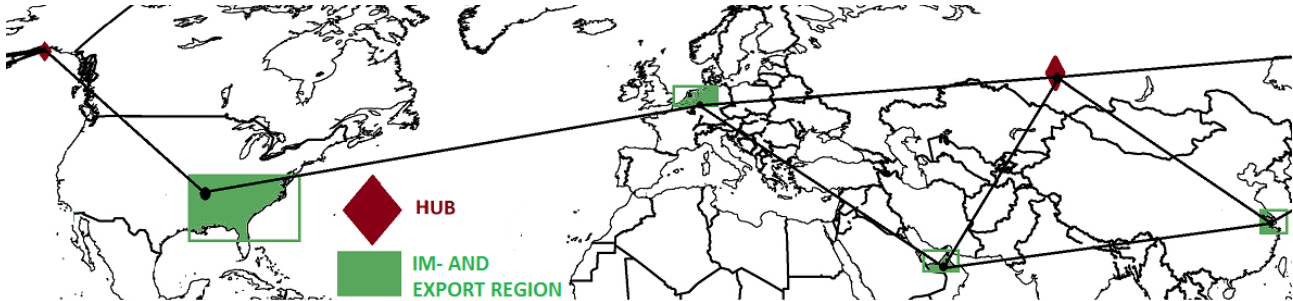


Figure 4.2.: The network of the HUULC.

given from 2030 until 2095. As it can be seen in Figure 4.3 the HUULC will operate with a maximum peak of 325 units from 2050 until 2075. With an availability assumed of 85 percent, there are 278 HUULCs operable ever day of the year. This availability percentage is based on the rationale presented in Table 4.2.

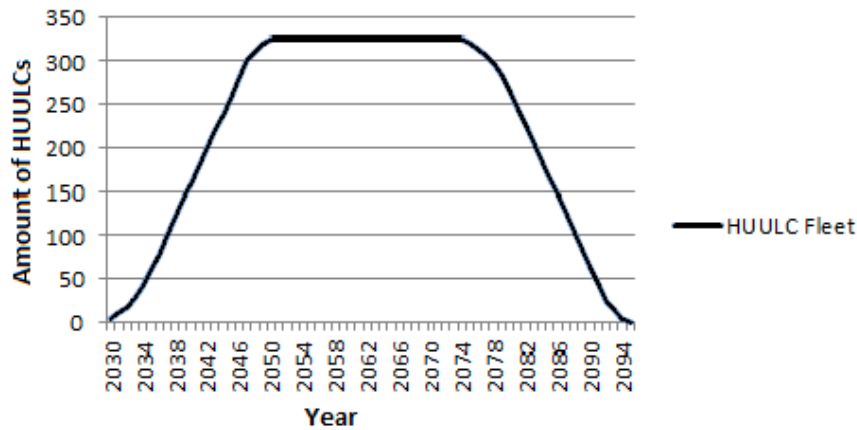


Figure 4.3.: Forecast of total number of operational HUULCs.

Table 4.2.: Availability based on typical aircraft maintenance checks [18]. A safety margin of double the maintenance duration is assumed to be sufficient.

Type	Duration	Scale up	Unit
A check			
<i>Required every</i>	15	26280	days
<i>Time in hangar</i>	0.5	876	days
B check			
<i>Required every</i>	186	26280	days
<i>Time in hangar</i>	3	424	days
C check			
<i>Required every</i>	620	26280	days
<i>Time in hangar</i>	14	593	days
D check			
<i>Required every</i>	26280	26280	days
<i>Time in hangar</i>	62	62	days
<b>Total</b>			
<i>Required every</i>		26280	days
<i>Cumulative time in hangar</i>		1955	days
Aspect	Value	Unit	
Maintenance	7.5	%	
Availability	92.5	%	
Safety margin	7.5	%	
Assumed availability	85	%	

### 4.3. Estimation of the amount of containers transported

For containerised transport, a value of 7.4% growth for each year is assumed [5]. With this value, the import and export of containerised goods is estimated from 2030 onwards. In Table 4.3 the sum of the import and export for every region is given. The data of the year 2013 is used to extrapolate the data from 2030 onwards. The market share is calculated using the number of operational HUULCs. This market share represents the market share of the route that is flown by the HUULC. For this calculation, one should keep in mind that the HUULC has an availability rate of 85 percent. The loading and unloading time is estimated on six hours and the time needed for refuelling is four hours. In Figure 4.4, the total number of TEU containers transported in every region is shown for the coming 80 years.

Table 4.3.: Number of containers for each region.

Year	2013	2030	2045	2070	2090
Number of operational HUULCs	0	5	260	325	65
<b>Im- and export: Western Europe</b>	37,369,000	125,772,084	366,985,141	2,186,530,370	9,116,772,997
<b>Im- and export: Yangtze River Delta Region</b>	56,260,000	189,353,140	789,510,915	3,291,878,258	13,725,538,516
<b>Im- and export: United Arab Emirates</b>	17,440,000	58,697,454	171,270,863	1,020,447,153	4,254,770,560
<b>Im- and export: South-East USA</b>	12,052,071	40,563,411	118,358,291	705,189,309	294,0297,986
<b>Im- and export: Total</b>	123,121,071	414,386,090	1,209,119,954	7,204,045,090	30,037,380,059
<b>Market share</b>	0%	0.07%	1.16%	0.24%	0.01%

As can be seen in Table 4.3 the maximum market share is reached in 2070. The numbers are still very low so the HUULC team is convinced that it is possible to win 1.16% market share from the containerised goods.

Since the distance from one point to another sometimes exceeds the 6000 km range, the HUULCs will be loaded with only 97 containers. If the distance does not exceed the 6000 km range, the HUULC will be fully loaded, as it is designed for. This is calculated in the payload range diagram in Section 6.1.3

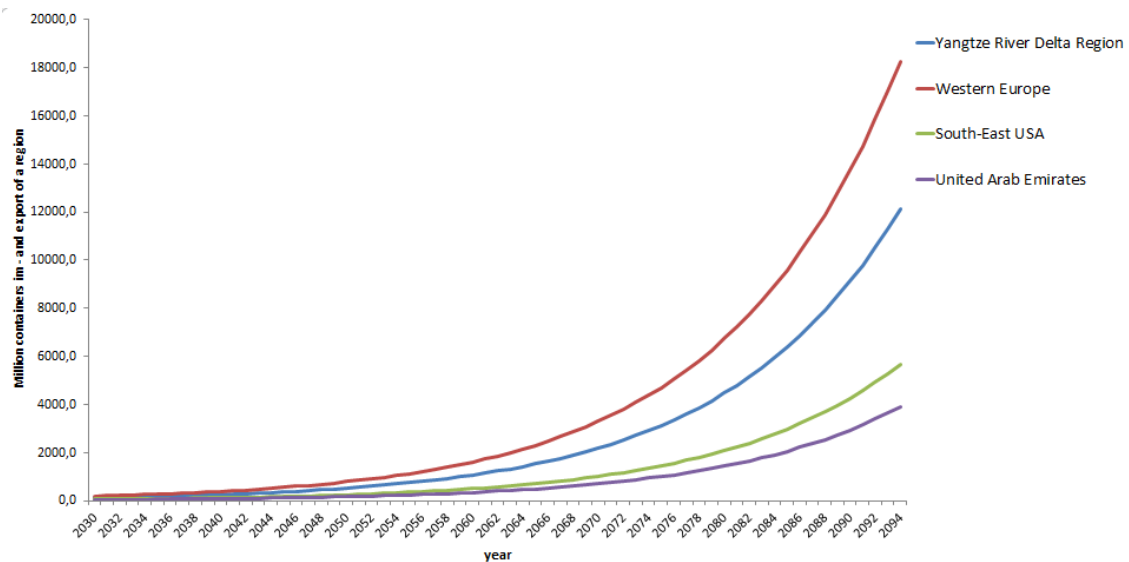


Figure 4.4.: Forecast of number of containers.

## 4.4. Hub-and-Spoke vs. Point-to-Point

Before setting up a network, the principles of Hub-and-Spoke and Point-to-Point are taken into consideration. This is to find an optimal network use between the supply and demand of the payload.

### 4.4.1. Hub-and-Spoke

The Hub-and-Spoke network can also be seen as a radial network, see Figure 4.5. The essential characteristics of such a network are [19]:

- All traffic is directed via the hub
- City-pair coverages are available
- Transfer at hub is necessary
- Concentration of departures and arrivals in banks (waves) of flights
- Increase in traffic density
- Protection from competition
- The total travel time increases
- High dependency on punctuality

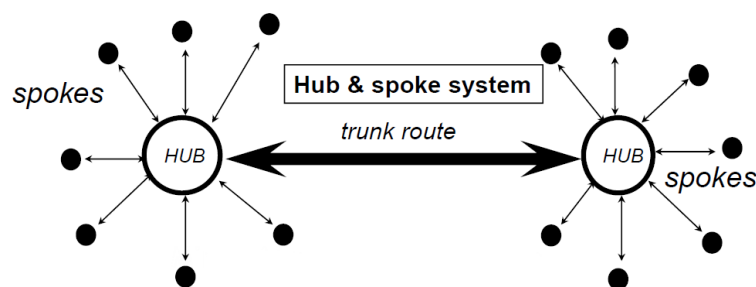


Figure 4.5.: Hub-and-Spoke system [19].

The main advantage is that the ability to reach a large number of destinations from any one origin gives the airline operating the hub system considerable market appeal [20]. Effective “hubbing” generates substantial volumes of additional traffic, and revenue, but most of it is transferring through the hub airport. Another advantage is that due to shorter distances and higher demand, by providing more connections, the flights can be performed more frequently.

As a result of increasing demand, the hub operator may also drop its fares on connecting services if it needs to undermine any new competition offering Point-to-Point services bypassing a hub. It can do this easily by cross-subsidising this service from other routes where it faces no direct competition. One of the most important benefits to arise from effective Hub-and-Spoke operations is the extent to which individual airline networks can become self-sufficient in meeting demand and enabling operators to keep passengers on their services.

To have a time-efficient hub, punctuality is important. Punctuality can be achieved by for example having a larger turnaround time than necessary. To comply with the efficiency, hubs will have a wave-system. A wave-system is a system consisting out of clusters of arriving and departing flights that create transfer possibilities. An example of such a wave-system for an European hub airport can be found in Figure 4.6. As an addition, the arriving and departing waves do not have to be intercontinental only. In the meanwhile, the hub can be served by local trucks or flights as well, keeping up with the inbound and outbound schedule of the HUULC.

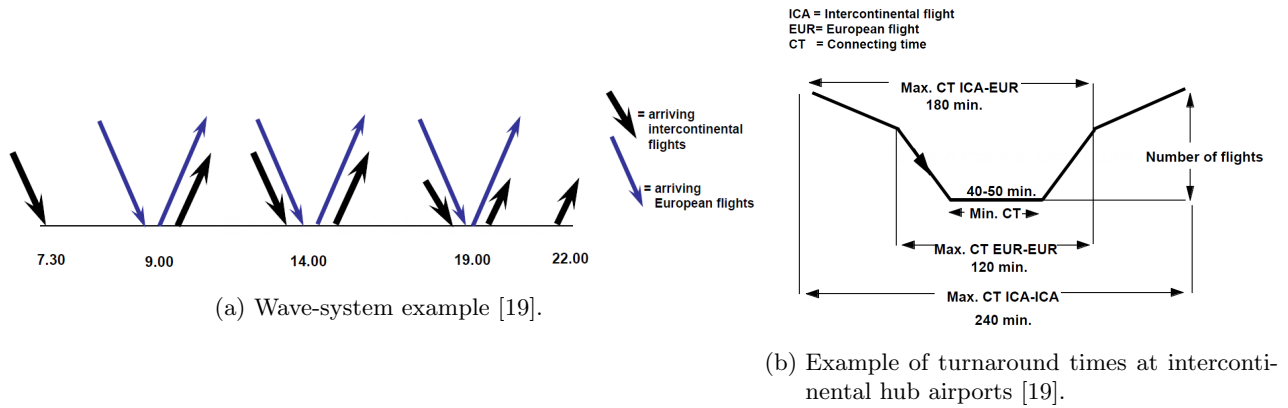


Figure 4.6.: Example cases of a wave-system and turnaround time.

To investigate the number of possible connections of the network, Table 4.4 has been created. It can be seen that using a single hub with three spokes, the total city pairs served is six. A single hub with four spokes serves a total of ten city pairs. The more city pairs will be served, the higher the market appeal will become.

Table 4.4.: Impact of “hubbing” on the number of city pairs served [20].

Number of spokes from the hub	Number of points connected via the hub	Number of points linked to the hub by direct flights	Total city pairs served
$n$	$n \cdot (n - 1) / 2$	$n$	$n \cdot (n + 1) / 2$
3	3	3	6
4	6	4	10

#### 4.4.2. Point-to-Point

A visualisation of the Point-to-Point connection principle can be found in Figure 4.7. The essential characteristics of this system are that it has non-stop connections between city pairs and that the travel time is minimal, due to direct routing and absence of transfers [19]. Due to non-stop connections, there is no single point of failure and delays are unlikely to cascade through the system [21]. On the downside, compared to a Hub-and-Spoke system, more routes are needed to provide the same amount of destinations from each single airport. As a result, the travel frequency per route will decrease as well.

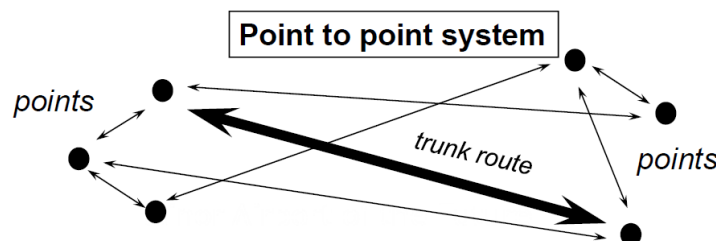


Figure 4.7.: Point-to-Point system [19].

### 4.4.3. Combination of networks

To conclude this section, the investigation led to the decision to make a combination of both Point-to-Point and Hub-and-Spoke routes. The Point-to-Point routes will be positioned between airports covering large distances, without the need of picking-up more payload along its route. To solve the problem of covering larger distances than the designed range of the HUULC, less payload will be carried in order to increase its range. For the routes where the demand and the chosen seaports and airports are closely positioned to each other and distances are within the design range of the HUULC, a Hub-and-Spoke system will be set up. Figure 4.2 will go in further detail to set up the network to be used by the HUULC.

## 4.5. Analysis of airports

The first intention of the group was to use already existing airports. Since the wingspan of the HUULC will be around 200 meters, a cost trade-off between enlargement and fees of an already existing airport and building a new airport has been done. The trade off had two important outcomes: The fees were extremely high because of the MTOW of the HUULC and possibilities for enlargements were very limited. Since the analysis of the existing airports is not relevant anymore for the project, this is not included in the final report but the content can be found in the midterm report [4]. The analysis of the new airports is done in Chapter 8.

## 4.6. Assigning the network

For assigning the network, the information of Sections 4.1, 4.2, 4.3, 4.4 and 4.5 is used. The first step in assigning a network is determine the demand of a certain zone. This step is called trip generation. The zones used in this network are the four regions and the two hubs. The production and attraction is calculated in Section 4.3.

In Table 4.5 the demand numbers for each region are given in terms of amount of HUULCs. At a certain point 325 HUULCS will be usable. This number is reduced to 278 operable HUULCs (85 percent availability rate) as illustrated in Table 4.2. For distributing the network the relative percentages are multiplied with the amount of HUULCS used in the network.

Table 4.5.: Relative size.

Region	Relative size	Generation (# HUULCs)
United Arab Emirates	14.16%	39
Yangtze River Delta	45.49%	127
Western Europe	30.35%	85
South East USA	9.79%	27
<b>Total</b>	<b>100 %</b>	<b>278</b>

These numbers are used for the production of each region. They have to be scaled for the attraction because production and attraction have to be the same. This process is iterated until production and attraction of every region are the same. Due to this the relative percentages are not the same anymore. At the moment 278 HUULCS enter fleet, the production and attraction of each region will be so large that the 278 HUULCs even can get one percent market share. So that the relative number are a bit out of proportion is insignificant.

In Figure 4.8 the simplified network is shown for the HUULC when the maximum amount of HUULCs are operable. As you can see the production and attraction is the same for every region. This is calculated in amount of HUULCs but for containers this is almost the same since the minimum amount of containers carried by a HUULC is 97. At the end Novosibirsk and Anchorage do not really serve as a hub anymore but more as refuelling place since the distances are to large to do it directly.

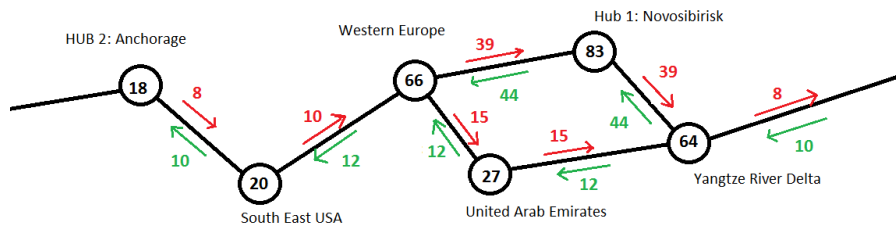


Figure 4.8.: Assigned network. The amount of flights shown here is per 19 hours.

The next step was calculating the amount of hours the HUULC is flying or the amount of hours the HUULC is loading and unloading on an airport. The HUULC needs four hours on an airport for refuelling and six hours on an airport for loading and unloading, this can be done parallel. The results are given in Figure 4.9.

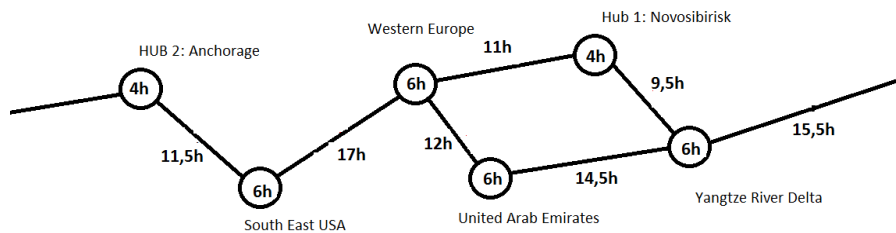


Figure 4.9.: Estimated time.

The final step was calculating the places needed in every airport for the HUULCs. A safety margin of 20 percent is assumed. The final result is shown in Figure 4.10. To do this, the flight hours are used. The average flight time is thirteen hours so if you multiply the amount of HUULCs that enter an airport with the relative time on an airport, the maximum amount of HUULCs at one place can be calculated. Chapter 8 gives a further analysis of the airports.

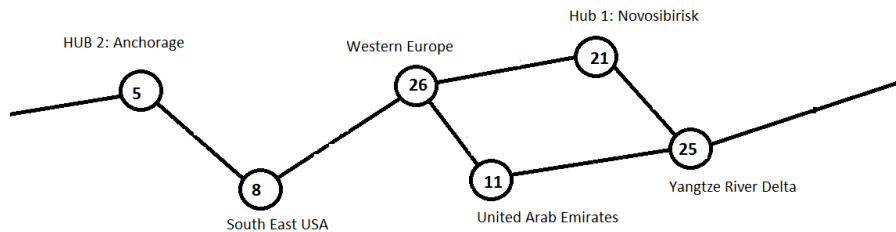


Figure 4.10.: Capacity required on every airport.

## 4.7. Conclusion and recommendations

Before making the network itself, ports were chosen in the regions of the Yangtze River Delta, Western Europe, South-East USA and the United Arab Emirates. These ports cover 33% of the worlds transport of containerised goods. To select the proper airports, the concept of Hub-and-Spoke vs. Point-to-Point and the runway type was investigated. It was decided that a combination of both Hub-and-Spoke and Point-to-Point will be used. Two hubs have been chosen to lower the travel distances and to gain the advantage of logistics: one in Novosibirsk and the other in Anchorage. The network of the HUULC will get between 1 and 1.5 percent market share of the containerised transport in the world. To get this target 325 HUULCs are needed.

Assigning the network was a hard job since the team did not know a lot about transport modelling. Research has been done but still there was not enough knowledge to use an appropriate model. Eventually the network is distributed using trial and error. A recommendation would be to use a mathematical model for distributing the flow. Another recommendation is that the team used average hours to calculate the amount of spots on the airports. This gives a sufficient idea but since some flights take 9.5 hours and some 17, the parking capacity is not that accurate. That is why a safety margin of 20 percent is assumed.

It would be interesting to look into other regions, for example South-America and Africa for an expansion of the network.

## 5. Cost budget

Cost budget and final price (i.e. freight rate in this project) are two parameters which heavily influence each other. For example, the cost budget may be set a priori and the cost modelling will be built forward based on this figure, to ultimately determine a final price. Alternatively, a final price may be set from the beginning, from which one may work backwards to determine the allowable maximum budget as to achieve the set price. The cost budget for the entire HUULC program is determined in the current chapter, whereas actual cost estimations and calculations will be made in Chapter 10.

One of the key requirements of this project is to achieve a maximum freight rate of 250% that of maritime transport. Hence, the second method of the two aforementioned will be used to determine the budget, since the price is its driving parameter. The budget will be determined as shown in Figure 5.1, where the right-most step is the key requirement of freight rate (in red), the left-most steps are the estimated budgets resulting from this process (in orange) and the blue diamond represents the profit margin of Team HUULC (manufacturer and operator of the HUULC). The six steps of Figure 5.1 are detailed in Sections 5.1 to 5.5 below, in which “aircraft purchase price” is defined as the R&D and production cost combined. Because Team HUULC is both the manufacturer and operator of the HUULC, the aircraft will not actually be purchased by any external party. The current terminology however has been chosen because it gives a clear indication of the different components of the total program cost.

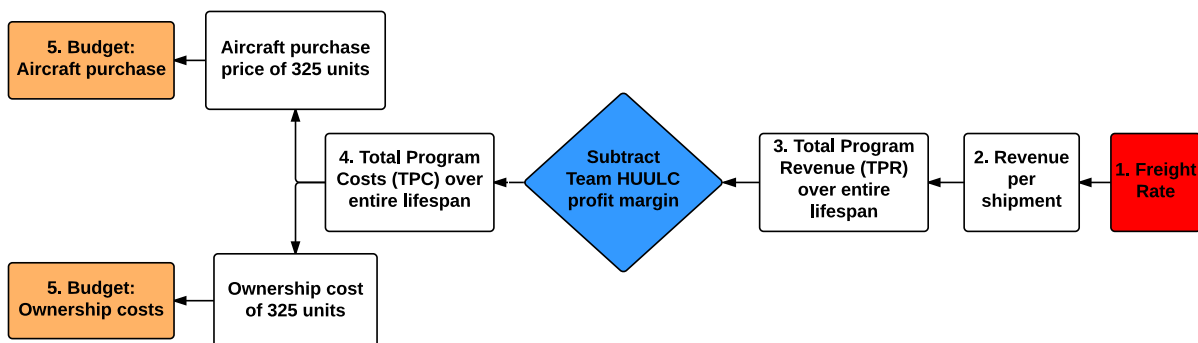


Figure 5.1.: The six steps of the backward cost budget process for the HUULC.

### 5.1. Freight rate

The cost of one TEU container shipped by maritime transport from the far-east to Northern Europe equals \$1,150 [10]. A key requirement is that cargo transport with the HUULC does not exceed 2.5 times the price of a container shipped by maritime transport, hence \$2,875 of freight rate. For a more specific price definition, one needs to look at the price per *tonne – km*. *Tonne – km* is a unit of freight carriage equal to the transportation of one metric *ton* over one *kilometer*, and is calculated by multiplying the amount of metric *tonnes* carried times the moved distance [22][23]. For the distance from the far-east to Northern Europe, the shortest distance between HUULC airports Shanghai and Terneuzen is taken as reference for comparison between maritime and HUULC freight rates. This has been done because in the end, the customer pays for his product to be transported from A to B and is less interested in the particular route taken.

In order to determine the maximum price per tonne-km for the HUULC program, first the price per *tonne – km* for maritime transport is computed. The shortest distance from Shanghai to Terneuzen is 8,812 *km*, and the maximum payload of one container is 12*ton*. Multiplying these gives a value of 105,744*tonne – km*. Dividing the cost of one TEU container shipped by maritime transport from Shanghai to Terneuzen of \$1,150 by 105,744*tonne – km* results in a price per tonne-km of \$0.010875. The price of HUULC transport is allowed to be 2.5 times the price of maritime transport, hence a maximum price per tonne-km of \$0.027188 is set. A specific freight rate for every HUULC shipment has been calculated using the maximum price per *tonne – km* and amount of *tonne – km* for every shipment, as shown in Table 5.1. Please note that the freight rate is defined as the price that the shipper pays to Team HUULC to ship the contents of one TEU of at most 12 *ton* from point A to point B.

Table 5.1.: Shipment-specific freight rates. One TEU weighs 12 ton, one tonne – km costs \$0.027188.

HUULC Shipment	Distance [km]	Avg. TEU	Tonne-km	Freight rate [\$]
Shanghai - Terneuzen	8,812	100	105,744	2,875
Shanghai - Dubai	6,460	97	77,520	2,108
Shanghai - Memphis	11,962	97	143,544	3,903
Terneuzen - Memphis	7,666	97	91,992	2,501
Terneuzen - Dubai	4,850	100	58,200	1,582
Memphis - Dubai	12,403	98.5	148,836	4,047
<b>Average</b>	<b>8,692</b>	<b>98.25</b>	<b>104,306</b>	<b>2,836</b>

## 5.2. Revenue per shipment

Every time a HUULC shipment is completed, revenue for the program is generated. How much revenue one shipment will generate is a function of amount of cargo on board and freight rate for that specific shipment. Table 5.2 presents the revenue for all shipments.

Table 5.2.: Revenue per shipment.

HUULC Shipment	Avg. TEU	Freight rate [\$]	Revenue per shipment [\$]
Shanghai - Terneuzen	100	2,875	287,500
Shanghai - Dubai	97	2,108	204,441
Shanghai - Memphis	97	3,903	378,564
Terneuzen - Memphis	97	2,501	242,607
Terneuzen - Dubai	100	1,582	158,236
Memphis - Dubai	98.5	4,047	398,590
<b>Average</b>	<b>98.25</b>	<b>2,836</b>	<b>278,323</b>

## 5.3. Total Program Revenue (TPR) over entire lifespan

In order to obtain the Total Program Revenue (TPR), which is defined as the total revenue all HUULC shipments combined in history will ever earn, the total amount of shipments needs to be known. The calculation of this number starts with taking the amount of flights between every HUULC airport per 19 hours when the fleet size is largest, see Figure 4.8 from Section 4.6. These numbers are then converted to amount of flights per day, after which they are multiplied by 365 to convert them to flights per year. Now these numbers are scaled up to the lifetime of the HUULC program, which the period in time from the moment that the first HUULC will enter into service until the moment that the last HUULC will retire. Hence the lifetime of the HUULC program is  $2095 - 2030 = 65$  years. The values obtained now, however, are assuming that all 325 HUULCs are operative in every year of the lifetime, which is not the case. As explained in Section 4.2, the amount of HUULCs per year differs. The average of this is taken, and is found to be  $221.59$  HUULCs/year. The last step that needs to be taken is to multiply the total flights over the entire lifespan by the average number of HUULCs per year. The procedure mentioned above is performed for every HUULC shipment route, for both initial and return flights. To finally find the generated TPR, these number of shipments are multiplied by the revenue per single shipment and are cumulated. The results of this process are presented in Table 5.3. The bottom-right value in the table is the generated TPR of \$923.89 billion.

## 5.4. Total Program Costs (TPC) over entire lifespan

Subtracting Team HUULC's net profit margin (assumed to be at 2%, based on commercial airlines [24]) from the TPR, the Total Program Costs (TPC) can be determined, where the TPC refers to the cumulative costs Team HUULC will incur as a result of the HUULC program. With the aforementioned TPR and profit margin, a TPC of \$905.41 billion can be incurred.

## 5.5. Budget

The TPC is divided into two main costs: a) Aircraft purchase price summed over 325 units and b) Ownership cost for 325 units. Aircraft purchase price is subdivided into two categories: i) Research and development costs

Table 5.3.: Overview of the process to obtain the TPR. The initial and return flights per 24h are summed. Some values have been left out because they do not add value.

<b>HUULC Shipment</b>	<b>Flights per 24h (summed)</b>	<b>Total flights ever</b>	<b>Revenue per shipment [\$]</b>	<b>Total route revenue [\$bn]</b>
Shanghai - Terneuzen	102.32	1,655,074	287,500	475.85
Shanghai - Dubai	34.11	551,691	204,441	112.79
Shanghai - Memphis	22.74	367,794	378,564	139.23
Terneuzen - Memphis	18.95	306,495	242,607	74.36
Terneuzen - Dubai	25.26	408,660	158,236	64.66
Memphis - Dubai	8.84	143,031	398,590	57.01
<b>Average</b>	-	-	278,323	153.98
<b>Total</b>	212.21	3,432,746	-	923.89

and ii) Production costs. Ownership costs are subdivided into three categories: i) Ground support equipment, initial spare parts & purchase additions costs, ii) Operations & Maintenance costs and iii) System phase-out & disposal costs, as seen from reference [25]. Because Team HUULC is the one big company that covers all aspects of HUULC program (meaning it both is the aircraft manufacturer and the operator), the entire TPC can be used to provide for all elements in the program.

From the \$905.41 billion that will ever be generated by the HUULC program, two main expenses have to be paid: the aircraft purchase price costs and ownership costs. It must hence be determined what percentage of this \$905.41 billion figure will be spent on manufacturing the 325 aircraft and on operating them. Table 5.4 provides all subcategories of the TPC and their respective estimated percentages. These figures are taken from reference [25], which shows the cost breakdown for a conventional aircraft program.

However, the HUULC differs from a conventional aircraft in many aspects. Therefore the conventional percentages from reference [25] have been adjusted to HUULC-specific percentages, the former and latter shown in the second and third column, respectively. The first important difference with conventional aircraft is that the HUULC is unmanned. This means less staff is needed for operating the aircraft, hence lower operational costs. For this reason, 2% has been removed from the percentage for conventional operational costs in Table 5.4, the reduction being a rough estimate.

The second important difference is the use of hydrogen, instead of kerosene as fuel. Since the production of hydrogen is part of this project and the use of energy is renewable, it is expected that the cost of operating with hydrogen nowadays will be higher than operating with kerosene as a result of the expected high costs of renewable energy generation. On the other side, the team expects government subsidies because of the sustainability of the HUULC. However, no or limited subsidies are assumed as a worst case scenario in this feasibility study. To surely have a sufficient budget available for hydrogen production, the HUULC operations & maintenance budget has been increased with 13%. To accommodate the operations budget with this net increase of 11% (-2 + 13 = 11), budget is taken away from the R&D, production and ground support budgets. The rationale behind this is HUULC's relatively long lifetime. HUULC aircraft have a lifetime of 45 years, which is significantly longer (+10 years) than the average lifetime of freighter airplanes. The average age of freighter airplanes at leaving service is approximately 35 years between 2003 and 2013 [26]. Therefore a relatively larger percentage of the budget can be reserved for recurring costs, which mainly are the operations and maintenance cost. It is expected that a percentage of the total operations and maintenance budget of 81% is required for producing hydrogen, as will be further explained in Section 9.5.3. As can be evaluated from Table 5.4, this implies a budget for hydrogen production of \$491.37 billion.

Another important difference is that Team HUULC does everything itself. In reference [25], a portion of the R&D and production costs is set aside as profit for the manufacturer. However, since Team HUULC is the company that undertakes all program elements, only one general profit margin is taken into account. This is the profit margin mentioned in Section 5.4.

From Table 5.4 it becomes clear that the estimated aircraft purchase price (R&D plus production costs) for one HUULC aircraft equals \$668.61 million. This crude, first estimate cost budgeting has thus predicted an aircraft purchase price of \$668.61 million, when the profit margin already is subtracted from the revenues. These figures seem to be within the order of magnitude of the current commercial aircraft market. According to Boeing, a 747 Freighter has a purchasing price of \$368.4 million per unit [27]. With the HUULC being a new aircraft, multiple times larger than the 747 and with new technologies, a price of almost double that of the 747 Freighter is arguably acceptable.

It must be noted that this estimate lacks many important parameters and inclusions, which should be taken

Table 5.4.: Estimated resource allocation. Research & Development and Production together are defined as the “Aircraft purchase price”. Ground support, initial spares & purchase additions, Operations & maintenance and system phase-out & disposal are defined as the “Ownership cost”.

<b>HUULC Program element</b>	<b>Percentage conventional [%]</b>	<b>Percentage HUULC [%]</b>	<b>Budget [\$bn]</b>
Research & Development <i>-Program management</i> <i>-Advanced R &amp; D</i> <i>-Engineering design</i> <i>-Equipment development &amp; test</i>	6	3	27.16
Production <i>-Manufacturing</i> <i>-Initial logistic support</i>	24	21	190.14
Ground support, initial spares & purchase additions <i>-Manufacturing</i> <i>-Construction</i> <i>-Initial logistic support</i>	12	7	63.38
Operations & maintenance <i>-Operations</i> <i>-Maintenance</i> <i>-System/equipment modification</i>	56	67	606.63
System phase-out & disposal	2	2	18.11
<b>Total</b>	<b>100</b>	<b>100</b>	<b>905.41</b>

into account when a more detailed design has been established. For example, no interest rate has been assumed, in the case economic means have to be lent from financial investors. Secondly, the price of each HUULC has been assumed to be constant, however one could expect that the price will fall over time, with later orders of the HUULC having lower prices than initial orders. Thirdly, with a first delivery 15 years from now, inflation must also be taken into account.

# 6. The design of the HUULC

Before the actual design of the HUULC can start, a configuration has to be chosen. The configuration trade-off is discussed in Section 6.1. After this trade-off, the preliminary sizing can start. This is also discussed in Section 6.1 which consists of the preliminary weight estimation and performance constraint analysis. From the preliminary sizing several parameters are needed to continue the design process. With these parameters, the aerodynamic analysis can start as well as the propulsion system design. These are discussed in Section 6.2 and Section 6.3, respectively.

When the engine placement and the aerodynamic characteristics are known, the structural sizing of the wing and fuselage is done in Section 6.4. When all major components are sized, the weight and balance estimation can be done, which is discussed in Section 6.5. It should be noted that the weight and balance calculations depend on the empennage and the landing gear sizing and position while the sizing of these components also depends on the weight and balance calculations. Sizing of the empennage, the landing gear and the weight and balance calculations therefore have a close relation and are constantly updated relative to one another. The stability and control characteristics of the HUULC are discussed in Section 6.6. Furthermore, the empennage and landing gear sizing are, together with the control surface design, discussed in Section 6.7. The assembly of all components is discussed and shown in Section 6.8.

Once the preliminary design of the HUULC is finished, a risk map is created to analyse the risks of this design, which can be found in Section 6.9. Finally all important design parameters are stated again in the conclusion in Section 6.10. It should also be noted that the RAMS (Reliability, Availability, Maintainability and Safety) are integrated in each section and discussed when applicable.

## 6.1. Preliminary configuration design

The configuration design starts with the configuration trade-off in Section 6.1.1. Once the configuration is known, a preliminary weight estimation is done in Section 6.1.2. When the fuel weight is known, the payload range diagram is constructed. This diagram is shown and discussed in Section 6.1.3. Section 6.1.4 elaborates on the preliminary constraint analysis. From this analysis, the preliminary aircraft design parameters. Finally the payload bay, which houses the containers and hydrogen tanks, is discussed in Section 6.1.6. The sizing of the containers and the hydrogen tanks is discussed in Section 6.1.5 and 6.1.7 respectively. Finally the conclusions and recommendations are stated in Section 6.1.8.

### 6.1.1. Configuration trade-off

After the mission analysis was described in Chapter 3, several designs were produced. This section gives an elaboration upon these designs and the trade-offs that were performed. A more elaborate description can be found in Team HUULC's midterm report [4]. The team obtained the following design configurations: conventional design, blended wing body, joined wing design, and twin-fuselage design. Each of these configurations is shortly described below.

- **Conventional design:** This design was favoured because of its reliable characteristics and the improvements that have been made over its existence. It can be seen in Figure 6.1a. The development costs of this aircraft are therefore lower than newer concepts and there is an abundance on available aircraft for initial design sizing and cost estimations leading to lower design risks. The conventional design also has a variant in which struts and external tanks are added to the wing to decrease the wing loading and increase the rigidity of the wings. Some of the consequences of this variant when compared to a conventional configuration are decreased aerodynamic efficiency and increased safety risks.
- **Blended wing body:** The blended wing body is chosen as a design option because of the size of the HUULC and can be seen in Figure 6.2a. It has a great advantage regarding the aerodynamic efficiency, since the entire body of the aircraft can be used to generate lift and is thus less influenced by the square-cube-law. This high aerodynamic efficiency leads to a reduction in fuel required for a given range and thus a more sustainable configuration. Since there are not many existing blended wing bodies, the concept has not been proven yet and thus design risks are present.  
A variant of the original blended wing body design is the flat nose configuration (inspired from Burnelli's designs) which is shown in Figure 6.2b. When compared to the original blended wing body configuration, this design presents new advantages, such as a higher structural and operational efficiency.
- **Joined wing configuration:** This configuration can be seen in Figure 6.1b. The main advantages of this configuration are the larger lift generating areas (two similarly sized lifting wings) when compared

to a conventional configuration. Some advantages that follow from this design are a decreased wing span (dimensional advantage) and an increased aerodynamic efficiency due to tip vortex reduction. On the other hand, this configuration has never been proven in real flight which induces some big risks and disadvantages such as bad manufacturability.

A variant of this design is the application of external tanks. These tanks can be fixed or attachable. The main advantage of this variant configuration is the use of the external tanks as stress relievers for the closed wing structure as well as a mean of connecting the two wings which would replace other joining methods.

- **Twin fuselage configuration:** This configuration is shown in Figure 6.1c. It proposes a higher operational efficiency. When the payload is loaded/unloaded, separate groups can work in parallel in order to maximise efficiency and minimise loading/unloading times. By dividing the fuselage in two, the payload weight gets distributed over the span of the aircraft and the lift generation over three wings. This decreases the loads that are exerted at the roots of the wings, allowing to increase the wing span with the same wing area (larger aspect ratio).

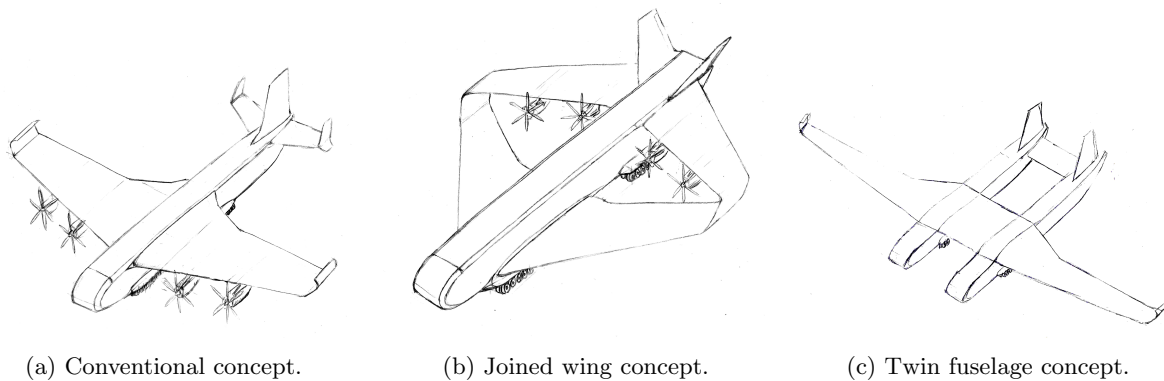


Figure 6.1.: Design concepts for the HUULC.

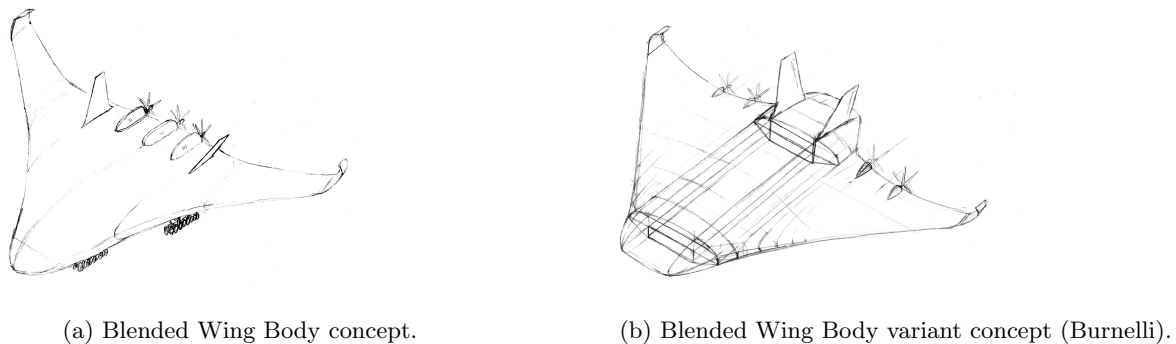


Figure 6.2.: Blended wing body design concepts for the HUULC.

After the design configurations were obtained, a trade-off had to be performed between them. Several existing trade methods were considered for the trade-off, such as the traditional method, the AHP (Analytical Hierarchy Process) and a graphical comparison method [28]. The traditional trade method is chosen because of its reliability and the knowledge the group has on this method.

The criteria were chosen in such a way that the different configurations would score differently. Having criteria for which most designs score the same is not useful since it does not help in choosing the most appropriate configuration. The criteria are evaluated with percentages obtained by reference aircraft, by using conducted research or by performing rough calculations. The criteria are listed below.

- **Safety:** Safety is defined as the ability of the HUULC to be protected from external and internal risks. It is an important criteria for aircraft design consideration and especially for the HUULC due to the size of the aircraft and the value and quantity of goods transported.
- **Payload handling:** Payload handling is one of the most important criteria defined by the team. Since the HUULC will handle large amounts of payload, doing this as efficiently as possible is of major importance.
- **Reliability:** This criteria is majorly influenced by the design maturity of the concept. Reliable concepts are (in general) the ones that are studied and applied most in aviation. Since one of the objectives is to gain 6-8% of the market share of containerised cargo, having a reliable HUULC is an important criteria.

- **Maintenance:** The hub-and-spoke system described in the previous chapter provides a network over the entire globe. Inspection and maintenance has to be performed at various airports. Designing the HUULC in such a way that maintenance is not too complex nor complicated is therefore important.
- **Sustainability:** The propulsion system will be using hydrogen as fuel. One of the objectives of the HUULC is to provide fast and environmental-friendly long-range transportation of goods. Sustainability is therefore of major importance.
- **Design risk:** Design risk is defined as the probability of the occurrence of undesired events during the design phase of the HUULC. Certain concepts have a higher design risk than others. Since 325 units are expected to be in operation by 2050, minimising the probability of the occurrence of undesired events is important.
- **Development cost:** A certain budget was allocated in the baseline report. This budget may not be exceeded. The development costs of the HUULC should therefore be minimised and monitored carefully. Since competitiveness is of major importance, minimising the development costs is of the greatest importance for the HUULC and is therefore the most important design criterion.
- **Noise:** Aircraft regulations have grown stricter over time and noise is a phenomenon that must be reduced as much as possible. Since the aim of the HUULC is to be environmental-friendly, noise reduction is a criteria that the different design options have been judged upon.
- **Aerodynamic efficiency:** The design options that are described above all have different characteristics regarding the aerodynamic efficiency. When looking at the characteristics of each configuration, the lift to drag ratio and wing span were considered as well as the aspect ratios.
- **Structural efficiency:** Structural efficiency is also a criteria on which the designs score differently. Having a high structural efficiency is beneficial for reducing the HUULC's empty weight and is judged as important as the aerodynamic efficiency.
- **C.g. range:** For all configurations an acceptable centre of gravity range for stability and controlability is required. However a larger centre of gravity range allows for greater flexibility in the allowable payload distribution inside the HUULC.
- **Manufacturability:** Some designs include shapes that are difficult to manufacture. When regarding concepts which involve a lot of curvature such as the blended wing body configuration or other consideration such as the difficult joining method for the joined wing configuration, difficult manufacturing processes can be expected.
- **Dimensions:** Allowing payload with a volume equal to 100 TEU containers requires dimensions that are not seen before in aviation. The different design concepts have certain advantages and disadvantages with respect to payload handling, but also require different dimensions. The span wise dimensions of the aircraft are regarded as one of the most important aspects.
- **Take-off/Landing performance:** Take-off and landing performance is defined as a criteria since the concepts have different characteristics. During the evaluation of this criteria for the different concepts, the stall speed was used as an indicator for the take-off performance.
- **Aesthetics:** Being defined as least important, this criteria is majorly based on personal opinion. The team does not want to end up with an aesthetically bad design and thinks that such a design would decrease the interest of the customer, therefore an election was held between the different designs.

Table 6.1 shows the trade-off criteria and weights for the configuration of the HUULC. It became clear that the Burnelli blended wing body won the trade-off. The aerodynamic advantages, payload handling capabilities and small dimensions resulted in the highest score in the trade-off. This configuration will therefore be used as the baseline configuration for the HUULC.

### 6.1.2. Preliminary weight estimation

Before starting the weight estimation, the mission needs to be analysed. With the requirements in mind, a mission profile was constructed. This mission profile can be seen in Figure 6.3. The main phase of the mission is phase five, which is the cruise over a range of 6000 *km*. To comply with the legal regulations of CS25, a loiter phase of 30 minutes and a second cruise phase of 600 *km* are added. This second cruise phase needs to be taken into account in case the aircraft is not allowed to land and has to divert to another airport. The value of 600 *km* is determined during the analysis of emergency procedures in Section 8.6.

After constructing the mission profile, the mission weights of the aircraft could be determined. These have first been determined for an aircraft that uses kerosene as fuel and have then been converted for an aircraft that uses hydrogen as fuel which is one of the driving requirements. The weight estimation process can be seen in Figure 6.4.

The take-off weight is first broken down in different elements such as the empty weight, fuel weight and payload weight. Each of these elements was rewritten in terms of the maximum take-off weight except for the payload weight. This can be seen in Equation 6.1.

Table 6.1.: Trade-off table for the configuration of the HUULC.

Criteria	Weight	Concept 1 Conventional configuration	Concept 2 Conventional variant (tanks)	Concept 3 Blended wing body	Concept 4 BWB variant (Burnelli)	Concept 5 Joined wing	Concept 6 JW variant (ext. tanks)	Concept 7 Twin boom
Aerodynamic efficiency	7	5	5	10	10	7.1	7.1	6
Structural efficiency	7	5	6	9	10	7	8	6
High stability	3	9	10	2	3	9	7	9
Safety	8	5	2	5	5	5	2	5
Payload handling	8	5	5	2.1	10	5	5	9.7
Aesthetics	3	7	6	9	9	9	5	6
Reliability	9	8	7	6	6	6	5	6
Noise	7	5	5	10	10	6	6	5
Manufacturability	6	10	9	5	6	8	7	8
Dimensions	5	5	5	8.7	8.7	10	10	2
Maintenance	8	9	10	6	7	6	6	8
Sustainability	9	5	5	10	10	7.5	7.5	5
Take-off / Landing	5	5	5	10	10	7.4	7.4	5
Design risk	9	10	8.75	10	10	10	8.75	5
Development cost	10	10	9	6	7	6	5	8
Operational cost	10	5	5	5	5	5	5	5
Overall grade	N/A	772	726.75	808.3	905.5	779.2	707.95	702.6

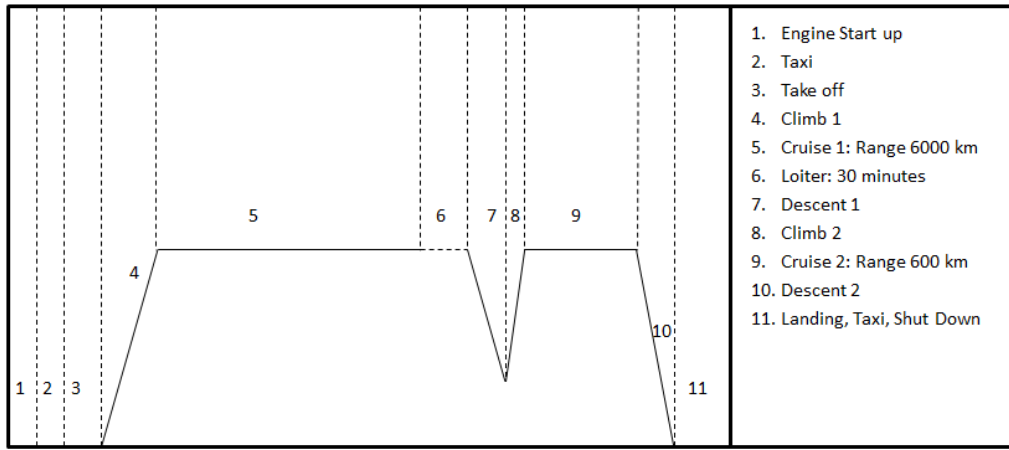


Figure 6.3.: Mission profile of the HUULC aircraft.

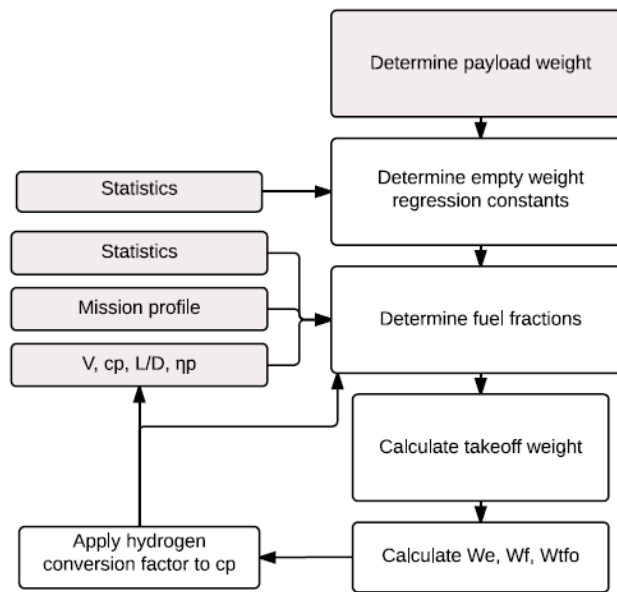


Figure 6.4.: Flowchart of the weight estimation.

$$W_{to} = aW_{to} + b + (1 - M_{ff})W_{to} + W_{pay} + M_{tfo}W_{to} \quad (6.1)$$

The parameters such as the fuel fractions and the empty weight regression constants in Equation 6.1 can be found using statistics [29]. For the empty weight, aircraft that fit the categories 'large civil cargo aircraft' and 'large military transporters' have been chosen as references because of the large payload requirement. The fuel fractions corresponding to the non-fuel-intensive mission phases of the mission profile were chosen from statistics in [29] and were later corrected for the use of hydrogen. The fuel intensive phases were estimated using the Breguet range and endurance equations. These are given in equation 6.2 and 6.3. It can be noted that these equations are the equations for a propeller aircraft. Propellers were chosen over a jet aircraft configuration because jet engines would consume too much fuel. Furthermore jet engines are less efficient because the HUULC flies at a relatively low cruise speed. The HUULC has a cruise speed of 483 km/h. Using propellers would therefore be more efficient for this cruise speed. Minimising the fuel is one of the driving requirements and therefore it was decided to use propellers.

$$R = \left( \frac{\eta_p}{g c_p} \right)_{cruise} \left( \frac{L}{D} \right)_{cruise} \ln \left( \frac{W_4}{W_5} \right) \quad (6.2)$$

$$E = \left( \frac{\eta_p}{V g c_p} \right)_{loiter} \left( \frac{L}{D} \right)_{loiter} \ln \left( \frac{W_5}{W_6} \right) \quad (6.3)$$

The parameters for this equation are shown in Table 6.2. The value for  $\eta_p$  was chosen from statistics in Roskam [29]. For  $c_p$  it is beneficial to have a value as low as possible. Initially a value of 0.4 lbs/hr/hp was

chosen from statistics [29]. However, later on it was found that for counter rotating propeller engines, this value could go down to  $0.36 \text{ lbs/hr/hp}$  [30]. The speed was chosen in an iterative manner. A starting value of  $500 \text{ km/h}$  was chosen. A higher speed would be less efficient when using propeller engines and require more fuel, however a higher speed would be more beneficial for the operations and time required to get to another airport. Reducing the speed would be more beneficial for the efficiency of the propellers and the required fuel and less for the time to get to another airport. Eventually a value of  $483 \text{ km/h}$  was chosen. Reducing the speed further would not make significant difference in the fuel weight and the speed is still within acceptable limits for reaching the next airport within the required time. Finally, a lift to drag ratio of 26 was chosen. From references it was found that blended wing bodies can have a lift to drag ratio up to 27 [31]. With a lift to drag ratio of 26, the required amount of hydrogen could be reduced to the amount that can be produced within the hydrogen production budget.

Parameter	Value
$\eta_p$ [-]	0.82
$c_p$ [lb/hr/hp]	0.36
$V$ [m/s]	134
$L/D$ [-]	26

Table 6.2.: Parameters of the Breguet equations.

Solving Equation 6.1 for the maximum takeoff weight leads to a value of 2.58 million kg for a kerosene powered aircraft. Hydrogen is 69% more efficient (see Chapter 9 and therefore a factor of 0.31 is applied to the specific fuel consumption. This results in a reduction of the maximum takeoff weight of 20%. The amount of fuel required is reduced by almost 30%. The weight of the HUULC compared to other aircraft can be seen in Figure 6.5. The final mission weights of the aircraft can be seen in Table 6.3. The fuel weight that is mentioned is the fuel required for the range of  $6000 \text{ km}$ .

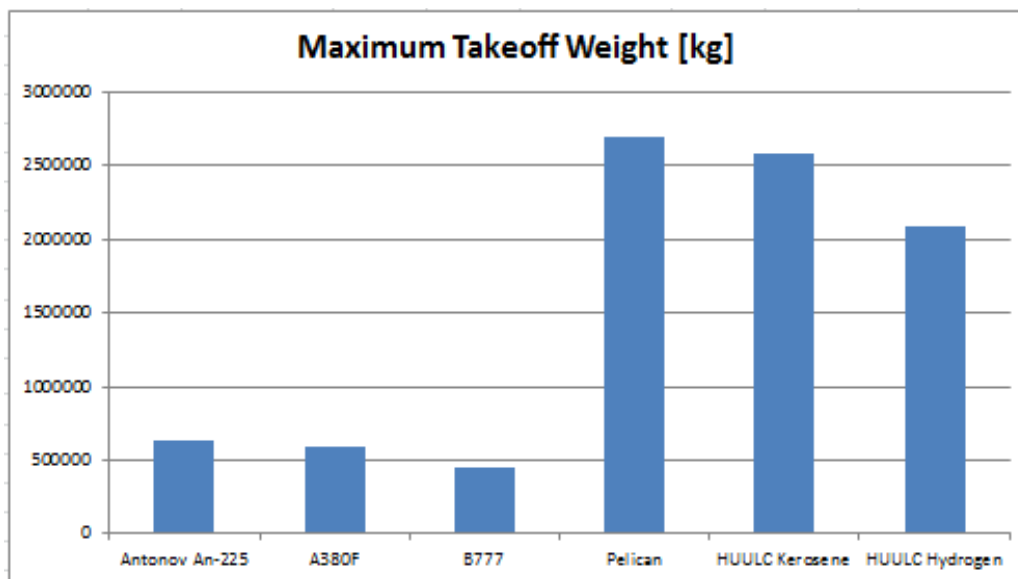


Figure 6.5.: The weight of the HUULC compared to other aircraft.

Weights [kg]	HUULC Kerosene	HUULC Hydrogen
$W_e$	856,000	701,000
$W_f$	477,000	141,000
$W_{tfo}$	2,600	2,100
$W_{pay}$	1,248,000	1,248,000
$W_{to}$	2,584,000	2,092,000

Table 6.3.: Mission weights of the HUULC with kerosene and hydrogen as fuel.

As part of the preliminary sizing of the aircraft, a sensitivity analysis is conducted. This is done in order to provide the designers with a relationship between important design parameters of the aircraft and the performance parameters that influence them. With the HUULC being the largest and heaviest aircraft in history, it must be ensured that the increase in weight throughout the design process is stable and does not increase

uncontrollably. Furthermore, runway pavements act as an upper limit on the maximal take-off and landing weight, to which the aircraft must conform.

The sensitivity of the maximum take-off weight is investigated against two aircraft characteristics, namely payload weight  $W_{pl}$  and empty weight  $W_E$ , and five performance parameters, namely range  $R$ , endurance  $E$ , lift-to-drag ratio  $L/D$ , specific fuel consumption  $c_p$  and propulsive efficiency  $\eta_p$ . These growth factors are shown in Table 6.4.

Table 6.4.: Growth factors of the maximum takeoff weight.

Growth Factor	Value
$\frac{\partial W_{to}}{\partial W_{pl}}$ [-]	1.61
$\frac{\partial W_{TO}}{\partial W_E}$ [-]	3.21
$\frac{\partial W_{TO}}{\partial R}$ [kg/km]	0.02
$\frac{\partial W_{TO}}{\partial E}$ [kg/s]	3.25
$\frac{\partial W_{TO}}{\partial \frac{L}{D}}$ [kg]	$-4.90 \cdot 10^3$
$\frac{\partial W_{TO}}{\partial c_p}$ [kg/kg/J]	$6.95 \cdot 10^{12}$
$\frac{\partial W_{TO}}{\partial \eta_p}$ [kg]	$-1.55 \cdot 10^5$

From this table it becomes clear that three of the performance parameters influence the weight the most. These are the lift to drag ratio, the specific fuel consumption and the propeller efficiency. Increasing the lift to drag ratio or the propeller efficiency and decreasing the specific fuel consumption is most beneficial to reduce the takeoff weight. The other way around, these factors are most dangerous for weight increases. If the specific fuel consumption is increased by a small fraction, the takeoff weight increases by a very large amount. Changes in any of these values should therefore be monitored closely.

### 6.1.3. Payload range diagram of the HUULC

With the estimated mission weights a payload range diagram could be constructed. This diagram is shown in Figure 6.6. When comparing to conventional payload range diagrams, this diagram looks very different. This is due to the extra multiplication factor to account for the use of hydrogen.

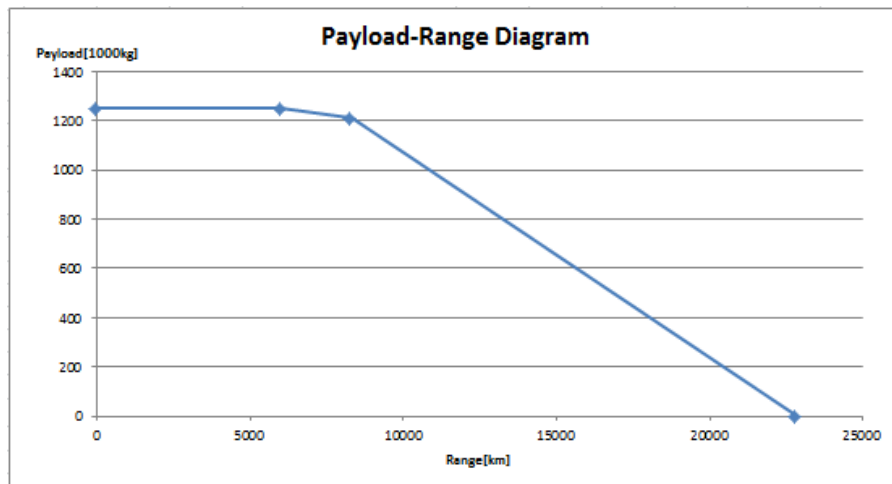


Figure 6.6.: Payload range diagram of the HUULC.

The diagram was constructed in a similar manner as for conventional aircraft using kerosene. One difference is that the second kink point in the diagram was chosen because of the range. To reach some of the airports in the network, an extended range was required. This is explained in Section 4.3. The exchange of payload for fuel was iterated until an extended range to approximately 8000 km was found. This was found by only taking three containers of payload out and replacing the weight of these 3 containers by extra hydrogen. It has to be noted that the hydrogen tanks should be sized for the amount of fuel that is needed to reach the range of approximately 8000 km. This amount is 172,000 kg.

Performing the same weight estimation and constructing the payload range diagram for the same aircraft that uses kerosene instead of hydrogen results in Figure 6.7.

It can be seen that for the same exchange of payload for fuel, only 300 km of extra range is achieved. The difference between the two payload range diagrams is due to the multiplication factor of 0.3 to the specific fuel

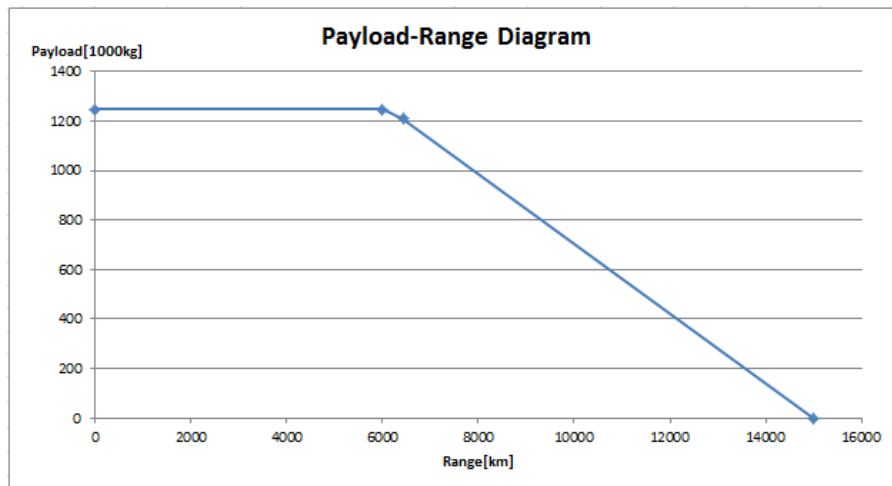


Figure 6.7.: Payload range diagram of the HUULC using kerosine.

consumption. Because of this factor, the aircraft is much more efficient. Only a small amount of extra fuel compared to the takeoff weight is required to reach a significant amount of extra range. Another consequence is that because of this multiplication factor, the total amount of fuel that is required is much smaller compared to an aircraft that uses kerosene. The ratio of fuel weight to takeoff weight is much smaller and the ratio of payload weight to takeoff weight is much larger. Therefore taking out payload results in a significant larger range for a hydrogen powered aircraft than for a kerosene powered aircraft.

#### 6.1.4. Preliminary performance constraint analysis

Another part of preliminary sizing is the determination of the wing loading and weight to power ratio. This is done by analysing the performance requirements. Each of the requirements is briefly explained and finally a diagram is shown in which all constraints are plotted. From this diagram a design point is chosen for the HUULC Aircraft. It should be noted that the weather conditions differ a lot at the airports where the HUULC operates at. Therefore the worst case condition has been taken into account which are the weather conditions at the airport in Dubai.

##### Stall speed constraints

There are no stall speed constraints defined by legal regulations. However, it is beneficial to keep the stall speed as low as possible. The stall speed was initially derived from the runway length but later in the process it was found that the stall speed,  $V_s$ , could be reduced from 71 to 60  $m/s$  because of the increased required wing area which is explained later in this section.

##### Landing distance constraints

As explained in Chapter 8 new airports are designed specifically for the HUULC aircraft. This means that when looking at these airports, the aircraft is not constrained by a landing or takeoff distance. However when the aircraft is not allowed to land on one of these airports for example in case of bad weather, it has to divert to another airport. In this case the aircraft is constrained by the runway length. It has therefore been decided to use a runway length of 3300 meters as a constraint which is a typical value for runways of large airports. It was also the value of the shortest runway of the set of airports that was initially chosen for the network.

##### Take-off distance constraints

For the takeoff segment the same constraints apply as to the landing segment. In this case, the constraint for the takeoff length is also set at 3300  $m$  in case the aircraft has to divert to another airport.

##### Climb constraints

The climb requirements that the aircraft has to comply with are the climb gradient requirements from the FAR25 regulations for an aircraft with four engines [29]. These are:

- FAR 25.111 (OEI) The climb gradient must be larger than 0.017 with take-off flaps and landing gear retracted.
- FAR 25.121 (OEI) The climb gradient must be larger than 0.005 with take-off flaps and landing gear down.
- FAR 25.121 (OEI) The climb gradient must be larger than 0.030 with take-off flaps.
- FAR 25.121 (OEI) The climb gradient must be larger than 0.017 in clean configuration.

- FAR 25.119 (AEO) The climb gradient must be larger than 0.032 with landing flaps and landing gear down.
- FAR 25.121 (OEI) The climb gradient must be larger than 0.027 with landing flaps and landing gear down.

Another requirement for the climb constraints is the rate of climb. This is set at 5  $m/s$ . This means that the aircraft should be at the cruise altitude of 8000  $m$  within 25 minutes.

### Manoeuvring constraints

There is one constraint set for the aircraft when it comes to manoeuvring. The aircraft has to be able to withstand a load factor of 3 [29].

### Determination of wing loading and weight-to-power ratio

After analysing all performance constraints, a  $W/S$  -  $W/P$  diagram can be constructed. This is shown in Figure 6.8. Each of the constraints is plotted in the diagram. Once this is done, a design point was chosen in an iterative manner. The constraints were initially plotted for large  $C_L$  differences and a very low aspect ratio. The first design point that was chosen can be seen at the right in the diagram. This value could be reached for relatively large  $C_{L_{max}}$  values. Using this design point for further calculations led to aerodynamic requirements that could only be reached at extreme angles of attack. Therefore it was decided to reduce the required  $C_{L_{max}}$  values and thus the wing loading could be reduced significantly. This led to a wing area large enough to deliver the reduced  $C_{L_{max}}$  values. The final parameters that were derived from this diagram can be seen in Table 6.5. In the end the  $W/S$  value of the design point was not so much constraint by the stall speed or the landing distance as it was by the aerodynamic requirements that followed from the chosen design point. The wing loading had to be decreased to obtain a wing surface area and a wing span that would be large enough to deliver the requirement amount of lift and the high lift to drag ratio. The  $W/P$  value however was constraint by the climb gradient requirements as can be seen in Figure 6.8.

Parameter	Value
$W/S$ [ $N/m^2$ ]	2867
$W/P$ [ $N/W$ ]	0.065
$S$ [ $m^2$ ]	7175
$P$ [ $MW$ ]	316
$b$ [ $m$ ]	200.1
$MAC$ [ $m$ ]	35.1
$C_{L_{max}}$ clean [-]	1.6
$C_{L_{max}}$ takeoff [-]	1.7
$C_{L_{max}}$ landing [-]	1.75
$A$ [-]	5.59
$e$ [-]	0.77

Table 6.5.: Parameters corresponding to the chosen design point of the HUULC aircraft.

### 6.1.5. Containers design

The HUULC is designed with the objective of being able to transport standardised container-like cargo. However, air freight is much more sensitive to container tare than maritime shipping. In order to improve efficiency and fuel consumption, several decisions are taken concerning the containers used and the operations related to them.

“Classic” containers are heavy. Their corrugated steel structure is designed to bear the loads of several other containers on top but is highly inefficient when it comes to air cargo. ULD’s on the other side are more lightweight but present lower structural properties. Table 6.6 shows some basic characteristics of several containers. As it can be seen, composite ULD’s present a specific weight reduction of 78% when compared to standard inter-modal containers.

The HUULC container logistics proposal suggest the usage of an alternative packaging solution (i.e. new container), which shall be lightweight and fit inside a TEU container. This decision, although costly in terms of new containers, is essential to achieve the HUULC’s objectives and reduce the operation costs. If standard TEU containers were to be used, the total weight of the empty containers in the aircraft would result in 223 tons, 18.6% of the payload. This is clearly highly inefficient. On the contrary, a new container design with a similar specific mass when compared to LD-6 (new container design tare 481.4 kg) would yield in a total empty containers weight of 48.14 tons, 4% of the payload weight. These new containers are designed as closed structures, in order to allow for air/humidity tightness. However, pallets or open frames with ropes could be used as well, reducing the tare by an even larger percent.

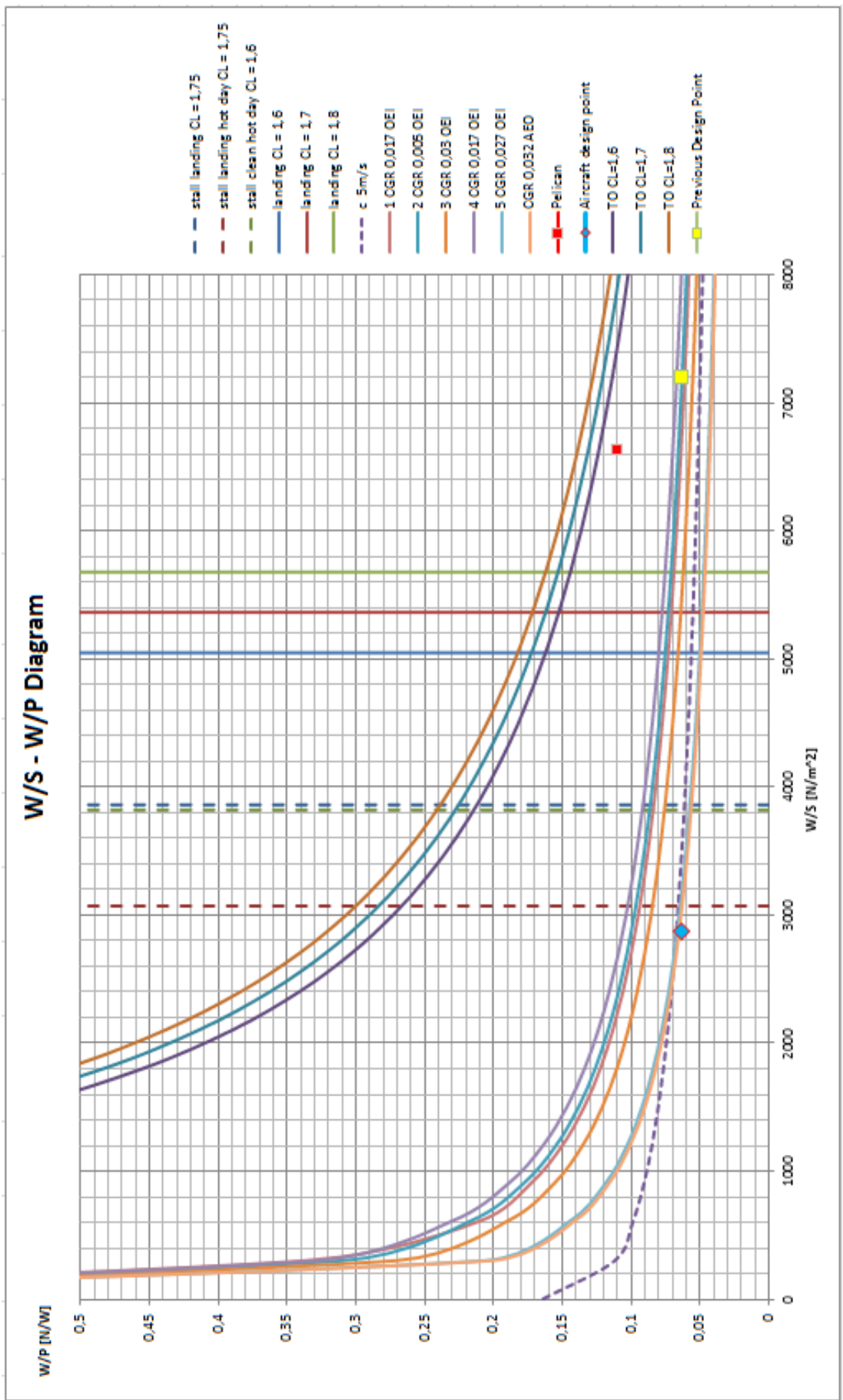


Figure 6.8.: W/S - W/P Diagram for the HUULC aircraft.

Table 6.6.: Containers comparison.

Denomination	Tare [kg]	Volume [m <sup>3</sup> ]	Specific mass [kg/m <sup>3</sup> ]	Reduction [%]
TEU Steel Container	2230	33.2	67.17	Baseline
TEU Composite Container	1784	33.2	53.73	-20
ULD-6 Standard Container	230	9.1	25.27	-62.37
ULD-6 Composite Container	132	9.1	14.51	-78.40

The new containers would be loaded by the customers and then transported to the HUULC's terminals. Due to the lower structural loading characteristics of the new packaging design, in order to allow for inter-modal operations and stacking storage, the new container could be fit inside a standard TEU. In the airport terminals, the steel classic TEUs would be opened, and only the lightweight containers would be transferred to the aircraft.

Finally, 40 ft (two TEUs) lightweight containers would also be supported. The major relevance of this cargo format makes relevant to keep compatibility with it. Therefore, the payload bay and the logistic support activities are also prepared to handle this kind of containers. More information on airport logistics can be found in Chapter 8.

### 6.1.6. Payload bay sizing

The design of the payload bay started with an analysis of blended wing body fuselage length to width ratios. This value is on average 0.30 [32] for these kind of aircraft. Once this ratio is known, it is possible to place the 100 containers in a determined row/column arrangement. The design hence resulted in nine columns and 12 rows of containers. Moreover, as it is further explained in Chapter 6.4, the payload bay has also a structural function. Therefore, structural-reinforcement ribs are present from bottom to top in between each of the columns (see Figure 6.9). Moreover, this requires the tanks to have the same width as the payload containers.

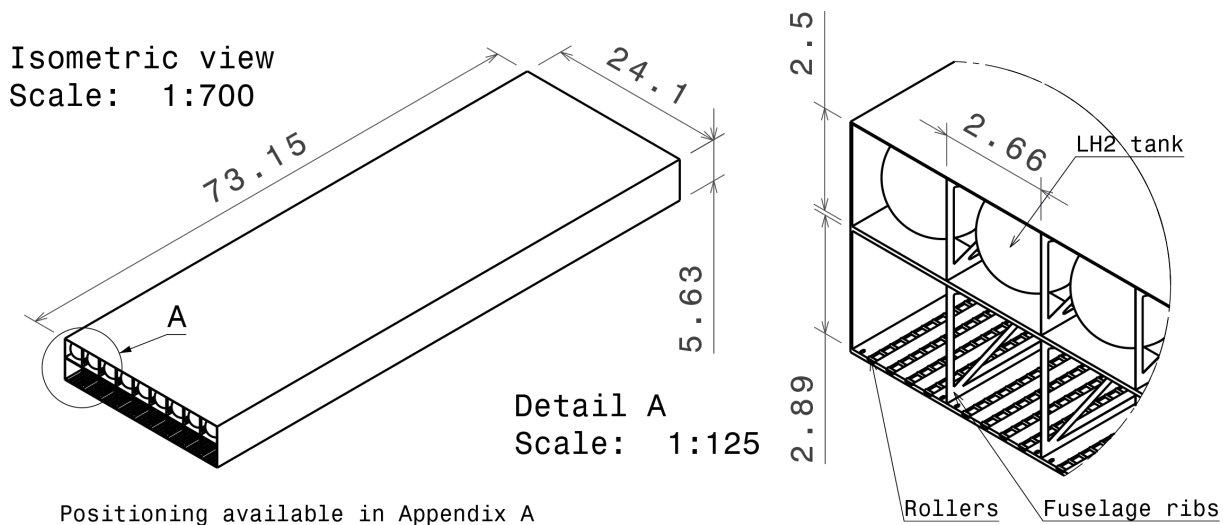


Figure 6.9.: Payload bay design [m].

### 6.1.7. Hydrogen tanks

From the weight estimations, a fuel mass of 172,229 kg was obtained. However, in order to determine the tanks volume the density of the fuel (hydrogen) is required. This property is proportional to the pressure and temperature of storage, which influence the design as well. In order to size the thickness of the tank walls, the longitudinal and hoop stresses of the tank walls are calculated using Equation (6.4). Carbon fiber reinforced polymer (CFRP) is selected due to its much lower weight when compared to metal alloys. CFRP usage in cryogenic tanks is a technology still in development, although already demonstrated [33]. For the preliminary sizing of these tanks, two idealised layers of composite are chosen in order to cope with the longitudinal and hoop stresses respectively. In order to calculate the mass, first the material volume is multiplied with CFRP density, thus the mass is obtained. A correction factor of three is applied for manufacturability.

$$t_{long} = \frac{p \cdot d}{4 \cdot \sigma} \quad t_{hoop} = \frac{p \cdot d}{2 \cdot \sigma} \quad (6.4)$$

Different hydrogen states were assessed for the sizing of the tanks: liquid hydrogen (LH2) and cryo-compressed hydrogen (CcH2). The operating regime of these states can be seen in Figure 6.10. An isolation layer is also included into the design, with a specific mass of  $1.8 \text{ kg/m}^2$  [34]. Moreover, nine tanks are assumed due to the payload bay sizing constraints described in Section 6.1.6, Table 6.7 shows the preliminary design of the tanks for the conventional configuration. The data shown gives the volume and dry mass of each of the nine tanks that would carry the total hydrogen amount for each of the hydrogen states. In this case, the previously calculated value for hydrogen mass is used. Additionally, the total dry mass and volume of the nine tanks is shown in Table 6.8.

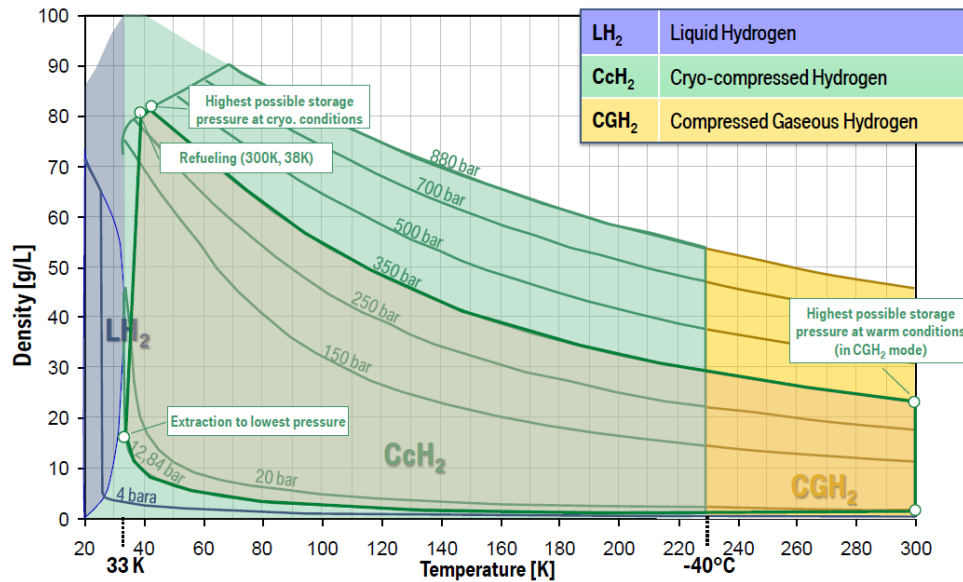


Figure 6.10.: Hydrogen storage [35].

Table 6.7.: Hydrogen storage tank preliminary design parameters (individual).

Abrev.	Denomination	Density [ $\text{kg/m}^3$ ]	Pressure [ $\text{MPa}$ ]	Temperature [ $\text{K}$ ]	Volume [ $\text{m}^3$ ]	Dry mass [ $\text{kg}$ ]
LH2	Liquid Hydrogen	80	0.4	25	239.20	2,756.97
CcH2	Cryo-compressed Hydrogen	80	35	40	239.20	171,189.535
CcH2	Cryo-compressed Hydrogen	50	35	110	382.73	272,798.06

Table 6.8.: Hydrogen storage tank preliminary design parameters (total).

Abrev.	Denomination	Density [ $\text{kg/m}^3$ ]	Pressure [ $\text{MPa}$ ]	Temperature [ $\text{K}$ ]	Volume [ $\text{m}^3$ ]	Dry mass [ $\text{kg}$ ]
LH2	Liquid Hydrogen	80	0.4	25	2,152.86	24,069.91
CcH2	Cryo-compressed Hydrogen	80	35	40	2,152.86	1,547,434.926
CcH2	Cryo-compressed Hydrogen	50	35	110	3,444.58	2,461,400.63

From Table 6.8, it can be seen that LH2 has the best characteristics in terms of weight and tank volume (important parameters for the aerospace industry). Moreover, due to volume and mass constraints of the aircraft, LH2 results to be the only feasible option. CcH2 can only achieve high densities at cryogenic temperatures and high pressures. This high pressures make the tanks much heavier in comparison to LH2. Additionally, in order to illustrate the volume required of hydrogen, we compare it with the container volume. If all the hydrogen could be stored in TEU containers, 56 containers would be necessary to do this. Hence, a volume of 56% the one of the payload is required. If low pressure CcH2 would be chosen, this figure would rise up to 89.45% in volume.

The internal diameter of the tanks is  $2.15 \text{ m}$ . This value was chosen to accommodate for the isolation layers, which drive total diameter up to  $2.44 \text{ meters}$ . This last value is constrained by the payload bay ribs design (see Section 6.1.6). The length of the tanks equals  $64.45 \text{ meters}$ . The tanks are placed in the payload bay, which on itself is  $73 \text{ meters}$  long. This leaves a margin of at least  $8 \text{ meters}$  in the payload bay (without additional fuselage length) for tank subdivision (easier to manufacture) and to install pipe connections and other subsystems.

The tank sections lying parallel to the propulsion system are to be shielded. This is due to safety requirements in case of propeller break-off. This reinforcement would be implemented in the fuselage skin for simplicity and

easiness of maintenance.

Finally, it has to be remarked that the used hydrogen mass is the one of extended range operations. Hence, during regular flights they will not be filled to the top of their capacity. More information on extended range operations can be found in Section 6.1.3.

### 6.1.8. Conclusion and recommendations

After the mission analysis, the team brainstormed about aircraft configurations. A trade off was done and the chosen aircraft configuration was the Burnelli inspired blended wing body. With this concept in mind the weight estimation was started. The analysis of the mission of the HUULC aircraft and its requirements were used as an input for the preliminary weight estimation and the wing loading sizing. This led to the parameters that are stated in Table 6.9. Another part of the preliminary sizing is the payload bay. The payload bay itself was sized as well as the payload containers and the hydrogen tanks that would fit in the payload bay. This resulted in a payload bay of 73 by 22 meters that accommodates containers which are designed especially for the HUULC. These containers are structurally more efficient and much lighter than conventional TEU containers. The hydrogen tanks are designed for an amount of 172,000 kg LH2.

Parameter	Value
$W_e$	701,000
$W_f$	141,000
$W_{tfo}$	2,100
$W_{pay}$	1,248,000
$W_{to}$	2,092,000
$W/S$ [ $N/m^2$ ]	2867
$W/P$ [ $N/W$ ]	0.065
$S$ [ $m^2$ ]	7160
$P$ [ $MW$ ]	316
$b$ [ $m$ ]	200.1
$C_{L_{max}}$ clean [-]	1.6
$C_{L_{max}}$ takeoff [-]	1.7
$C_{L_{max}}$ landing [-]	1.75
$A$ [-]	5.59
$e$ [-]	0.77

Table 6.9.: Preliminary design parameters of the HUULC aircraft.

It is recommended by the team to do more iterations in both the weight estimation process as the wing loading estimation process. A driving requirement is to get the hydrogen weight as low as possible because of the high production costs. This led to design choices that are very optimistic and make some parts of the design phases very difficult further on in the process. An example is the high lift to drag ratio of 26. This value was chosen because at this point the cost of the amount of hydrogen that has to be produced fit the budget. If the budget was not constraining, a less optimistic and more realistic value for the lift to drag ratio could be chosen. This would relax the aerodynamic requirements on the aircraft and make the aerodynamic design less complicated.

Another recommendation is to do more research on how to integrate the effect of using hydrogen on the weight estimation. In this case the specific fuel consumption was multiplied by a factor of 0.3 because hydrogen is 69% more efficient. This leads to quite different weight ratios for hydrogen powered aircraft than for kerosene powered aircraft. This in combination with the very low value for specific fuel consumption leads to a payload range diagram that looks very optimistic when comparing it to a kerosene powered aircraft.

Furthermore there are also recommendations for the wing loading estimation. The method used for this estimation was taken from Reference [29]. This method however is not made for aircraft of the size of the HUULC and on top of that it is developed for aircraft with a conventional configuration. Because of the limited amount of time, it was decided to still use this method but to relax the requirements for the aircraft if the requirements constrained the design freedom too much. To perform a more accurate estimation, different methods should be researched for the performance constraint analysis.

The requirements that constrained the design space significantly were the climb requirements. The climb gradient requirements defined in Reference [29] are only stated for aircraft using up to four engines. The HUULC aircraft will use more than four engines because of the large power requirement. It is therefore recommended to define new requirements for an aircraft that uses more than four engines. The team decided to use the requirements for an aircraft with four engines because the lack of time to perform enough research on how

to determine the values for adapted requirements. Another recommendation concerning the amount of power, the climb requirements and the engines is to do more research on assisted takeoff and climb. The large power required is mainly needed for climbing. Therefore options such as rockets or extra batteries were considered. However these options would consume too much extra fuel. Therefore it is recommended to look into 'green' solutions or solutions that do not consume as much fuel as the solutions that exist nowadays for assisted takeoff.

## 6.2. Aerodynamic model

The aerodynamic model is based on the aerodynamic properties of the three dimensional model of the HUULC, which is in the form of a planform design. To have a three dimensional model, first a two dimension airfoil analysis has to be made, see Section 6.2.1. Then, the airfoils are used to make a three dimensional model, or planform design, as described in Section 6.2.2. At last, the high lift devices will be designed. This will be described in Section 6.2.3. For design of the aerodynamic model, the program called XFLR5\_v6 [36] has been used.

### 6.2.1. Airfoil design

The first aim of designing an airfoil is to pick an airfoil which has a very high lift coefficient in clean configuration. This is due to the fact that for clean configuration, a maximum lift coefficient of 1.60 is required. For the transformation from a two dimensional model into a three dimensional model, the lifting properties of the airfoil will decrease. Therefore, it is decided to choose an airfoil delivering the highest lift coefficient possible. Also, a thick airfoil and a flat bottom is requested for positioning the payload bay. Research leads to the airfoil called the FX 74-CL6-140 [37], which has the ability to reach a maximum lift coefficient of 2.4. An impression can be found in Figure 6.11. The Reynolds numbers used for the model are based on the velocity and chord lengths of the aircraft and the characteristics of the air. The values are in between the 50,000,000 for take-off and landing procedures and the 500,000,000 during cruise phases.

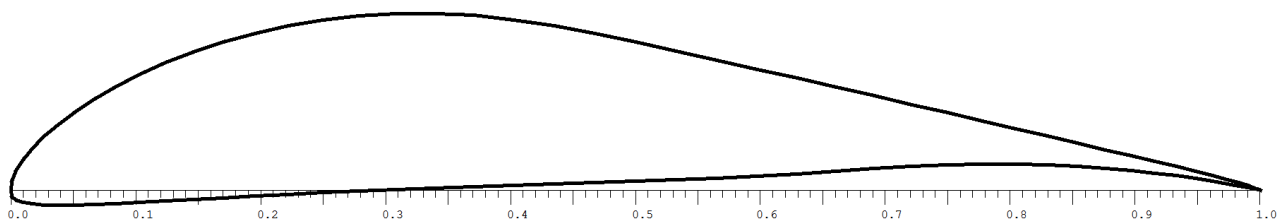


Figure 6.11.: FX 74-CL6-140 Airfoil.

Further analysis in the three dimensional model turns out that this airfoil easily delivers its required lift, but it does not give the lift over drag ratio of 26 which was aimed for in the preliminary design. To have a more drag efficient aircraft, a new airfoil is designed. The final airfoils chosen for the three dimensional model are:

- NACA 2415
- NACA 2420
- NACA 2422
- NACA 2424

An impression of these four airfoils can be found in Figure 6.12. As in the next Section will be explained, the three dimensional model will consist out of four different NACA airfoils. One for the fuselage, two for the fairing between the fuselage and the wing and one for the wing itself. The airfoil does not show the flat bottom as required for the payload bay, but because of its high thickness the payload bay will still easily fit in. On the other hand, some structural adjustments are needed to cope with the integration of the curved airfoil and the straight payload bay.

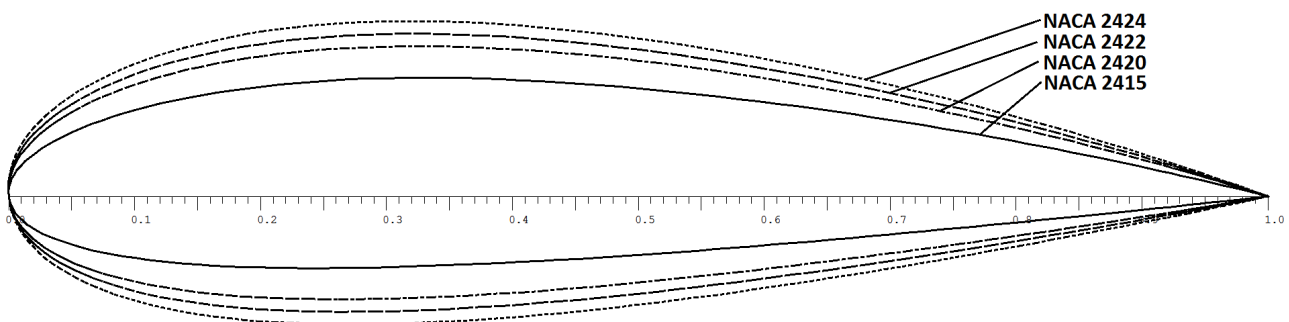


Figure 6.12.: NACA Airfoils.

## 6.2.2. Planform design

To transform a two dimensional airfoil into a three dimensional model, a planform design is made. The planform design gives the complete aerodynamic properties and the actual sizing of the aircraft. With this sizing, work can be completed on for example the structural, propulsion and the airport design. The aerodynamics have to match the numbers which have been calculated in the preliminary design. Examples on this are the lift coefficient during cruise, take-off and landing and the lift over drag ratio.

The final planform concept is designed by going through multiple design iterations. The iterations are performed to optimise the lift over drag ratio to the aimed value of 26. The final planform design is shown in Figure 6.13. With this design, the lift coefficient and the lift over drag ratio meet the requirements set in the preliminary design, as well as the stable moment coefficient. This will be further described in Section 6.6, the section where the stability analysis will be performed.

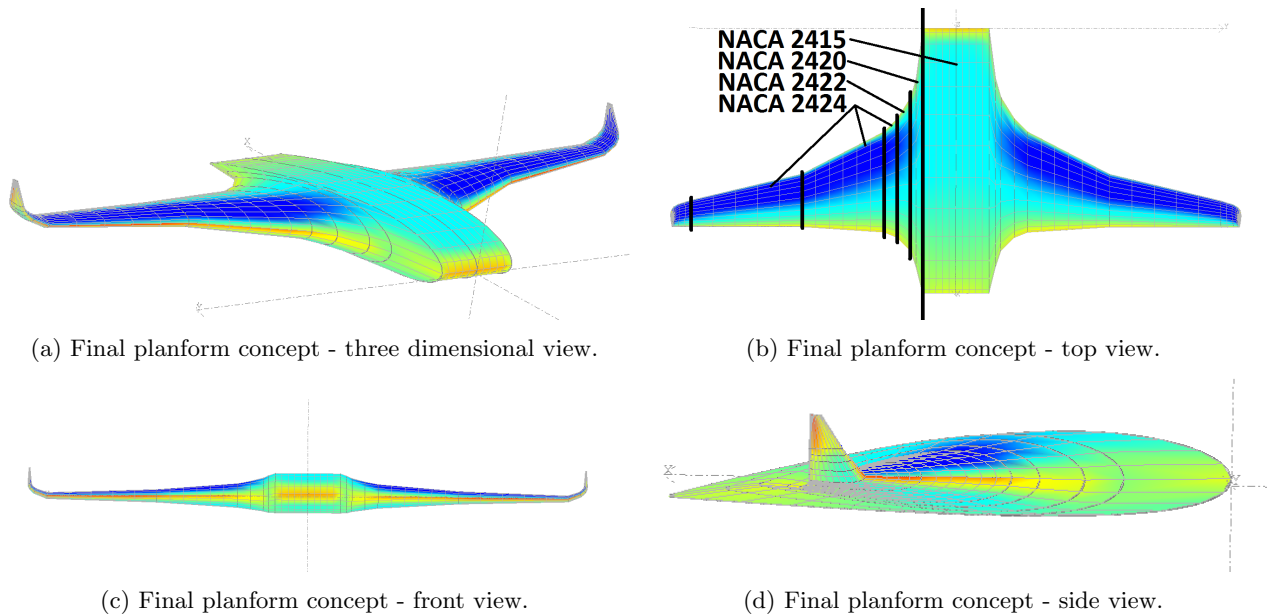


Figure 6.13.: Final iterative concepts.

The reason for having such a large wingspan is because of the aspect ratio. The aspect ratio is the leading factor for the drag coefficient and the aspect ratio itself is dependent on the wingspan and the surface area of the aircraft. Keeping the aircraft as narrow as possible with the same surface area, the aspect ratio drops and the drag coefficient increases, while the lift coefficient remains constant. This can also be seen in Equations 6.5 to 6.7.

$$A = \frac{b^2}{S} \quad (6.5)$$

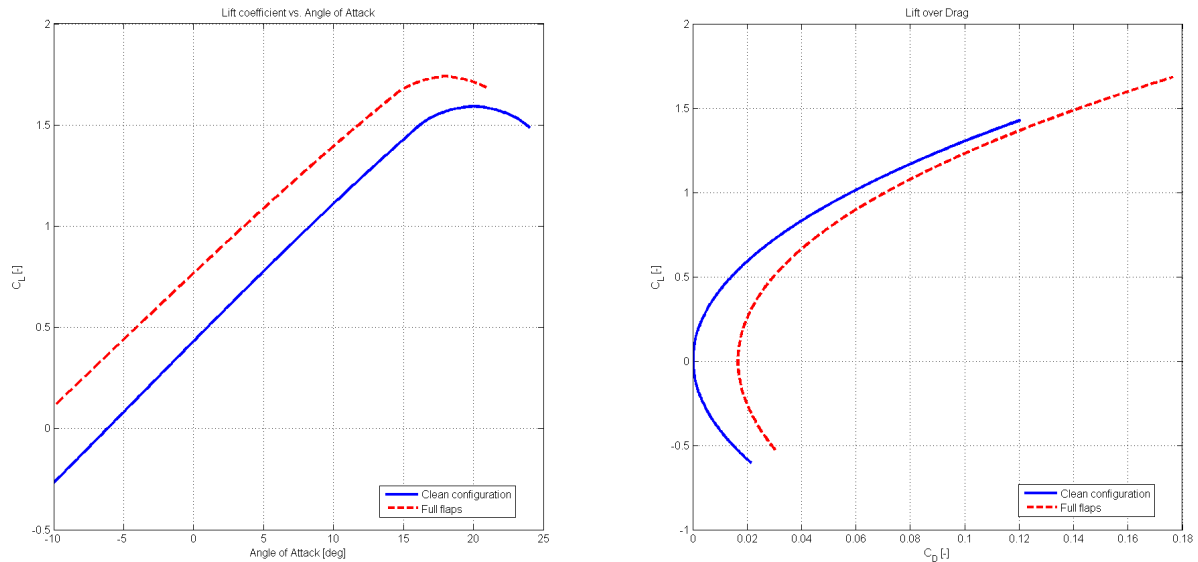
$$C_L = C_{l_0} \frac{a}{a_0} \quad (6.6)$$

$$C_D = C_{D_0} + \frac{C_L^2}{\pi A e} \quad (6.7)$$

It is found that for a surface area of  $7175 \text{ m}^2$  and a wing span of  $200 \text{ m}$ , during cruise the lift over drag ratio is 28.3 along with an aspect ratio of 5.58. Now, one has to be aware that this value will change due to the propulsion system, landing gear, high lift devices and control surfaces which are not taken into account in this model. During cruise, the aircraft will fly at a lift coefficient of 0.62, which is reached at an angle of attack of 3 degrees. Its drag coefficient is 0.022, the zero lift drag ratio is estimated at 0.0002 and the taper ratio is estimated to be 10. Values for the lift coefficient per angle of attack and the lift over drag ratio can be found in Figure 6.14a and 6.14b.

To go into further detail about the sizing of the aircraft, the fuselage will have a length of  $100 \text{ m}$  and a width of  $25 \text{ m}$ , while the total wingspan (fuselage and wing combined) is 200 meters long. The aim was to have a wingspan as small as possible, so it could fit in the current airport regulations. In the end, it turned out that such a wing span should be able to lift the HUULC, but the lift over drag ratio will be too small.

To show the influence of the wingspan on the lift over drag ratio, a comparison between a 200 meter wingspan



(a) Lift coefficient versus angle of attack plot.

(b) Lift over drag plot.

Figure 6.14.: HUULC characteristics plots.

HUULC and a 136 meter wingspan HUULC is made. To have the same lift requirements, it is made sure both concepts have the same surface area. This means during cruise flight, a lift coefficient of 0.62 is required. It is found that for this scenario the 136 meter wingspan HUULC has a lift of drag ratio of 15.1, while the 200 meter wingspan HUULC has a lift over drag ratio of 28.3. This clearly shows that the lift over drag ratio almost halves by increasing the wingspan by a factor of about 1.5. For the hydrogen strategy, a lift over drag ratio of 26 is assumed. If this value would lower due to a shorter wingspan, the costs of the hydrogen would grow out of the allocated budget. This will be further explained in Chapter 9. This actually means that technically it is feasible to shorten the wingspan and still lift the HUULC, even with its increased drag. In the case of this design, the HUULC is bounded by its costs and an increase in drag results in a budget which may not be profitable any more. Therefore, it is chosen to have a wingspan of 200 m to comply with the lift over drag ratio of 26.

The airfoils used to build this model are set in an twist angle of three degrees for the fuselage to five degrees for the wing. This is because the lift coefficient needed during cruise will exactly match the angle of attack the fuselage is positioned into. Therefore, the payload bay has to be put into an angle of attack of minus three degrees with respect to the fuselages reference frame to keep the containers horizontal during loading and unloading on the ground. The dimensions of both the wing and the fuselage can be found in Figure 6.20.

As a last remark on the three dimensional model, the software tool used for the rendering of the aerodynamics has some problems concerning the wingtips. Even if winglets are included in the model, still a lot of vortexes are generated at the wing tips. In fact, the vortexes should decrease and the drag will lower. In the model this is not the case. Therefore, if a more professional CFD tool will be used, the drag coefficient is likely to be lower than the one from the current tool and the lift over drag ratio will further increase.

### 6.2.3. High lift devices

For take-off and landing, a higher lift coefficient is required than the maximum lift coefficient of 1.60, which is designed for during cruise flight. Calculations indicated that during take-off a maximum lift coefficient of 1.70 is needed, while during landing it requires a maximum lift coefficient of 1.75. In order to provide a higher lift coefficient, high lift devices are used. Because engines will be placed at the leading edge of the wing (see Section 6.3), only the trailing edge is left to place the flaps.

The aim is to make the high lift devices as simple as possible. Because of the enlargement of wing area by moving multiple slotted flaps further backwards, the chord length will increase by twenty percent. Therefore, a flap system which only exist out of a single hinge, in the form of a single slotted flap, is chosen.

To calculate the sizing of the single slotted flap system, Equation 6.8 is used. Due to a safety factor,  $\Delta C_{L_{max}}$  is estimated to be 0.20 (which means that the maximum lift coefficient needed during landing is 1.8), while the  $\Delta C_{l_{max}}$  (the extra lift coefficient generated in the two dimensional model by the flap system) is estimated to be 1.30 [38]. The angle of the hinge line is assumed to be zero degrees. From this, the area needed for the high

lift devices over the total surface area is determined. As a result, the area needed for the high lift devices is estimated to be  $1227 \text{ m}^2$ .

$$\Delta C_{L_{max}} = 0.9 \Delta C_{l_{max}} \frac{S_{wf}}{S} \cos \Lambda_{h,l} \quad (6.8)$$

An impression of the single slotted flap system can be seen in Figure 6.15a. The total area used for the single slotted flap system can be found in Figure 6.15b. The single slotted flap is located from 27 meters to 58 meters in the wingspan direction, measured from the centreline of the fuselage. It has to be noted that the flap system is estimated to have a  $S_{wf}$  of about  $1700 \text{ m}^2$ , which means the flaps are over-designed. It has to be noted that the engines in front of the high lift devices may cause some extra turbulence, which mean the lifting behaviour of the single slotted flap system may drop a little. Also, a more professional CFD software tool may even lower the expected maximum lift coefficient. Therefore, the assumption of over-designing the high lift devices is said to be acceptable, by not introducing major designing problems.

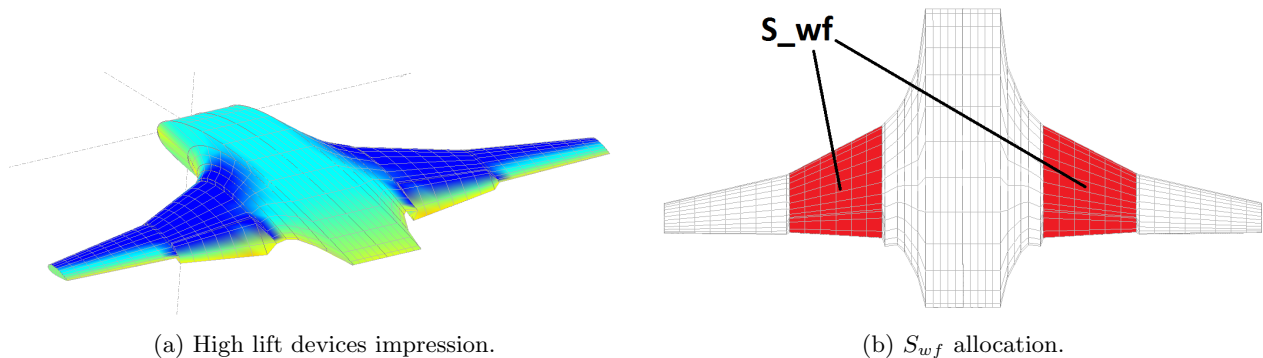


Figure 6.15.: Impression of the high lift devices.

#### 6.2.4. Conclusion and recommendations

The design of the aerodynamic model turns out that the Burnelli blended wing body is able to generate a maximum lift coefficient of 1.60 during cruise. The wing span has to increase to 200 meters in order to deliver its lift over drag ratio of 28.6. A lower wingspan still delivers the required lift coefficient, but an increase in drag coefficient leads to complications for the fuel efficiency of the aircraft. The length of the aircraft will be 100 meters, with a payload bay width of 25 meters. The aircraft will consist out of four different NACA airfoils, namely the NACA 2415 for the fuselage, the NACA 2420 and NACA 2422 for the fairing between the fuselage and wing and the NACA 2424 for the wing itself. Along with the surface area of  $7175 \text{ m}^2$ , the aspect ratio is 5.58 and the taper ratio is ten. During cruise, the lift coefficient is estimated to be 0.62 at an angle of attack of three degrees, along with a drag coefficient of 0.022. The zero lift drag coefficient is estimated to be 0.0002.

For the take-off and landing procedures, high lift devices are designed in order to increase the maximum lift coefficient. The lift coefficient has to be increased by 0.20, in order to meet the landing requirements. This is done by putting single slotted flaps at the trailing edge of the wing. The  $S_{wf}$  should have a minimal surface area of  $1227 \text{ m}^2$ , but for the preliminary design performed in XFLR5, which may contain some errors, the real  $S_{wf}$  is designed to be  $1700 \text{ m}^2$ . The flap system is located from 27 to 58 meters in the wingspan direction, measured from the centreline of the fuselage.

In order to have a better aerodynamic approximation, more professional CFD software tools are required. The program used for this estimation, XFLR5\_v6, only gives a first approximation and the program has issues regarding wingtip vortexes. Even if a winglet was included in the design, the vortexes did not reduce. A more professional CFD software tool can accommodate for this. Subsystems like the propulsion system and the landing gear are not included in the model. These subsystems are likely to increase the drag coefficient and therefore the assumption is made that the lift over drag ratio will drop from 28.3 to 26.

### 6.3. Propulsion system selection and integration

In this chapter, the process that led to the configuration of the HUULC propulsion system is explained in five sections. Section 6.3.1 will discuss possibilities for the general architecture of the propulsion system and the subsequent selection. Following the general architecture, Section 6.3.2 will investigate the various types of engines that may be used, such as turboprops or propfans, after which one type will be selected. With the type of engine having been chosen, Section 6.3.3 will optimise the propeller size and the number of required engines. Once the engines have been chosen and sized, the most appropriate placement on the aircraft will be evaluated

in Section 6.3.4, both longitudinally and span-wise. Finally, a conclusion and recommendations will be given in Section 6.3.5.

It should be mentioned that for the choice of the propulsion system many technologies and design options have been assessed in a qualitative (rather than quantitative) manner. This is a result of the limited scope of this project. For example, thoroughly assessing the benefits of distributed propulsion is an entire DSE project on its own [39]. Hence, instead of conducting an in-depth analysis, most decisions have been made with reference material and general impressions on the benefits and drawbacks of a particular technology.

### 6.3.1. General architecture

The entry into service of the HUULC will be 2030. This makes it possible to consider uncommon propulsion technologies that may be feasible in the future but not in the present day. For the general architecture, three options have been considered: fuel cells connected to electric motors (concept 1), gas turbines coupled to cryo-cooled electric generators & electric motors (concept 2) and finally gas turbines directly connected to a shaft (concept 3). The energy conversion flows of these three architectures are shown schematically in Figure 6.16 and are elaborated upon below.

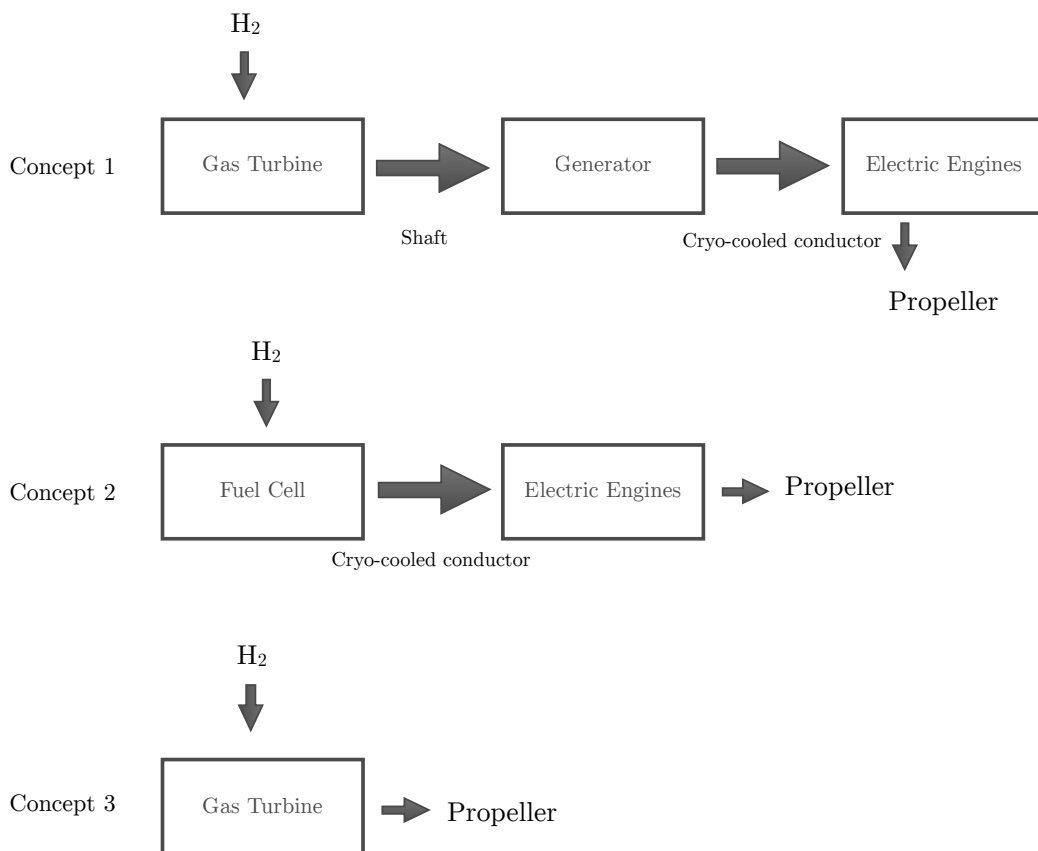


Figure 6.16.: Possible propulsion architectures for the HUULC

#### 6.3.1.1. Gas turbines coupled to cryo-cooled generators & fans

This architecture is based on the N3X concept by NASA [40]. The NASA concept uses cryo-cooled superconductive electric generators powered by gas turbines located at the wingtips. The electricity is then transferred to electric motors, which power multiple fans embedded in the fuselage, enabling a distributed propulsion technology. According to NASA, this concept improves fuel consumption by up to 72% compared to a Boeing 777-200LR. The propulsion architecture of the N3X is shown in Figure 6.17.

An advantage of using electric propulsion is that it eliminates the need of close proximity of cores and fans that is required by mechanical connections, such as belts and shafts. This gives the opportunity to separate cores and fans and place them each in optimal positions. For example, the N3X has cores on the wing tips, to ingest free-stream airflow, whilst having fans embedded in the fuselage, allowing for boundary layer ingestion. For the HUULC, however, the embedding of propulsors into the fuselage would interfere with the cargo bay. A remedy to this would be to elevate the upper surface of the fuselage which would, however, increase the wetted area



Figure 6.17.: The NASA N3X concept [40].

and thus skin drag.

Despite the benefits claimed by NASA, a few considerations must be addressed when evaluating this architecture:

- **Development time and costs:** Although the authors of the paper claim that the N3X could fly by 2030 [40], it is believed by the propulsion team that using cryo-cooled superconductive electric systems may be too complicated and costly to develop in the current time frame. Superconductivity is still in very early stages of development and will need many years before its price will be low enough to be used commercially.
- **Added weight and complexity:** Furthermore, even if the concept does reach an acceptable price level, the added weight and complexity of all the extra components, such as electric generators and electric motors, would need to be addressed before this architecture may become beneficial on the scale of an aircraft the size of the HUULC.

#### 6.3.1.2. Fuel cells connected to electric motors

This architecture would use fuel cells with a power density of  $967 \text{ W/kg}$ , which could potentially increase to  $1500 \text{ W/kg}$  with future improvements [41]. The electricity generated by these fuel cells would power electric engines which then generate thrust for the HUULC, by means of fans. The main advantage of fuel cells is their higher efficiency compared to gas turbines. Current fuel cells have an efficiency of about 60%, compared to 50% of gas turbines [42]. This means that the main consideration is whether or not the increased efficiency of fuel cells outweighs their low power density. Although weight and efficiency are considered as main aspects of fuel cells, a few other considerations must be addressed when evaluating this concept:

- **Fuel cell heat dissipation:** Given the 60% efficiency of fuel cells, the remaining energy needs to be dissipated with a cooling system. This presents significant challenges due to lower operating temperatures and almost no heat carried away by the product stream [43].
- **Cost:** Current fuel cells have a cost of €1,100 per  $\text{kW}$  [44]. Given a total power required of  $316 \text{ MW}$  for the HUULC, this would mean a total fuel cell cost of €348 million per aircraft. The fuel cells then need to be connected to electric engines, which add to the costs. Moreover, in order to save cable weight, the electric propulsion system would have to use superconductivity, which requires cryo-cooling, adding further complexity and cost to the system.

#### 6.3.1.3. Gas turbine directly connected to a shaft

This architecture is the simplest option of the three, by using conventional engines with integrated cores and propulsors. It has the advantage of being a tried and tested architecture but is also expected to be the lightest of the three options, as there is no need for fuel cells, electric generators or electric motors.

#### 6.3.1.4. Architecture selection

For the general architecture, fuel cells and gas turbines connected to cryo-cooled generators are disregarded as viable options for the HUULC. Fuel cells are very heavy, expensive and an elaborate cooling system would have to be designed to accommodate them. The other option, gas turbines coupled to cryo-cooled generators is

considered too complicated, costly and risky for the HUULC, which must be ready by 2030. Furthermore, it is possible that the downside of the extra energy conversion steps (extra weight, loss in efficiency, see Figure 6.16) will be more important than the benefits of electric propulsion. This means that the last option is chosen: gas turbines directly connected to a shaft. This widespread architecture poses the lowest risk, weight and cost of the three.

### 6.3.2. Engine and propeller type

In this section, the engine type and propeller selection is addressed. First, a discussion on the power required and the disk loading values is conducted. Finally, the concept of counter-rotating propfan engines is elaborated upon.

#### 6.3.2.1. Total power and required disk loading

The preliminary design of the engine was initiated once the final required gross power was determined. For an aspect ratio of 5.59, this power was estimated at  $316\text{MW}$  in Section 6.1.4. The Boeing Pelican ULTRA, the concept most similar to the HUULC's scale, requires a gross power of  $240\text{MW}$ , 41% less than that of the HUULC. In order to give an indication of the gross power of one HUULC, approximately 10 Airbus A400M aircraft would be needed to deliver the same power, or a total of 40 of their Europrop TP400 engines.

With the Europrop TP400 being one of the most powerful propeller engines to date, it becomes clear that no engine model currently available on the market will be suitable for the HUULC, as a prohibitive number of engines would be required or otherwise prohibitive propeller diameters. The key to limiting the number of engines and propeller diameters is maximising propeller disk loading, defined as the power per unit area. The disk loading of an engine is heavily dependant on the type of engine used, such as a turboprop or a propfan. Hence, the selection of the engine type will be based on the highest disk loading.

Table 6.10 lists disk loadings for current engines and design concepts. The last entry states the theoretical scalability of disk loading when using propfan technology plus counter rotating blades.

Table 6.10.: Propeller disk loading value for current and concept engines.

Engine Type	Propeller loading ( $\frac{kW}{m^2}$ )
Standard Turboprop [45]	100 - 200
Pelican ULTRA (concept) [46]	340
Europrop TP400 [47] [48]	368
Propfan + Counter Rotating Blades (theoretical) [45]	600

As was previously discussed, using the Europrop TP400 would require about 40 engines or unrealistic propeller diameters. Hence, according to Table 6.10, if the Europrop TP400 cannot be used, neither can anything with a lower disk loading. This means standard turboprops will trigger unrealistic engine numbers and propeller diameters, more-so than the TP400. The only remaining option is the theoretical upper value of a propfan concept combined with contra-rotating blades. This concept is now be elaborated upon.

#### 6.3.2.2. Contra-rotating propfan technology

Patented in 1919 by Frederick W. Lanchester, the contra-rotating propeller technology (also known as CRP) is a technology that due to its major improvements in performance has attracted the attention of designers and researchers since its invention. Until recently, its presence on the market has been minimal due its noise drawbacks, complexity, higher costs and manufacturability difficulties.

Its high performance characteristics lie behind the elimination of the tangential velocity or swirl losses. This leads to a great improvement in efficiency and therefore reductions in fuel consumption [51]. A counter-rotating turboprop, the NK-12 can be seen on the left of Figure 6.18.

A propfan is a propeller engine concept characterised by multiple (usually eight or ten), swept blades which allow for an increased disk loading, thus shorter blades. Its special blade design and configuration enhance rotation speed reductions and according to Ruijgrok [45], when combined with contra-rotating blades, increase the propeller disk loading up to three times that of a standard turboprop, hence reaching  $600\text{kW}/\text{m}^2$  [45]. With the HUULC's extensive power requirements, contra-rotating propfan technology may be the only way to attain realistic engine numbers and propeller diameters. The D-27, the world's first commercial contra-rotating propfan, is seen on the right of Figure 6.18.

Although Ruijgrok states that contra-rotating propfans may potentially reach disk loadings of  $600\text{W}/\text{m}^2$ , Dr Leo Veldhuis of Delft University of Technology questioned this number when consulted by the propulsion team. A



Figure 6.18.: NK-12 [49] and D-27 [50] Counter-Rotating Propeller Engines.

more attainable disk loading of  $500 \text{ kW/m}^2$  was thus chosen for the contra-rotating propfan concept. This disk loading still surpasses that of other engine types. Hence, the contra-rotating propfan is still the most appropriate engine for the HUULC in terms of disk loading.

Current contra-rotating propfan technology presents one major disadvantage: noise. The harmonic interactions between the multi-bladed propellers cause an increase of 30dB in the axial direction and 10dB in the tangential [51]. With noise being one of the key elements in the HUULC's sustainability plan, such noise footprints seem to limit the use of these engines. However, large efforts are being made to face the technical challenges that the open rotor contra-rotating technology presents. In this line, several EU-funded programmes (DREAM [52], NACRE [53], JTI [54]) are currently investigating solutions to reduce the noise footprint of these engines, but also other aspects such as its mechanical or control systems [55]. It is reported that the DREAM (validation of Radical Engine Architecture systems) is succeeding in its goal of reducing the noise generated by open rotor contra-rotating engines and it is predicted that in the future, these engines will be at similar noise levels as conventional turboprops [55].

### 6.3.3. Engine number and propeller sizing

The determination of the engine numbers & propeller sizing and the position of the engines is an iterative process, as the position of the engines depend on their dimensions and vice-versa. In this report, the engine positioning section is written after engine numbering and sizing but the reader should be aware that this process is iterative in nature.

In order to determine the optimal number of engines for the HUULC, the following constraints must be met:

1. A total propulsive power of  $316 \text{ MW}$  during climb
2. A disc loading of  $500 \text{ kW/m}^2$
3. The diameter of the propellers shall be less than  $15 \text{ m}$  for ground clearance (this requirement was set after the positioning of leading edge was selected)
4. The helical tip velocity (combination of angular and forward velocity) of the blades shall not exceed Mach 0.85, to avoid transonic efficiency reductions [56]
5. According to Roskam [57], propeller efficiencies increase with propeller diameter, hence it is desirable to maximise propeller diameter, within the constraints of ground clearance and tip velocity
6. The number of engines shall be even so that the same number of engines may be placed on each wing

An optimiser was created, in which the aforementioned constraints were entered as inputs. The values are used to calculate the required total swept area, based on the total power required and the assumed blade loading. The area is then divided into combinations of number of engines and propeller diameters, which are the two outputs. With the values stated above, the optimal number of engines is given as eight (four on each wing), each with a diameter of  $10.05 \text{ m}$  and eight blades per shaft (16 blades per engine due to two contra-rotating shafts). The power produced by each engine amounts to  $39,664 \text{ kW}$ , which is about four times as powerful as the most powerful turboprops currently on the market. This may seem extreme, however the Boeing Pelican ULTRA concept was planned to have  $59,656 \text{ kW}$  propeller engines of  $15 \text{ m}$  propeller diameter [46].

#### 6.3.3.1. Propeller tip velocity considerations

The helical tip velocity is defined as the combination of the rotational velocity component due to the propeller's rotation and the axial velocity component due to the aircraft's forward motion. With the propeller diameter

set, the upper limit of angular speed  $\omega$  of the engine must be determined, such that requirement four regarding a maximal helical tip Mach number of 0.85 is met. From Ruijgrok, the helical tip velocity is given as [45]:

$$V_{helical} = \sqrt{V_{rotational}^2 + V_{axial}^2} \quad (6.9)$$

Re-arranging for the rotational component of velocity yields:

$$V_{rotational} = \sqrt{V_{helical}^2 - V_{axial}^2} \quad (6.10)$$

The limiting condition for the rotational velocity will be during take-off and climb, when maximal thrust is required. Hence, an axial velocity of  $72\text{ m/s}$ , the take-off velocity, is selected along with sea-level atmospheric conditions. At sea-level, a Mach of 0.85 produces a maximal helical velocity of  $290\text{ m/s}$ . Substituting these values into equation 6.10 yields a maximal rotational velocity component of  $281\text{ m/s}$ . With a radius of  $5.025\text{ m}$ , the maximal angular speed is found to be  $\omega = 55.92\text{ rad/s}$  or 534 rotations per minute, by  $\omega = \frac{V_{rotational}}{r}$ . Hence, according to this estimation, during take-off the angular speed of the propellers may not exceed 534 rotations per minute.

It must be noted, however, that this estimation is relatively simple and does not account for the special swept blade design of the propfan engine, designed to increase the allowable angular velocity. Hence, it is expected that a slightly larger maximal angular speed  $\omega$  will be allowed, before the helical velocity reaches Mach 0.85.

### 6.3.4. Engine positioning

The positioning of the propulsion system is just as crucial as the design of the propulsion system itself, particularly when discussing the integration of the engine(s) to the rest of the aircraft. The position of the propulsion system must be chosen in a manner which optimises parameters such as drag, noise and fuel efficiency, to name a few. First, longitudinal positioning of the propulsion system on the aircraft is discussed, followed by the span-wise position.

#### 6.3.4.1. Longitudinal positioning

Even with an assumed disk loading of  $500\text{ kW/m}^2$ , it is expected that multiple engines will be required. Hence, some form of distributed propulsion is inevitable.

Several concepts are proposed for the positioning of the propulsion system.

- **Concept I:** All engines at the trailing edge.
- **Concept II:** All engines at the leading edge.
- **Concept III:** All engines embedded into the planform, to benefit from boundary layer ingestion.
- **Concept IV:** All engines located in pylons on top of the wing.
- **Concept V:** Some engines embedded into the fuselage, to benefit from boundary layer ingestion and the rest at the leading edge of the wing.

Based on these six concepts, a trade-off is conducted, shown in Table 6.11. The most important considerations during this trade-off is noise and take-off rotation obstruction. Noise is an important part of the HUULC's sustainability plan, hence why it was given a weight of five out of five. If take-off rotation is obstructed by the propellers, a higher take-off velocity would be required so as to eliminate the need to rotate. This would ultimately lead to a longer runway, which is not desirable when the required runway length is already long, hence why this criterion was also given a weight of five out of five. Structural & integration difficulty was given the lowest weight, as these difficulties could only be very roughly estimated by the structural engineers of the group. Furthermore, the implications on subsystem criterion was also given the lowest weight, since the HUULC has a very large wetted area, allowing for more placement option of the subsystems.

Although concept V obtains the most points during the trade-off, during the second iteration of propeller sizing it was discovered that having engines embedded in the fuselage, so as to benefit from boundary layer ingestion, is not feasible for the HUULC. Propeller sizing revealed that even with a large number of embedded propellers, spanning the entire fuselage, the propeller diameters would still need to be considerably large in order to provide the required power. This would increase the upper surface of the fuselage by an unrealistic amount. As a result, the second best option is selected, that of concept II: engines on the leading edge of the wings. This has the consequence of locking the propulsive configuration to that of a tractor configuration.

Table 6.11.: Propulsion system longitudinal positioning trade-off table

Criteria	Weight	C. I	C. II	C. III	C. IV	C. V
Noise	5	1	2	5	4	3
Take off rotation	5	1	5	5	5	5
Structural and integration difficulty	1	5	4	1	3	3
Size of propellers	4	3	5	1	2	3
Number of engines / Wing span interfaces	2	5	2	2	5	4
Fuel Efficiency	4	1	3	5	1	5
Development risk	2	5	5	1	5	3
Implications on subsystems (HLDs, control surfaces)	1	1	5	1	3	3
<b>Total</b>		<b>52</b>	<b>90</b>	<b>82</b>	<b>83</b>	<b>92</b>

### 6.3.4.2. Span-wise positioning

With the longitudinal positioning of the propulsion system having been set to the leading edge of the wing, the span-wise positioning of the engines must be determined. There are multiple considerations to account for before the engines' positions may be set:

- **Aerodynamic efficiency:** According to Veldhuis [58], for an aircraft with propeller engines in a tractor configuration at the leading edge, the aerodynamic efficiency  $\frac{C_L}{C_D}$  of the wing improves the closer the propellers are to the tip of the wing.
- **Structural characteristics:** Bending relief of the wingbox is improved, the closer the propellers are to the tip of the wing.
- **Wing vibrations during landing:** The further the engines are from the root, the larger the fluttering will be during touch-down. For a 200m span aircraft like the HUULC, this may be a real problem, whose remedies would include the reinforcement of the wingbox, or the attachment of small landing gears at the tip of the wings, called 'outriggers', as is the case for the B52 Stratofortress [59].
- **Engine failure yaw control:** The out-most engine must be close enough to the root, such that if it fails, the rudder will be able to compensate for the moment differential. This is explained in more detail in Section 6.7.6.4, for the largest-moment scenario, when the outer-most engine is located at the tip.
- **Lateral ground clearance:** According to Roskam, the angle subtended by the out-most landing gear and the out-most propeller must be greater than five degrees [57].

With these five considerations in mind, the aerodynamic and structural characteristics would benefit from having the engines as close to the tip as possible. Temporarily setting the outer-most engine to the wing tip, the remaining three considerations will shift the engines closer to the root.

For brevity, only the limiting consideration will be discussed, which turned out to be the lateral ground clearance. At the time of engine positioning, for a required ground clearance angle of five degrees, the outer-most engine had to be located a minimum of 14.98m from the tip. This position was set and given to the structural team for their structural analysis. However, after the structural analysis had been finalised and frozen, the landing gear design changed with a decrease in the landing gear height. This decreased the ground clearance angle from 5 degrees to 2.51. At this point, time did not allow for repositioning the engines closer to the root, as the structural analysis had already been frozen. Hence, the clearance angle remains at 2.51 degree. Further information on this issue is given in the upcoming conclusion and recommendations section.

With the out-most engines having been positioned, it was decided to position the six remaining engines symmetrically on each wing, to distribute their loads evenly but also for aesthetic purposes. This results in an engine spacing of 15m, giving a distance between adjacent propeller tips of 4.95m.

### 6.3.5. Conclusion and recommendations

A contra-rotating propfan engine in a tractor configuration (like the D-27 engine shown on the right of Figure 6.18) has been selected, with an assumed disk loading of  $500kW/m^2$ , a maximal output power of 39,664kW and a propeller diameter of 10.05 m. Each engine will consist of two shafts, with eight blades per shaft. Eight of these engines shall be fitted on the aircraft, four on the leading edge of each wing. The maximal allowable

angular speed of the propellers during take-off shall be upper of 534 rotations per minute.

The primary recommendation involves the shortening of the landing gear, which triggered a decrease in the ground clearance angle under the required five degrees. This was a time-related issue and if more time was available, the structural team would have re-conducted their structural analysis, allowing for the correct shifting of the out-most engine. Of course in the designing of real aircraft, the excuse of limited time is not acceptable. Hence a possible recommendation would be to develop and use a structural analysis tool, which easily incorporates iterations in other parts of the aircraft, such as the landing gear or engine positioning. This way, design changes in other systems could be accounted for easily, rather than having the structural team manually change their inputs.

A further recommendation would involve a more accurate determination of the maximal allowable propeller angular speed, with a calculation that would incorporate the special swept design of propfan blades. This way, the team would have a better estimation of when the tip would reach Mach 0.85. Along the same line of thought, it would be beneficial for a future project with a wider scope to undertake an in-depth analysis of engine design, to determine exact blade shapes and angular speeds required in order to reach a high power output, like to  $39,664kW$  of the HUULC engines. This was out of the scope of this project but would be required by an engine manufacturer in the designing of such a propulsion system.

Although of great interest to the propulsion team, evident by the amount of time spent on its research, the concept of distributed propulsion was unfortunately not widely incorporated in the HUULC propulsion design. Despite the team's extensive efforts to discover more about the concept from literature and a fellow DSE team [39], its complexity meant an in-depth analysis had to be made, which was not allowable by the limited resources of the propulsion team. The NASA N3X's boundary layer ingesting distributed propulsion system was a main candidate for the HUULC, as the propulsion team saw potential for improved fuel consumption. However, after the complexity of the system was measured against the propulsion team's limited resources, it was not looked into further.

Therefore, as a final recommendation the propulsion team believes a project with more time and a greater scope would potentially benefit from conducting a deeper analysis into this concept. Rolls-Royce and EADS have a comparable distributed propulsion design concept, called the 'E-Thrust Hybrid Electric Aircraft', which may also prove fruitful. The interested reader is referred to [60].

## 6.4. Structural characteristics

In this section, the preliminary structural designs of both the wing and the fuselage are presented along with their integration analysis. The structural analysis of the wing and the fuselage has two main purposes: first, to deliver a consistent structural skeleton for the aircraft; and second, to provide an accurate and realistic weight prediction. This weight estimation is indeed of great importance due to the fact that the HUULC presents an unconventional configuration. The design is subdivided in two parts: wing design in Section 6.4.1 and fuselage design in Section 6.4.2. Both designs were modelled as box shaped structures consisting of plates, spars, ribs and stringers.

### 6.4.1. Wing sizing

The following section explains the entire process for the structural sizing of the wing box. Firstly, The reference frame and the load cases are described. Then the forces are modelled and the sizing of the different sub-components is performed. Finally the structural iteration process and results are explained.

#### 6.4.1.1. Reference frame

The reference frame chosen is an orthogonal 3-axis inertial system with the origin placed at the bottom left corner of the wing box tip cross section. The  $z$ -axis points in the vertical direction of the cross section parallel to the vertical spars. The  $x$ -axis runs along the bottom plate of the cross section. Finally, the  $y$ -axis points in the direction of the fuselage, perpendicular to the  $z - x$  plane. This axis system is shown in Figure 6.19.

#### 6.4.1.2. Wing box geometry

The geometry of the wing box is primarily derived from the planform design of the HUULC. As it is shown later, the main design constraints result from the integration of high lift devices, ailerons and other wing subsystems.

The wing box cross section is modelled as a rectangular-shaped box, consisting of plates, stringers and spars running along the span (see Figure 6.19). Moreover, a trapezoid was chosen as wing box top view outline. This shape (shown in Figure 6.20) greatly simplifies the model, and it is used for this preliminary phase of the structural design. A proposal for further steps is outlined as well. The geometry involves taper in the  $x - z$  and

$z - y$  planes, as well as front and backward sweep in the  $x - y$  plane. In order to maximise the dimensions of the wing box and enhance the efficiency of the structure, a wide range of parameters was implemented in the sizing tool (sweep angles, taper angles, piecewise load distributions, etc.).

In Figure 6.20, the integration of the wing box within the wing is shown. In this figure, the wing box is represented by a shaded green area. To maximise the efficiency of the wing box, it is important to model and integrate the wing box such that it occupies the maximum volume available inside the wing. From figure 6.20, the wing box is modelled as a trapezoid that occupies the maximum chord available (45% of chord) from the tip of the wing until the kink located at 42 metres from the tip. After the kink the wing box still follows the geometry defined by the trapezoid. Thus after the kink, the wing box does not occupy 45% of the chord anymore and this is because initially, the wing box was modelled as a single trapezoid. However after the aerodynamic planform analysis was complete, the analysis determined that a kink was needed. This reduces the efficiency of the wing box after the kink and thus, for an improved structural sizing the kink should be implemented in the wing box geometry in the future.

The value of 45% of the wing chord arises from the need of high lift devices, ailerons and the integration of other such subsystems. More precisely, the front spar is located at 15% of the chord and the back spar at 60% [61].

The ribs limit the effective length of the stringer (beneficial for buckling). An equal rib spacing of  $1.5m$  was selected. Conventional aircraft present a rib separation of  $0.75m$  due to fuel loads [62]. The HUULC does not encounter this problem as no fuel exists in the wings. Hence, its rib spacing is larger.

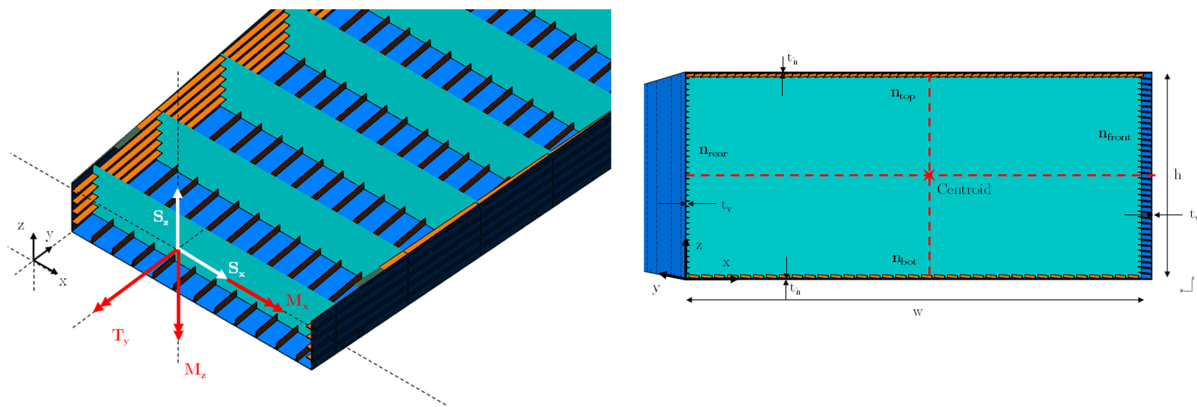


Figure 6.19.: Left: Wing box axis system and sign conventions. Right: Wing box cross section geometry.

### 6.4.1.3. Load discovery and modelling

In order to determine the maximum loads acting on the wing, a flight envelope at maximum takeoff weight of the aircraft (which is the most critical case) was created for both manoeuvres and gusts (see Figure 6.21). From these diagrams, the maximum load factors were obtained (3 and  $-2$ ). By scaling the forces acting on the vertical direction ( $z$  axis), the load factors are implemented in the design. The theory behind these plots can be consulted in [63].

**Aerodynamic forces:** From the aerodynamic analysis, the lift distribution was obtained. The lift forces were assumed to be acting on the quarter chord of the wing and are modelled as a quadratic distribution. Moreover, the shadowed area in Figure 6.20 is used to calculate the lift (i.e. a piecewise function is used to obtain the lift chord). Drag forces are neglected (explanation in Section 6.4.1.4).

**Engines:** The forces induced by the engines are thrust and weight, acting in the in the  $x$  and  $z$  directions respectively. These forces are modelled as point loads acting on the wing box. As the horizontal and vertical offsets of the engines with respect to the wing were unknown until the very last phases of the development, the point loads were located at the centroid of the wing box. However, in further work these offsets will have to be implemented, as they induce considerable additional torque along the span of the wing box.

**Structural weight:** The weight distribution of the wing box itself was also accounted for. An initial wing box sizing was performed based solely on the other load cases described previously. Based on this initial sizing, the weight distribution was modelled and added to the load calculations. This triggers an iterative process which is described in detail in the upcoming sections. The weight distribution of the wing box is assumed to be acting in the centre of the wing box at every cross section. This positioning arises from the fact that the wing box centroid is located in the geometric centre of every cross section (the centroid is equivalent to the centre of mass of every cross section in this case since the material density is the same everywhere on the wing box, Aluminum 7075 T-6).

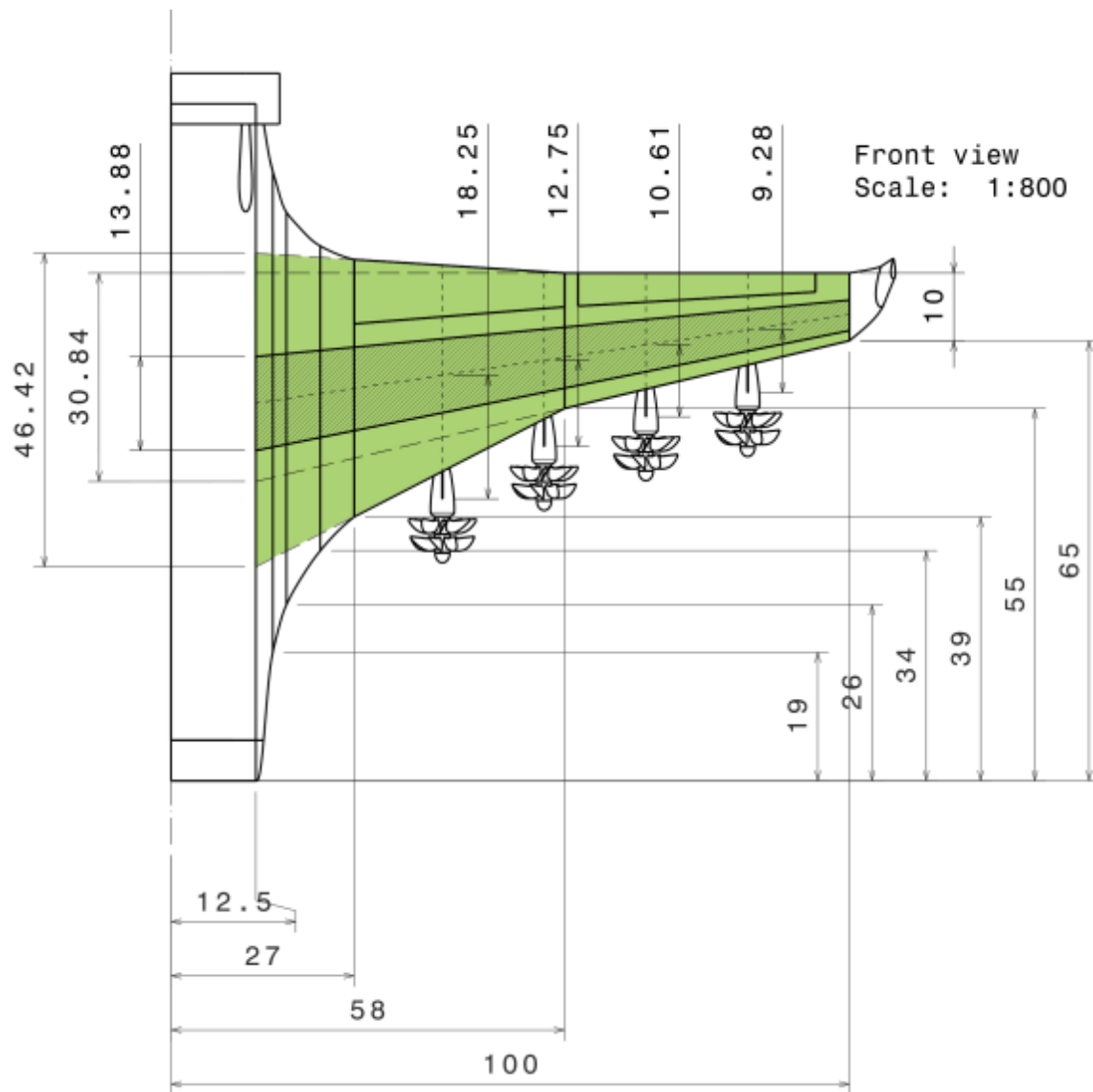


Figure 6.20.: Planform outlines.

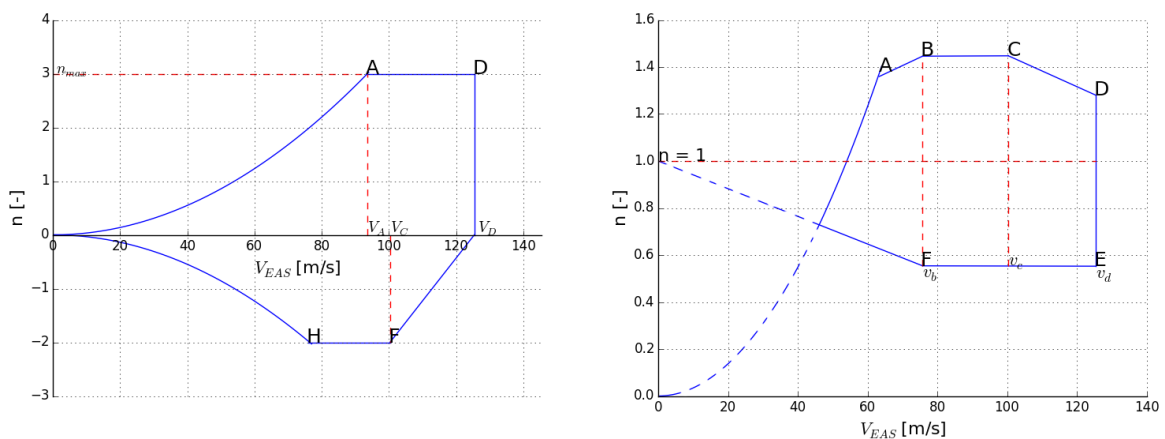


Figure 6.21.: Manoeuvres Diagram (left) and Gust Diagram (right) at MTOW.

**Landing gear:** This subsystem induces shear forces and bending moments. Landing gears also create additional torque due to their positioning offset from the centroid of the wing box. However the landing gears induce a stress relieving moment during the flight phase as well as on the ground, thus by neglecting the landing gear, the wing box is actually being oversized. The load induced by the landing gears were not included in the model

due to the late finalisation of the landing gear subsystem design.

**Other forces:** Moreover, additional forces were evaluated but not included into the load model. These include the weight of the skin, but also the loads exerted by the high lift devices, ailerons and other subsystems attached to the wing box frame. To introduce such loads into the model, more refined design of these subsystems should be performed to determine their exact position and mass distribution. Since these load cases could not be considered, the bending moments, the shear forces and torques modelled are undersized.

As a result of the forces present, moments are present around every axis. The modelling of the different forces acting upon the wing box is shown in Figure 6.23. In Figures 6.24, 6.25 and 6.26 the diagrams of the lift distribution, shear forces and moments acting on the wing box about  $x$ ,  $y$  and  $z$ -axis are depicted with the convention for positive forces and moments shown in Figure 6.19.

Figure 6.22 shows the totality of the forces that would in reality be acting upon the wing. This diagram shows the forces included in the script model as well as the ones not included but stated previously.

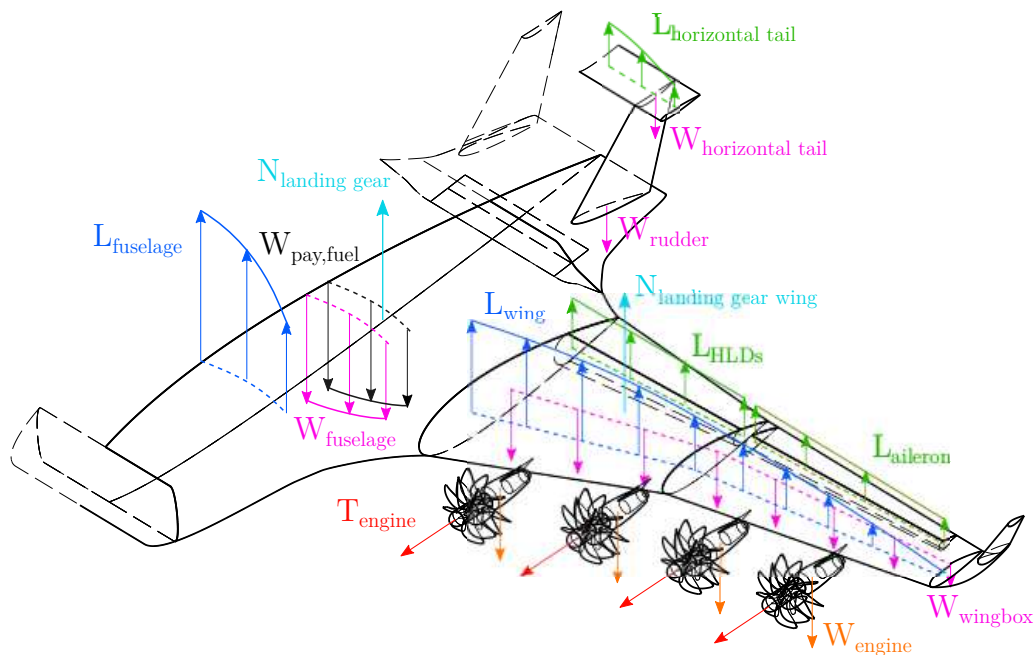


Figure 6.22.: Totality of forces acting on the HUULC (in reality).

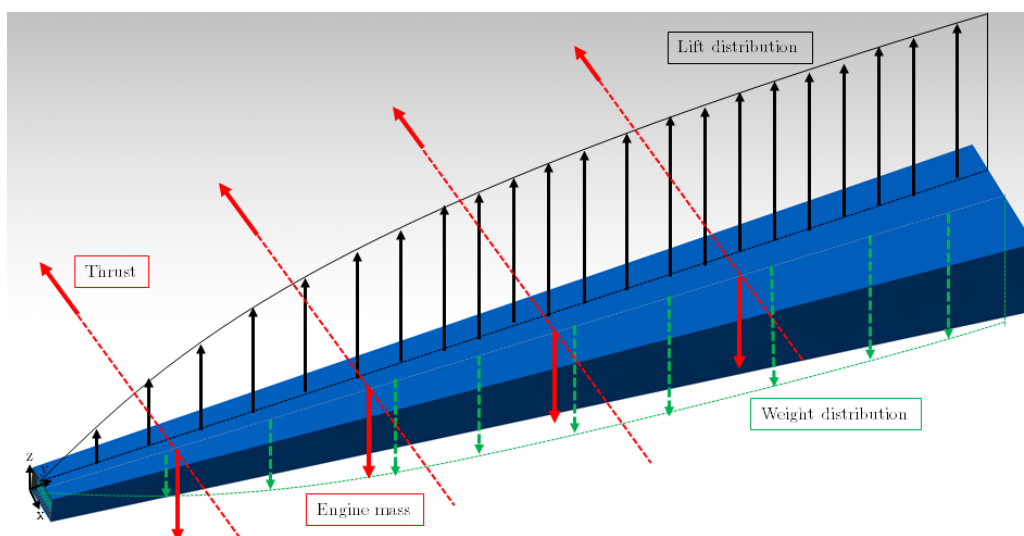


Figure 6.23.: Modelling of forces present on wing box.

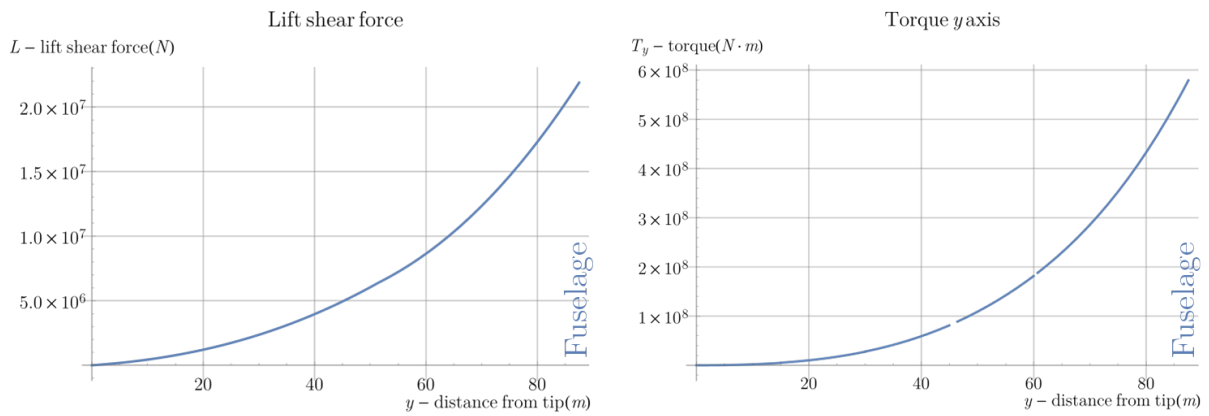


Figure 6.24.: Lift shear distribution (left) and Torque about  $y$ -axis (right).

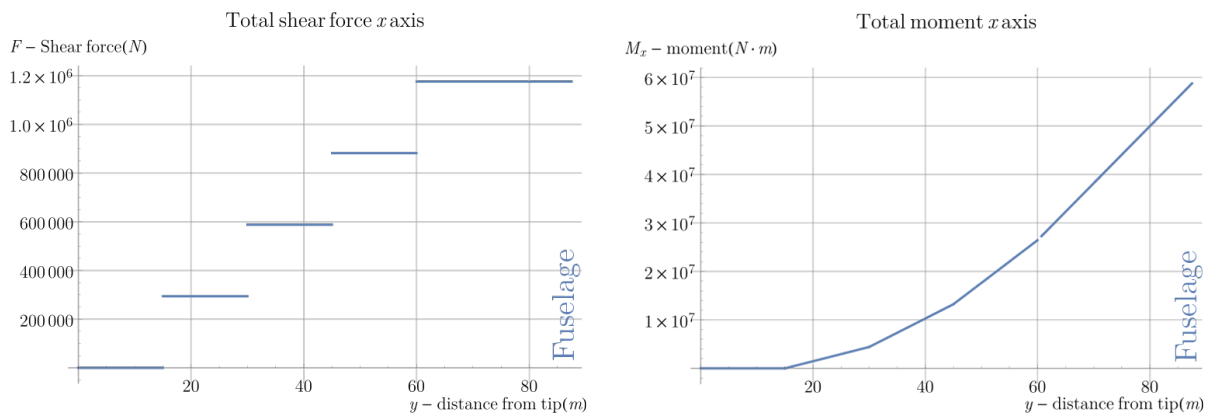


Figure 6.25.:  $x$ -axis diagrams:  $x$  shear (left),  $x$  moment (right).

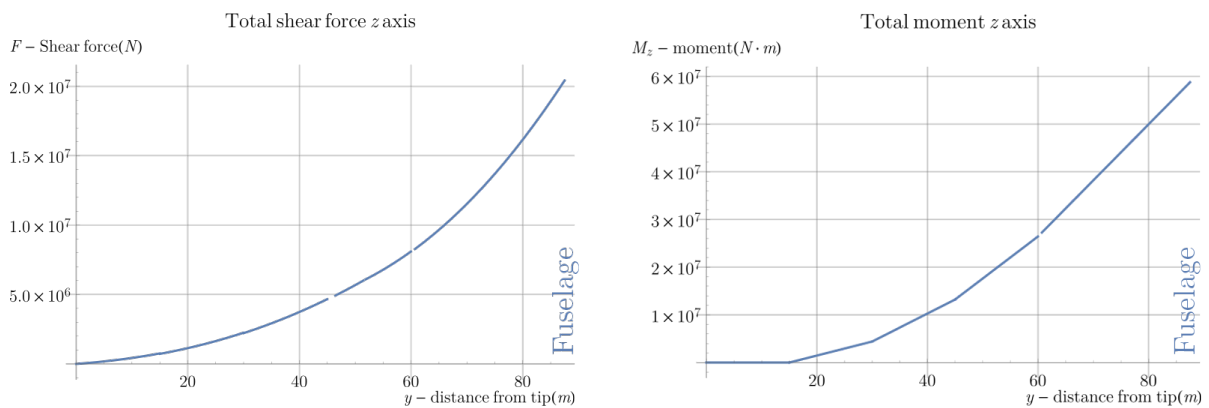


Figure 6.26.:  $z$ -axis diagrams:  $z$  shear (left),  $z$  moment (right).

#### 6.4.1.4. Theory and assumptions

In this section, the general assumptions which are implemented in the structural sizing script and which are applicable to both the wing and fuselage boxes, are presented and the impact of each of these assumptions on the design is explained.

##### General assumptions:

- **Torsion does not induce direct stresses:** This is a common and valid assumption performed in structural analysis (see reference [64]).
- **The effective stringer distances are equal to rib spacings:** Important while considering buckling loads on stringers. It also means that ribs are sized such as to carry loads.
- **Thin wall assumptions are taken into account:** Cubed thickness terms are neglected in the calculations of moments of inertia. Since the width and height dimensions of the wing box are much larger than the expected thickness, this assumption is reasonable.
- **Lift is modelled as a quadratic distribution:** The lift distribution is obtained from the aerodynamic model of the HUULC at take-off condition which is discussed in Section 6.2. Interpolating this distribution to a quadratic function leads to very high correlation coefficients ( $R^2$ ) and thus leads to a great fit.
- **The material used for the sizing of the wing box is Aluminum 7075-T6:** due to its high strength properties as well as its relatively low density compared to other aluminum alloys [65]. Moreover, its behaviour is greatly understood which makes the modelling achievable within the allocated time for the structural design.

##### Wing and fuselage box specific assumptions:

- **The stringers in the boxes are assumed to carry all the direct stresses due to bending moments around the  $x$  and  $z$ -axis:** This is a common conservative assumption performed in the structural analysis of wing boxes [64] and ensures that no plate buckling occurs.
- **The plates of the boxes are assumed to carry the shear stresses due to the forces in the  $z$  and  $x$ -axis as well as the torque around the  $y$ -axis:** This is also a common valid and conservative assumption made for structural sizing [64].
- **The thickness of the top plate and bottom plate are equal and given by  $t_h$  and the thickness of the front and rear plate are equal and given by  $t_v$ :** As a result, the shear centre of the wing box is located in the geometric centre of the shear-carrying box.
- **Load factors of 3 and  $-2$  are applied to the loads induced by the bending moment (around  $x$ -axis) to size the top and bottom stringers:** These load factors are directly resulting from FAR-25 regulations [63].
- **The engine thrust and weight are modelled as point forces:** Engine forces are normally distributed forces. To simplify the model, these forces were taken as point forces. Modelling the engine forces as point loads produce slightly different moments and force distribution near the engines location do not significantly influence calculations.
- **No drag is acting on the wing and fuselage:** Since the wing and fuselage box are sized for maximum engine thrust (at takeoff), and during flight the drag force is usually close to or smaller than the thrust force, drag forces are not taken into account for sizing.
- **All forces are carried by the wing and fuselage box:** In reality part of the stresses induced in the wing are carried by the other components present in the wing and fuselage. This assumption means that the wing and fuselage box are slightly over sized but this is of minor influence since for example the leading and trailing edge devices in the wing usually carry a minor portion of the loads present.
- **The stringers present on each of the wing and fuselage box plates are equally spaced:** This allows for symmetry around the  $z$ -axis of the wing and fuselage box for direct stress sizing, or  $I_{xz} = 0$ .
- **The effective length of the stringer is set by the rib spacing and the clamping of stringer is assumed to be pinned:** This means that ribs are reinforced such as to limit the effective length of stringer but do not carry bending moments.
- **A safety factor of 1.5 is applied to the yield stress of the Aluminium 7075-T6 material in the program:** This causes the wing and fuselage boxes to be slightly over-sized, however this safety factor is necessary to deal with the uncertainties of the model.

#### 6.4.1.5. Program flow diagram

To perform the structural sizing of the HUULC, the program built in Mathematica used a certain sequence of inputs and outputs to perform the sizing. Figure 6.27 illustrates the program flow process used for the structural design. The different blocks represented in the flow diagram are explained in the subsequent sub-chapters.

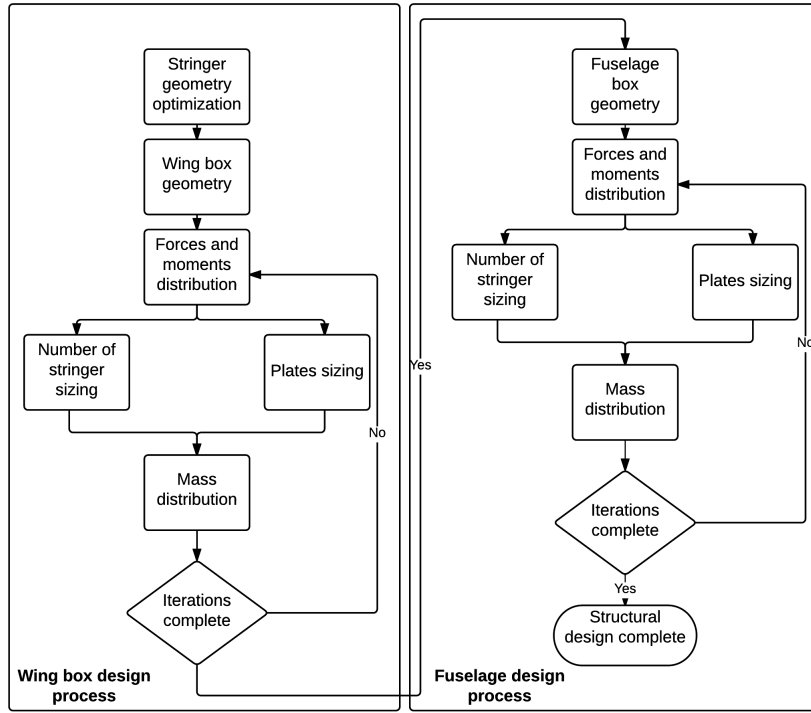


Figure 6.27.: Program flow diagram.

#### 6.4.1.6. Stringer optimisation

Inside the wing box, stringers are the most efficient direct stress carrying components. As previously stated in the assumptions, the stringers carry all the direct stresses. It is thus crucial to optimise their geometry to obtain the best results.

The most beneficial characteristic of a stringer towards its resistance to loads is its inertia. Hence, this value should be maximised. However the stringer cross sectional area should be minimised to reduce the weight of the wing box as much as possible. Thus the chosen optimisation function for the stringer is to maximise the inertia to cross sectional area ratio of the stringer.

The chosen shapes for the stringers used in the wing box are L-shaped stringers as shown in Figure 6.28. The reason for this choice of stringer is its simple shape which allows for cheap manufacturing costs (only one bending operation required), which become crucial due to the size of the HUULC's wing box. From Figure 6.28, the area and inertia properties of this stringer are derived such that:

$$A_s = w_s \cdot t_s + (h_s - t_s) \cdot t_s \quad (6.11)$$

$$I_s = t_s \left[ \left( \frac{h_s^3}{12} \right) + w_s \left( h_s - \frac{h_s^2}{2} + w_s h_s \right)^2 + h_s \left( \frac{h_s}{2} - \frac{h_s^2}{2} + w_s h_s \right)^2 \right] \quad (6.12)$$

To maximise the ratio of inertia to area of the stringer, the `NMaximize` function from Mathematica was used [66]. This function uses multiple optimisation algorithms to find the global maximum of a given objective function under set constraints. For the optimisation of the wing box stringers the following objective function, optimisation variables and constraints were set as listed in Equation (6.13).

$$\left\{ \begin{array}{l} \text{Objective function: } \frac{I_s}{A_s} \\ \text{With optimisation variables: } t_s, h_s, w_s \\ \text{Subjected to constraints:} \\ A_s \geq 0, h_s - t_s \geq 0, w_s \geq 0, t_s \geq 0, h_s \geq 0, t_s \leq 0.01, h_s \leq 0.1, w_s \leq 0.05 \end{array} \right. \quad (6.13)$$

The first five constraints above ensure that the solution is compatible with the geometry of the stringer and that the solution outputs positive values only. The last three constraints define the upper limits of the allowable stringer dimensions set according to usual aircraft stringer dimensions as well as the maximum dimension that would allow the number of stringers to fit inside the wing box.

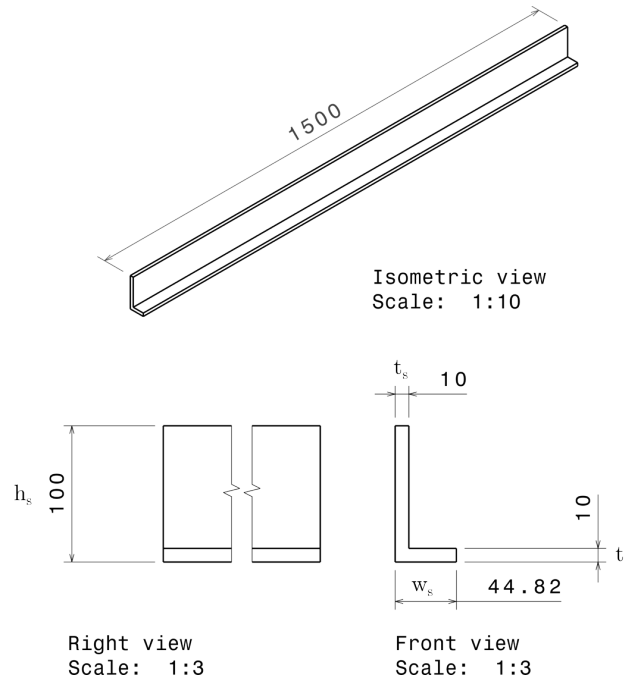


Figure 6.28.: L-stringer dimension for wing box.

Based on this objective function and the given constraints, the results obtained for optimum stringer dimensions are  $t_s = 0.01$  m,  $h_s = 0.1$  m and  $w_s = 0.0448$  m. These dimensions resulted in a maximum inertia to area ratio of  $(\frac{I_s}{A_s})_{max} = 0.001192$ . These optimised stringer dimensions are used for all the stringers present in the wing box. Table 6.12 and Figure 6.28 show the final dimensions of the stringer.

Table 6.12.: Stringer properties used for wing box

	Thickness [m]	Height [m]	Width [m]	Inertia [m <sup>4</sup> ]	Area [m <sup>2</sup> ]
<b>Stringer</b>	0.01	0.1	0.0448	$1.60709 \cdot 10^{-6}$	0.00134823

#### 6.4.1.7. Sizing for direct stresses

This section explains the process and methods used for the sizing of the number of stringers (top, bottom, rear and front stringers) required for the wing box design.

##### Sizing for top and bottom stringers

In order to size the number of stringers for direct stresses induced by bending moments, the moments around the  $x$  and  $z$ -axes were treated separately.

Firstly, the top and bottom stringers were sized to take bending moments around the  $x$ -axis. The stringers were sized to ensure no stringer buckling occurs. Since load factors of 3 and  $-2$  are required for this bending moment (see Figure 6.21), both top and bottom stringers are designed to take the critical buckling stress in compression. Also since the compression load factors between top (load factor 3) and bottom (load factor  $-2$ ) differ, the number of stringers between the top and bottom plates varies.

Figure 6.19 shows the schematic of the distribution of the top and bottom stringers used for sizing. Given the number of stringers present on the top plate ( $n_{top}$ ) and on the bottom plate ( $n_{bot}$ ), the direct stress distribution due to the bending moment  $M_x$  along the vertical axis is given by Equation (6.14).

$$\sigma_y = \frac{M_x}{I_{xx}}(z - \bar{z}) = M_x \frac{1}{n_{top}A_s \left(h - \frac{n_{top}h}{n_{top}+n_{bot}}\right)^2 + n_{bot}A_s \left(-\frac{n_{top}h}{n_{top}+n_{bot}}\right)^2} \left(y - \frac{n_{top}h}{n_{top}+n_{bot}}\right) \quad (6.14)$$

The buckling stress for a stringer is calculated using Euler column buckling Equation (6.15)[64].

$$\sigma_{buck} = \frac{I_s \pi^2 E}{A_s K^2 L^2} \quad (6.15)$$

where  $I_s$  and  $A_s$  are the stringer inertia and area respectively obtained from optimum stringer sizing.  $E$  is the material's Young's modulus of Aluminum 7075 T-6. Also,  $K$  and  $L$  are the clamping constant and the effective stringer length respectively. For buckling stress, a value of one was chosen for the clamping constant as pinned stringers are assumed [64]. A value of  $1.5m$  was chosen for the effective length from the rib spacing.

Now to size the stringers Equations (6.14) and (6.15) are set equal to each other such that:

$$\frac{M_x}{I_{xx}}(z - \bar{z}) = M_x \frac{1}{n_{top} A_s \left(h - \frac{n_{top} h}{n_{top} + n_{bot}}\right)^2 + n_{bot} A_s \left(-\frac{n_{top} h}{n_{top} + n_{bot}}\right)^2} \left(y - \frac{n_{top} h}{n_{top} + n_{bot}}\right) = \frac{I_s \pi^2 E}{A_s K^2 L^2} \quad (6.16)$$

Then to solve for the number of stringers  $n_{top}$  and  $n_{bot}$ , Equation (6.16) is solved for two conditions which are given by Equation (6.17).

$$\begin{cases} M_x(N_{load} = 3) & \text{for } z = h \\ M_x(N_{load} = -2) & \text{for } z = 0 \end{cases} \quad (6.17)$$

These conditions state that the top stringers must comply with a compressive stress with a load factor of 3 and the bottom stringers must comply with a tensile stress with a load factor of  $-2$  (or in other words a compressive stress of load factor 2).

These two conditions given by Equation (6.17) combined with Equation (6.16) form a system of two non-linear equations. Solving it, the required number of top stringer  $n_{top}$  and bottom stringer  $n_{bot}$  is obtained (the `Solve` function from Mathematica was used to solve the non-linear system of equations). Figure 6.29 (left) shows the obtained distribution of required top and bottom stringer obtained along the span ( $y$ -axis). The number of stringers is calculated at each ribspace since the distribution varies along the wingspan.

### Sizing for side stringers

The side stringers (front and rear) are sized for the buckling stress induced by the bending moment around the  $z$ -axis ( $M_z$ ). This yields in an equal number of stringers for the front and rear plate of the wing box. Hence, the number of front and rear stringers are solved in a similar way to the top and bottom stringers but with load factors of 1 and -1. The side stringers number expression can be derived as Equation (6.18). Solving it, the distribution of front and rear stringers along the wingspan can be obtained.

$$n_{front} = n_{rear} = \frac{M_z L^2 K^2}{2E \pi^2 I_s w} \quad (6.18)$$

#### 6.4.1.8. Shear stress optimisation

As previously stated, the shear stresses are assumed to be carried by the wing box plates. To size the wing box, the thickness of the rear and front plates are assumed to be equal and are denoted by vertical thickness  $t_v$ . Similarly, the top and bottom plate are assumed to have a thickness of  $t_h$ . As a result, the shear centre of the skin carrying wing box is located in the geometry centre of the box for every cross section (see Figure 6.19).

To size the plates of the shear stress skin carrying box, the shear flows due to the forces in  $z$  and  $x$  direction as well as the torque around the  $y$ -axis are calculated separately and finally superimposed into a total shear flow  $q_t$ . The equations used to find the shear flow distributions due to the different forces and torque applied on each cross section and the total shear flow  $q_t$  are given by Equation (6.19).

$$\begin{cases} q_z = \frac{-S_z}{I_{xx}} \int_0^s t \cdot s \cdot ds \\ q_x = \frac{-S_x}{I_{zz}} \int_0^s t \cdot s \cdot ds \\ q_{torque} = \frac{T}{2A} = \frac{T}{2wh} \\ q_t = q_z + q_x + q_{torque} \end{cases} \quad (6.19)$$

The final step is the optimisation. From the model of shear flow two variables could be optimised which are the horizontal  $t_h$  and vertical thickness  $t_v$ . Varying these two variables completely change the shear flow distribution along the plates of the cross sections. As a result to optimise these dimensions, an objective optimisation function was defined.

Since the plates run along the entire span of the wing box, the objective function was set as the summed cross sectional area of all the plates at a certain  $y$  location. Similar to what was done for the stringer optimisation; the function `NMinimize` was used to find the global minimum of the total area of plates objective function subject to constrains.

Note that minimising the total area of the plates of each cross section is equivalent to minimising the weight of the plates in each cross section since the same material is used throughout the wing box. These constraints include non-negative constraints such that the `NMinimize` function only output the global minimum for positive thickness values. The other constraints ensure that the yield stress of the material is not exceeded at the location of maximum shear flow in each cross section.

The minimisation optimisation functions and constrains can be written as:

$$\begin{cases} \text{Objective function: } f = \min(A_p) = \min(2 \cdot h \cdot t_v + 2 \cdot w \cdot t_h) \\ \text{Subjected to: } \frac{\max(q_t)}{t} \leq \tau_y, t_h \geq 0, t_v \geq 0 \end{cases} \quad (6.20)$$

Using this optimisation function, the required horizontal and vertical plates thickness  $t_h$  and  $t_v$  required to obtain minimum total plate area (or weight) were obtained for each cross section and can be seen in Figure 6.29 (right) as a function of  $y$  (along the span). The plates thicknesses are calculated along the wingspan at every ribsapce interval. Also, the stringer distribution along the wingspan is shown in Figure 6.29 (right).

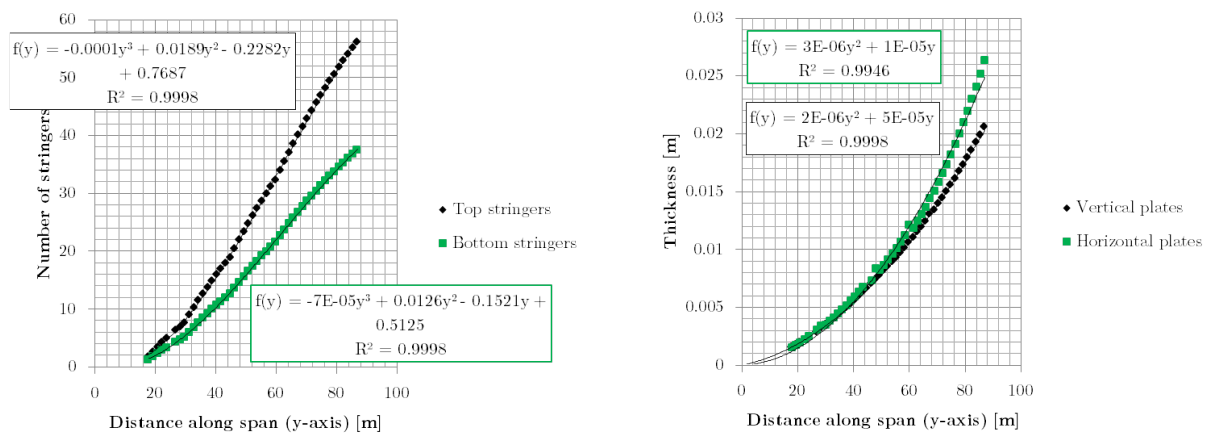


Figure 6.29.: Number of stringers (left) and plates sizing (right) along the wingspan (1<sup>st</sup> iteration).

#### 6.4.1.9. The iteration process

In the previous sections, the structural elements had only to cope with the lift and engine forces. However, the weight of these structural elements should be also taken into account. Hence, an iterative process was conducted to improve the sizing and weight results.

Firstly, an initial wing box sizing is obtained without including the structural elements weight distribution as illustrated in Figure 6.29. Afterwards, the results of this initial sizing are used to construct an initial mass distribution function (as shown in Figure 6.30, left) for the structural elements of the wing box, which is fed back as a force distribution in the program to resize the wing box, to obtain a new mass distribution and so on. This cycle is repeated for three times. The schematic of this process for the wing box can be seen in the program flow diagram in Figure 6.27.

Figure 6.30 (right) shows the new mass distribution obtained after the iteration cycle was completed once. The cycle is repeated once more (iteration three) to obtain the final sizing of the wing box. Figures 6.31 and 6.32 (left) show the results obtained for the number of stringers required, plate thicknesses and mass distribution of the final (third) iteration of the wing box. The results given by these figures were then used to size the final wing box for the HUULC aircraft.

In Figure 6.32 (right), the percentage reduction in mass of the fuselage box at every ribsection between the initial mass distribution (iteration one, shown in Figure 6.30) and the final mass distribution (iteration three, as in Figure 6.32, left) can be seen. As expected, the highest reduction in mass occurs near the root of the wing box where the bending moments are the highest.

Table 6.13 shows the total wing box mass obtained at each iteration. The reason for stopping after three iterations is because the percentage difference between iterations three and two is already  $-0.14\%$  and thus increasing the number of iterations would barely change the results. From Table 6.13, it can be seen that due to the iteration process a total mass reduction of  $-1.828\%$  is obtained when compared to the initial mass estimated (iteration one). This shows that the mass of the wing box itself contributes quite significantly to the sizing of the wing box. As can be seen the final total weight of the wing box obtained from the last iteration is  $98,576.75\text{ kg}$  and is used for all further calculations.

Table 6.13.: Iteration results for wing box sizing.

	Iteration 1 (initial)	Iteration 2	Iteration 3 (final)
Total mass [kg]	100,378.4	98,723.57	98,576.75
Percentage difference between iterations [%]	0	-1.676	-0.149
Percentage total mass reduction with respect to iteration 1 [%]	0	-1.676	-1.828

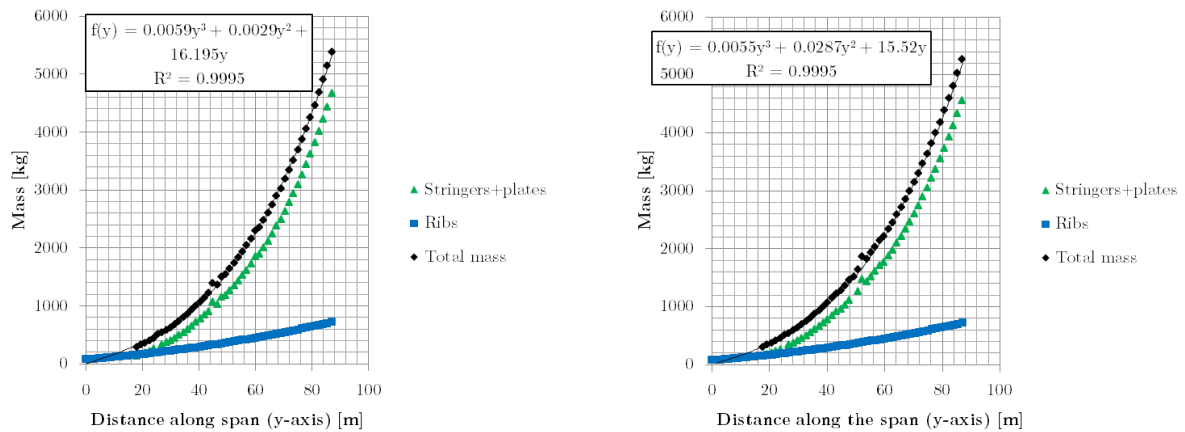


Figure 6.30.: Initial mass distribution of the wing box (left, 1<sup>st</sup> iteration) and after one cycle (right, 2<sup>nd</sup> iteration).

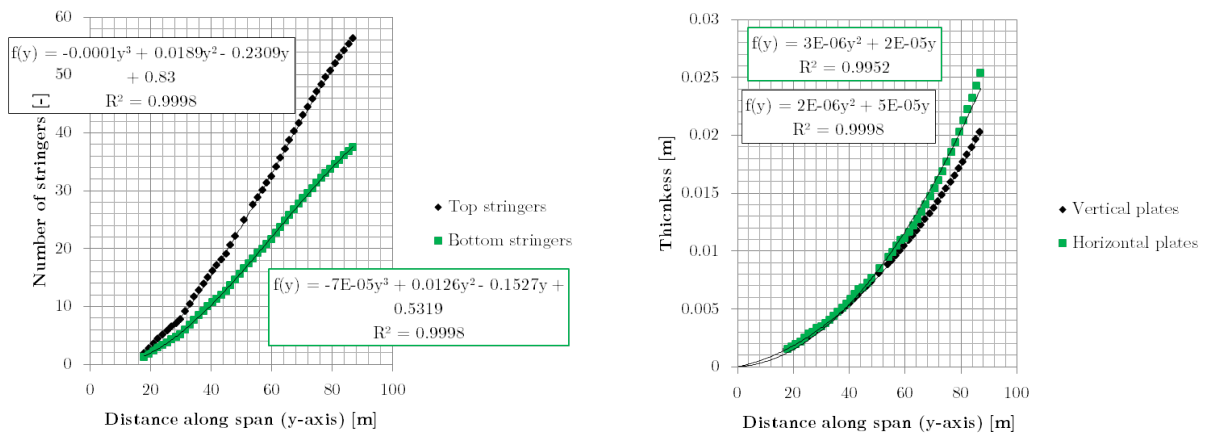


Figure 6.31.: Final number of stringers (left) and plate sizing (right) along wingspan (3<sup>rd</sup> iteration).

## 6.4.2. Fuselage sizing

For the next step of structural design, the fuselage box was designed. The following section explains the entire process for the structural sizing of the fuselage box. The section starts by defining the reference frame used, the force and are then modelled followed by the sizing of the different components (stringers and plate) of the fuselage box and finally the structural iteration process is explained.

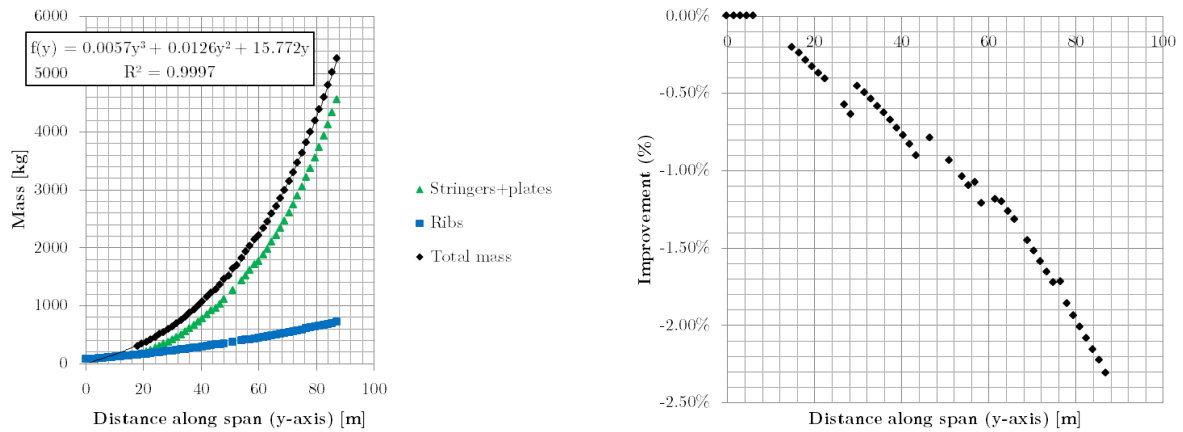


Figure 6.32.: Left: Final mass distribution of the wing box (left, 3<sup>rd</sup> iteration). Right: percentage mass reduction at every rib section along the wingspan ( $y$  axis) between iteration one and three.

#### 6.4.2.1. Reference frame

The reference frame chosen to size the fuselage box is a 3-axis inertial system with origin placed at the bottom left corner of the fuselage box-cross section at the beginning of the fuselage box, that is, at the intersection between the wing box root and the fuselage box. The  $z_f$ -axis points in the vertical direction of the cross section parallel to the vertical spars. the  $x_f$ -axis runs along the bottom of the cross section perpendicular to the  $z_f$ -axis. Finally, the  $y_f$ -axis point perpendicular to the  $z_f - x_f$  plane in the direction of the centre of the fuselage box. The reference frame used for the fuselage can be seen in Figure 6.33.

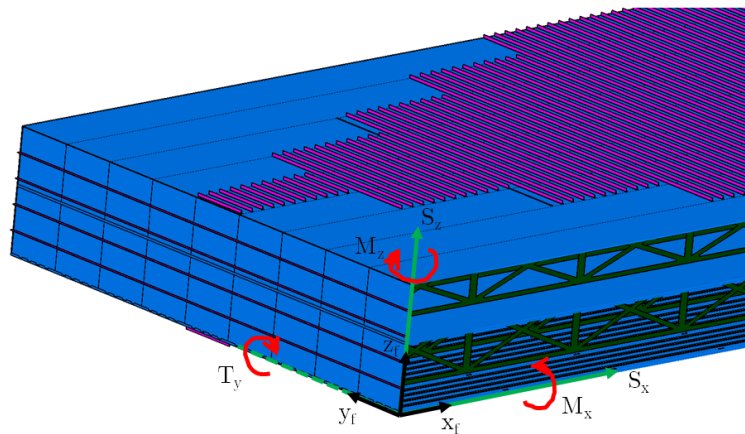


Figure 6.33.: Fuselage box axis system and moment and forces convention.

#### 6.4.2.2. Fuselage box geometry

The fuselage box is modelled in a way similar to the wing box however for the box fuselage the geometrical properties such as length, width and height of the fuselage box are constant. Fuselage ribs run along the longitudinal direction of the fuselage and their spacing are defined by the width of the payload containers. Figure 6.34 shows the setup of top, bottom, rear and front stringers as well as the shear carrying plates inside the wing box.

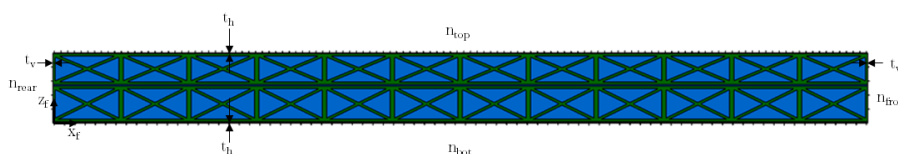


Figure 6.34.: Fuselage box cross section.

### 6.4.2.3. Force discovery and modelling

For the fuselage box, the forces and moments present at the root of the wing are transmitted to the fuselage box via the interface of both boxes. Since moments and forces transmitted from the wing are required for the fuselage sizing, the wing box sizing must be completed before the fuselage box can be sized (Figure 6.27). Once again, the fuselage box is sized according to the load factors introduced in the wing box design in figure 6.21. The different load cases experienced by the fuselage are explained below:

**Forces and moments transmitted by the wing:** At the intersection between the fuselage and wing box, the load carried by the wing box are transmitted to the fuselage. These load include the shear forces, bending moments and torque that act at the root of the wing box. These forces and moments act at the geometric centre of the root cross section of the wing box and are taken into account in the Mathematica script.

**Lift distribution of the fuselage:** Since the HUULC has been designed as a blended wing body aircraft, a lift distribution is present on the fuselage. From the aerodynamic analysis of the HUULC (see section 6.2), the lift distribution over the fuselage was modelled as a quadratic distribution. Once again the lift distribution over the fuselage is placed at the quarter chord line of the fuselage.

**Payload and hydrogen weight:** These are known and given from section 6.1. Since the mass distribution of payload and hydrogen within the fuselage bay are uniform on the  $y_f - x_f$  plane, the forces induced by the payload and hydrogen mass are modelled within the script as uniform distributed force along the  $y_f$  axis of the fuselage box.

**Structural weight:** The weight distribution of the fuselage box itself was also accounted for. An initial fuselage box sizing was performed based solely on the other load cases described previously. Based on this initial sizing, the weight distribution was modelled and added to the load calculations. This triggers an iterative process which is described in detail in the upcoming sections. The weight distribution of the fuselage box is assumed to be acting in the centre of the fuselage box at every cross section. This positioning arises from the fact that the fuselage box centroid (or equivalently, centre of mass, since the density of material is the same everywhere in the fuselage box) is located in the geometric centre of every cross section.

**Landing gear:** Once again due to the late design of the landing gears, the forces induced by the landing gears on the fuselage are not included in the script. If the landing gears were modelled in the script, shear forces and bending moments would be induced. Also due to the offset of the landing gears from the centroid of the wing box, additional torque can be expected. The landing gears are more influential in the fuselage box design rather than in the wing box since more landing gears are present over the fuselage.

**Forces due to the horizontal tail and rudder:** The horizontal tail of the aircraft generates a lift distribution itself causing a bending moment and a torque due to the offset of the position of the tail to the centre of the fuselage box. Due to the late design of the horizontal tail however, the force induced by this subsystem could not be integrated into the script. We can expect the horizontal tail contribution to influence quite significantly the stresses within the fuselage and should be taken into account in the future. The lift force due to the horizontal tail would then be modelled as a distributed force acting at quarter chord line of the horizontal tailplane. Also the horizontal tail and rudder mass have an influence that should be taken into account however, the mass of both of these subsystems were not computed at this stage of the design and could not be implemented in the model either.

**Other forces:** Moreover, a series of forces were not included into the load model that act on the fuselage. These include the weight of the skin, but also the loads exerted by the hydraulics and other subsystems (such as the unmanned subsystem) attached to the fuselage box frame. To introduce such loads into the model, a more refined design of these subsystems should be performed to determine their exact position and mass distribution. Since these load cases could not be considered, the bending moments, the shear forces and torques modelled are undersized.

Figure 6.35 shows the modelling of the forces and moments present on the fuselage box. Also shown in Figures 6.36, 6.37 and 6.38 are the force and moments distribution present on the fuselage box.

Figure 6.22 shows the totality of the forces that would in reality be acting upon the fuselage. This diagram shows the forces included in the script model as well as the ones not included but stated previously.

### 6.4.2.4. Stringer sizing

For the fuselage box, the stringer geometry was chosen to be different than the stringer geometry of the wing box however the same L-shaped stringer was used as shown in Figure 6.28. This choice was made due to geometrical constraints set by the fuselage box size. The fuselage box stringers were based on a new of constraint given by 6.21.

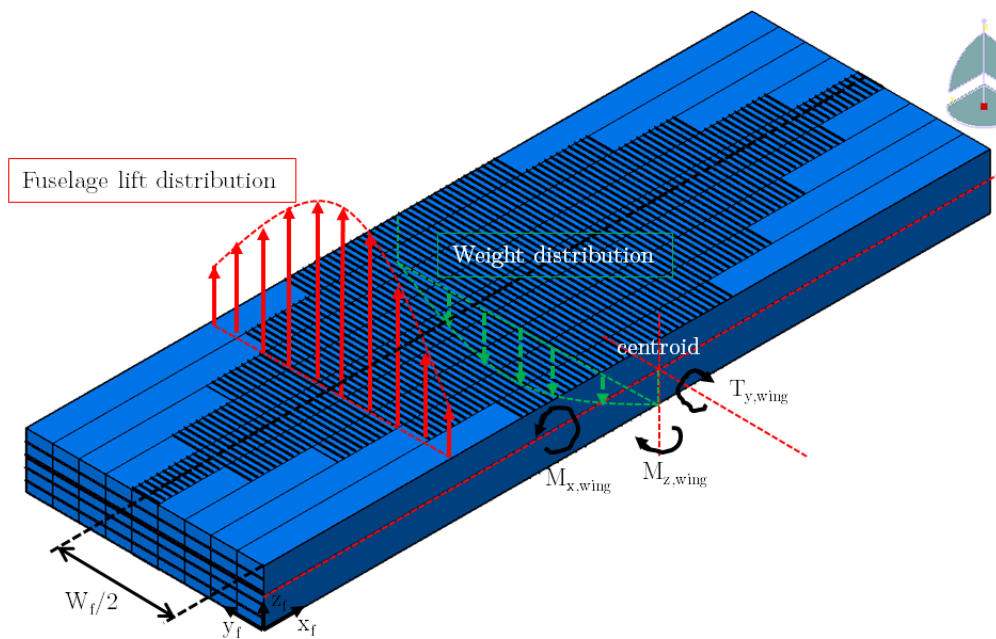


Figure 6.35.: Modelling of forces present on fuselage box.

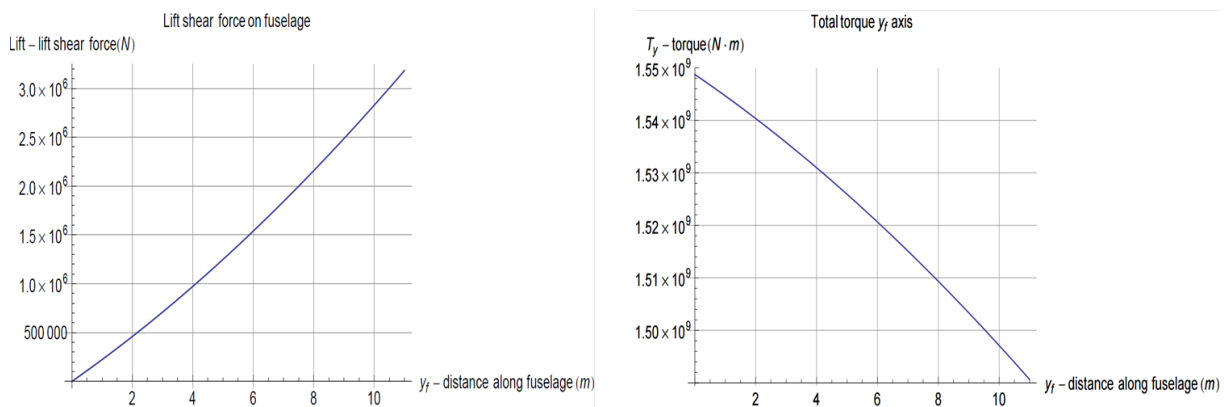


Figure 6.36.: Lift shear distribution (left) and Torque about  $y$ -axis (right) of fuselage box.

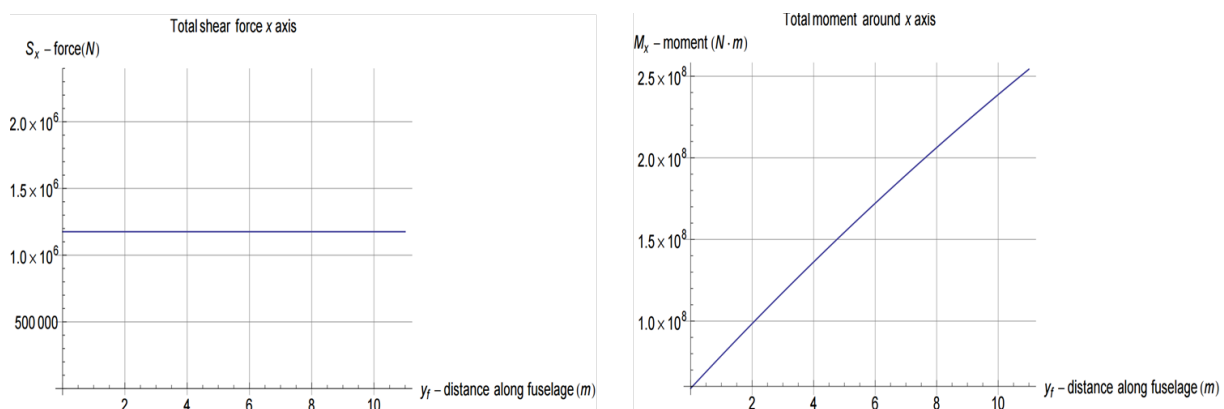


Figure 6.37.:  $x$ -axis diagrams of fuselage box:  $x$  shear (left),  $x$  moment (right).

$$\left\{ \begin{array}{l} \text{Objective function: } \frac{I_s}{A_s} \\ \text{With optimisation variables: } t_s, h_s, w_s \\ \text{Subjected to constrains:} \\ \quad A_s \geq 0, h_s - t_s \geq 0, w_s \geq 0, t_s \geq 0, h_s \geq 0, t_s \leq 0.015, h_s \leq 0.15, w_s \leq 0.1 \end{array} \right. \quad (6.21)$$

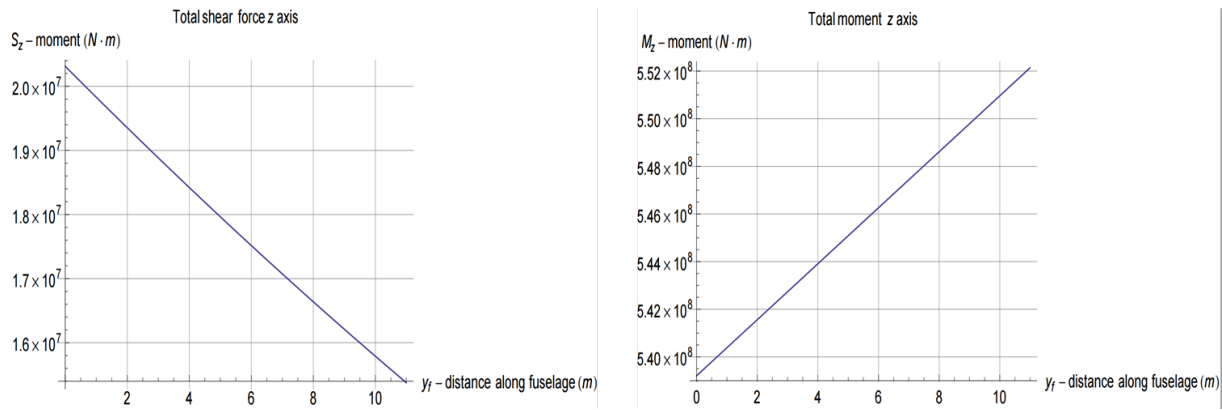


Figure 6.38.:  $z$ -axis diagrams of fuselage box:  $z$  shear (left),  $z$  moment (right).

Based on this objective function and the given constraints, the results obtained for optimum stringer dimensions of the fuselage box are  $t_s = 0.015 \text{ m}$ ,  $h_s = 0.15 \text{ m}$  and  $w_s = 0.0672314 \text{ m}$ . These dimensions resulted in a maximum inertia to area ratio of  $(\frac{I_s}{A_s})_{max} = 0.002682$ . These optimised stringer dimensions are used for all the stringers present in the fuselage box. Table 6.14 shows the final dimensions of the stringer.

Table 6.14.: Fuselage box stringer properties.

	Thickness [m]	Height [m]	Width [m]	Inertia [m <sup>4</sup> ]	Area [m <sup>2</sup> ]
<b>Stringer</b>	0.015	0.15	0.0672314	$8.13576 \cdot 10^{-6}$	0.00303347

For the top and bottom sizing of the fuselage stringers, the same method as the one used for the stringer sizing of the wing box was used. Once again the load factors of 3 for the top stringer and -2 for the bottom stringers were used. The stringers are designed for every fuselage rib section using Equation 6.16.

The number of front and rear stringers is obtained using Equation 6.18 with the moment distribution around the  $z$ -axis induced in the fuselage box.

Figure 6.39 (left) shows the obtained distribution of required top, bottom and side stringers obtained along the fuselage box ( $y_f$  axis). The number of stringers is calculated at each ribspace since the stringer are set to vary only after every ribspace distances in the fuselage box design. Also, the stringer distribution shown in Figure 6.39 (left) shows the required stringer distribution for half of the fuselage, such that the  $y_f$ -axis extends until the centre fuselage box. The distribution can be mirrored around the centre of the fuselage to obtain the entire stringer distribution of the fuselage box since the aircraft is symmetric around the centre of the fuselage box (see Figure 6.35).

#### 6.4.2.5. Plates sizing

For the sizing of the lateral plates, the plates are sized using the same approach as the one used for the plate sizing of the wing box. The obtained required thickness distributions for the horizontal and vertical plates of the fuselage box are shown in Figure 6.39 (right).

#### 6.4.2.6. Iteration process

Similar to the wing box iteration process, the obtained mass distribution of the the initial sizing of the fuselage box model (Figure 6.40, left) is fed back into the model to obtain a more accurate estimation of the fuselage box total mass distribution. Once again the iteration process is stopped after three iterations when the difference between the second and third iterations is negligible. The schematic of this process for the fuselage box can be seen in the program flow diagram in Figure 6.27.

Figure 6.40 (right) shows the new mass distribution obtained after the iteration cycle was completed once. The cycle is repeated once more (iteration three) to obtain the final sizing of the fuselage box. Figures 6.41 and 6.42 (left) show the results for the number of stringers required, plate thicknesses and mass distribution of the final (third) iteration of the fuselage box. The results given by these figures were then used to size the final fuselage box for the HUULC aircraft. Note that the Figures 6.41 and 6.42 (left) give the the number of stringers required, plate thicknesses and mass distributions of half of the fuselage (from root of the wing-box to

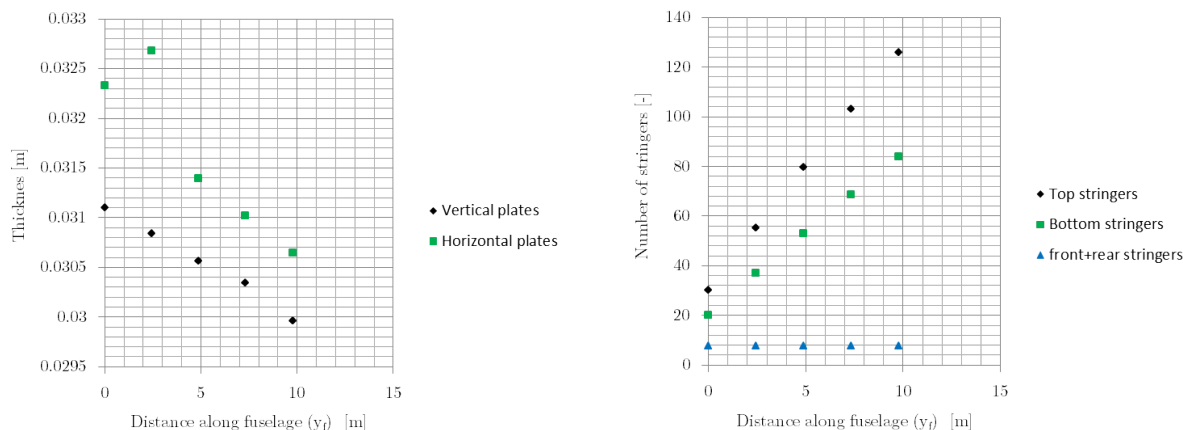


Figure 6.39.: Number of stringer (left) and plates sizing (right) required per ribsection along fuselage box (iteration one).

centre of fuselage box), these distributions can be mirrored around the centre of the fuselage box to obtain the entire sizing of the fuselage box.

In Figure 6.42 (right), the percentage reduction in mass of the fuselage box at every ribsection between the initial mass distribution (iteration one, 6.40, left) and the final mass distribution (iteration three, 6.42, left) can be seen. As expected, the highest reduction in mass occurs at the centre of the fuselage where the bending moments are the highest.

Table 6.15 shows the total fuselage box mass obtained at each iteration (complete fuselage box). The reason for stopping after three iteration is because the percentage difference between iterations three and two is already 0.0507% and thus increasing the number of iteration would barely change the results. Also from Table 6.15, it can be seen that due to the iteration process a total mass reduction of  $-0.716\%$  is obtained when compared to the initial mass estimated (iteration one). This shows that the mass of the wing box itself contributes quite significantly to the sizing of the wing box. As can be seen the final total weight of the fuselage box obtained from last iteration is 203,618.6 kg and is used for all further calculations.

Table 6.15.: Iteration results for fuselage box sizing.

	Iteration 1 (inital)	Iteration 2	Iteration 3 (final)
<b>Total mass [kg]</b>	205,076.6	203,515.4	203,618.6
<b>Percentage difference between iterations [%]</b>	0	-0.767116395	0.050682993
<b>Percentage total mass reduction with respect to iteration 1 [%]</b>	0	-0.767116395	-0.716044605

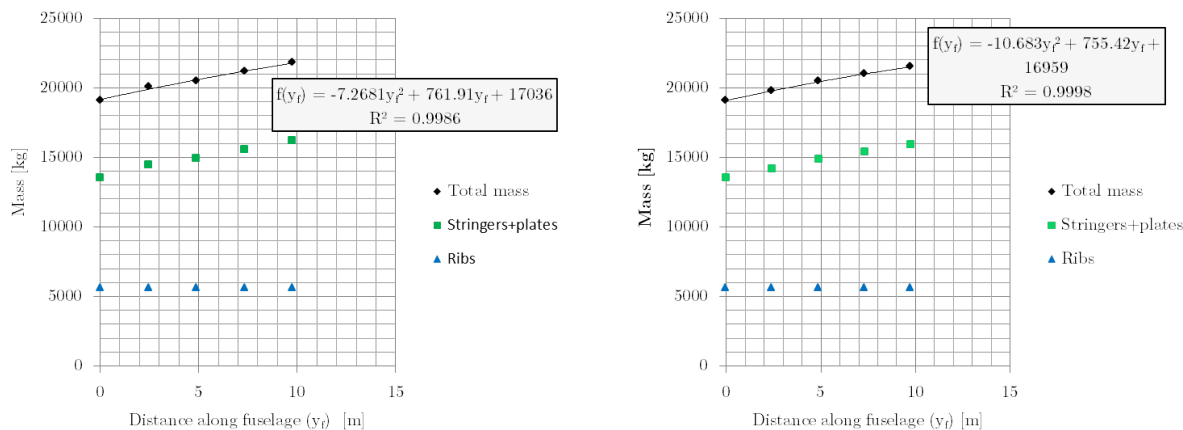


Figure 6.40.: Initial mass distribution (left, iteration one) and mass distribution after one cycle (right, iteration two) of the fuselage box.

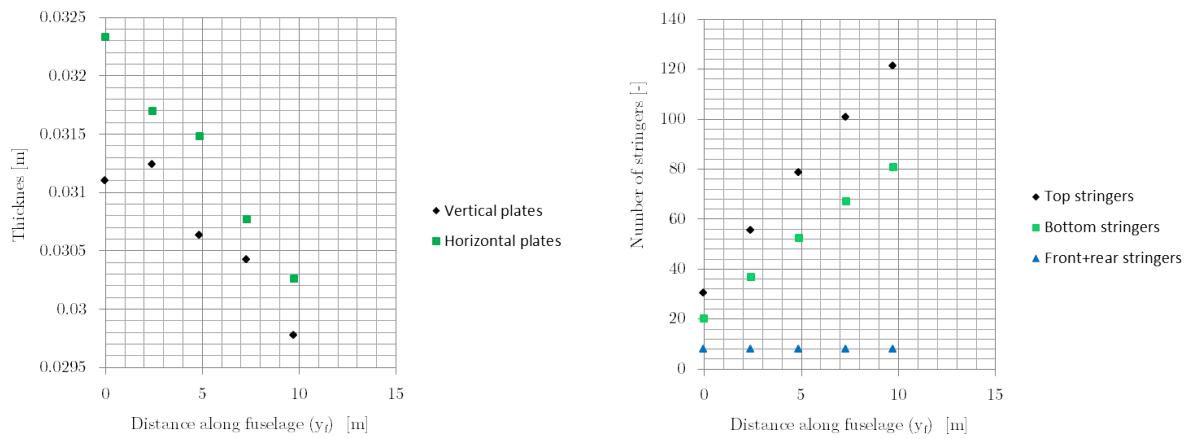


Figure 6.41.: Final number of stringers (left) and plates sizing (right) required per ribsection along fuselage box (iteration three).

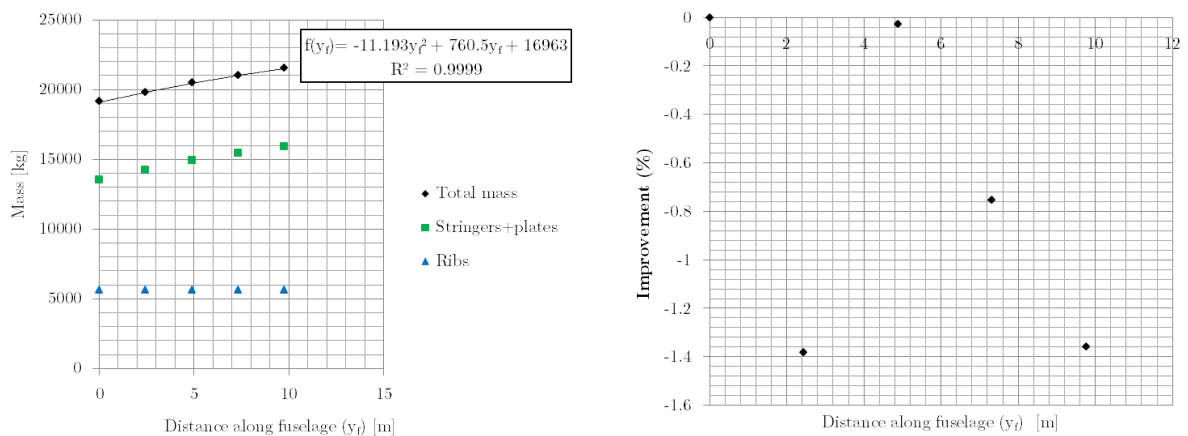


Figure 6.42.: Final mass distribution of the fuselage box (iteration 3, left) and percentage mass reduction (or improvement) at every rib section along the fuselage box width ( $y_f$  axis) between iteration 1 and 3 (right).

### 6.4.3. Conclusion and recommendations

Combining the total mass obtained from the final iteration of the wing box and fuselage box, the total wing box plus fuselage box mass inside the aircraft was found to equal 400,772.1 kg.

It should be noted that in the obtained results for the number of stringers and plate sizing required for the wing box (Figures 6.29 and 6.31), some of the result points near the tip of the wing box and the location of the engines were removed as they showed outliers. This is because the optimisation functions `NMinimize` and `NMaximize` as well as the non-linear solver `Solve` do not converge for small solution values and shows peaks near the engine locations (this is because engines are modelled as point loads and thus create “jumps” in the force and moment distributions, in reality engines are a distributed loads and thus should not create these peaks in the results) and thus equations fit were used to interpolate the result based on the obtained result points without outliers.

As was stated in the force modelling of the wing box and the fuselage box, a significant range of forces were not yet included in the script. These include, the landing gears, the horizontal tail, the high lift devices, ailerons and other subsystem. Since these subsystems were designed at a late stage of the HUULC design, due to time constrain and the need for a more refined design of such subsystems it was not possible to implement them into the structural sizing script. As a result it can be expected that the actual structural mass of wing and fuselage box obtained will change as compared to the mass obtained (400,772.1 kg). For the future, once these forces will be well defined, a more accurate mass of the wing and fuselage box will be obtained.

In the wing and fuselage box model presented in this section, the fuselage was assumed to carry the bending loads induced in the wing. Upon further research (see reference [67] and [68]) it is stated that in case of a blended wing body aircraft configuration, the bending moment induced by the wing should not be carried by

the fuselage box structure. This is mainly because transferring the bending loads carried by the wing box to the modelled fuselage box would drastically increase the fuselage box weight.

In a conventional aircraft configuration, a centre box cutting through the fuselage or passing above or under it carries the bending load introduced by the wings. In our case, due to the position of the wing with respect to the fuselage, the only option would be to integrate a centre box cutting through the payload and hydrogen bay. This however is not possible, since cutting through the payload bay would prevent the loading and unloading of cargo. A solution presented by the reference [67] would be to keep the internal structure as a wing box and a fuselage box as was modelled in this chapter but construct a wing-fuselage transition structure that would drastically reduce the bending moments transmitted by the wing to the fuselage. The proposed solution in this case would be to use a system of shear panels at the location of the wing-fuselage transition to transfer bending moments from the wing as torsional moments to the fuselage box. This solution takes advantage of the geometry of the blended wing body and would be more adapted than a conventional centre box. Due to limited time and the complexity associated with the design of this shear panel structure (without using a FEM software), this solution could not be implemented or designed. However, for the future such a structure should be designed to prevent bending load from the wing to be transmitted to the fuselage and thus reduce the computed fuselage box weight significantly.

Another recommendation that could be made is the use of an alternative material or a combination of materials that could be used to design the wing and fuselage box. Aluminium 7075 T-6 was chosen here due to its high strength properties and its wide use in the aircraft industry over the years. However aircraft industry nowadays tends more towards the use of composites in the structural design of an aircraft due to the high strength and low density properties of composites. It would therefore be beneficial to investigate the use of such composite materials in the wing and fuselage box design of the HUULC to assess their feasibility. However, mainly due to the huge complexity that would be required to implement composites or multi-material distribution (to due anisotropy and fibre orientation for example) in the script used for the wing and fuselage box sizing, this was judged to be out of the scope of the preliminary HUULC design. In a more advanced design of the HUULC, using for example an industrial Finite Element software that would include the possibility to use of carbon fibre in the structural design would allow to investigate the possible use of multi-materials and composites.

A verification process is missing in this chapter but due to the complexity of the written code used in the structural sizing a verification was judged unfeasible. The reason of this is that the Mathematica code built includes global optimisation function such as `NMinimize` and `NMaximize` as well as non-linear equation systems in the stringer sizing using the function `Solve`. Since these functions are near impossible or very difficult to reproduce by hand or on other software such as Excel or Python, a simple verification is unfeasible. To perform an effective verification, a more advanced Finite Element Method (FEM) software should be used.

To conclude, quite some improvements could be made to the wing and fuselage box model, especially in the modelling of the forces acting over the wing and fuselage boxes. However as was stated before, the reason why forces induced by subsystems such as high lift devices, landing gears, horizontal tail and other subsystems could not be implemented into the structural sizing model was either due to the late design of such subsystems or the lack of information (such as location and mass) of such subsystems (see figure 6.22). Once all the subsystems have enough information to implement them into the script, they will be implemented in the future. Also the model should be improved by implementing a wing-fuselage box transition structure such that the fuselage box does not carry bending moments from the wing. The transition structure should be designed in a more advanced Finite Element software. Overall even though improvements should be made in the future and more time should be allocated for the structural design, it is believed that the overall sizing model is correct and should be further developed.

## 6.5. Weight and balance

The design of the empennage and sizing of the landing gear depends on the centre of gravity location. This however depends on the location of the empennage and the landing gear. The determination of centre of gravity location and the sizing of the empennage and landing gear is therefore done in an iterative manner. The c.g. positioning is discussed in this chapter. First the weight breakdown is discussed in Section 6.5.1 after which the c.g. location is determined in Section 6.5.2.

### 6.5.1. Weight breakdown

The weight breakdown is done according to the steps presented in Roskam [57]. The mission weights of the aircraft have been determined and discussed in Section 6.1.2. These weights are used to determine the weight breakdown. As also mentioned in Section 6.1.2, the category that is used for reference aircraft is the one for large military transporters. This category is therefore also used for the weight breakdown of the HUULC aircraft. It has to be noted that the weight fractions that are taken from this category are adjusted for the blended wing

body configuration of the HUULC.

The next step is to define the important aircraft components that have to be taken into account in the weight breakdown. A list of these components can be found in the first column of Table 6.16. Weight fractions are mentioned for each of these components in [63]. However these fractions are for a kerosene powered aircraft with a conventional configuration. The fractions therefore need to be adapted for the HUULC aircraft. Not all fractions are estimated using the data from Roskam [63]. Some component weights have already been estimated during the structural sizing and during the propulsion system design of the HUULC. These are the weights of the wing, the fuselage and the engines. When looking at the fractions of these components it can be seen that the fractions seem reasonable for a blended wing body. The wing weight to takeoff weight ratio is normally about 9 to 10% for a conventional configuration. For a blended wing body, the wing takes up more of the takeoff weight. Therefore this fraction was estimated to be approximately 15% of the takeoff weight. From the structural sizing calculations, it followed that the wing structure will take up approximately 9% of the maximum takeoff weight. This is excluding the skin of the structure. Therefore the weight fraction of the wing was taken as 12.5% to account for the skins. The statistics show that the fuselage usually takes up about 11% of the takeoff weight. However the fuselage is normally pressurised. The fuselage of the HUULC aircraft is not pressurised and thus this fraction can be reduced. It should be taken into account that the fuselage is still significantly larger than the fuselage of a conventional configuration. The weight fraction was therefore set to 9%. The weight estimation from the structural design procedure showed that the weight fraction is 9.7%. Finally the engine weight was estimated by looking at existing engines and extrapolating to find an approximation for the weight. Other fractions that were taken from Roskam [63] but that were adapted are for example the landing gear and fuel system. The landing gear will be significantly larger and heavier for an aircraft like the HUULC than for a conventional aircraft such as the B747. The loads acting on the landing gear are very large and thus a lot of wheels are required. These wheels are needed not just to take up all the loads during landing and providing enough redundancy but also to not inflict any damage on the runway. The fuel system was also designed specifically for the HUULC aircraft. The aircraft uses cryogenic hydrogen as fuel. The fuel needs to be kept at a certain pressure and it needs to stay at very low temperatures. Therefore the tanks need to be pressurised and insulated which adds a lot of extra weight. This weight has been estimated and is discussed in Section 6.1.7. All other weight fractions and their corresponding weights can also be found in Table 6.16.

Number	Component	Fraction Estimated	Weight [kg]
	<b>Flight Design Gross Weight</b>		<b>2092389</b>
I	Structural Weight $W_{struct}$	0.275	575,407
1	Wing	0.125	261,549
2	Empennage	0.005	10,462
3	Fuselage	0.097	202,962
4	Nacelles	0.003	6,277
5	Landing Gear	0.045	94,158
5.1	Nose Gear	0.005	10,462
5.2	Main Gear	0.040	83,696
II	Powerplant Weight	0.034	71,230
1	Engines and Propellers	0.013	26,800
2	Air Induction System	0.001	2,092
3	Fuel System	0.020	42,338
III	Fixed Equipment Weight	0.031	64,864
	Empty Weight	0.335	701,129
IV	Trapped Fuel and Oil $W_{tfo}$	0.001	2,092
V	Fuel Weight $W_f$	0.067	141,026
VI	Payload Weight $W_{pay}$	0.597	1,248,140
	Weight Breakdown Estimated Takeoff Weight	1.005	2,102,759
	Class I estimated Takeoff Weight	1.000	2,092,387

Table 6.16.: Weight Breakdown of the HUULC aircraft.

After assigning the weights to all components, the new maximum takeoff weight could be calculated. Several iterations were done by reallocating the weight until the difference between the new takeoff weight and the takeoff weight that was estimated with the class I method was less than 1%. Resulting in a difference of 0.05%.

### 6.5.2. Weight and balance calculation

Once all major component weights are determined they can be used to locate the centre of gravity of the aircraft. For each of these components, the c.g. was determined. The distances of these centres of gravity were taken with respect to the nose of the aircraft. And a reference line that is 4.2m below the fuselage. Each of the

components with their corresponding weights and coordinates are stated in Table 6.17. Since the aircraft is symmetric along the  $XZ$ -plane, the  $y$ -coordinates are zero and are therefore not shown in the table.

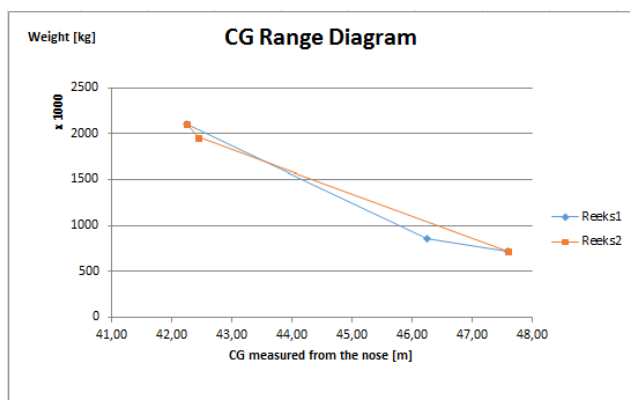
Component	Weight kg	x m	c.g. x m	z m	c.g. z m
Wing	$2,62 \cdot 10^5$	50.8	-	10.4	-
Empennage	$1.04 \cdot 10^4$	93.0	-	15.2	-
Fuselage	$2.03 \cdot 10^5$	50.0	-	10.4	-
Nacelles & Engine Pair 1	$8.79 \cdot 10^3$	40.7	-	10.4	-
Nacelles & Engine Pair 2	$8.79 \cdot 10^3$	48.4	-	10.4	-
Nacelles & Engine Pair 3	$8.79 \cdot 10^3$	52.8	-	10.4	-
Nacelles & Engine Pair 4	$8.79 \cdot 10^3$	56.4	-	10.4	-
Nose Gear	$1.04 \cdot 10^4$	7.00	-	3.93	-
Main Gear	$8.37 \cdot 10^4$	52.5	-	4.76	-
Fixed Equipment	$6.49 \cdot 10^4$	50.0	-	10.4	-
Fuel System	$4.23 \cdot 10^4$	39.5	-	11.8	-
Empty Weight	$7.12 \cdot 10^5$	-	47.6	-	9.09
Trapped Fuel and Oil	$2.09 \cdot 10^3$	39.5	-	11.8	-
Fuel	$1.41 \cdot 10^5$	39.5	-	11.8	-
Operating Empty Weight	$8.55 \cdot 10^5$	-	46.2	-	9.54
Payload	$1.25 \cdot 10^6$	39.5	-	8.71	-
Takeoff Weight	$2,10 \cdot 10^6$	-	42.2	-	9.05

Table 6.17.: Centre of gravity position of the HUULC for different mission weights.

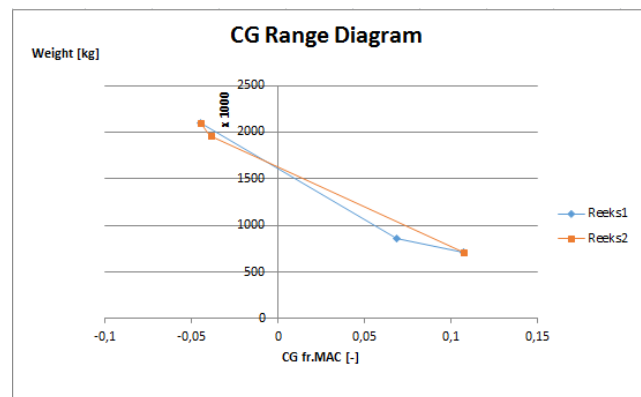
Once the c.g. position is known, it can be determined for different cases. The cases that are considered are:

- Empty Weight
- Operational Empty Weight
- Takeoff Weight

There are two loading sequences that are considered for the HUULC. Starting at the empty weight, the fuel or the payload can be loaded first. The blue line in Figure 6.43a indicates the sequence empty weight + fuel weight + payload weight. The orange line shows the sequence empty weight + payload weight + fuel weight. Figure 6.43a indicates the c.g. excursion diagram expressed in meters while Figure 6.43b shows the center of gravity excursion expressed as a fraction of the mean aerodynamic chord. From these figures it can be seen that the most forward c.g. position is at 42.2 meters from the nose while the most aft c.g. position is at 47.6 meters from the nose. The difference falls within 30% of the mean aerodynamic chord fraction.



(a) Centre of gravity excursion diagram in meters.



(b) Centre of gravity excursion diagram as a fraction of the MAC.

Figure 6.43.: Centre of gravity excursion diagrams.

### 6.5.3. Conclusion and recommendations

From the weight breakdown several components have been estimated by calculations from the structural sizing or the propulsion system design while other component weights are estimated by using weight fractions. Once

all weight components were known, the centre of gravity was estimated for each of these components. With the component weight and centre of gravity coordinates, the centre of gravity of the entire aircraft was estimated. The c.g. ranges from 42.2 to 47.6 meters.

A recommendation is to estimate the weight of each component by calculations. At this point this was done for only the main components. By calculating the weight for each component, a more accurate weight breakdown can be done. The same holds for the weight and balance calculations. If the component weights are more accurate, the estimation of the c.g. location is also more accurate.

## 6.6. Stability and control

A stability analysis was done using the aerodynamic model of the HUULC in XFLR5. The symmetric and asymmetric eigenmotions are analysed. This is done in Subsection 6.6.2 and 6.6.3 respectively.

### 6.6.1. Stability and controllability

To ensure that the HUULC is stable and controllable, an empennage is designed. The design of the empennage system can be found in Section 6.7.6. Figure 6.44 shows the static stability characteristics of the HUULC. The blue continuous line represents the HUULC without an empennage and the red striped line represents the stability curve of the HUULC with tail. The blue continuous line shows a negative slope and a negative  $C_{m_{ac}}$  value. This indicates that the aircraft without tail is stable but hard to control. Adding the tail leads to the red striped curve. The positive  $C_{m_{ac}}$  value and the negative slope of the curve indicate that the aircraft is both stable and controllable.

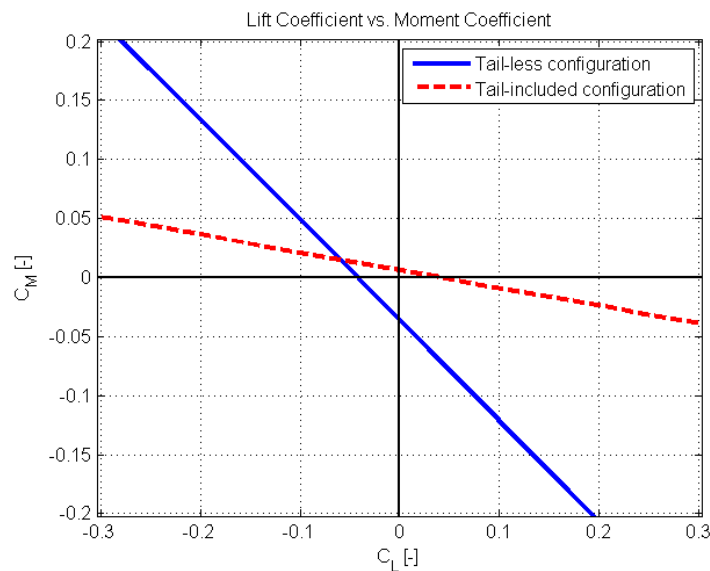


Figure 6.44.: Lift coefficient versus moment coefficient plot.

### 6.6.2. Symmetric Eigenmotions

By using XFLR5 the data in Table 6.18 was obtained. This data shows the eigenvalues for the longitudinal eigenmotions. These are the short period motion and the phugoid motion. The real numbers of both motions are negative which indicate that the motions are stable. The imaginary numbers indicate that the motions are oscillating.

Table 6.18.: Eigenvalues for the symmetric eigenmotions.

Longitudinal Modes	Eigenvalues
Short Period	-1.34439- 2.39760i
	-1.34439+ 2.39760i
Phugoid Motion	-0.00105- 0.02500i
	-0.00105+ 0.02500i

#### Short period motion

The short period motion is induced by a step input on the elevator during the entire manoeuvre. Figure 6.45

shows the short period motion of the HUULC. The damping ratio that corresponds to the short period is equal to 0.489. This is a relatively high damping ratio which indicates that the motion will be damped out quickly. This can also be seen in Figure 6.45.

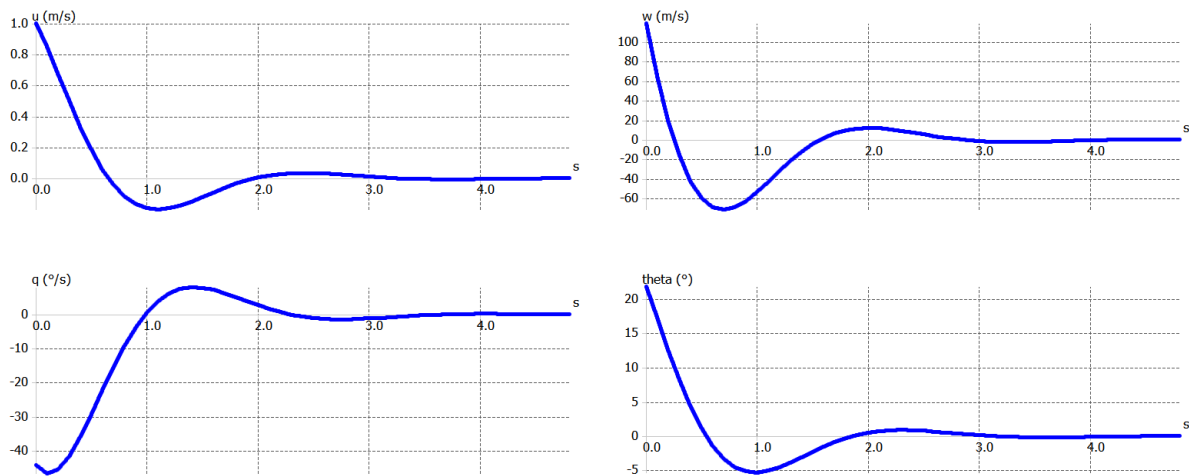


Figure 6.45.: Short period motion of the HUULC.

### Phugoid motion

The phugoid motion is initiated in a similar fashion as the short period motion. This is by means of a step input on the elevator. Figure 6.46 shows the phugoid motion of the HUULC. It shows that the period will be damped out after approximately 3000 seconds. The damping ratio of the phugoid motion is 0.042, which is relatively small damping ratio. It takes a long time to damp the phugoid motion because of the relatively small damping ratio and the very large weight of the aircraft. Decreasing the weight would lead to a significantly shorter phugoid motion.

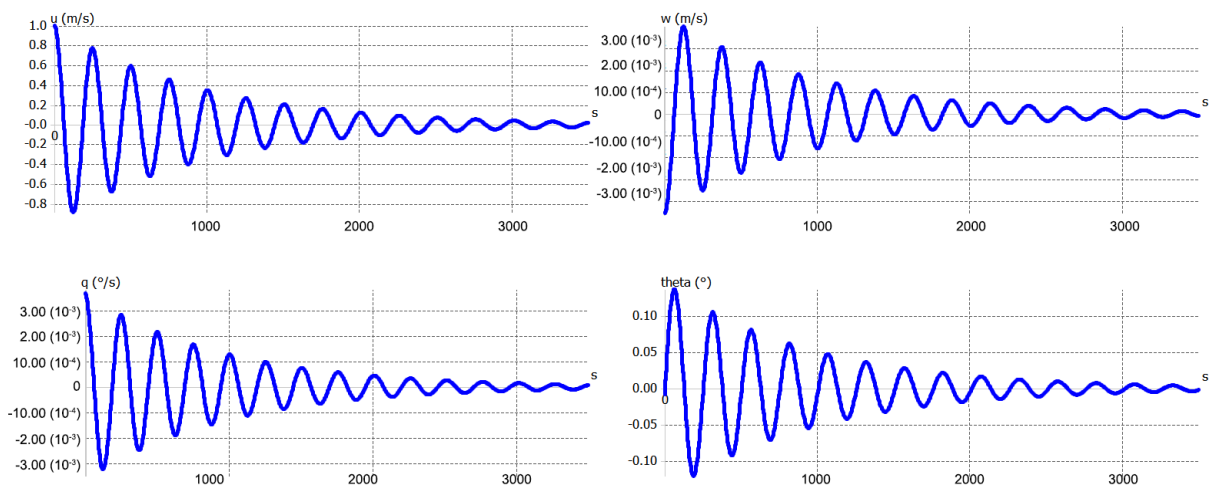


Figure 6.46.: Phugoid motion of the HUULC.

### 6.6.3. Asymmetric eigenmotions

A similar analysis can be done for the asymmetric eigenmotions. From the XFLR5 analysis, the data in Table 6.19 was obtained. The table shows the eigenvalues of the asymmetric eigenmotions. From this table several conclusions can be drawn. The negative real parts show that a motion is stable. The aperiodic roll and the dutch roll are therefore stable motions. The spiral however is unstable. Secondly the imaginary numbers show that a motion is oscillating. It can be seen from the table that the dutch roll is the only asymmetric motion that oscillates.

#### Aperiodic roll motion

The aperiodic roll is initiated by performing two step inputs on the aileron in opposite direction. Figure 6.47 shows the aperiodic roll motion of the HUULC. The figure shows that the aperiodic roll is stable. It also shows that the roll will be damped out within two seconds.

Table 6.19.: Eigenvalues of the asymmetric eigenmotions.

Lateral Modes	Eigenvalues
Aperiodic roll	$-4.09117 + 0.00000i$
Dutch roll	$-0.09879 - 1.08688i$
Spiral motion	$0.00154 + 0.00000i$

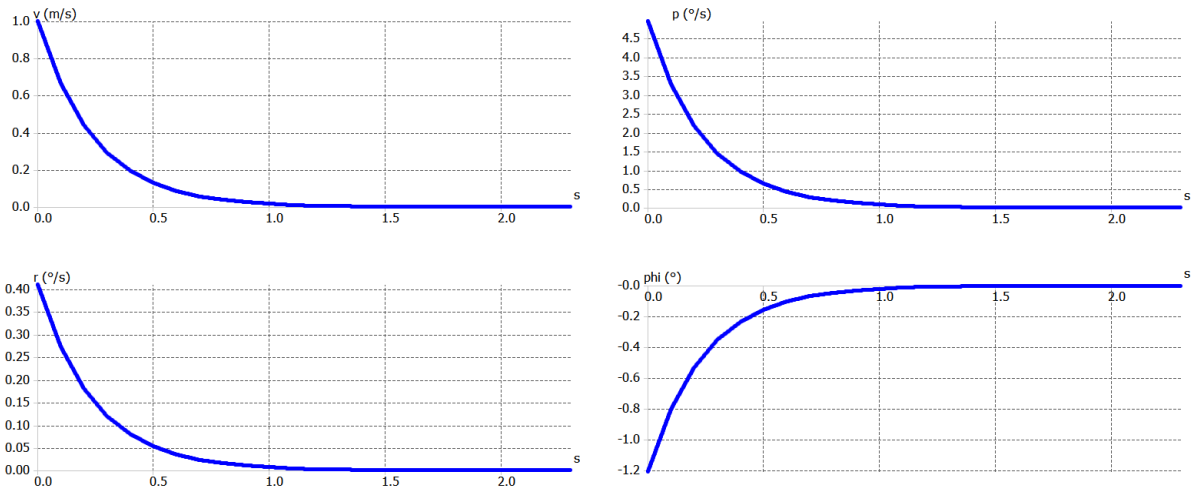


Figure 6.47.: Aperiodic roll motion of the HUULC.

### Dutch roll motion

The dutch roll is initiated by applying three pulses on the rudder, a positive, a negative and finally another positive pulse. This results in an oscillating yaw motion which then introduces a roll motion as well. In the figure it can be seen that the dutch roll motion is stable and that it oscillates like the eigenvalues indicated. The figure shows that the motion will be damped out in approximately 50 seconds. The damping ratio that corresponds to the dutch roll motion is 0.091.

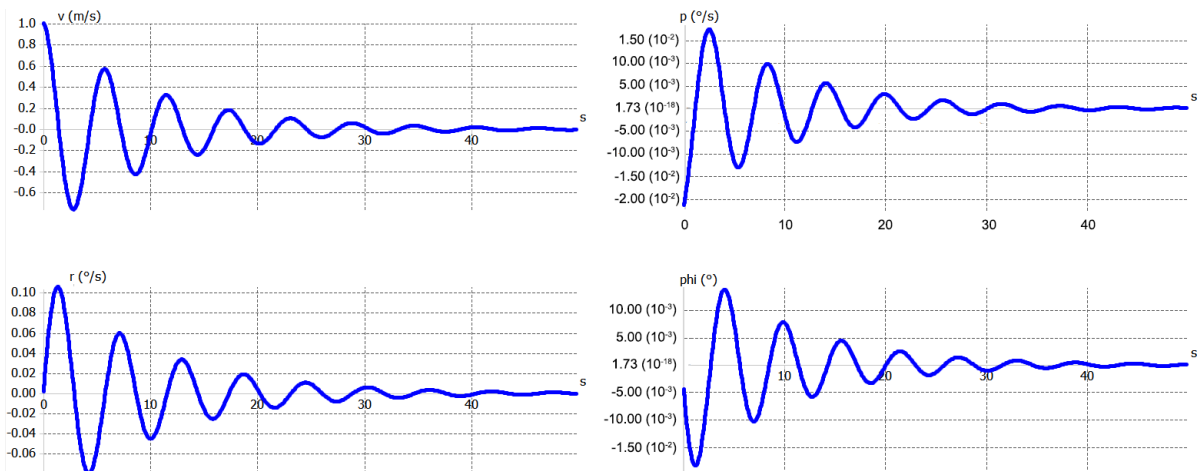


Figure 6.48.: Dutch roll motion of the HUULC.

### Spiral motion

The spiral motion is generated by giving the airplane an initial roll angle. The positive real part of the eigenvalue of the spiral already indicated that the spiral motion of the HUULC is unstable. This can also be seen in Figure 6.49. The line diverges and it can be seen that the roll angle will increase by eight degrees in approximately 50 seconds. In spite of this instability, the aircraft is still safe to fly because the roll angle increases very slowly which leaves a large response time for the ground control.

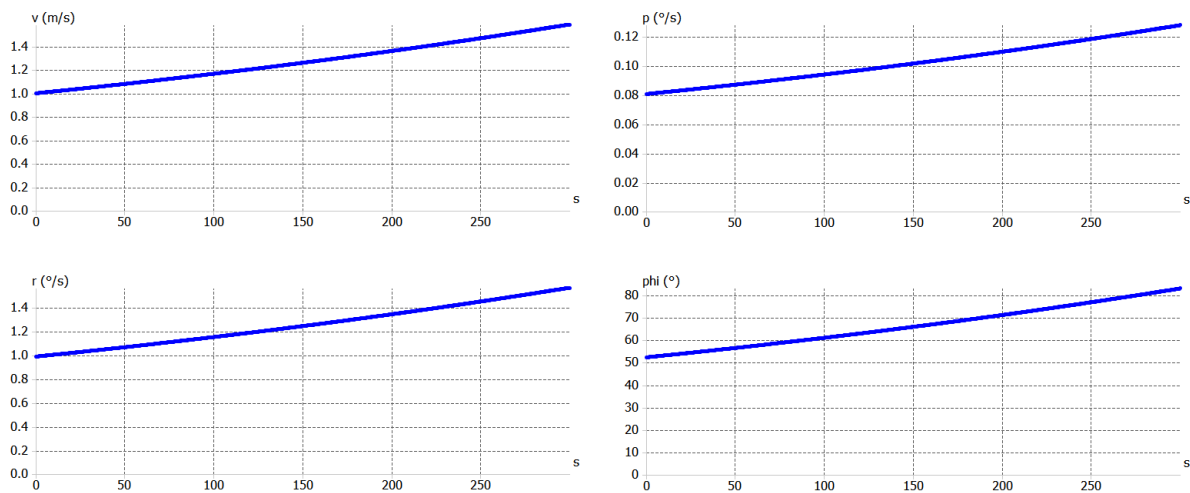


Figure 6.49.: Spiral motion of the HUULC.

## 6.7. Subsystems design

This section outlines the design of the subsystems of the HUULC. Given the size of the HUULC, some systems can be more challenging to design than for conventional aircraft. For example the tail can easily become too large if one is not careful while designing it. This section outlines the design process of different systems of the HUULC. The systems presented are the ones that are relevant for ultra large aircraft like the HUULC. Initially internal systems are presented: namely fuel systems, hydraulic systems and electrical systems. Then environmental systems are discussed: pressurisation, air conditioning, hydraulic and pneumatic systems. This is followed by a section dealing with de-icing, anti-icing, rain removal and defog systems. Then the tail is sized and designed in section 6.7.6 and finally section 6.7.8 outlines the design of the landing of the HUULC.

### 6.7.1. Fuel systems

Because the HUULC uses hydrogen fuel instead of kerosene, the fuel system is expected to be different when compared to conventional aircraft. With this in mind, several aspects regarding the hydrogen fuel system need to be taken into account. This section will elaborate upon the tank sizing and positioning, piping systems, and the eventual fuel pumps.

### 6.7.2. Fuel pump and hydrogen tank to engine connection

Given the use of liquid hydrogen, two options are available for transporting the hydrogen from the tanks to the engines:

- Pipe flow as liquid
- Pipe flow as gas

The first option would imply that the entire piping system would have to be kept at cryogenic temperatures. Furthermore, if no active cooling system is used, at startup the piping is expected to be at ambient temperatures, which means that a lot of hydrogen would vaporise until sufficient hydrogen has been sent through the system for the system to be cold enough. The second option is implemented by converting the hydrogen to gaseous form at the exit of the tank. A heat exchanger extracting heat from the outside air could be used to add heat to the liquid hydrogen and convert it to gas form. Once converted to gas form, the hydrogen could be routed to the engines in gas pipes that do not need to be isolated. This process would have to be properly controlled to avoid any excessive pressure buildup in the system because of the hydrogen expansion ratio of 865 from liquid to gas [69].

### 6.7.3. Hydraulic vs. electrical systems

One of the main functions of hydraulic systems is to move primary flight controls. Current technologies tend to use electrical systems for this purpose instead of hydraulic systems. Where a fluid reservoir is necessary for hydraulic systems, an electrical power generator is required for electrical systems. Since the HUULC will be driven by hydrogen, using fuel cells for electrical power generation is a feasible option. This section elaborates further upon the use of electrical systems for the purpose of controlling the aircraft and providing power to subsystems that require this.

### 6.7.3.1. Normal operation

The maximum amount of power required for the operation of an aircraft usually occurs in the landing phase. The primary and secondary flight controls, the landing gear and speed brakes may all have to be operated simultaneously. These functions would normally be powered hydraulically, but using electrical power is also possible. Electrical power is also necessary for internal and external lightning, flight instruments/avionics systems and engine starting systems. The flight instruments are not present in the HUULC, but rather in the ground control station. Nevertheless, the communication system will also require electrical power and it is assumed that this will be in the same order as the total package of flight instruments.

### 6.7.3.2. Electric power generation

Power generation is a very important design consideration for the HUULC, especially since there is a trend of converting more and more systems that were traditionally pneumatic or hydraulic to electric power [70]. In order to generate power for the HUULC, power may be extracted by putting a generator on the engine shaft, by using an APU or by using the hydrogen to power a fuel cell. Fuel cells are considered for electricity generation on current aircraft because they also produce water as a byproduct [71]. However, since the HUULC does not need water for crew or passengers, the advantage of water as a byproduct is canceled. Furthermore, fuel cells have a low power to weight ratio of about 1000W/kg [41], and they cannot provide bleed air for engine startup. In order to provide power while the engines of the HUULC are turning, generators are to be installed on the shaft of the engines. On the ground an APU can be used when the engines are shut down. This also allows to provide backup power in case of a failure of all the engines.

### 6.7.4. Environmental systems

Environmental systems are generally a necessity in passenger aircraft to provide conditions for the survival of human life. The four main systems for environmental control are:

- Pressurisation system: the purpose of this system is to maintain sufficient cabin air pressure during flight so that passengers remain comfortable.
- Pneumatic system: this system is necessary on the HUULC for ice protection system (See next section)
- Air conditioning system: the purpose of this system is to regulate cabin air in terms of temperature and humidity
- Oxygen system: this system is required in case of failure of the pressurisation system

Since the HUULC will be an unmanned cargo aircraft, pressurisation and oxygen systems are not present on the HUULC. The air-conditioning system is also not a necessity since the environmental conditions for the commodities will be provided by the specially designed containers. This is chosen in such a way because providing these conditions in the payload bay would require different payload bays with different environmental conditions. The pneumatic system however, will be present on the HUULC since air is a necessity for the de-icing systems (See Section 6.7.5). The primary source of air will be the engine compressor. A secondary source can be the APU described in Section 6.7.3, but since the HUULC will have  $N$  engines it is assumed that the amount of bleed air from the compressors will be sufficient. AC powered valves will control the delivery of engine bleed air into the pneumatic manifold. A pre-cooler will not be necessary in this system since this is mainly used in the supply of air for the air-conditioning [72].

### 6.7.5. De-icing, anti-icing, rain removal and defog systems

The HUULC is expected to be operated into known icing conditions. To prevent the accumulation of ice and/or to remove ice which has already formed, special systems need to be installed. An issue that may arise with de-icing is that the HUULC has control surfaces which are excessively large. This means that deicing boots which rely on pneumatic air to “break” the ice away will require large systems. Hence, electro-impulse systems will be used for the purpose of de-icing. These systems rely on impulses delivered by electromagnetic coils installed on the leading edge of the wing and other control surfaces.

The HUULC will rely more on the anti-icing systems than on the de-icing systems. An air heated system which provides hot air from the engines to the leading edges of the wings will be installed for this purpose. An electrical heating system will also be implemented to prevent ice formation on pitot tubes, stall vanes, total air temperature probes and engine inlet lips. To prevent ice hitting the rest of the structure, it is far better to prevent ice formation than to remove it after it has formed.

Rain removal on the HUULC is not as important as anti-icing since this is mainly necessary for manned aircraft in which low visibility conditions may cause problems. The optical sensor at the front of the fuselage will need a small wiping system for rain removal. Defogging the camera can be done with bleed air from the engines that is led to the area. A complicated defogging system that is used in manned aircraft would be superfluous and is therefore not designed.

### 6.7.6. Control surfaces and empennage sizing

The aileron sizing and the empennage configuration, along with the empennage sizing and control surface sizing are provided in this section.

#### 6.7.6.1. Empennage configuration

Multiple configurations for the empennage are considered, as given by Roskam, including a single vertical tail, multiple vertical tails, V-tail, T-tail, vertical tails on wings and twin-boom tail.

Before selecting the appropriate empennage configuration, it is important to look at the specific aircraft configuration in question and how it will affect the empennage configuration selection. The HUULC is a blended wing body aircraft, with an airfoil-shaped fuselage. This allows for a more synergistic integration of longitudinal control surfaces. For example, the trailing edge of the fuselage may be used as an elevator control surface, reducing the need for a horizontal tail.

As was explained in Section 6.5, the centre of gravity of the aircraft is longitudinally close to the line of the wing tips. Hence, wing-mounted tails would need to be sized largely, as a result of the small moment arm between the rudder and the centre of gravity. Hence, wing-mounted vertical tails may be excluded from the list.

This leaves the options of one tail or multiple vertical tails. This choice must be made on the basis of the required size of the vertical tail. If the required vertical tail is small in size, it would be beneficial to use a single tail, which would be lighter in weight than two tails of equivalent area. However, if the required size of the vertical tail is large, two smaller tails may be required, in order for the aircraft (which is already considerable in size) to fit in a hangar and to allow for easier accessibility for empennage maintenance.

#### 6.7.6.2. Scissors plot for horizontal tail sizing

In order to design the horizontal tail, one must take into account controllability and stability of the aircraft. This results in the so called “scissors plot”. The scissors plot is generated using two equations: one that puts a limit on controllability and another on stability. These equations are given below:

$$\frac{S_h}{S} = \frac{1}{\left[ \frac{C_{L\alpha_h}}{C_{L\alpha}} \left(1 - \frac{d\varepsilon}{d\alpha}\right) \frac{l_h}{\bar{c}} \left(\frac{V_h}{V}\right)^2 \right]} \bar{x}_{cg} - \frac{\bar{x}_{ac} - 0.05}{\frac{C_{L\alpha_h}}{C_{L\alpha}} \left(1 - \frac{d\varepsilon}{d\alpha}\right) \frac{l_h}{\bar{c}} \left(\frac{V_h}{V}\right)^2} \quad (6.22)$$

$$\frac{S_h}{S} = \frac{1}{\frac{C_{L_h}}{C_{L_{A-h}}} \frac{l_h}{\bar{c}} \left(\frac{V_h}{V}\right)^2} \bar{x}_{cg} + \frac{\frac{C_{m_{ac}}}{C_{L_{A-h}}} - \bar{x}_{ac}}{\frac{C_{L_h}}{C_{L_{A-h}}} \frac{l_h}{\bar{c}} \left(\frac{V_h}{V}\right)^2} \quad (6.23)$$

All coefficients given in the equations above need to be estimated. For the stability curve, parameters in cruise flight are used, while for controllability parameters at landing speed and altitude are used. This is because those are the two flight phases at which the tail size is critical for stability and controllability respectively. Coefficients such as  $C_{L\alpha}$  were estimated using the DATCOM method. The location of the aerodynamic centre is estimated as shown in reference [73]. The final scissors plot is shown in Figure 6.50. The horizontal line shows the ratio of  $S_h/S$ . For the HUULC, the wing area without the fuselage area is  $4675m^2$ , so the required tail area from the scissors plot is  $1683m^2$ . This area may be reduced by adding an elevator at the trailing edge of the fuselage airfoil. This would allow to add more moment around the centre of gravity if required.

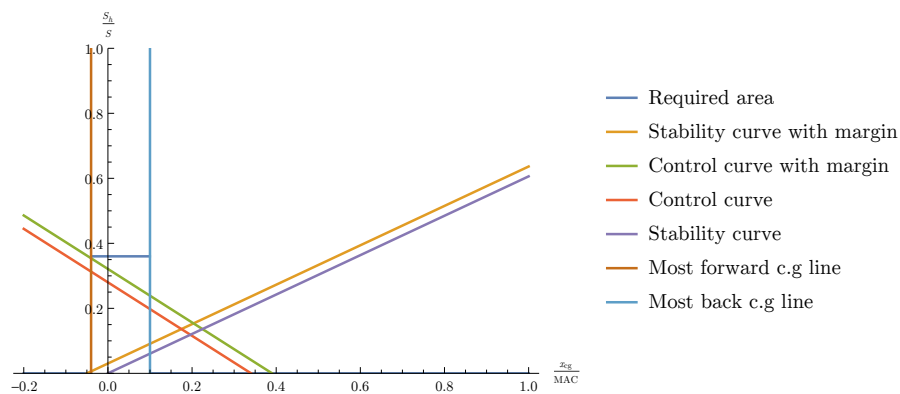


Figure 6.50.: Scissors plot for the HUULC

### 6.7.6.3. Vertical stabilizer

The empennage is now sized using the tail volume coefficient method, as outlined by Roskam. This is done by determining the required tail volume ratio through statistics and from that choosing a corresponding tail area and distance from the centre of gravity. The tail volume coefficients are given by Roskam as:

$$V_v = \frac{x_v S_v}{S b} \quad (6.24)$$

From Roskam, values of tail volume coefficients for different aircraft are given. By removing one outlier and calculating the average,  $V_v$  is 0.072. However, due to the unconventional nature of the configuration of the HUULC, the volume coefficients of a flying wing are used. This is given to be 0.02 for  $V_v$  [74].

By using the current HUULC dimensions, putting numbers in formula 6.24 and rearranging yields a tail area of  $398 \text{ m}^2$ . This is done by taking a most aft center of gravity position of  $47.6 \text{ m}$ .

With such a large tail area aeroelastic effects and fitting the aircraft in a hangar become a concern. Hence, a double tail configuration would be more appropriate. This would imply that one vertical tail would be positioned on the left and another rudder on the right of the fuselage, as much aft as possible to increase the moment arm with respect to the center of gravity. Sweep would further increase the effective moment arm. Multiple tails have the following advantages [75]:

- Reduced rolling moment due to rudder deflection.
- Slipstream improvement of one of the vertical tails in case of engine failure.

Now that the required area of the tail is found, reference [76] gives typical values for aspect ratios and sweep angles for the tail of different aircraft. For the HUULC, a low aspect ratio (AR) for the vertical tail is preferred to limit the height of the two vertical tails. Also, as it is planned to locate the horizontal tail on top of the vertical tails, a large value of the chord at the top of the vertical tails is preferred in order to meet the required horizontal tail area. From reference [76], it can be seen that the given vertical tail ARs range from 0.95 to 1.88 (the Wright flyer with an AR of 6.3 is ignored). For the HUULC, the average value of 1.48 is used. This yields a tail height of  $17.12 \text{ m}$ . Taper is applied as well, for the CATIA model a value of 0.64 is used, however further research is needed to optimise this value.

For the sweep, the average value from aircraft given in reference [76] is used. This gives a sweep angle of  $37.03^\circ$ .

### 6.7.6.4. Empennage sizing check in case of one engine inoperative

In this section, the required coefficient of lift from the tail to counter the moment by one engine inoperative is estimated. This gives an indication to check if the area given in the previous section is realistic.

The total power of the HUULC is given to be  $316 \text{ MW}$ , dividing this over eight engines means that the power per engine is  $39.5 \text{ MW}$ . Dividing the power by the takeoff speed yields the thrust that needs to be compensated by the rudder (assuming 90% efficient propellers). With a takeoff speed of  $72 \text{ m/s}$ , the thrust is given by  $0.9 \cdot 39.5 \cdot 10^6 / 72 = 493 \text{ kN}$ .

The tails are located  $50 \text{ m}$  from the centre of gravity of the HUULC, if the failing engine is located at the wingtip (assuming worst case scenario) the distance would be  $100 \text{ m}$ . The takeoff speed of the HUULC is given to be  $72 \text{ m/s}$ . So given the current size of the tails of  $398 \text{ m}^2$ , the required  $C_l$  can be calculated.

$$C_{l_{rudder}} = \frac{L_{required}}{1/2 \rho V^2 S} = \frac{(100/50) \cdot 494 \cdot 10^3}{0.5 \cdot 1.225 \cdot 72^2 \cdot 398} = 0.78 \quad (6.25)$$

It should be mentioned that this is a substantially simplified analysis, and that for a detailed design other factors should be taken into. For example, in case of sideslip the fuselage induces disturbances on the airflow around the wing, which is not taken into account here.

### 6.7.7. Ailerons

Figure 6.51 is used to size the ailerons. From Raymer it can be seen that the aileron chord to wing chord ratio and the aileron span to wingspan ratio are dependent between on each other [77].

Raymer states that most aircraft have ailerons that span 60 to 90% of the span [77]. The last 10% are rarely used because of the vortex flow at the wingtips [77]. For the HUULC, the aim is to have 35% of the span consisting of ailerons, so the ailerons will extend from 60 to 95% of the span. Given the large dimensions of the HUULC, a 5% margin with respect to the wingtip still represents a distance of 5 meters. From Figure 6.51 the chord of the aileron should be equivalent to 32% of the wing chord. The wing allows for the aileron to extend up to 35% of the wing chord, so this space will entirely be used to make sure effective roll control is possible. Further analysis in the future may allow for a more accurate and optimised aileron design. The aileron can be tapered with the same ratio as the wing to provide a constant aileron chord to wing chord ratio.

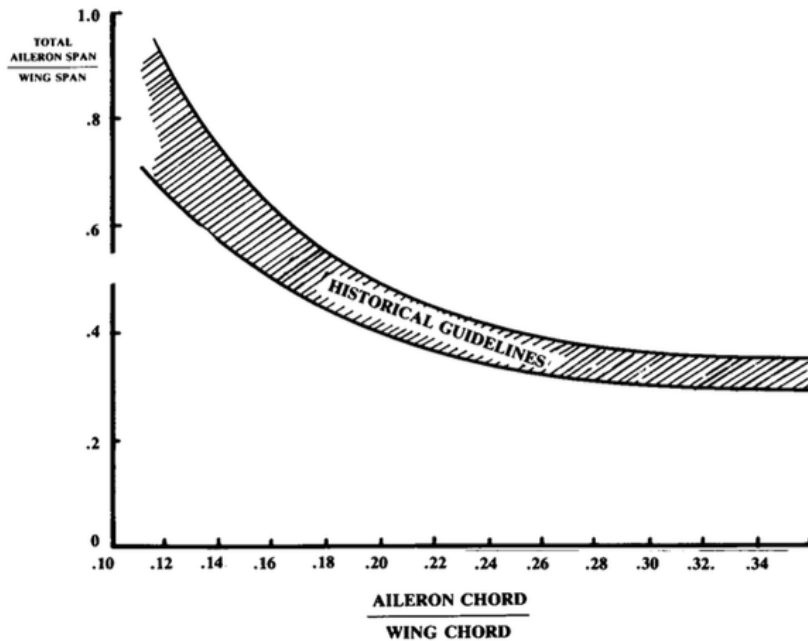


Figure 6.51.: Aileron guidelines [77].

### 6.7.8. Landing gear

The HUULC needs to be able to land at various airports. Designing a landing gear for an aircraft such as the HUULC imposes several challenges. Class One Weight estimations are performed using the Roskam approach [57]. The Raymer approach is chosen for the conceptual placing and sizing of the struts and the tires [78]. This section elaborates further upon the design process of the landing gear, by showing the process in a flow diagram and explaining the choices that are made during the process.

#### 6.7.8.1. Design process

The Roskam approach required several steps in order to choose, size and design the landing gear for the HUULC. After a certain step it was found that the Roskam approach was too elaborate for this early preliminary design and the team switched to the Raymer approach. This approach is more conceptual, but still provides sufficient characteristics for the design of the landing gear.

The process consists of the steps described below, in which iterations are made. The static and dynamic loads determined in the tire and strut sizing part will determine the longitudinal and lateral positioning of the gears. If the positioning is not chosen correctly, the gears will bear loads that cannot be withstand or are too small for adequate steering.

#### Decide on retractable or fixed landing gear

Raymer and Roskam both state that the drag penalty for fixed wings becomes too large for flights above 150 knots. Since the HUULC will be flying above this speed, the landing gear is chosen to be retractable.

#### Overall configuration

Several options for landing gear arrangement exist. The most common ones are the taildragger, bicycle and tricycle configurations. According to Roskam, the tricycle configuration is the most conventional one and overall provides the best characteristics. The HUULCs landing gear is therefore chosen to have a tricycle configuration.

#### Determine center of gravity range

The range for the c.g. was determined in Section 6.5. The most forward c.g. is located at 42.2 meters from the front of the fuselage. The most aft c.g. is located at 47.7 meters from the front of the fuselage. The lowest c.g. is at 4.827 meters height and highest c.g. is at 5.317 meters height. The position of the c.g. is important for the criteria that will be discussed in the next process.

#### Longitudinal and lateral positioning

The longitudinal and lateral positioning of the gears is done by complying with the clearance angles shown in Figure 6.52. The tip-over angle shown in the upper left illustration must be larger than the clearance angle shown in the lower left illustration. A 15 degrees tip-over and clearance angle are recommended by both Roskam and Raymer. However, there is an issue with this angle, because the profile of the fuselage airfoil does not provide sufficient height difference between the back of the fuselage and the longitudinal position of the

main landing gear. The eventual approach was to place the main gear at 52.496 meters from the front of the fuselage, providing the 15 degree angle between the vertical of the gear and the most aft c.g..

The clearance angle for rotation at the back is then a function of the height of the struts. Providing 15 degrees for the rotation angle requires struts with an height of 10 meters, which would have negative consequences for the loading time of the HUULC, since lifting containers over this height would take too much time. Therefore the strut height is chosen to be four meters, resulting in a clearance rotation angle of only 11.6 degrees. This means that the HUULC will have to perform take-off with minimal rotation.

The calculations for speed and take-off were performed on a runway distance of 3300 meters, but the minimal runway distance that the HUULC will encounter is now set at 4000 m (except for alternate airports). A check whether take-off is possible can be made by calculating the lift coefficient needed for take-off. With a take-off speed of 72 m/s, a wing area of 7175 m<sup>2</sup>, a sea-level density of 1.225 kg/m<sup>3</sup>, and a required lift force of 20,526,336 N, the required lift coefficient equals 0.9009. Figure 6.14a in Chapter 6.2 shows the  $C_L - \alpha$  curve with full flaps. A lift coefficient of 0.9009 is attainable at an angle of attack of 2.5 degrees, meaning that the 11.6 degrees clearance angle is sufficient for rotation during take-off.

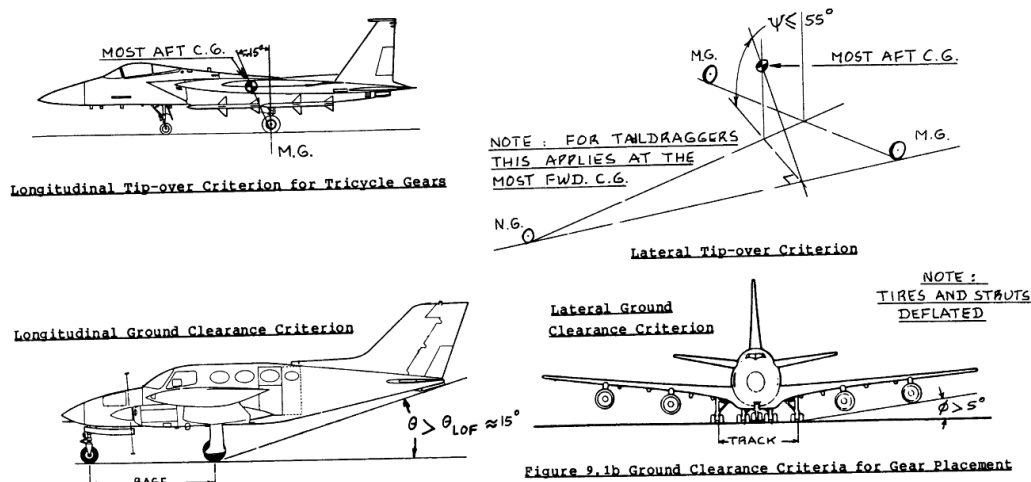


Figure 6.52.: Clearance angles for landing gear placement.

The overturn angle should have a maximum value of 55 degrees according to Roskam. A visualisation of this angle can be seen in the left upper illustration in Figure 6.52. Complying with this 55 degree angles determines the longitudinal position of the nose gear and the lateral position of the main gears. The nose gear is placed at seven meters from the front of the fuselage. The main gear track is 48.6 meters. This provides an overturn angle of 38.9 degrees. The longitudinal position of the nose gear also determines the loads that act on the nose gear and therefore it is an iterative process to determine the exact position.

The last criterion is the lateral ground clearance. The angle between the bottom of the propeller blade and the ground contact point of the main gear should at least be five degrees. However, it is decided by the team that the engines would be placed in such a way that this angle would be feasible after the landing gear was designed. The final height of the landing gear was however changed to four meters (without tires). The resulting clearance angle with the propeller resulted in 2.5 degrees. This is smaller than the required five degrees and a revision on landing gear placement or propeller placement will have to be made.

### Tire and strut determination and sizing

In order to determine the amount of tires and struts, the loads acting on the nose and main gear need to be determined. The total dynamic plus static load on the nose should be at least 0.05 times the maximum take off weight [78]. This is required for adequate steering of the HUULC. The longitudinal position of the nose gear is therefore also a function of this and is determined in an iterative process. Placing the nose gear at seven meters from the front of the fuselage ensures 0.0549 times the maximum take off weight acting as the load. The main gear should have a maximum of 0.20 times the maximum take-off weight [78]. With the current positioning, a total static load of 0.1774 times the maximum take off weight acts on the main gear.

The total static load on the nose gear equals 863,175.9 pounds. Three Part Name tires can take the highest loads, so the best tire for the HUULC is chosen from this category in Table 6.20.

The maximum load this tire can take is 63,700 pounds. Dividing the nose gear by this allowable load per tire results in 13 tires. The static load acting on the main gear is 4,447,972 pounds, resulting in 70 tires.

It is chosen to use struts with six and two tires. This results in two struts with six tires and one strut with two tires for the nose wheel, and twelve struts with six tires for the the main gear. The total amount of tires

Table 6.20.: Tire specifications.

Speed	235 <i>mph</i>	378.2 <i>km/h</i>
Max Load	63700 <i>lb</i>	28894 <i>kg</i>
Pressure	195 <i>PSI</i>	1345 <i>kPa</i>
Max width	20.5 inches	0.5207 <i>m</i>
Max Diameter	52 inches	1.3208 <i>m</i>
Rolling radius	21.3 inches	0.54102 <i>m</i>
Wheel diameter	23 inches	0.5842 <i>m</i>
Number of plies	30	-

is therefore 86. Considering the fact that both Raymer and Roskam approach the landing gear loads as point loads, it is determined to place all the main landing gears spanwise instead of in a longitudinal direction.

The final step of this process is to check if the chosen tire complies with the kinetic braking energy. The equation for the kinetic braking energy is:

$$KE_{braking} = \frac{1}{2} \cdot \frac{W_{landing}}{g} \cdot V_{stall}^2 \quad (6.26)$$

In this equation the units are in feet, pounds and seconds. The stall speed equals 196.85 *ft/s*, the landing weight is the MTOW minus the fuel weight and equals 4,612,881 pounds, and 'g' equals 32.2 *ft/s<sup>2</sup>*. This results in a total kinetic braking energy of 34,980,105.93 *ft - lb/s*, corresponding with a wheel diameter of approximately 23 inches for large transport aircraft [78]. This means that the chosen tires are applicable on the HUULC.

### Shock absorber

The first decision was on the type of shock absorber. The oleopneumatic (oleo) shock strut is chosen because of its conventionality. In order to size the oleo, the required deflection must be determined first. This is also called the stroke. The stroke of a shock absorber is calculated with Equation 6.27.

$$S = \frac{V_{vertical}^2}{2g\eta N_{gear}} - \frac{\eta_T}{\eta} S_T \quad (6.27)$$

Where the vertical speed is 12 feet per second (FAR25),  $\eta$  equals 0.97 (metered orifice in the oleo),  $N_{gear}$  equals 3,  $\eta_T$  equals 0.47 and the tire stroke  $S_T$  equals 0.39 feet. This results in a stroke of 9.48 inches including a two inch margin. The length of the oleo is approximately 2.5 times the length of the stroke. By adding a small margin, the total length of the oleo becomes 37.93 inches. Converting these values to meters the oleo has a stroke of 0.24 meters and the total length of the oleo is 0.964 meters.

The diameter of the oleo approximately equals 0.04 times the square root of the load on the oleo. The loads on the nose and main gear and the amount of necessary struts are determined above. Dividing these loads by the amount of struts, substituting the correct values and converting to meters results in a diameter of 0.6185 meters for the main gear oleo's and 0.525 meters for the nose gear oleo's.

The diameter of the oleo's determines the diameter of the struts and thus the minimum pitch between the wheels on the same strut. Adding a 0.06 meter margin to the distance results in a pitch of 0.6785 meters between the wheels. The same pitch is used for the nose gears for manufacturing convenience.

The total width of one strut is then determined as two times the tire width plus the wheel pitch. The total width (with margins) equals 1.70713 meters.

### Gear retraction geometry

The dimensions of the HUULC make gear retraction possible at different locations. However, the wing box was already sized before the design of the landing gear and thus putting gears in the wing would require cutting of the wing box, which is not preferred. The width of the fuselage equals 25 meters. If the required 12 struts would be placed spanwise in the fuselage, the remaining pitch between the struts would be too small. Therefore it is chosen to put one strut at each wing root and the remaining ten struts in the fuselage. The pitch between the wheels in the fuselage is then 0.766 meters. The most outer gears are placed at 24.3 meters lateral direction from the center line of the fuselage. This distance is chosen because of feasibility; the wing box shall not

be interrupted and the required height for retraction is approximately 2.3 meters, which is available at this point.

A four point pivoting retraction system is chosen. The nose gears and all the main gears in the fuselage will be retracted forward. The most outer main gears will be retracted inwards because of the increasing volume inwards towards the centre line of the fuselage.

The six wheels on the strut can rotate about their centre wheel, so when retracted forwards, the required height can be minimised. The required height then becomes slightly larger than the diameter of the wheels, which equals 1.3208 meters. The inward retracting gears will not rotate and need approximately two meters height, because of the width of the entire gear.

The strut with two wheels for the nose wheel will be placed at the centre line of the fuselage. The two remaining struts with six wheels are then aligned with the most outward main gears, resulting in a triangular configuration for the three struts, so the overturn angle does not change. The actual geometry of the landing gears can be found in Appendix A. Tables 6.21 and 6.22 below specifies all characteristics of the landing gears.

Table 6.21.: Main gear characteristics.

Main Gear	
Struts (6wheels)	12
Strut height	6.5 m
Strut Diameter	0.62 m
Wheel pitch (single strut)	0.67 m
Wheel pitch (between struts)	0.77 m
Track	48.6 m
Longitudinal position	52.94 m

Table 6.22.: Nose gear characteristics.

Nose Gear	
Struts (6wheels)	2
Struts (2wheels)	1
Strut height	8.10 m
Strut diameter	0.53 m
Wheel pitch (single strut)	0.58 m
Lateral pitch struts	2.06 m
Longitudinal pitch struts	4 m
Height of fuselage	4.66 m

### 6.7.8.2. Verification and validation

The Excel file has been verified by performing all calculations analytically by hand. An actual validation of this is not feasible, since the inputs and outputs could not be found on actual reference aircraft. It is therefore assumed that the verification of the Excel file is sufficient.

### 6.7.8.3. Conclusion and recommendations

The final specifications of the landing gear are listed in Tables 6.21 and 6.22. The specifications for the tires can be found in Table 6.20. A visualisation of the geometry can be found in Appendix A.

The main gear and the nose gear can take all the loads. In general, multiple main gears are positioned with certain offsets behind each other. Since the Raymer and Roskam approaches both assume point loadings (from a side view) for the landing gear, the team chose for a spanwise distribution. One of the consequences is that if the HUULC has a banking angle during landing, the most outer gears will take all the loads. Therefore, this distribution is not considered as reliable. The actual distribution of the landing gears will have to be revised in later design stages.

The rotation angle is one of the only requirements that could not be complied with. The profile of the HUULCs fuselage required a strut height that is too large for the purpose of the HUULC. Manufacturability would also become a problem with struts of 10 meters. Containers will have to fit under the HUULC for loading, so a minimal height of three meters is necessary for the fuselage. Adding some margins for loading/unloading systems, the total height from ground to the bottom of the fuselage is 4.7 meters. The clearance rotation angle is then put at 11.6 degrees. The B52 Stratofortress takes off without rotation and needs a runway of 2900 meters for this, which is regarded as a large runway [59]. It is shown that the required lift coefficient of 0.9009 is attainable at an angle of attack of 2.5 degrees, meaning that take-off is possible in the current scenario.

Another issue might be the large wingspan, which can cause the tips of the wings to touch the ground. This is undesirable and the B52 actually uses outriggers to make sure that this does not happen. However, no load bearing calculations and actual sizing of the outriggers is performed. It is recommended that further research shall be conducted on the design and implementation of outriggers.

## 6.8. Integrated design

The integration process of the HUULC was itself a big challenge. Accommodating all the subsystems while taking care of the geometry constraints and the mass distributions was not an easy task. The use of CAD Software (CATIA) helped the team to effectively visualise the design and to thus detect integration problems early on and take all necessary actions.

After modelling the wing and the fuselage surfaces and integrating the wing box into the CATIA product, it was realised that the dimensions used during the structural sizing were not accurate enough. However, due to the time limitations this correction is proposed as a recommendation for further work.

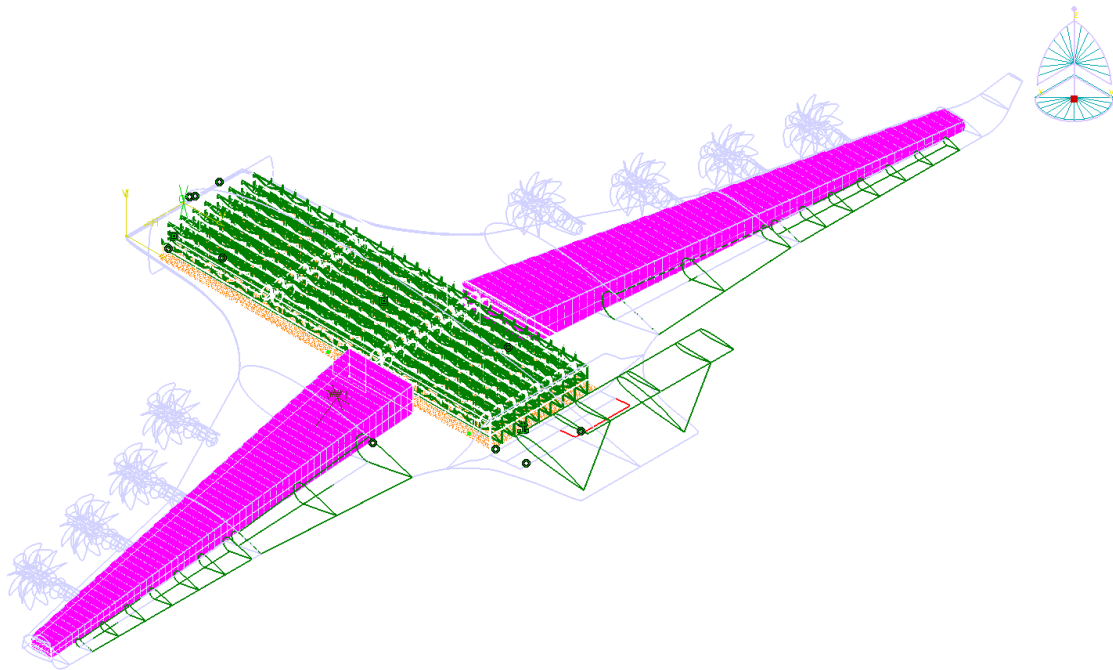


Figure 6.53.: Wireframe model overview.

During the tail integration it was detected that the dimensions of the design seemed excessively large compared with the blended wing body and Burnelli concepts examined during the research phase. Hence, a short research was performed, and it was found that the use of conventional configuration statistics was clearly not compatible with the HUULC concept. Finally, a new tail volume coefficient of 0.02 was chosen, based on the proposed tail volume coefficient of a blended wing body from [74] and the tail was resized accordingly.

Finally, the CATIA model proved to be extremely useful during the landing gear design. The use of a 3D model made it possible to determine the most adequate locations for the aircraft undercarriages based on the storage volume and planform design. A wide variety of drawings may be found in Appendix A.

## 6.9. Aircraft design riskmap

The Technical Risk Assessment (TRA) is performed to give insight in the level of risk as an item is likely to fail. The items are based on the sub-systems and its associated technologies chosen in the sections above.

The level of risk is based on the likelihood an item will fail and the impact it will have on the entire system if it fails. Out of these two parameters, the level of risk can be determined. It is set that if the likelihood of an item to fail is lower than 0.01%, the likelihood is said to be “unlikely”. If the likelihood of an item to fail is between the 0.01% and 1%, the likelihood is said to be “less than likely”, whilst if the likelihood of an item to fail is larger than 1%, the likelihood is said to be “more than likely”.

The impact can be divided into three categories, namely “minor”, “moderate” and “major”. Major levels of impact may cause the system to entirely shut down and/or damage itself even more. A moderate impact will include urgent fixes if a problem occurs. The system will come to a hold, but some sub-systems will still behave as designed for. A minor impact has the least negative influence onto the system. If one part fails, the system

can still continue its mission, without coming to a hold or damage itself even further. For all three scenarios, maintenance is required before the next mission is started.

Table 6.23.: TRA Likelihood/Impact matrix [79].

Likelihood	Impact		
	Minor	Moderate	Major
More than likely: >1%	Medium	High	High
Less than likely: 0.01-1%	Low	Medium	High
Unlikely: <0.01%	Low	Low	Medium

For the convenience, the level of risk has a background colour to intuitively point out the importance of risk. The level of risk is divided into three categories, namely “low (green)”, “medium (yellow)” and “high (red)”. The level of risk shows the safety for using a particular technology for a (sub-)system. The higher the level of risk, the larger the risk on the entire system becomes.

All sub-systems are judged on their likelihood and impact. The results of this analysis are shown in the risk map in Table 6.24. Again, for the convenience, the level of risk has a background colour to intuitively point out the importance of risk.

Table 6.24.: Risk map for all sub-systems.

Sub-system	Likelihood	Impact	Level of Risk
Container design	Less than likely	Minor	Low
Payload bay	Less than likely	Major	High
Structural integrity	Unlikely	Major	Medium
Propulsion	Unlikely	Major	Medium
Hydrogen tanks	Less than likely	Moderate	Medium
Internal fuel transportation	Unlikely	Moderate	Low
Hydraulic system	Unlikely	Major	Medium
Electrical system	Unlikely	Major	Medium
De-icing / anti-icing	Less than likely	Moderate	Medium
Horizontal stabilisers	Unlikely	Major	Medium
Vertical stabilisers	Unlikely	Moderate	Low
Ailerons	Unlikely	Major	Medium
High lift devices	Unlikely	Moderate	Low

The level of risk is dependent on the combination of choices made from the likelihood and the impact. Therefore, the following list is created to clarify the decision of choosing a certain parameter for both the likelihood and the impact of each sub-system:

- **Container design:** The likelihood chosen for this sub-system is “less than likely”. The containers designed for the HUULC may be prone to weather changes while being stored, or it may be damaged while being transported from the payload bay onto a truck. Therefore, because daily a lot of containers will be handled, the chance of one to show some form of damage is estimated to be between 0.01% and 1%. The impact of such an failure does not influence the system as a whole. The containers can easily be replaced by another one and the payload just has to be transferred from the damaged one into the new one. The rest of the containers do not depend on the broken container and therefore, the impact is said to be “minor”. As a result, the level of risk for this sub-system is estimated to be “low”.
- **Payload bay:** The likelihood chosen for the payload bay to fail is “less than likely”. This is because the payload bay will be used along with a couple of hundred of rollers in the floor. Because the rollers have to withstand a lot of force and friction and will be used on a daily basis, the chance of failing is estimated to be within the 0.01% and 1%. The impact of a roller to fail may be devastating for the flow of the loading and unloading of the containers, which is set to “major”. Therefore, the level of risk is estimated to be “high”.
- **Structural integrity:** The structural integrity is “unlikely” to fail. The theory of structural sizing is already proven for years, but if a component fails, it may have a “major” impact on the performance of the aircraft. The level of risk is therefore estimated to be “medium”.
- **Propulsion:** The propulsion system also is “unlikely” to fail. The theory is proven for years and the engines will be optimised when the HUULC will go into service in the year 2030. The impact of an engine to fail is “major”, because this will definitely influence the performance of the aircraft. The level of risk is therefore set at “medium”.

- **Hydrogen tanks:** Because of the pressurisation of the hydrogen tanks, the likelihood of failure is due to the stresses set at “less than likely”. The impact is set to “moderate”, because a damaged hydrogen tank can easily be replaced. Also, during flight, one single damaged hydrogen tank will not result in a shortage of fuel. The level of risk is therefore set at “medium”.
- **Internal fuel transportation:** The internal fuel transportation is performed by pipes and is “unlikely” to fail. The impact is “moderate”, because the multiple pipes are used to pump the fuel to the right destination. Therefore, the level of risk is set at “low”.
- **Hydraulic system:** The hydraulic system is “unlikely” to fail, because of its proven technology. However, the impact is “major”, because the aircraft may become uncontrollable. Therefore, the level of risk is “medium”.
- **Electrical system:** The electrical system is “unlikely” to fail, because of its proven technology. The impact may be “major”, because if the APU for example fails, the whole aircraft may become uncontrollable. Therefore, the level of risk is set to “medium”.
- **De-icing / anti-icing:** The de-icing system is unlikely to fail. However, because of the cold temperatures faced in Novosibirsk, the system faces harsh weather conditions and therefore the likelihood of failure is set to “less than likely”. The impact is set to “moderate”, because the aircraft generates a lot of lift, so a decrease in lift due to ice may be counteracted by increase in angle of attack. The level of risk is set to “medium”.
- **Horizontal stabilisers:** The horizontal stabilisers have, due to their proven technology, an “unlikely” likelihood of failure. The impact of failure is set to “major”, because the aircraft may become uncontrollable. The level of risk is “medium”.
- **Vertical stabilisers:** The vertical stabilisers also have an “unlikely” likelihood of failure due to its proven technology. The impact of failure is set to “moderate”, because an aircraft may still be able to manoeuvre without its vertical stabilisers. Therefore, the level of risk is set to “low”.
- **Ailerons:** Due to its proven technology, the ailerons are “unlikely” to fail. However, the impact is set to “major”, because a failing aileron will make the aircraft uncontrollable. The level of risk is set to “medium”.
- **High lift devices:** The high lift devices are set with an “unlikely” likelihood, because of its simple and proven technology. The impact is set to “moderate”, because the change in increase in lift coefficient between cruise and landing is just 0.2. A simple solution may be to just land with a slightly higher velocity. The level of risk is therefore set to “low”.

## 6.10. Conclusion

In this chapter a lot of important characteristics have been determined that are specific to the HUULC. Table 6.25 gives an overview of these characteristics. More specific conclusions to each subsystem can be found in the corresponding sections as well as recommendations.

Table 6.25.: Main design characteristics of the HUULC.

<b>Mission Weights</b>	
$W_e$ [kg]	701,000
$W_f$ [kg]	141,000
$W_{tfo}$ [kg]	2,100
$W_{pay}$ [kg]	1,248,000
$W_{to}$ [kg]	2,092,000
<b>Preliminary Sizing Characteristics</b>	
$W/S$ [ $N/m^2$ ]	2867
$W/P$ [ $N/W$ ]	0.065
$S$ [ $m^2$ ]	7160
$P$ [MW]	316
$b$ [m]	200.1
$C_{L_{max}}$ clean [-]	1.6
$C_{L_{max}}$ takeoff [-]	1.7
$C_{L_{max}}$ landing [-]	1.75
$A$ [-]	5.59
$e$ [-]	0.77
<b>Aerodynamic Characteristics</b>	
Airfoils	NACA 2415; NACA 2420; NACA 2422; NACA 2424
High lift devices	Single slotted flaps (0.27b/2 - 0.58b/2; 0.75c - 1c)
Cruise $C_L$	0.62 @ $AoA$ 3 deg
Cruise $C_D$	0.022
<b>Propulsion System Characteristics</b>	
Type of Engines	Counter rotating propfans
Number of Engines	8
Power per engine [kW]	39270
<b>Structural Characteristics</b>	
Wing weight	$0.094W_{to}$
Fuselage weight	$0.097W_{to}$
<b>Weight and Balance Characteristics</b>	
Most forward cg [m]	42.24
Most aft cg [m]	47.60
<b>Stability Characteristics</b>	
Eigenvalues of Longitudinal Modes	
Short Period	-1.34439- 2.39760i -1.34439+ 2.39760i
Phugoid Motion	-0.00105- 0.02500i -0.00105+ 0.02500i
Eigenvalues of Lateral Modes	
Aperiodic roll	-4.09117+ 0.00000i
Dutch roll	-0.09879- 1.08688i -0.09879+ 1.08688i
Spiral motion	0.00154+ 0.00000i
<b>Subsystem Characteristics</b>	
$S_h$ [ $m^2$ ]	342
$S_v$ [ $m^2$ ]	398
Ailerons	0.6b/2 - 0.95b/2; 0.65c - 1c
Number of Struts	12 (main gear), 3 (nose gear) 12 main; 3 nose
Number of wheels	12x6 72 (main gear), 14 (nose gear)

## 7. Unmanned operations

One of the requirements for the HUULC is TR-OPS-FLIGHT-2, which states that “The HUULC shall have no crew and no crew support systems”. In order to meet this requirement, the HUULC will have to be an unmanned air vehicle. Most uses of UAVs are currently for military purposes. However, unmanned cargo vehicles (UCAs) are becoming an interesting topic, since several conferences are being held over the world and the use for civil applications is growing fast [80].

This chapter elaborates upon the benefits of having an unmanned cargo vehicle in Section 7.1, the implications that being unmanned has on the design of the HUULC in Section 7.2, the ground control station in Section 7.3, communications protocol in Section 7.4, commands and control in Section 7.5, and finally the technical specifications and signal to noise ratio in Section 7.6.

### 7.1. Benefits of an unmanned cargo vehicle

Where UAVs were mainly used in order to decrease the risk of losing well-trained man during military operations, the civil use of UAVs is becoming more convenient nowadays [80]. However, an unmanned replacement for passenger aircraft does not seem feasible. The presence of a crew will always be necessary for serving the passengers and to assist in, for example, evacuation in case of emergencies [81]. This does not automatically mean that a pilot has to be present to operate the aircraft. The aircraft can still be flown from the ground, but in case of trouble one may need ‘ears and eyes’ in the plane. One of the advantages of an UCA is therefore the transition step that it provides from military purposes to civil purposes. If it can be proven that UCAs are reliable and safe, the public might start to feel comfortable with an unmanned aircraft that provides passenger transport.

Another advantage is the flight time that may cause issues with intercontinental flights if the aircraft is manned. The absence of a crew on board provides possibilities regarding optimisation of flight speed for efficient and environmentally friendly engines. The flight speed of the HUULC is chosen to be 480 km/hr and the minimum flight distance is almost 6000 km [11]. This means that a pilot will have to fly the HUULC for more than 10 hours. According to FAA regulations, a pilot is allowed eight hours of flight time per 24 hour period (with some acceptances when it comes to exceeding this limit) [82]. Looking at the network assigned in Chapter 4 a rough estimation of salary savings can be made. The flights calculated in Chapter 4 are per 19 hours. Converting this to a 24 hour time scale, the flight crew operational costs for being manned and unmanned are calculated. Assuming an average salary of \$60 per hour, four pilots per HUULC, 365 days of availability, the total operational costs for all 287 HUULCS flying in the network is \$364,907,789.00, if all the HUULCs would be manned. For the unmanned operational costs, a total amount of 24 pilots is assumed to operate all ground control stations and alternate airports. This amount is chosen since we have six airports with three alternate airports in direct proximity of every airport. Assuming double the salary (\$120) for the responsibility the pilots have to take, a total operational cost of \$31,886,400.00 is calculated for all mission flights performed in a single year. This is 8.71% of the manned costs, and gives an insight in the operational cost savings that can be obtained by being unmanned. Note that this is only accounting for operational cost savings for flight crews on board. Another advantage is the operational efficiency; because there are no crews to be scheduled, the HUULC can fly to a destination, unload cargo, load new cargo and continue to its next destination, largely avoiding cargo denial and empty return flights. A rough calculation shows that one cargo denial between Yangtze River Delta region and Terneuzen would result a revenue loss of \$287,500. One can see that avoiding these empty return flights is beneficial for the operational costs of the HUULC.

### 7.2. Implications on the design of the HUULC

Unmanned aircraft have certain degrees of freedom compared to conventional manned aircraft regarding the design of control systems. The first advantage is the freedom in design configuration. Since the fuselage is not pressurised, the design is not constrained to a cylindrical fuselage and a blended wing body configuration is possible. Keeping the payload bay unpressurised and having a manned cockpit would result in large cabin dimensions, increasing the drag encountered.

In manned aircraft, control systems are generally located in the cockpit where the pilots have full control over the aircraft. The HUULC does not need a cockpit of this kind, since the pilots controlling the aircraft will be located in ground stations. The benefit of this is that the system components can be distributed over the aircraft, which comes with advantages regarding centre of gravity range. The control systems and indicators

that would be present in manned aircraft are now located at ground stations. This slightly reduces the weight, but this reduction is compromised by the additional weights of necessary communication systems on the aircraft. Transmitters, receivers and antenna's are part of this communication system. For the purpose of the HUULC, a full development of the system to control the vehicle is out of the scope. A concept for the communication flow is created and a link budget is calculated. The fact that no human life form will be present during flight makes the presence of passenger (emergency) doors unnecessary. Cut-outs in a fuselage have to be strengthened in order to prevent failure. The cargo entrances are the only necessary entrances and can be used for internal inspection. The absence of passenger doors simplifies the structural design of the HUULC in some degree and is regarded as an advantage for the structural engineers. One of the requirements of the HUULC is that it should be able to resist unauthorised control requests. For this reason, all data transmitted to and from the HUULC will be encrypted.

### 7.3. Ground control station

Ground control stations (GCS) are necessary in order to operate the aircraft. Every selected airport will have a GCS from where the HUULC can be operated. Take-off and climbing are flight phases performed by the controller in the GCS. The controller will have to operate all HUULCs departing from the airport he is located at, meaning that multiple HUULCs will be operated by a single controller. Since six airports are selected, six GCS will be present during the lifetime of the HUULC. The GCS will have interfaces for two communications systems; for Line of Sight operations and for Beyond Line of Sight operations. Interfaces for both systems will be implemented for the purpose of operation. Finally, it has to be stated that one controller can operate multiple HUULCS from the GCS. If the amounts of HUULCS departing from an airport gets excessively large, another controller can be added in order to decrease the operator workload. Finally, a telephone communication system will be added for the purpose of informing the ATC towers of the presence of the HUULC. The alternate airports will not have a GCS, but they will have the communications hardware necessary for performing LOS-operations in case of an emergency landing. The controllers at these airports do not need to be assigned for the full mission, but skillful pilots will have to be present in case of an emergency scenario.

### 7.4. Communications protocol

The controller in the GCS has full control over the line-of-sight (LOS) operations, using a flight stick controller. After the LOS operations, the HUULC enters the beyond-line-of-sight (BLOS) operations. This is mostly autonomous flight as will be explained in Section 7.5. At every entrance in a air zone of a new region/country, the GCS will inform the corresponding ATC tower about the presence of the HUULC. At the same time, a transponder will inform the ATC tower about the flight state and path of the HUULC.

As the HUULC enters the air zone of the region/country where its destination airport is located, the GCS at the departure airport will inform the corresponding ATC tower for the last time. After this, the satellite communications will be switched to GCS of the destination airport. A break before make system is chosen for this purpose, since the communications are not provided by a C2 link but rather by a SATCOM link and the aircraft is still in autonomous flight state, the make before break handoff seems redundant and is not chosen for the hand off of the communications [83].

When the HUULC enters its loiter phase(if necessary) the recovery procedure starts. This is part of the LOS operations and an instrumental landing system (ILS) will land the HUULC. The communications protocol is illustrated in Figure 7.1.

### 7.5. Command and control

The pilot located at the ground station has to perform flight operations. However, a large part of the mission will be performed autonomously with remote piloting during the important flight phases, such as take-off. An ILS system, based on differential GPS positioning, will be added for assisted landing in case visibility is low. Two phases of operations can be distinguished, namely: Line of Sight (LOS) operations and Beyond Line of Sight (BLOS) operations. The take off and landing are LOS operations, whereas climb and cruise are BLOS operations. Two different communication systems are designed for these operations. These are described in the sections below.

#### 7.5.1. Line of sight operations

For the Line of Sight operations, a direct, low-power link will be used between the HUULC and its ground centre. Take off and landing are important flight phases in which a live video feed is required for the GCS. The bandwidth of the communication system should be large enough to transmit live video feed data for the remotely piloted take-off. In Section 7.6.2 the required specifications for the line of sight operations are calculated.

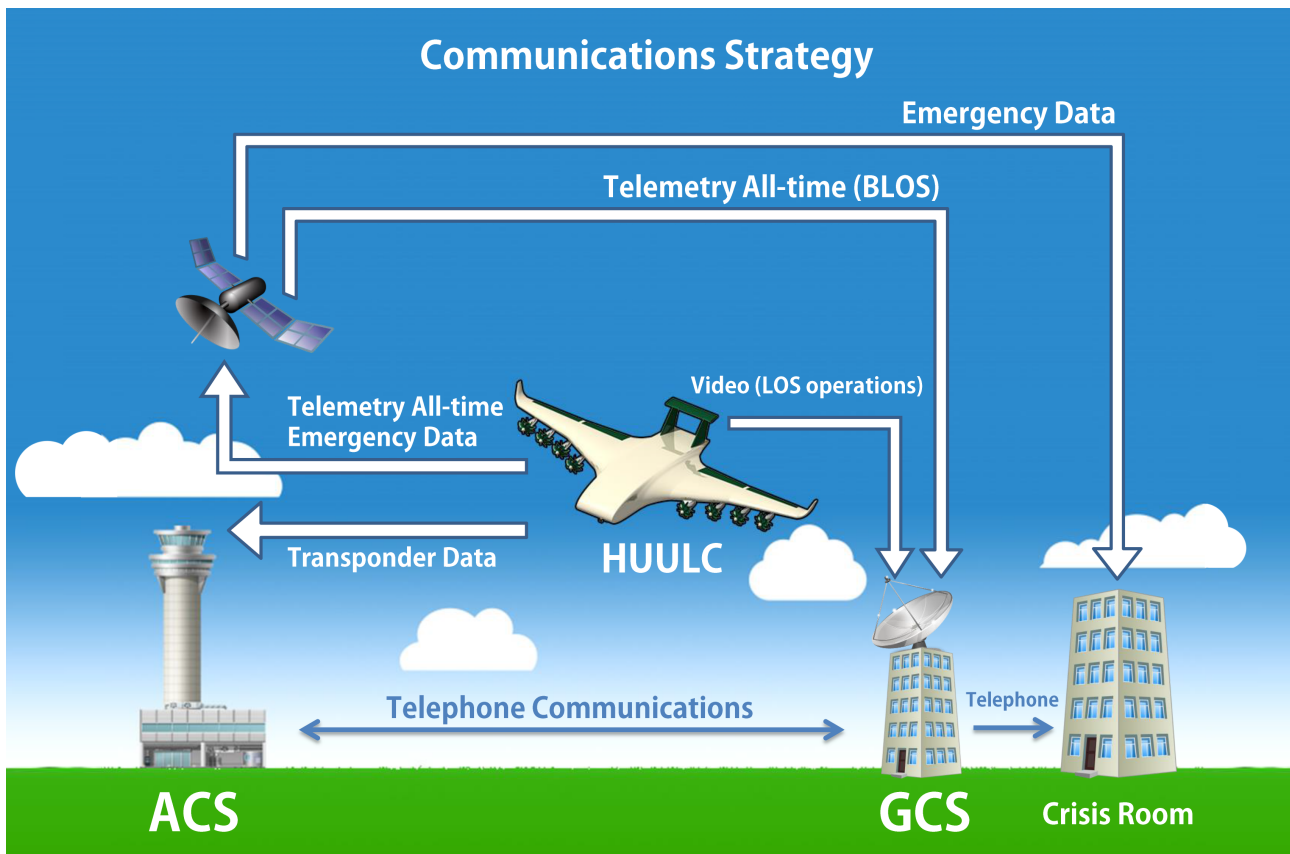


Figure 7.1.: A visual overview of the HUULC communications strategy. White arrows indicate communication between airborne systems, blue arrows indicate communication between systems on ground.

### 7.5.2. Beyond line of sight operations

After the LOS operations, the HUULC will enter the BLOS operations. These are mainly autonomous flight phases in which the HUULC will send data over a SATCOM link at all times. The data will contain all parameters of the flight state and path. These parameters are listed in Table 7.1.

The geostationary satellites deployed by Inmarsat are capable of receiving this data from the HUULC and transmitting it to the GCS [84] [85]. A proper communication system that complies with the needs of the HUULC is already available on the market. *Gilat BlackRay Parabolic System* is the name of this system and its technical specifications can be found in Table 7.2. A data link budget was calculated using the method described by Jay Gundlach in reference [83]. The calculation of this data link budget can be found in Section 7.6.1.

Cruise flight will be quasi-autonomously managed. A provisional flight plan will be loaded into the aircraft at the start of each flight. During cruise, the SATCOM link will be used to inform the GCS of the flight state and to transmit flight plan updates to the flight management system (FMS) of the HUULC. A live video feed during cruise would be expensive and add no more value to the system. In case of emergencies, the GCS will inform a crisis room where engineers are located to solve the problem. The bandwidth of the SATCOM link is large enough to transmit video feed for emergency cases. If there is an emergency, this large bandwidth will also be used to send more variables than the ones shown in Table 7.1 to the crisis room. Those variables can represent any data for which there is a sensor on the HUULC. This can include for example various engine parameters or data from the hydrogen tanks. All sensor data will be sent to a central computer, engineers in the crisis room will then be able to request values from specific sensors by sending requests to the HUULC.

### 7.5.3. GCS and ATC towers

The third communication link is between the operating GCS and the ATC towers of the air zones that are entered by the HUULC. Every time the HUULC will enter a new air zone, the operating GCS informs the corresponding ATC tower by telephone communication. Since this is a simple telephone communication link, a data link budget calculation is not performed on this communication flow.

Table 7.1.: Flight state parameters

	State variable	Notes
Position in Earth coordinates	$x_e$	Relative to a fixed longitude
	$y_e$	Relative to fixed latitude
	$z_e$	Relative to Earth's surface
Airspeed	$V$	Total airspeed
	$u$	Airspeed along x-axis(body)
	$v$	Airspeed along y-axis(body)
	$w$	Airspeed along z-axis(body)
Aerodynamic angles	$\alpha$	angle of attack
	$\beta$	angle of sideslip
Euler angles	$\psi$	Heading angle (relative to north, positive in west direction)
	$\theta$	Pitch angle (relative to horizontal, positive up)
	$\phi$	Roll angle
Accelerations in body axes	$a_x$	
	$a_y$	
	$a_z$	
Angular rates in body axes	$p$	Roll rate
	$q$	Pitch rate
	$r$	Yaw rate
Geographic position	$\lambda$	Latitude, can be related to $y_e$
	$\mu$	Longitude, can be related to $x_e$

## 7.6. Technical specifications and signal to noise ratio

Two different communication systems are present on the HUULC. One for BLOS operations and the other for LOS operations. The technical specifications of these two systems are given in Section 7.6.1 and Section 7.6.2. The required subsystems for flying unmanned are elaborated upon in Section 7.7.

### 7.6.1. BLOS operations

The communication link for the BLOS operations will be a SATCOM link. Inmarsat is chosen as a commercial retailer providing GEO-stationary satellites. *Gilat BlackRay Parabolic System* is chosen as the communication system on the HUULC. The technical specifications of this system can be found in Table 7.2. From this table, the total weight of the communication system may be estimated. The mass of the parabolic antenna is  $12kg$ , the block upconverter (BUC)  $3.6kg$  and the modem's mass is  $4.3kg$ . This combines to a total mass of about  $20kg$ , which is negligible when compared to the total mass of the HUULC. The system may be heavier however since redundancy will be used and also because some elements such as cabling and antenna radome are not taken into account. Also with Table 7.2 a data link budget may be calculated for the link margin. Jay Gundlach recommends a 10 dB link margin between the required signal to noise ratio and available signal to noise ratio. The calculations can be found below:

$$SNR_{available} = P_{carrier}(dBm) - P_{noise}(dBm) \quad (7.1)$$

$$SNR_{required} = \frac{Eb}{N_o} + 10 \log_{10} R_{data} B \quad (7.2)$$

$$P_{carrier}(dBm) = EIRP(dBm) + L_{Ptotal}(dB) + G_R(dBm) + L_R \quad (7.3)$$

$$P_{noise}(dBm) = 10 \log_{10} (1000kT)(dBm/Hz) + 10 \log_{10} (B) + NF(B) \quad (7.4)$$

$$(7.5)$$

Only the parameters that are not directly specified in the table will be elaborated upon in the following section.  $L_{Ptotal}(dB)$  is the propagation loss. In the case of the HUULC, atmospheric losses and precipitation losses are neglected, leaving only the free space loss. The free space loss can be calculated with Equation 7.6.

$$L_{Ptotal}(dB) = 20 \log_{10} \left( \frac{\lambda}{4\pi R} \right) \quad (7.6)$$

In which  $R$  is the distance between the HUULC and the satellite. This distance is assumed to be  $40000km$ . The height of the satellite above the earth's surface is  $35786 km$ . A margin of approximately  $5000km$  is taken for convenience. The total propagation loss is:

$$L_{Ptotal}(dB) = 20 \log_{10} \left( \frac{0.023}{4 \cdot \pi \cdot 40 \cdot 10^6} \right) = -206.76dB \quad (7.7)$$

$G_R(dBi)$  is the antenna gain of the receiver, which is the satellite in our case. This value is not known and left unsubstituted for now. As soon as the available and the required signal to noise ratios are calculated, one can choose an appropriate antenna gain receiver in order to comply with the recommended  $10dB$  link margin.

$L_R$  is the receiver loss and is the decibel sum of the receiver line losses, polarisation losses and the spreading implementation losses. The polarisation loss is a function of the bank angle. A maximum bank angle of  $45^\circ$  is assumed for the HUULC and this corresponds with a loss of six decibels. Spreading implementation losses are up to two decibels for links that use the spread system and the line loss can go up to one decibels.

$$L_R(dB) = (-6) + (-2) + (-1) = -9dB \quad (7.8)$$

The generated noise must also be calculated. The average temperature on earth is 250 K, which corresponds with a thermal noise of  $-174.6 dBm/Hz$ . The bandwidth noise is calculated with 7.9:

$$10 \log_{10} (B) = 10 \log_{10} \left( \frac{R_{data}}{\frac{R_{data}}{B}} \right) \quad (7.9)$$

Where  $R_{data}$  equals 20 Mbps and  $R_{data}/B$  equals 0.5 for BPSK systems.

$$10 \log_{10} \left( \frac{20 \cdot 10^6}{0.5} \right) = 76.02dB \quad (7.10)$$

The receiver noise figure is also a contributor to the generated noise. For Ku-bands this can be optimised to three decibels.

Substituting the values in the equations above yields:

$$P_{carrier}(dBm) = 81 + (-206.76) + G_R(dBm) - 9 = G_R(dBm) - 134.76 \quad (7.11)$$

$$P_{noise}(dBm) = -174.6 + 76.02 + 3 = -95.58 \quad (7.12)$$

$$SNR_{available} = P_{carrier}(dBm) - P_{noise}(dBm) \quad (7.13)$$

$$SNR_{available} = (G_R(dBm) - 134.76) - (-95.58) = G_R(dBm) - 39.18 \quad (7.14)$$

$$(7.15)$$

$$SNR_{required} = 0.8 + 10 \log_{10} 0.5 = -2.2102dB \quad (7.16)$$

In order to comply with the  $10 dB$  link margin, the available signal to noise ratio has to have a minimum value of  $7.79 dB$ . So the antenna gain of the receiver must have a minimum value of  $46.97 dBm$ . The relation between the gain and the size of the antenna is:

$$G = \eta_{antenna} \cdot \left( \frac{\pi D}{\lambda} \right)^2 \quad (7.17)$$

To convert this to decibels, the following operation is performed:

$$46.97 = 10 \log \left( \eta_{antenna} \cdot \left( \frac{\pi D}{\lambda} \right)^2 \right) \quad (7.18)$$

$$\eta_{antenna} \cdot \left( \frac{\pi D}{\lambda} \right)^2 = 10^{4.697} = 49773.7085 \quad (7.19)$$

$$D = 1.95m \quad (7.20)$$

$$(7.21)$$

Geostationary satellites have large antenna diameters and it is assumed that the parabolic dishes of the Inmarsat satellites comply with the minimum value of  $1.95 m$  [84] [85]. The data link budget was only calculated in one direction. Taking the EIRP of the BlackRay system, it is possible to calculate the transmitting power of the system (without transmitting gain). This power was calculated to be 25 Watts. It is assumed that the Inmarsat satellite has the same transmitting power and the communication flow can be realised in both directions. Now the available signal to noise ratio becomes:

$$SnR_{available} = 46.97 - 39.18 = 7.79dB \quad (7.22)$$

$$SnR_{required} = 0.8 + 10 \log_{10} 0.5 = -2.2102dB \quad (7.23)$$

$$LinkMargin = 7.79 - (-2.2102) = 10.0002dB \quad (7.24)$$

The link margin of 10 dB is desired according to J. Gundlach [83]. However, it is also stated by Gundlach that this 10 dB link margin is slightly exaggerated. Nevertheless, it is taken as the margin since the calculations do not take the presence of a radome around the antenna into account, which will cause losses in the transmitted power.

Table 7.2.: Gilat BlackRay Parabolic technical specifications

BlackRay Parabolic BRPKu/30B	
Antenna Size	60cm
Frequency $T_x$	13.75-14.5GHz
Frequency $R_x$	10.95-12.75GHz
Polarization	Linear
$T_x$ Gain	36dB
EIRP	81dBm
Data rates	over 20Mbps
Modulations	BPSK, QPSK, 8PSK
Spread Spectrum	Spreading factor 1-16
SNR	-12 to +13dB
Typical Eb/No for BER=10-8	0.8dB(BPSK $\frac{1}{2}$ LDPC 12k block length)
Dimensions	Antenna: 62L $\times$ 62W $\times$ 62H [cm] BUC(40W Ku): 22.6L $\times$ 13.7W $\times$ 10.7H [cm] Modem: 25.5L $\times$ 24.5W $\times$ 8.4H [cm]
Weight	Antenna: 12Kg BUC(40W Ku): 3.6Kg Modem: 4.3Kg
Temperature	-40 to +55 deg
Vibrations	Mil Stf 810F
Voltage	22-32VDC
Data(IP)	Ethernet 10/100/1000 Base-T

## 7.6.2. LOS operations

For the landing and takeoff phases, constant video stream will be sent from the HUULC to the GCS at the airport. Even though the satellite link above has sufficient capacity to provide video feed to the airport, a direct HUULC to airport link will be used for two key reasons:

- No need to pay for satellite bandwidth capacity
- Lower latency, which can become significant for geostationary satellites

For the LOS operations it is assumed that the HUULC will transmit live video feed and telemetry data for a distance of up to 30km with respect to the airport. The purpose of this section is to describe the characteristics of a system that could allow to close the link budget for a distance of 30km and a data rate of 20 MBps.

Since the same bitrate is used and assuming the same modulating technique, from section 7.6.1 the  $SNR_{required}$  does not change and is still -2.2102 dB. Furthermore, since the distance is much smaller, it is assumed that a simple isotropic antenna can be used. With this in mind, the carrier power can be written as:

$$P_{carrier}(dBm) = EIRP(dBm) + L_{Ptotal}(dB) + L_R \quad (7.25)$$

Since an isotropic antenna is used,  $G_R$  is omitted. Assuming an emission power of 10W for the EIRP and the same value for  $L_R$  as for BLOS operations, the carrier power is as follows:

$$P_{carrier}(dBm) = 92.1(dBm) - 20 \log_{10} \frac{0.125}{4 \cdot \pi \cdot 30 \cdot 10^3} - 9dB = -46.49 \quad (7.26)$$

If the same noise temperature is assumed as in Section 7.6.1, the signal to noise ratio is given by  $SNR_{available} = -46.49 - (-95.58) = 49.1dB$ . Since the  $SNR_{required}$  is -2.21 dB, this means that an important margin is

available if a transmitter power of just 10 W is used.

However this is useful as the receiver noise figure might be different for LOS operations compared to BLOS operations. Also, the antenna was assumed to be isotropic, which means that power is equally radiated in all directions. As this is rarely the case it should be expected that the emitted power is less in some directions, which adds to the argument of keeping an important signal to noise ratio [83]. Other factors such as losses due to multipath propagation are not taken into account, so the emitter power is kept at 10W to allow for sufficient margin. If communication is lost, an alternative control sequence should take over control of the HUULC. For example, the first could be to keep the altitude for several seconds, If after those few seconds the connection hasn't resumed, data could be sent over the satellite communication link. Furthermore, since communication during the takeoff and landing phase a communication link is critical, multiple backup systems could independently be installed on the HUULC.

## 7.7. Software and hardware

In order to operate the HUULC unmanned, several sensors and actuators will have to be implemented in the design. This section elaborates further upon on the necessary systems and the implemented software. The allocation of the sensors and antennas can be found in Figure 7.2.

**Flight management system** The flight management system (FMS) performs flight critical and unmanned aircraft operation functions. Interfacing to command and control communication systems, subsystems and the autopilot is part of the FMS. The flight paths for autonomous cruise phase will be implemented into the flight management system. A contingency management algorithm will be implemented to provide limited controller interaction in case of contingencies. The FMS will be hosted by one computer, but a back up computer will be added that can take over in case the main computer fails. In case of communication loss, the FMS will be able to resume the flight plan until either the satellite link is re-established or the LOS link is connected near the destination airport. In case the connection loss takes longer than 10 minutes, the HUULC will fly to a pre-ordered alternative airport on its route where an ILS landing would be performed.

**Navigation sensors** The navigation sensors will rely on the GPS system available with GEO satellites. This system provides optimal information on location and flight state. The parameters described in Section 7.5 include several position parameters which can be provided by the GPS system. Since this system is critical for the HUULC, a high level of redundancy will be applied. This is done by integrating multiple navigation sensors that work separately. If one of the sensors fails, the system relies on the other sensors that will provide sufficient information. Another back-up system will be the use of an altimeter and radio-navigation in order to validate the GPS measurements or as secondary system if the satellite receiver fails.

**Air data systems** A pitot-tube and static port will be implemented in order to measure the dynamic pressure. From this dynamic pressure, the equivalent airspeed can be derived. The equivalent airspeed can be converted to the true airspeed by correcting for the density at altitude. Pitot tubes are generally installed at several locations for redundancy. Multiple pitot tubes will be present on the HUULC for this purpose.

**Airspace integration systems** The HUULC will share airspace with other (manned) aircraft. Several systems help support safe integration to avoid collisions. The GCS will inform the ATC tower of the corresponding air zone about the presence of the HUULC. A transponder will be implemented so the HUULC is able to inform other air traffic of its presence. The transponder type is chosen to be a Mode S type. This transponder supports anti-collision systems (ADS-B and TCAS). It protects against excessive interrogation and works with modes 3/A and C, which provide indent, pressure altitude and position. A Traffic Collision Avoidance System (TCAS) will be added for warning in case of collision hazards. The TCAS works with Mode S transponders from other aircraft. It also identifies mutual avoidance maneuvers when there is a collision risk. Autonomous airborne response is used to actually perform the maneuver.

The HUULC will also be illuminated to avoid midair collisions. The same lightning systems that are used for manned aircraft can be applied here. The two primary types of lightning are navigation and anti-collision lightning. It is assumed that applying all these systems provides a sufficient level of redundancy for the airspace integration.

**Take-off and landing aids** During take-off the HUULC is controlled by the GCS. An optical sensor will be present to provide the GCS with live video feed. The commands from the GCS are uploaded to the flight management system, which will use actuators to control the lifting surfaces. A detailed elaboration upon the control and command for LOS-operations is out of the scope of project HUULC and is not performed.

An instrument landing system is implemented for landing. Landing aids are necessary because the landing point of the HUULC must be intercepted within an acceptable tolerance. RF-based methods generally use a

narrow beam to guide the aircraft to the touchdown point. An example for this system is the UAV Common Automatic Recovery System (UCARS), which will be implemented in the HUULC.

Relative GPS positioning method determines the relative point between two GPS receivers. This is commonly known as differential GPS (DGPS). This system does not improve the absolute positioning accuracy; rather, it improves the accuracy of the position between two receivers.

The height of the HUULC will be estimated using AGL sensors. These sensors provide the height above the local surface. Radio altimeters will be used for this purpose.

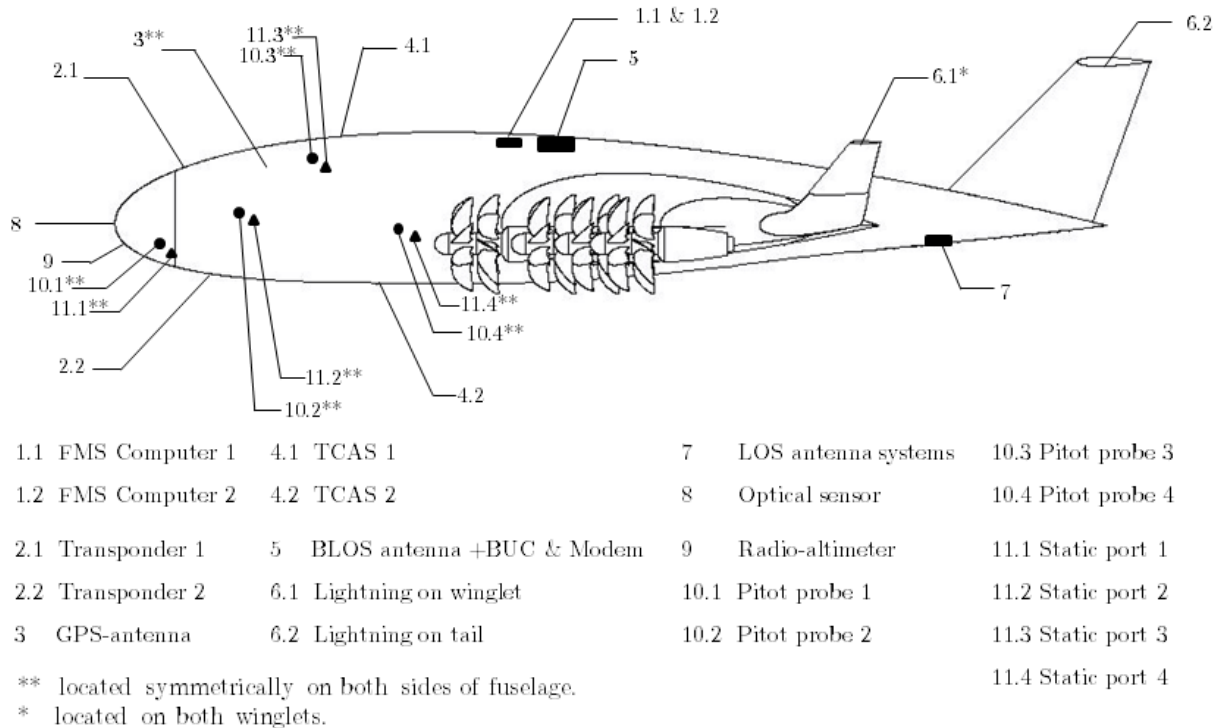


Figure 7.2.: Hardware diagram.

### 7.7.1. Conclusion and recommendations

The market for large unmanned cargo aircraft is not large enough to make a conclusion about the incorporation of the HUULC in this market [81]. The belly freighters that are used for the purpose of cargo transport are not used to their full potential. However, the HUULC will also compete with maritime transport, for which there is already a large market. The freight rate is low enough to convince customers to use the HUULC for their cargo transport. The benefits and operational cost savings described in the sections above are therefore assumed to outweigh the extra costs of the systems that will have to be added. Neglecting subsystems that would have to be added for a manned aircraft, such as a pressurised cockpit, also relieves some tension. Most subsystems described above are systems that are already present on manned aircraft and thus do not add actual costs. Installing the GCS is assumed to add initial costs. However, not having scheduling issues, multiple flight crews on a single flight and not pressurising the HUULC comes with great cost and life-time advantages. The current regulations for unmanned aircraft do not have many degrees of freedom. The strict regulations even allow small unprofessional UAV operators to operate more freely than the professional dedicated companies [81]. Revising these regulations is of great importance for full authorised operation of the HUULC. However, the intercontinental flights take place in international air zones where the regulations are not as strict. The problem is therefore restricted to certain countries where widely populated regions are present.

The team strongly believes that having the HUULC unmanned comes with certain doubts, but it is acknowledged that with improving regulations, the HUULC will find a stronghold in the current economy. The targeted market already provides enough possibilities and the low freight rate makes convincing the potential customers easier than the case in which only air cargo market would be targeted.

# 8. Airport analysis

This chapter includes an analysis of the airports that the HUULCs are going to use. In Section 8.1 the facilities and required area at the airport are discussed. In Section 8.2 the costs of building an airport are analysed. Next the analysis of the runways is done in Section 8.3 and Section 8.4 explains the loading and unloading systems used on the airports. One airport is chosen to give an idea of the overall architecture of the airport, this is shown in Section 8.5. Section 8.6 elaborates on the emergency procedures of the HUULC.

## 8.1. Required facilities

The first consideration that has to be taken into account when analysing an airport is how much space is required for the operation of the HUULC. Space is needed for: cargo storage, hydrogen storage, cargo handling but more importantly for the HUULCs. In Table 8.2 an overview is given of which facility is needed where and how much space is needed for each facility. Safety margins for the area have been used. The total area needed is given for each airport.

It has been decided that the Yangtze River Delta and the Western Europe region need two runways otherwise the time between two aircraft is too small. The same holds for Novosibirsk only it will need three runways. Table 8.1 shows the time between two aircraft landing or taking-off.

Table 8.1.: Amount of runways.

Region	Flights in 24 hours	Runways	use runway every...min
Yangtze River Delta	162	2	17.8
Western Europe	167	2	17.3
South East USA	51	1	28.5
United Arab Emirates	68	1	21.1
Hub 1: Novosibirsk	210	3	20.6
Hub 2: Anchorage	45	1	31.6

There are three major reasons why the HUULC will operate from dedicated airports instead of existing airports.

- Since landing fees are strongly dependent on MTOW, the cost for the HUULCs would be extremely high. The cost of the fees would be about half of the hydrogen costs. This could never work since hydrogen is 81 percent of the operating budget.
- In 30 years there will be 325 HUULC's in service. This means that every 3.5 minutes somewhere in the world a HUULC is departing or arriving. On average every 21 minutes a HUULC is departing or arriving on an airport. If a regular airport is used this means the HUULC should almost have a private runway.
- The last reason is that the HUULC will have a wingspan of 200 meters. This is something that normal airports cannot handle without enlargement of the run- and taxiways.

With these three reasons in mind, the team decided on building dedicated airports.

Table 8.2.: Area needed on airports

Region	Type of facilities	Amount	$m^2$	$km^2$
Yangtze River Delta	Hydrogen Storage	1	1,037.64	0.001
	Cargo Storage in containers	2500	14,862	0.014
	Places for HUULC's	25	750,000	0.750
	Cargo handling and taxi		2,250,000	2.25
	Runway	2	4,000,000	4.00
	<b>Total</b>			<b>7015900</b>
Western Europe	Hydrogen Storage	1	1,037.64	0.001
	Cargo Storage in containers	2600	15,457	0.0154
	Places for HUULC's	26	780,000	0.780
	Cargo handling and taxi		2,340,000	2.34
	Runway	2	4,000,000	4.00
	<b>Total</b>			<b>7136494</b>
South East USA	Hydrogen Storage	1	1,037.64	0.001
	Cargo Storage in containers	800	4,756	0.004
	Places for HUULC's	8	240,000	0.24
	Moving place		532,800	0.532
	Runway	1	2,000,000	2.00
	<b>Total</b>			<b>2778593</b>
United Arab Emirates	Hydrogen Storage	1	1,037.64	0.001
	Cargo Storage in containers	1100	6,539	0.006
	Places for HUULC's	11	330,000	0.33
	Cargo handling and taxi		990,000	0.99
	Runway	1	2,000,000	2.00
	<b>Total</b>			<b>3327577</b>
Hub 1: Novosibirisk	Hydrogen Storage	1	1037.64	0.001
	Places for HUULC's	21	630,000	0.63
	Maintenance Facilities	47	1,410,000	1.41
	Taxi		4,080,000	4.08
	Runway	3	6,000,000	6.00
	<b>Total</b>			<b>12121037.64</b>
Hub2: Anchorage	Hydrogen Storage	1	1037.64	0.001
	Places for HUULC's	5	150,000	0.15
	Taxi		450,000	0.45
	Runway	1	2,000,000	2.00
	<b>Total</b>			<b>2601037.64</b>

## 8.2. Budget for building the airports

The budget available for building a new airport and operating on an airport is the remaining 19 percent of the operational budget. This budget equals 115.26 billion dollar.

The relative percentages for the structural cost of building an airport and the operating cost are respectively 8 and 92 percent. The total amount of \$bn 19.21 is addressed with respect to the relative percentages. A cost estimation of one of the six airports is given in Table 8.3.

To estimate the cost of an airport, the following costs can be verified:

- Land price. An average of the price of land in every region is given in Table 8.4. There is a safety margin of 50 percent on required area.
- By taking into that that a runway at Schiphol airport costs 500 million euro and the HUULC project needs 10 runways, the total amount for runways and taxiways is \$bn 6, this will be feasible.
- In the midterm report the fees to fly over a country were estimated to around €42.5bn over the total lifespan. In this budget of table 8.3 there is around \$42.4 billion estimated for the fees. This is slightly under budget but the team expects to have funding or discount because these taxes are mainly calculated using distance and MTOW.

Table 8.3.: Costs of building one airport.

	Percentages	Percentages	\$bn
<b>Structural</b>	100	8	1.54
Land cost	5	0.4	0.0768
Research	2	0.16	0.0307
Permits	3	0.24	0.0461
Runway	65	5.2	0.999
Lighting, markings and navigation	3	0.24	0.0461
Equipment	3	0.24	0.0462
Hangars	9	0.72	0.138
Others	10	0.8	0.154
<b>Operation &amp; maintenance activities</b>	100	92	17.7
Personnel costs	14	12.88	2.47
Cargo handling	10	9.2	1.77
Maintenance runway	15	13.8	2.65
Maintenance aircraft	8	7.36	1.41
Runway operations	5	4.6	0.884
Insurance	6	5.52	1.06
Others	2	1.84	0.354
Fees	40	36.8	7.07
<b>Total</b>		<b>100</b>	<b>19.2</b>

Table 8.4.: Land prices by region.

Region	Cost per hectare [Dollar]	Land needed [ $km^2$ ]	Total [Million Dollar]
Yangtze River Delta	90,000	10.52	94.71
Western Europe	80,000	10.70	85.64
South East USA	50,000	4.17	20.84
United Arab Emirates	70,000	4.99	34.94
Hub 1: Novosibirsk	1,000	18.18	1.818
Hub2: Anchorage	40,000	3.90	15.61
		<b>Total [Millard Dollar]</b>	<b>0.254</b>

### 8.3. Runway

The runway is a crucial part in the design of the HUULC. For the loading and unloading of the payload, the aircraft has to take-off and land on different airports. Runways are required to perform this action and therefore, runways in general have to be investigated. The types of the most common runways [86] can be divided into the following list:

- Asphalt
- Concrete
- Grass
- Gravel
- Ice
- Sand
- Snow
- Water

Because the HUULC will have a large MTOW, the loads from the aircraft acting on the ground are too high for a runway made out of grass, gravel, ice, sand or snow. The design of the aircraft will not allow for lower loads to land on these kind of surfaces. Therefore, the remaining kind of surfaces to investigate are asphalt, concrete and water.

The advantage of a runway made out of asphalt or concrete is that these kind of runways already exist on current major airports and that the required infrastructure for the logistics is present. A runway made out of water does not have the issue related to loads from the aircraft to the water, but, in fact, it is the other way around. Because none of the HUULC concepts allows for take-off and landing in water, the only type of runway left for further research is asphalt or concrete.

### 8.3.1. Load identification

To investigate the loads of the aircraft acting on the runway, an analysis based on existing aircrafts has been made. This clearly shows the maximum allowable load needed per wheel, in order to land on the runway without damaging the asphalt or concrete itself. The results can be found in Table 8.5.

Table 8.5.: Load identification.

Aircraft	MTOW [kg]	# of wheels	Weight per wheel [kg]
Airbus A350-900 [87]	268,000	8	33,500
Airbus A380F [88]	592,000	20	29,600
Antonov An-225 [89]	640,000	28	22,857
Boeing C-17 [90]	265,350	12	22,113
Boeing 747-8 [91]	448,000	16	28,000
Boeing 777-300 ER [92]	351,500	12	29,292
Boeing 787-10 [93]	253,000	8	31,625

It is assumed the wheel load is purely based on the load acting on the main landing gear. One also has to be aware of the fact that during landing, the wheel load increases due to impact when touching down. Furthermore, a bumpy runway may cause the aircraft to bounce over the pavement, generating small impacts during the run. The pavement of the runway is designed to comply a maximum load (including impact) of 45,000 *kg* per wheel [94]. In Section 6.7.8, it is found that the landing gear allows this loads.

When designing a landing gear, one also has to account for the load interaction between the wheels themselves. This holds that if the spacing between wheels is too small, the loads of the wheels will interact with each other, generating higher load peaks which can still cause damage to the pavement. Therefore, a design has to be made in order to have the correct number of wheels, but also to have an adequate distance where no load interaction onto the pavement occurs [94].

### 8.3.2. Wheels vs. weight

To get a feeling of how the landing gear influences the weight of the aircraft, one can assume two methods. The first method is the “theoretical line neglecting interaction”. This holds that a 50% increase in the number wheels leads to a weight increase of 50% as well. The second method is the “capacity based on current FAA procedures”. This holds that a 50% increase in the number of wheels leads to a weight increase of 30%. Therefore, it can be assumed that the weight of the HUULC will increase between the 30%-50% if the amount of wheels doubles [94].

### 8.3.3. Pavement type

Investigating the runway itself, the runway can be divided into a rigid and a flexible pavement. The rigid pavements is usually made out of concrete, while the flexible pavement is usually made out of asphalt [95]. A rigid pavement characterises itself by distributing the load over a wide area of sub-graded soil. Rigid pavement is laid in slabs with steel reinforcement. A flexible pavement characterises itself by reflecting the deformation of sub-grade and the subsequent layers to the surface. This kind of pavement is laid with no reinforcement, or with a specialised fabric reinforcement that permits limited flow or repositioning of the roadbed under ground changes. However, the maximum loading stresses between a rigid and flexible pavement are about the same. Therefore, no distinction between an asphalt or concrete runway can be made and both can be assumed to be useful to use for the HUULC.

## 8.4. Loading and unloading architecture

The HUULC project is a huge initiative. With 325 projected units to be produced, each with a 97-100 TEU capacity and an availability of 85%, airports will not only be strained by the sheer size of the aircraft but also by the number of containers that must be loaded and unloaded within a strictly-defined turn-around time of six hours. For example, the busiest airport of HUULC operations, the airport of Western Europe, will be accommodating 26 HUULCs at any given time. This results in approximately 2,550 containers needing to be handled at a single given time. This difficult task, coupled with the fact that no existing air cargo handling system has been designed to process anything the size of a TEU container, leads to the need for a new and innovative cargo handling logistical system.

The development of such a system will be done in three steps: first, the skeleton of the airport will be designed, namely the parking formation of the aircraft. Secondly, the circulation of the containers will be developed, including the vehicle of transport. Finally, the interface between the aircraft and the cargo handling system will be designed.

### 8.4.1. Aircraft parking formation

With a wingspan of  $200m$  per aircraft, parking these aircraft for unloading and loading operations will require a very large area. Therefore, the first step in reinventing a logistical system is to determine an efficient parking formation. A traditional airport formation with terminals was initially considered, as this seemed to concentrate operations at the centre and minimise the total surface area required. However, manoeuvring 26 aircraft of large wingspan between terminals will not only be time-consuming but will also run the risk of damaging an aircraft or a terminal.

Instead, a simpler and more straight-forward parking formation was selected, which is believed to minimise transit times between the runway and the loading/unloading area. HUULC aircraft will be parked side-by-side, in a tip-to-tip manner, in groups of five. Another five aircraft will be parked directly in front of this group, with the two groups facing each other. Hence, a one kilometre line will be made, where two groups of five HUULCs will be on either side, facing one-another other, as shown in Figure 8.1. This parking formation will be repeated side-by-side, with container storage hangars at the end.

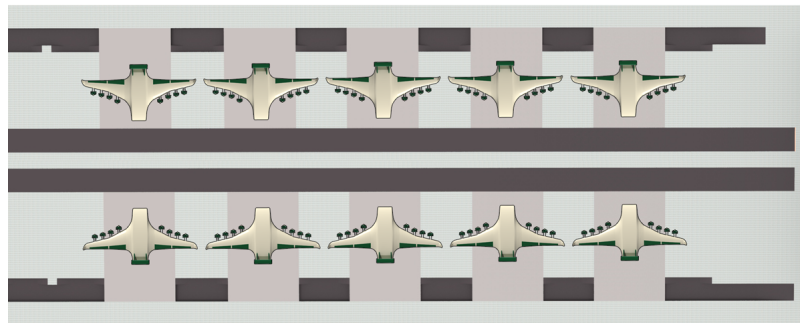


Figure 8.1.: Top view of a single set of the HUULC airport parking formation

Initially, one may think that this formation creates an unnecessarily long parking 'strip', which is much less compact than the traditional airport parking formation. However, the runways required for the HUULC are also long and thus placing such a parking area between two runways ensures minimal surface area between runways and parking areas is wasted. At the same time, this parking formation makes taxiing between the parking terminal and runways very streamlined and quick. Figure 8.2 shows the difference between these two parking formations and the aforementioned advantages of the new parking concept, where the short lines represent a HUULC aircraft each. The traditional airport has the advantage that runways that are closely spaced, the landing and departures on the two runways can not be conducted independently. Since the spacing between the runways is  $1357\text{ m}$  (as can be seen in the figure on page 103) and the minimum separation for two runways that can operate completely independent is  $1311\text{ m}$  the HUULC will not experience any disadvantage of the new architecture.

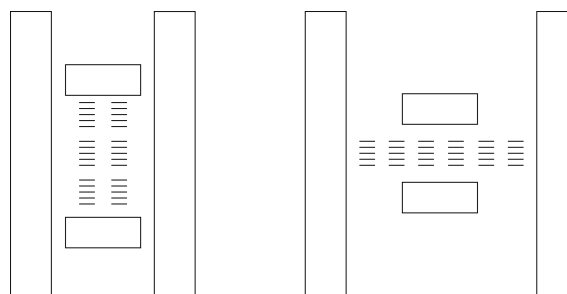


Figure 8.2.: Top view of new HUULC airport architecture (left) vs traditional terminal architecture (right)

### 8.4.2. Container circulation network

Now that the skeleton has been established, the second step in the development of a new cargo handling logistical system is to select how the cargo will be transported between the aircraft and the container storage hangars. Concepts from ports were studied, where containers are transported by cranes. This is a very efficient method for maritime containers, as they can directly be lifted off the vessel by crane and placed onto the storage area. This method will not be as efficient with the HUULC, as the cargo must first be removed from inside the vehicle, before it can be lifted by crane.

Further research showed that certain large ports use automated vehicles to transport TEUs, known as automatic guided vehicles, or AGVs [96]. These vehicles are simply a flat platform large enough to hold a single TEU, on

four wheels. With the simplicity of these vehicles, many can be ordered at a comparable price to only one large crane with the added benefit of increased flexibility and a much higher throughput. Each HUULC will have 97-100 containers, each of which may need to be brought to a separate section of the storage hangar or even a different storage hangar. Multiple AGVs will allow this more complex circulation.

The AGVs must travel on a route that minimises the time to reach an aircraft but also a route that does not interfere with the aircraft when they leave the terminal to taxi. This is where the selected parking formation shows its usefulness: In between each row of aircraft, there will be four straight roads, two adjacent roads called 'travel roads' and two roads closer to the aircraft, called 'loading roads', as seen in Figure 8.3. AGVs will travel on the travel roads, single file, in the same direction. Once the AGV has reached the correct aircraft, it will enter the loading road and park directly in front of the aircraft. With the benefit of automation, the AGV will park along the same longitudinal line that its TEU will enter the aircraft. Since the HUULC carries TEUs in rows of nine, a total of nine containers will line up side-by-side in front of the HUULC nose. The same procedure will occur on the rear side of the aircraft for unloading, except now the travel road must be underground, so that aircraft may enter and leave their parking spots without AGV interference. In the back, the road closer to the aircraft is called the 'unloading road', as this is where AGVs will park to unload cargo from the rear. The AGVs will use the travel roads to travel to and from the aircraft and the storage hangars. Upon arrival in the storage hangar, the contents of the special HUULC TEU containers will be repacked into a traditional corrugated steel TEU, ready to be transported out of the airport.



Figure 8.3.: Side view showing travel roads, loading roads (near nose) and unloading roads (near tail)

### 8.4.3. Aircraft - cargo handling system interface

The most efficient method of loading and unloading that comes to mind is using a ramp. However, the rectangular shape of the TEUs will make the use of a ramp difficult at the top and bottom of the ramp. Furthermore, a complicated system will be needed to push the TEU up the ramp. Hence, a hydraulic device which lifts the payload vertically into the aircraft seems more appropriate for this application. Having a loading and unloading mechanism on-board the aircraft increases the weight of the system and thus the fuel used. Instead, it is desired to keep such a system at the airport. For this reason, the HUULC will have two access points to the payload bay: the aircraft nose rotating upwards (similar to the Boeing 747 cargo aircraft) and a hatch on the underside of the aircraft, near the tail. The AGVs will be fitted with hydraulic actuators, enabling the lifting of each TEU up into the nose access point and through the aircraft hatch at the rear. Once the TEU is in the access point and level with the payload bay, it will be rolled into the payload bay by means of rollers or a rail system.

Having two payload doors greatly decreases the turnaround time, as compared to having only one. They can be used to unload cargo from both doors and then load new cargo from both doors. However, this method is not well-suited for the one-way travel roads. Two AGVs, one carrying cargo to an aircraft and one carrying cargo from an aircraft, would be travelling on the same road, creating clutter. Instead, loading will be done from the nose door, whilst at the same time unloading will be done from the rear door, as seen in Figure 8.4. This way, each travel road will be dedicated to the loading or the unloading of all aircraft. A loading AGV will be present at the nose of the aircraft, whilst at the same time its unloading-partner AGV will be present at the rear of the aircraft. Both AGVs will lift their platforms into their respective doors, the loading AGV with a new TEU on its platform, the unloading AGV with an empty platform. As the new TEU will roll from the loading AGV's platform into the payload bay, all TEUs in the aircraft will shift backwards with it. The rear-most TEU will roll onto the unloading AGV's empty platform. Both AGVs will lower their platforms, the loading AGV with a now empty platform and the unloading AGV with an old TEU, which will head to the container storage.

## 8.5. Airport architecture

In this section, the overall architecture of the airports is shown. First the locations of the 6 airports are shown using Google Earth. The pink area's are the areas used for the airports. When the airports were chosen a few particularities had to be considered:

- Water should be available for hydrogen production.
- The airport should not be too close to other airports and cities.

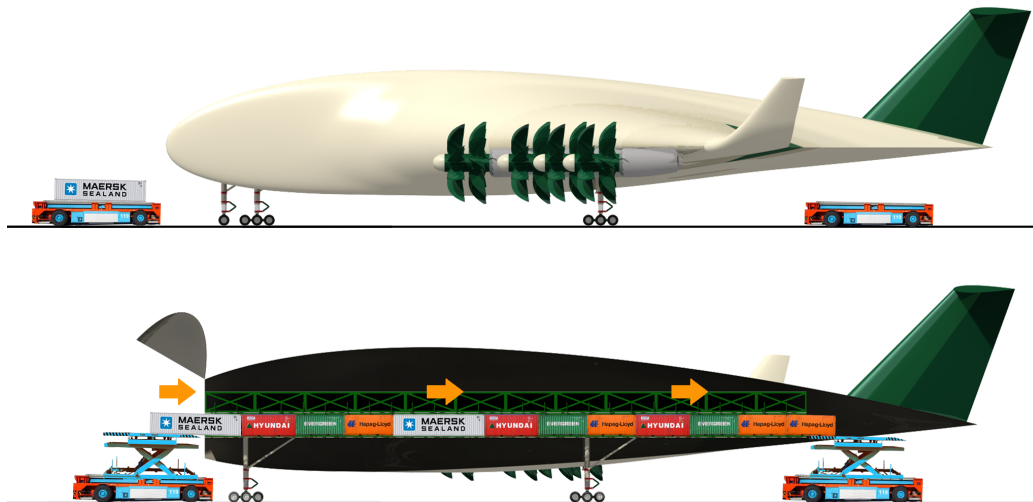


Figure 8.4.: Illustration of the simultaneous loading and unloading procedure, with nose-to-tail cargo flow

- The airport needs enough space without any interruption like roads or buildings
- The airports should be close to a main road to transport the cargo easily.

The airports are shown in the following pictures. The airport of Yangtze River Delta of  $10.52 \text{ km}^2$  can be seen in Figure 8.5. In Figure 8.6 the airport of Western Europe of  $10.70 \text{ km}^2$  is shown. Figure 8.7 presents the airport of South East USA of  $4.17 \text{ km}^2$ . The place of the airport of Arab Emirates of  $4.99 \text{ km}^2$  is displayed in Figure 8.8. Figure 8.9 shows the first hub: Novosibirsk of  $18.18 \text{ km}^2$ . The Second hub, Anchorage of  $3.9 \text{ km}^2$  is shown in Figure 8.10.

To have a good view on how the airports will look. The team decided to draw one airport with the right dimensions. In Chapter 4 the maximum places on an airport for the HUULCs are discussed. The maximum amount of HUULC parking spots will be in Western Europe. This is why the airport of Terneuzen will be elaborated upon. In figure on page 103 one can see the entire airport.

The space calculated for the airport is too large. The dimensions of the airport are  $4583\text{m} \times 1771\text{m}$ . This is slightly smaller than the dimensions calculated in Table 8.2. The dimensions of the runway, HUULCs, cargo handling and cargo storage are given in figure on page 103. The team decided on making the runway 4000 meters so that there will be no constraints in taking off. The width will be 200 meters. This is large because the wheels cover an area  $45 \text{ m}$  wide.



Figure 8.5.: Airport of Yangtze River of  $10.52 \text{ km}^2$



Figure 8.6.: Airport of Western Europe of  $10.70 \text{ km}^2$



Figure 8.7.: Airport of South East USA of  $4.17 \text{ km}^2$



Figure 8.8.: Airport of Arab Emirates of  $4.99 \text{ km}^2$

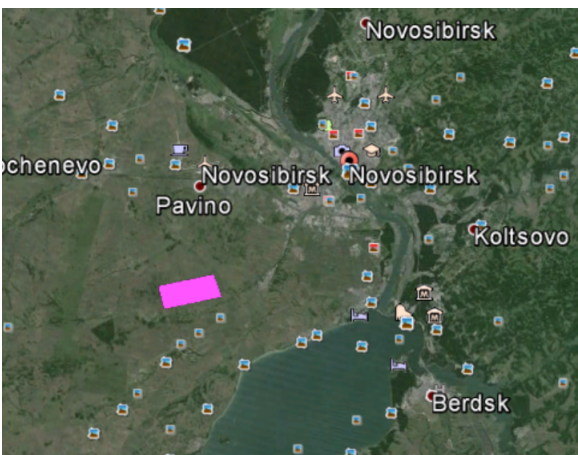


Figure 8.9.: Hub 1: Novosibirsk of  $18.18 \text{ km}^2$

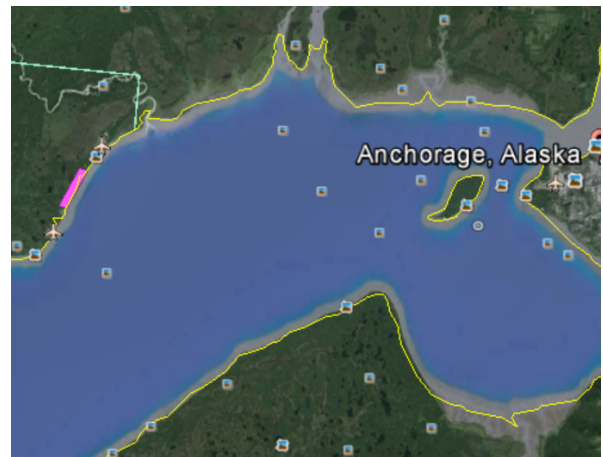
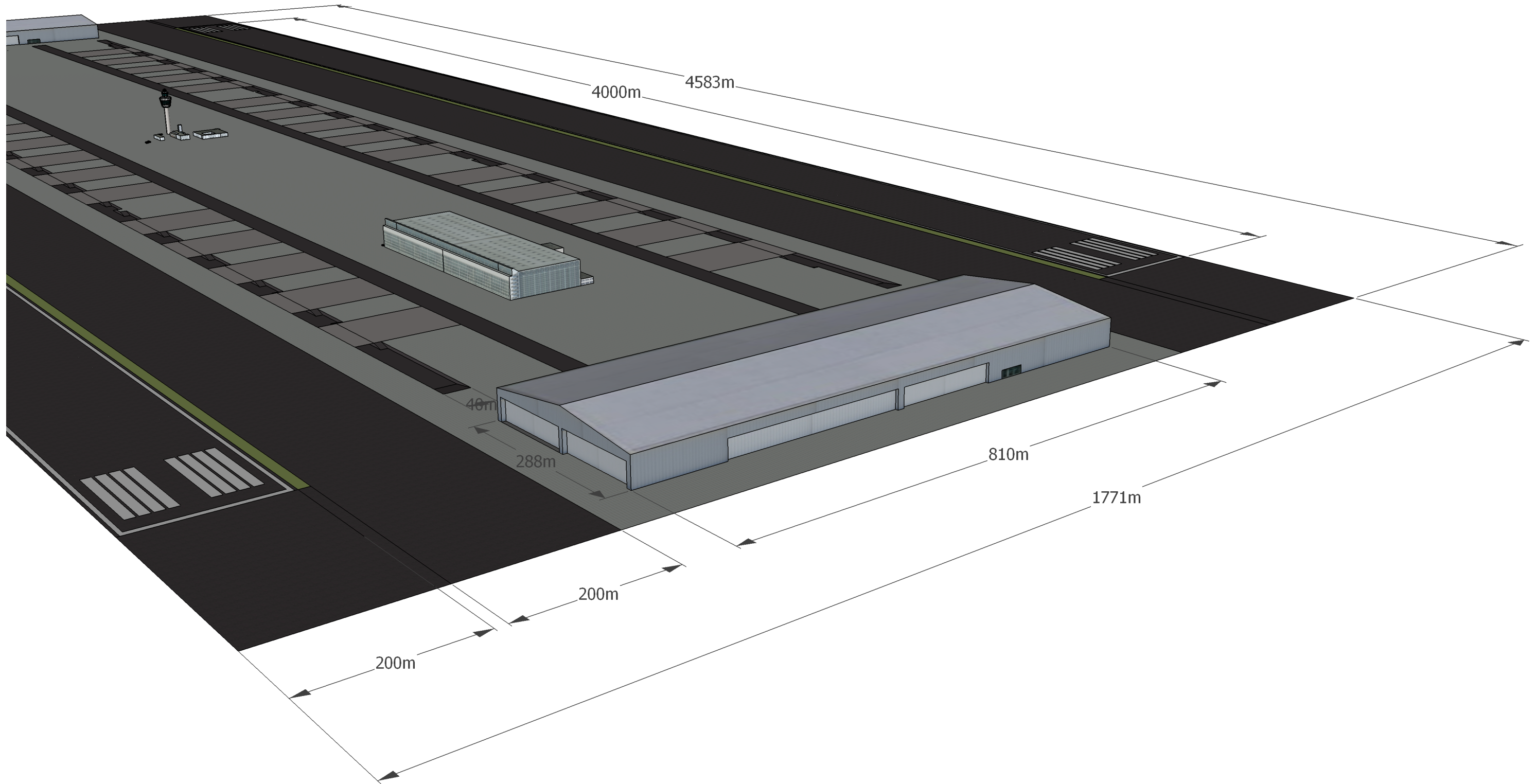


Figure 8.10.: Hub2: Anchorage of  $3.9 \text{ km}^2$



## 8.6. Emergency procedures

In case of any unpredicted events affecting the mission of the HUULC, an alternative procedure has to be followed in order to safely solve the situation. To accomplish this, several unpredicted events are taken into account, in which multiple solutions or procedures are designed. A distinction between the solutions will be made and in case of an emergency, the controller of the HUULC has to decide which procedure fits the situation best. This chapter describes two unpredicted events, which are diverting to an alternate airport, Section 8.6.1, and the need to land when the HUULC's weight still exceeds the Maximum Landing Weight (MLW), Section 8.6.2.

### 8.6.1. Alternate airport

The HUULC may find itself in the situation where no possibility can be found to land on its destination airport. In order to solve this problem, alternate airports around the destination airports are investigated in order to deliver the best possible solution. Examples in which an airport may be unavailable to land on are:

- Runway closed due to unpredicted maintenance
- Runway closed due to extreme weather situation
- Runway closed due to aircraft with problems (eg. fire, crash, terrorist attack) standing on the runway
- Runway and/or airport closed due to bomb threat

In case of long closure times, the HUULC must divert to an alternate airport. This is for the reason that at some point in time the HUULC will run out of fuel. To select the best possible alternate airport, a selection of airports in the region of the destination airport will be investigated. The investigation is based on the runway length, diverting distance to alternate airport, parking space and expansion possibilities.

The investigation of alternate airports around Memphis, Table 8.6, has led to the decision to use one primary and two secondary airports. The primary airport chosen is Arkansas International Airport. The two secondary airports chosen are Huntsville International Carl T. Jones Field and Nashville International Airport. The reason to have three airports is that one alternate airport will not be designed to completely park all HUULCs. The amount of HUULCs will therefore be distributed over three airports if necessary. The primary airport will be the first airport to be approached for landing and parking the HUULCs if necessary. This is due to its large parking spaces, runway length and the travel distance between the airport and Memphis International Airport. The two secondary airports may not be able to store as many HUULCs as the primary airport, but they will still function properly if necessary. Another downside of the two secondary airports is that the travel distance is around 300 kilometers, what automatically holds that additional fuel is needed to divert to these airports. The length of the runways of the three alternate airports are all longer than the required take-off distance of the HUULC. Therefore, no implications will be expected for the take-off and landing procedure.

Table 8.6.: Alternate airports around Memphis

Alternative airport	Runway length [m]	Airport distance [km]	Parking spaces [Lots, few, none]	Expansion possibilities [Lots, few, none]	Allocation [Primary, secondary]
Arkansas International Airport	3526	100	Lots	Lots	Primary
Huntsville International Field	3840	300	Few	Few	Secondary
Nashville International Airport	3362	320	Few	Few	Secondary

The downside of diverting is that not all facilities may be present to operate the HUULC while it is parked. For instance, the hydrogen fuel needed for the HUULC will not be present and therefore has to be transported from Memphis International Airport to the alternate airport. In case the payload has to be unloaded, specialised trucks are needed in order to ship the payload from the alternate airport back to Memphis International Airport.

Table 8.7 shows the investigation of alternate airports around Dubai. Even though Dubai has two additional airports, they have the allocation of being a secondary choice because of the business of the airports and the few places left to park the HUULC. Two slightly less busy airport with the proper space to park the HUULCs are Abu Dhabi International Airport and Al Ain International Airport. Because of the busyness and the parking spaces, these two airports are chosen to be the primary alternate airports. It has to be noted that Al Ain International Airport does not have many parking spaces on the tarmac, but, because of the condition of the ground, it is possible to park on the sand next to the tarmac. The third secondary choice airport is Muscat International Airport. This airport is relatively far located from Dubai, but it may provide enough parking spaces if necessary. All runways are longer than 4000 meters and therefore no implications for the take-off and landing procedures are expected.

Table 8.7.: Alternate airports around Dubai

Alternative airport	Runway length [m]	Airport distance [km]	Parking spaces [Lots, few, none]	Expansion possibilities [Lots, few, none]	Allocation [Primary, secondary]
Abu Dhabi International Airport	4100	70	Lots	Lots	Primary
Al Ain International Airport	4000	85	Lots	Lots	Primary
Dubai International Airport	4450	45	Few	None	Secondary
Sharjah International Airport	4063	60	None	Lots	Secondary
Muscat International Airport	4000	350	Lots	Few	Secondary

Not many alternate airports are available in the region of Anchorage, as shown in Table 8.8. All nearby airports have runway lengths which are too short for the HUULC. The only airport with a proper runway length is Fairbanks International Airport. Therefore, this airport is directly chosen as the primary alternate airport. The parking spots of the airport are already occupied, but if the private jets stationed at those spots are reorganised and properly parked, enough space is created to store the HUULCs. The secondary airport is Kenai Municipal Airport. The runway is in good condition, but it is not long enough to let the HUULC take-off with its MTOW. Therefore, landing on this airport has its consequence. Payload has to be unloaded from the HUULC in order to lower the aircraft weight and to shorten the take-off distance. Therefore, the secondary airport should only be used if no other options are left.

Table 8.8.: Alternate airports around Anchorage

Alternative airport	Runway length [m]	Airport distance [km]	Parking spaces [Lots, few, none]	Expansion possibilities [Lots, few, none]	Allocation [Primary, secondary]
Fairbanks International Airport	3597	420	Lots	Few	Primary
Kenai Municipal Airport	2387	95	Few	Lots	Secondary

The region around Shanghai shows a total number of four alternate airport, as shown in Table 8.9. All airports, except for Ningbo Lishe International Airport, have runways long enough to perform take-off and landing procedures at MTOW. The selection is therefore based on the availability of parking spaces and the flying distance to the alternate airport. It may be easy to say that the nearest located airport, called Shanghai Hongqiao International Airport, is the most logical choice for the primary alternate airport, but, because this is a very busy airport and just a few places are available for parking the HUULC, this airport is chosen to be a secondary alternate airport.

Table 8.9.: Alternate airports around Shanghai

Alternative airport	Runway length [m]	Airport distance [km]	Parking spaces [Lots, few, none]	Expansion possibilities [Lots, few, none]	Allocation [Primary, secondary]
Nanjing Lukou Airport	3400	290	Lots	Few	Primary
Hangzhou Xiaoshan International Airport	3600	165	Lots	None	Primary
Shanghai Hongqiao International Airport	3400	45	Few	None	Secondary
Ningbo Lishe International Airport	3200	150	Lots	None	Secondary

The region Western Europe has a lot of airports close to each other. A selection has been made to choose the best possible solution. The results are shown in Table 8.10. The new airport in Berlin, called Berlin-Schönefeld International Airport, still has to be finished, but therefore it also gives possibilities to include an expansion for parking places for the HUULC. Therefore, this airport is chosen to be the primary airport. Four secondary airports are chosen in the acceptable region near Zeeland. These airports are Luxembourg Findel Airport, Amsterdam Airport Schiphol, Hamburg Airport and Hannover Airport. The airport in Luxembourg is chosen because of its long runway and the yet existing cargo facilities. Amsterdam Airport Schiphol is chosen because of the long multiple runways and the possibility to expand the parking places. Also, this airport already has a lot of experience with large cargo aircrafts. The two German airports in the table are chosen because of their high quality runways and the parking places available.

Table 8.10.: Alternate airports around Terneuzen

Alternative airport	Runway length [m]	Airport distance [km]	Parking spaces [Lots, few, none]	Expansion possibilities [Lots, few, none]	Allocation [Primary, secondary]
Berlin-Schönefeld International Airport	4000	670	Lots	Lots	Primary
Luxembourg Findel Airport	4000	250	Few	None	Secondary
Amsterdam Airport Schiphol	3800	125	Few	Lots	Secondary
Hamburg Airport	3666	480	Few	Few	Secondary
Hannover Airport	3800	420	Few	Lots	Secondary

The region around Novosibirsk does not have many airports with large runways. For this region, three airports are chosen to be an alternate airport, as can be seen in Table 8.11. The primary airport chosen is Kemerovo

International Airport. This airport is located at 220 kilometers, while the Yemelyanovo International Airport, the secondary airport, is located at 600 kilometers. Both airports have the enough parking spaces and expansion possibilities. The Kemerovo International Airport has a runway of 3200 meters. This means that some payload needs to be unloaded from the HUULC in order to meet the take-off requirements of 3390 meters. Also, an tertiary alternate airport has been chosen. This airport is Yeltsovka Airport, which is located at the other side of the city of Novosibirsk. Because only a few airports are located within the region of Novosibirsk, it may occur that nearby the hub a real important emergency landing is required. The facilities of this airport are minimal and the condition of the runway is low, but a small investment will turn this airport into an acceptable alternate airport in case of important emergency landings.

Table 8.11.: Alternate airports around Novosibirsk

Alternative airport	Runway length [m]	Airport distance [km]	Parking spaces [Lots, few, none]	Expansion possibilities [Lots, few, none]	Allocation [Primary, secondary, tertiary]
Kemerovo International Airport	3200	220	Lots	Lots	Primary
Yemelyanovo International Airport	3700	600	Few	Lots	Secondary
Yeltsovka Airport	3350	25	None	Few	Tertiary

## 8.6.2. Exceeding MLW during landing

Another situation the HUULC may find itself in, is the possibility that it has to land while its weight still exceeds the Maximum Landing Weight (MLW). In order to solve this problem, the HUULC has to lose weight in order to be able to land safely. Therefore, this section will treat the multiple possibilities of decreasing the HUULC's weight.

### 8.6.2.1. Dumping fuel

The most common way of losing weight is by dumping fuel. The fuel will be dumped via a channel leading from the hydrogen tanks to the outside of the aircraft. The liquid hydrogen will be dumped into the air and will vaporise due to its very low boiling point. It has to be noted that hydrogen gas has the property to explode when in contact with fire or electrical charges. Therefore, the hydrogen has to be dumped in such a way that the hydrogen does not explode due to one of these factors.

### 8.6.2.2. Flying around

Another option of losing weight is flying around. This option takes considerable more time compared than dumping fuel, but this is one of the safest options for losing weight. In order to make this take the least possible time, the HUULC needs to fly at low altitude with landing gear down in order to increase the drag of the aircraft. As a result, more power is required and fuel is burnt much faster. The HUULC has to fly around until the weight of the aircraft is below the MLW.

### 8.6.2.3. Dumping payload

A less favourable option is dumping payload. If fast weight reduction is required and the fuel dumping system fails, this may be a considerable option. However, for the HUULC, payload is equal to revenue. The customer will not find itself into the position where it is glad its payload is dumped out the aircraft and smashed onto the ground. To avoid this, the containers might be equipped with parachutes to lower the impact on touchdown. Also, to avoid damaging properties on ground, this procedure can only be performed in inhabited regions, like above a desert or sea. After this procedure, a search and rescue team has to be set up to locate and retrieve the dumped payload and bring it back to the nearest airport.

### 8.6.2.4. Landing with overweight

If the three procedures above are not possible to perform, the only thing left for the HUULC is to take its weight for granted and land with a weight exceeding the MLW. This brings several risks along with it. Hereby, the largest risk one has to think about is that the landing gear will fail during touchdown and the HUULC will make an uncontrollable belly glide over the runway. In the worst case scenario, the aircraft might even break into pieces, set fire or explode. Then, the aircraft will be unrepairable and can be transported to the recycling facility. Another scenario is that the landing gear does not fail, but that the landing gear gets twisted or multiple tires will explode. These kind of damages can still be repaired, but it will take extra non-scheduled time. If the MLW is exceeded, the braking system may not be able to land the HUULC in time and the aircraft will run out of runway. This will cause some serious problems related to retrieving the very heavy aircraft which is sunk away in grass or sand. Also, during such a landing, the payload may encounter severe damage. The customer wants undamaged and on-time delivered payload, so this emergency procedure may cost a lot of money. Therefore, this procedure is the least favourable option.

### 8.6.3. Emergency procedures conclusion

Two unpredicted events affecting the mission of the HUULC were investigated. The two events were the selection of alternate airports and landing with exceeding MLW. For each destination, multiple airports were chosen based on their runway length, diverting distance, parking spaces and expansion possibilities. Four different procedures were treated for what to do if the HUULC's weight exceeds the MLW during landing. The two best solutions were found in the form of dumping fuel and flying around, while the two unfavourable solutions found were dumping payload and landing with a weight exceeding the MLW. One has to be aware that there is no perfect solution for each situation. In case of an emergency, the controller of the HUULC has to decide which procedure fits the situation best.

## 8.7. Conclusion and recommendations

Building the airports within the budget should be feasible. The result is that six airports are going to be built in the coming years. If something occurs that cannot be predicted there are emergency procedures that can be followed.

Some recommendations for a following project could be to think out a way for the road network. At this moment the team only thought about the cargo handling from the airport to the cargo storage but there is another challenge in handling the cargo from the storage to the customer.

Another recommendation is that at this moment there are six airports where a HUULC can take-off this is of course not optimal so it could be an option to look into other airports and what it should take to take off with an airplane of a wingspan of 200 meters.

The areas chosen for the airports are chosen using Google Earth but the team does not know if the landlords are willing to sell. That's why there should be a reserve option close by for building an airport.

There is no hangar that already can accommodate the HUULCs so the team recommends to look further in hangars of dimension around 500 *m*x 150 *m* so that the hangar can easily place 2 HUULC's for maintenance.

## 9. Hydrogen strategy

Hydrogen is the most abundant and lightest element in the universe [97]. At point-of-use, hydrogen is environmentally and climatically clean. Nowadays, using hydrogen comes with higher cost than using conventional fossil fuels, which is one of the main reasons why hydrogen is not widely used in aviation yet. Due to ever diminishing fossil fuel reserves and increases in hydrogen production technology maturity, it is expected that the production price of liquid hydrogen (LH2) will come down to equal the production price of kerosene in 2037 [98], after which it will drop even further.

Considering the facts given above, hydrogen is the obvious choice for the HUULC fleet to fly on. Hydrogen is abundant, will become cheaper and is sustainable. Also, in order to stand out in a market of fierce competition, one not only needs to be as good as the competition, but one needs to be better than the competition. This is especially the case when entering an existing market with large and experienced players. Hydrogen is one of HUULC's key aspects which enables the HUULC program to compete with the existing market. On Earth, hydrogen is only available in compounds. To produce pure hydrogen, it is required to free the hydrogen from their compound molecules, like  $H_2O$ . This process is more complicated than it seems at first sight. Doing this requires energy, compound molecules from which hydrogen will be subtracted and a sophisticated process. The current chapter addresses the hydrogen generation process by presenting an elaborate plan in which it is described how the hydrogen will be produced, stored and transported.

In Section 9.1 the complete LH2 production process is described, after which renewable energy generation is elaborated upon in Section 9.2. An overview of the process can be found in Section 9.3. A study of the possible hydrogen generation scenarios per airport is provided in Section 9.4, after which cost budgeting is performed in Section 9.5. In Section 9.6 the implications of using liquid hydrogen compared to kerosene are discussed. Subsequently, a landscape analysis can be found in Section 9.7 and in Section 9.8 a discussion on how the hydrogen plan should be executed is presented. An analysis of the feasibility conditions and parameters is included in Section 9.9. Recommendations and the conclusion are provided in Section 9.10.

### 9.1. Liquid hydrogen production

Processes to produce liquid hydrogen are numerous but all contain the same characteristic aspects of which the methods can vary. The dissection can be made by dividing into: energy input, chemical reaction, hydrogen source, liquefaction and storage. The different methods with regard to the aspects and rationale of design choices is provided in Section 9.1.1 to 9.1.4, respectively. The energy source is further elaborated upon in Section 9.2. The HUULC program will pioneer in sustainable transport by merely making use of renewable resources, which in combination with the financial aspect is the main driver in the LH2 production strategy.

#### 9.1.1. Hydrogen generation

The implications of the sustainable HUULC vision pose a challenge as present day hydrogen generation consists for 90% out of steam reformation, a thermal process which produces hydrogen by reacting hot steam with natural gas e.g. methane [99]. This process consists of multiple reactions of which the end products are carbon dioxide and hydrogen. Carbon dioxide can be sequestered which involves capturing and storing the carbon to prevent it attributing to global warming, which adds significantly to the cost of hydrogen production. Furthermore usage of fossil fuels makes the process non-sustainable and will therefore not be considered to power the HUULC fleet [100].

Renewable hydrogen production consists of three processes which can be utilised independently or combined. These processes are electrolysis, thermolysis or biologically through microorganisms of which merely electrolysis is currently implemented on a relatively large scale. Hydrogen production directly through biomass using biochemical or thermochemical has been disregarded, for reasons provided in Section 9.2.

Thermolysis can not be efficiently implemented as temperatures above 2500 K are required for water to dissociate into oxygen and hydrogen [101]. The high temperatures are usually generated by nuclear generators, not considered sustainable, and the high temperatures cause significant wear on the facility [102]. Biohydrogen makes use of organisms which convert hydrogen from water, but the production rates are too low to currently consider practical usage [103]. Electrolysis is applied all over the world to produce hydrogen for commercial purposes [104], and is considered the most practical and sustainable approach to generate hydrogen on large scale. Major improvements are made during the past years and the future is even more promising for the efficiency of electrolysis and will be the technology implemented in the HUULC's hydrogen production facilities.

Water electrolysis is widely implemented but accounts only for four percent of global hydrogen production [105]. The process of electrolysis is performed by drawing direct current through water with a salt solution where a membrane splits the reaction room with the cathode and anode on different sides of the membrane. Hydrogen gas will gather at the cathode and oxygen at the anode [106]. Electrolysis is expected to become more efficient, even though efficiency today is measured to be as low as 96% [105]. Using the theoretical specific power consumption of the higher heating value of  $39.4 \text{ kWh/kg}$ , this results in an electrolyser specific power consumption of  $41.0 \text{ kWh/kg}$  [107]. The costs to transform water into hydrogen and oxygen are threefold: the specific power consumption which dictates the required power generation facilities, the construction of the facilities and maintenance of the electrolysis facilities. The construction cost of the electrolysis facilities is estimated at \$780,000 in 2015 for a 50MW plant [108]. Using the process efficiency of 96%, the plant would produce 29,300  $\text{kg/day}$ . Maintenance costs are a function of the electrolysis capital value, costs are estimated at two percent of the initial investment per year [109].

### 9.1.2. Hydrogen source

To produce pure hydrogen gas, a hydrogen chemical compound is required from which hydrogen can be obtained. For electrolysis the source is water, which is abundant in the proposed airport locations. Terneuzen, Novosibirsk, Anchorage and Memphis are located near fresh water sources such as the Mississippi river and the Novosibirsk reservoir. River water in these countries is regarded as surface water and no abstraction fees are required [110]. In Dubai fresh water is scarce and in Shanghai surface water abstraction fees are charged so instead sea water will be used to produce the hydrogen [111]. Electrolysis of sea water results in the production of hydrogen, chlorine gas and sodium hydroxide [112]. The different byproducts can be used to capture carbon from the environment, implicating that the HUULC program not only has zero emissions, but improves the Earth's atmosphere [112].

Construction of the electrolysis facilities near the rivers or oceans allows the usage of kinetic or potential energy to transport the water to the facilities. Employing the kinetic flow energy of the rivers, the water can be pumped to the electrolysis facilities. If no flowing water is available, the electrolysis facilities can be constructed below sea level where a pipe connects the ocean to the electrolysis plant.

### 9.1.3. Hydrogen liquefaction

The products of water electrolysis are gaseous oxygen and hydrogen. Gaseous hydrogen has a density of  $0.0899 \text{ kg/m}^3$  at 273.15 K and atmospheric pressure, requiring large storage tanks, even when pressurised [113]. Liquid hydrogen is more dense with a density of  $80.0 \text{ kg/m}^3$  which makes it, in volumetric sense, easier to store [114]. Storage volume is especially important when hydrogen is used to fuel aircraft, where large storage volume directly increases operating cost [115].

To liquefy hydrogen it has to be cooled down to temperatures below 21.15 K [116]. Liquefaction technology of natural gas (LNG) is implemented since 1863, and experience in combination with technological advancements of liquefaction have made the process efficient [117]. Current day liquefaction methods are performed with a specific power consumption of  $4.0 \text{ kWh/kg}$ , which seems the highest efficiency possible [118]. The costs do not only consist of these operating costs; an initial investment is required to build the liquefaction capacity and maintenance has to be performed on the liquefiers. Current state-of-the-art facilities have a capacity cost of \$2600 per  $\text{kg/h}$ , which shows the relatively high investment and low operating costs for liquefaction compared to the hydrogen production cost [118]. Maintenance costs are included as a function of the liquefier capital value, wherefore budget is allocated to accommodate for four percent of the initial investment cost per year [119]. The combination of the high initial investment and maintenance cost requires a significant amount of the fuel budget for liquefaction.

### 9.1.4. Storage & transport

As mentioned in Section 9.1.3, the condensation temperature is 21.15 K [116], requiring the storage tanks to be extremely well isolated to counteract boil-off losses [120]. The well-isolated tanks are an initial investment and boil-off losses can be fed back directly to the liquefier to ensure no hydrogen is lost. Dewars exist where the capital cost for storing liquid hydrogen is \$28 per kilogram adjusted to present-day dollars [121].

Hydrogen transport will be done through pipelines to the airport storage tanks. Pipelines have certain losses due to the energy required to keep the gas flowing, which is 10% per 1000 km for hydrogen, relatively high compared to other gasses [122]. The effect of these losses is however minor and neglected as the hydrogen will be generated in the near vicinity the airports. The storage, transport and refuelling infrastructure system will be designed in such a way that one HUULC aircraft can be refuelled completely within a period of four consecutive hours. In order to do this, pumps with capacity of at least  $7000 \text{ L/second}$  will be used [123]. Using these pumps at full power, refuelling a completely empty HUULC aircraft will take only approximately five minutes, hence a refuelling time of four hours allows for sufficient time margins.

The maximum refuelling duration has been set to four hours because the maximum time on ground at hub airports (Anchorage and Novosibirsk) equals four hours and at hub airports HUULC aircraft are not unloaded and loaded, but solely refuelled, as explained in Section 4.3.

## 9.2. Renewable energy generation

As already stated, the HUULC program will only make use of renewable energy resources (renewables). This means that not only the hydrogen used to propel the HUULC fleet, but also the energy required to generate that hydrogen should be sustainable. If this would not be the case, the HUULC program would not be sustainable after all. In this subsection all renewables that have been taken under consideration are assessed on their applicability to the HUULC program.

**Ocean energy generation.** This energy resource makes use of the energy stored in the sea, generally by subtracting wave energy using electricity generators placed on the water surface. The sea technically is a huge basin full of energy, and hence has potential to provide energy to the HUULC program. Current wave energy technologies however are far away from technological maturity. The survivability and reliability of wave energy devices are parameters that still have to be demonstrated. The potential of wave energy is large, but it still is highly dependent on political and financial support [124]. Ocean energy generation is relatively expensive; it has a price of approximately 0.369  $\$/kWh$  as compared to 0.084  $\$/kWh$  for onshore wind energy generation [125]. Taking into account the technological immaturity, dependence on political and financial support and high costs per MWh, this renewable is not considered as a viable option for the HUULC program. The HUULC team will keep track of the progress of this technology in order to reconsider it, might it get more attractive in the coming decades.

**Solar photovoltaic energy generation.** In Germany, solar photovoltaic (solar PV) costs have been reduced by approximately 80% in the last ten years. In the near future, solar power will be the cheapest form of electricity in many sunlit areas of the world. Solar PV power might get as cheap as 0.0337 to 0.0675  $\$/kWh$  by 2030 and its costs will reduce even further to 0.0225 to 0.0450  $\$/kWh$  (depending on annual local sunshine) by 2050. This is a conservative scenario, assuming no major technological breakthroughs [126]. Inverters are a standard part of solar PV systems and ordinarily make up for of 8.62% of total costs for solar PV energy and optimally run at 97.5% efficiency [127][128]. The inverter converts the direct current supplied by the solar panel into alternating current, such that the electricity generated is compatible with the public grid. Grid electricity networks namely run on alternating current. Electricity generated for the HUULC hydrogen production facility does not enter the public grid, however; this energy enters the hermetic HUULC grid only. To reduce energy costs and increase efficiency, the entire HUULC hydrogen production facility is designed to run solely on direct current, eliminating the need for inverters. Total solar PV costs are hereby expected to decrease with 8.62%, resulting in an expected solar PV costs range of 0.0308 to 0.0616  $\$/kWh$  by 2030 and 0.0206 to 0.0412  $\$/kWh$  by 2050. It should be noted that solar PV energy rates generally include 0.007  $\$/kWh$  for long-distance high-voltage electricity transmission [129]. Due to the short transmission distances of energy generated for the HUULC program (energy and hydrogen production facilities lie close to each other), these transmission rates are assumed to be negligible. The outcome of this assumption is that solar PV costs ultimately are expected to range from 0.0238 to 0.0546  $\$/kWh$  by 2030 and from 0.0136 to 0.0342  $\$/kWh$  by 2050. In addition to that, solar PV has proven itself to be technologically mature and successful. This is a conclusion made on the exponentially growing solar PV total world capacity, which already reached 70GW by 2011 [130]. Based on these facts, solar PV power will definitely be considered as a viable renewable for the HUULC program.

**Onshore wind energy generation.** Onshore wind energy generation prices depend on numerous different aspects like wind speed, wind availability, subsidies and project costs. Different areas in the world hence hold different prices. The lowest-priced onshore wind energy is produced at highest-speed wind sites, like the interior of the United States. Admittedly focused on the highest-speed wind farms in the US, energy rates at the interior of the US have fallen to approximately 0.02  $\$/kWh$  in 2012. From 2016 onwards, the price of onshore wind energy decreases even further to 0.018  $\$/kWh$ , provided high-speed wind is an available natural resource [131]. Wind power technology has been sufficiently demonstrated in the past, according to its global capacity of 238GW in 2011 [130]. Onshore wind energy is economically competitive and technologically mature, hence this renewable is a viable option for the HUULC program.

**Offshore wind energy generation.** Offshore wind energy prices range from 0.14 to 0.19  $\$/kWh$  in 2010 [125][132], which is significantly more expensive than onshore wind power. In contrast to the onshore wind industry, the offshore wind industry is just at the beginning of its development, which makes estimates on cost reduction quite uncertain. Recent cost analysis however indicate potential cost reductions of 11% to 30% by 2030, depending on how fast the offshore wind industry grows [132]. Assuming an average of 20.5% reduction of costs, offshore wind costs will range from 0.11 to 0.15  $\$/kWh$  in 2030. Its industry being less developed and its price being higher, offshore wind will be kept in mind as a proper alternative to onshore wind. A (partial) switch to offshore wind power might be made when there exist a lack of land area at a hydrogen production facility, or when land area rates get too expensive.

**Biomass energy generation.** An additional complexity of biomass energy in comparison with the other renewables mentioned in this section is that biomass energy requires a supply of feedstock. To generate electrical energy by consuming feedstock, biomass energy hence not only requires the energy generation facility itself, but also a complete supply chain. Usually, primary biomass feedstock consists out of residues from forestry and agricultural harvesting, leftovers from food and fibre processing, organic parts of solid waste, animal manures or waste water [130]. The vital supply of these materials directly implies that these materials will somehow have to be transported from their origin to the biomass energy facility, which in turn requires trucks, boats, trains or airplanes. These means of transportation generally are not sustainable, which makes them unattractive for the HUULC program. Designing and producing sustainable feedstock carriers and a worldwide feedstock supply chain in addition to designing a biomass energy facility solely for the purpose of generating electricity for hydrogen production would be a very devious process. This is why the conclusion was made to not consider biomass energy as a viable option for energy generation.

**Hydroelectric energy generation.** Hydroelectric power makes use of water attracted by Earth's gravitation, causing the water to contain potential or kinetic energy. World's leading countries in terms of hydroelectric energy capacity are China, Brazil, the US, Canada and Russia, altogether accounting for 51% of global installed capacity [130]. Hydroelectric energy is estimated to come down to a rate of 0.02 to 0.04 \$/kWh from 2020 onwards [133][134][135]. Large hydroelectric plants will produce energy at an even lower rate of 0.015 \$/kWh in 2030, which makes this energy source cost-competitive [136]. Life span of hydroelectric energy facilities also seems quite bright. In North America for example, the average life span of installed facilities exceeds 50 years [137]. A possible drawback of a hydroelectric energy facility is its essential close proximity to flowing or falling water. This natural resource is available at some HUULC airports, which is why this energy source is considered potential for the HUULC program. Availability of hydroelectric energy will be discussed per airport in Subsection 9.4.1.

**Geothermal energy generation.** Geothermal power generation converts energy contained as heat inside the Earth into energy in the form of direct heat (2/3) and indirect electricity (1/3) [130]. In 2002 geothermal energy rates ranged from 0.02 to 0.10 \$/kWh, which makes it quite competitive. Apart from that, geothermal energy has been proven to be reliable for at least 25 years and the geothermal industry already is highly developed [138]. For the long term and under favourable conditions, the lowest cost for producing electricity using geothermal energy will be 0.01 to 0.02 \$/kWh [133]. Reference [133] originates in 2000, hence 2030 is considered the long term here. Geothermal energy generation altogether sounds promising so far, there are some drawbacks, though. Geothermal energy is concealed deeply underground Earth's surface, generally at depths of kilometers. This fact poses a particular uncertainty called "mining risk" among geologists, which sometimes is high and often is unpredictable [138]. Deciding to use an energy source with a significant level of uncertainty will make the hydrogen strategy of the HUULC program less reliable. This level of unpredictability thus makes geothermal energy less favorable for the HUULC program. Another drawback of geothermal energy is its limited geographic availability. Not many areas in the world hold the essential geological conditions for geothermal energy generation on an industrial scale. Figure 9.1 visualises the geothermal fields which already are being exploited (triangles) and the fields with potential of being exploited in the future (dots). None of the HUULC airports lie in proximity to neither a triangle nor a dot. Taking into account both drawbacks of geothermal energy, this resource is not considered as a viable option for the HUULC program.

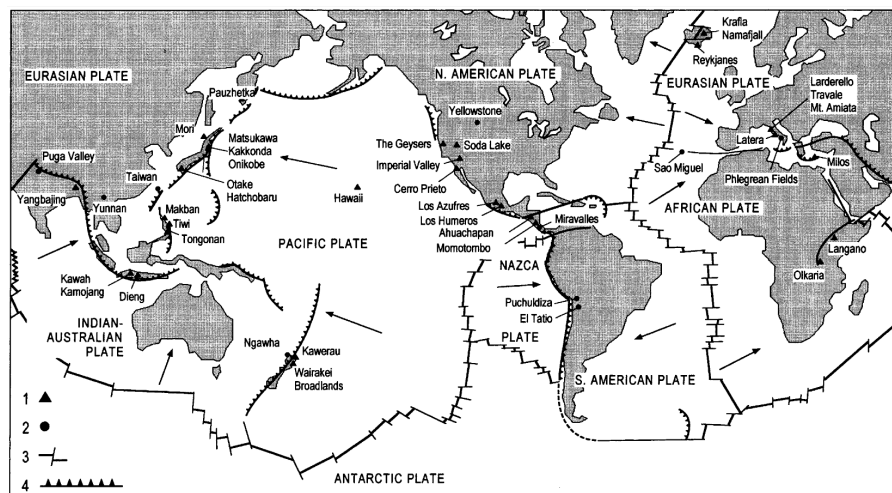


Figure 9.1.: World map displaying geothermal fields which already are being exploited (triangles) and fields with potential of being exploited in the future (dots) [138].

### 9.3. Hydrogen and energy generation overview

In Section 9.1 and 9.2 the HUULC strategy for the hydrogen and energy generation have been presented. This short section aims to give a concise overview of the hydrogen and energy generation methods chosen.

A visual representation of the HUULC hydrogen strategy is provided in Figure 9.2. As explained in Section 9.2, hydroelectric-, wind- and solar PV energy will be used in order to supply the hydrogen production facilities with sufficient energy. Then, as discussed in Section 9.1, electrolysis is the method chosen to produce gaseous hydrogen from electricity and water. The gaseous hydrogen subsequently is converted into the end product in the liquefaction facility, after which it is stored in tanks. Finally the liquid hydrogen is transferred into the HUULC aircraft before departure.

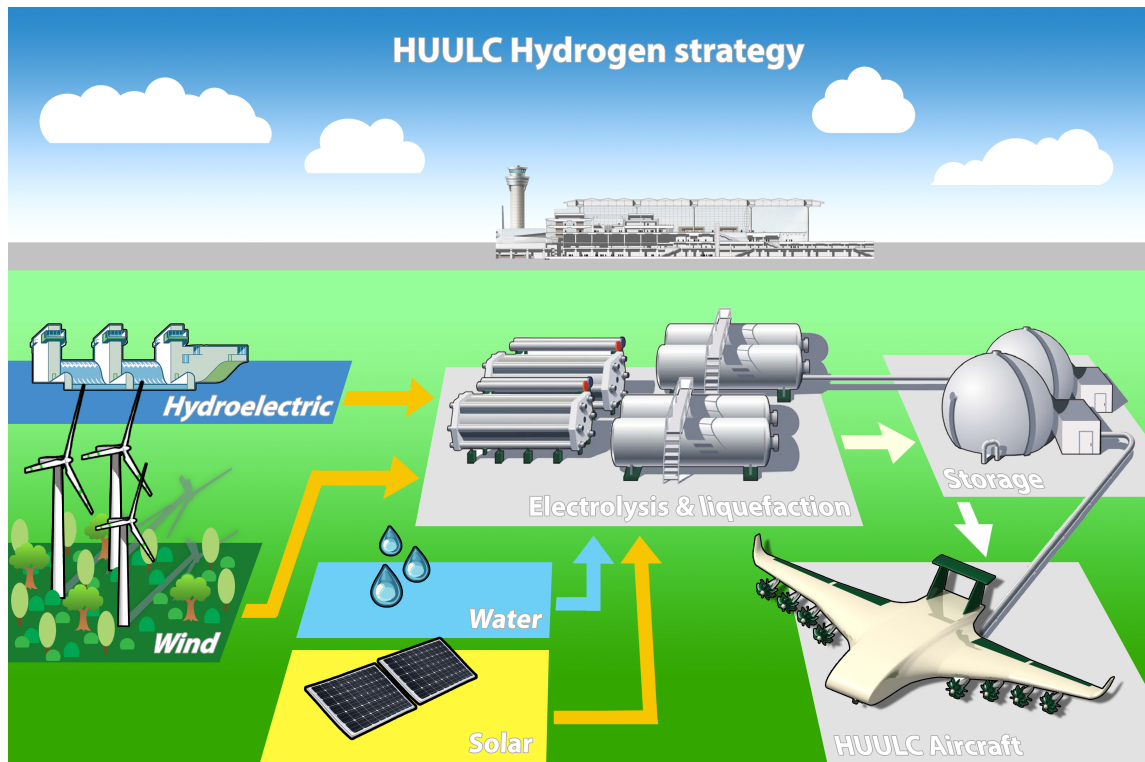


Figure 9.2.: A visual overview of the HUULC hydrogen strategy. Orange arrows indicate electricity flows, the blue arrow indicates water flow and the white arrows indicate the flow of liquid hydrogen.

### 9.4. Airport analysis

As the hydrogen generation process with the possible renewable energy generation methods has been defined, two airport characteristic factors are discussed in this section. Section 9.4.1 discusses the renewable energy source per airport according to natural availability. The required liquid hydrogen capacity per airport is analysed in Section 9.4.2.

#### 9.4.1. Airport energy analysis

Now that the renewables with potential for the HUULC program have been selected, it is of utmost importance to make optimal use of them. Every renewable is dependent on natural resources, whose availability is dependent on geographic location. Also, higher natural availability leads to lower costs per kWh. In Table 9.1 it is stated which natural resources the selected renewables require.

As explained in Section 4.6 of this report, the HUULC fleet will operate at six airports: Terneuzen, Dubai, Novosibirsk, Shanghai, Anchorage and Memphis. In order to assess the natural resources available, an analysis has been performed per airport, starting with Terneuzen, moving East from there on.

##### **Terneuzen**

Terneuzen is situated on the coast at the border of the Netherlands and Belgium, where the government increasingly starts to stimulate renewable energy [139]. In Figure 9.3 it can be seen that Terneuzen is situated in a high wind zone, where large wind turbine projects are feasible for low prices. For this reason a wind turbine farm will be realised for the hydrogen production in Terneuzen.

Table 9.1.: Required natural resources for viable renewables.

Potential renewable	Natural resource
Solar PV energy generation	Solar irradiation
Onshore wind energy generation	Kinematic wind energy
Hydroelectric energy generation	Potential or kinetic water energy

### Dubai

Dubai is located in the United Arab Emirates, a country with an abundance of solar irradiance as can be seen in Figure 9.4. Solar power can be harvested efficiently and cost-effective in sun-drenched areas, resulting in the decision that the HUULC’s Dubai airport will be powered by solar photovoltaics.

### Novosibirsk

The Novosibirsk reservoir is formed where the Inya river joins the Ob river and a dam is situated to power the third largest city in Russia: Novosibirsk [140]. The Novosibirsk hydroelectric plant can be upgraded to provide the power supply for the HUULC hydrogen facilities situated near the airport. Costs will be low as the dam has been built and installments merely involve an expansion of the power generating installments.

### Shanghai

Shanghai lies on the coast of the east China sea and as can be seen from Figure 9.3 has strong sea winds. The HUULC program will make use Shanghai’s sea wind and generate the required local power by building a wind farm.

### Anchorage

By inspection of Figure 9.3 it becomes clear that Alaska has large potential for wind power generation. The choice for the HUULCs program power generation in Alaska will therefore be by wind turbines.

### Memphis

Memphis is located in the interior of the United States where the potential for wind power is high as illustrated by Figure 9.3. Costs are low for wind power in the U.S. interior and a wind farm will be constructed [141].

## 9.4.2. Airport capacity analysis

The frequency of HUULC turnarounds differs greatly per airport as discussed in Section 4.6 and hydrogen availability has to be sufficient. The required amount of liquid hydrogen, the required daily power and storage capacity per airport are listed in Table 9.2. The numbers provided in Table 9.2 correspond to the condition where the maximum amount of HUULCs are operational, starting in 2050 as discussed in Section 4.2. The cost of the strategy can be found in Section 9.5.

Table 9.2.: Total capacity required for liquid hydrogen production and storage per airport.

Component	Novosibirsk	Terneuzen	Shanghai	Dubai	Memphis	Anchorage
LH2 consumption [ $kt/day$ ]	9.7	9.1	8.0	4.0	3.1	2.7
Required power [ $GW h/day$ ]	436.2	408.5	361.0	179.6	141.3	122.6
Storage capacity [ $m^3$ ]	121,180	113,482	100,276	49,886	39,249	34,045

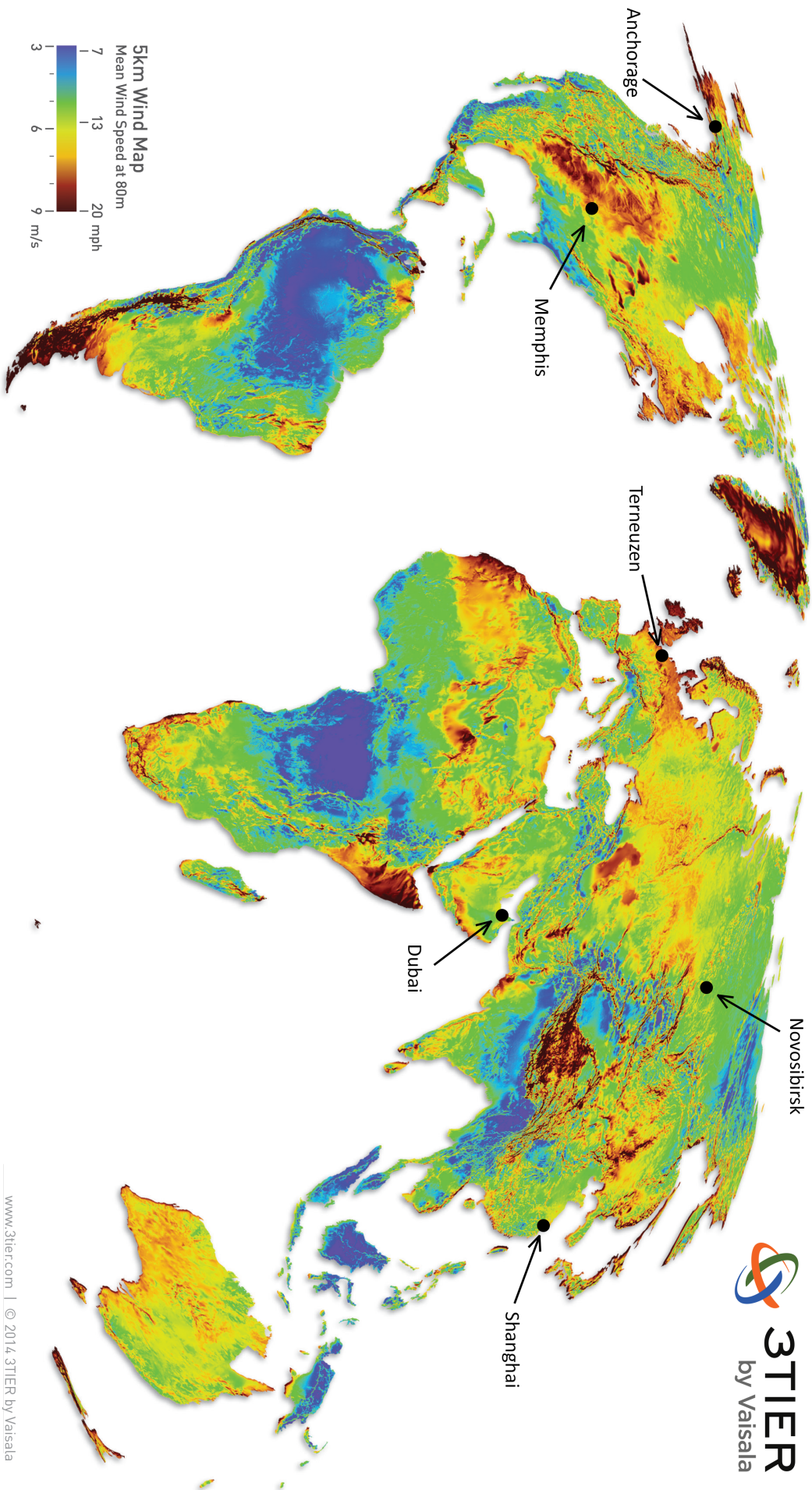


Figure 9.3.: World map displaying local wind speeds with regard to wind power generation [142].

www.3tier.com | © 2014, 3TIER by Vaisala



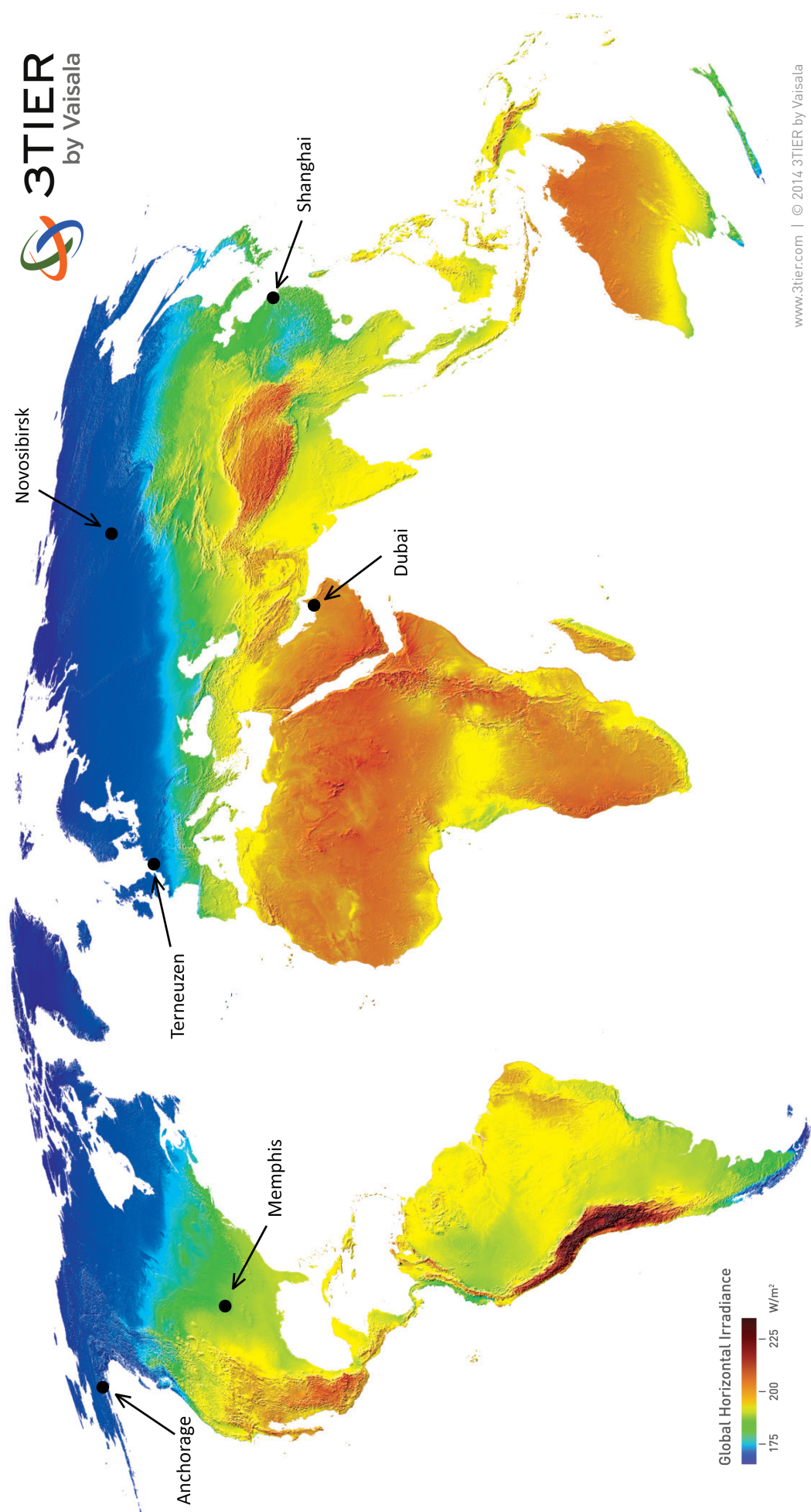


Figure 9.4.: World map displaying local solar irradiance with regard to solar power generation [142].

## 9.5. Fuel cost budget

The HUULC program faces challenges which never have been faced before by any other aircraft program. One of the top level requirements is the maximum freight rate of 250% with respect to maritime shipping, to be competitive in the global long-distance transport of containerised cargo market. This freight rate hence is the parameter which is the foundation of all budget estimations made. Hydrogen generation is, speaking of HUULC flavor, a truly huge enterprise and a critical part of the current feasibility study. This section addresses the preliminary cost budget for the hydrogen strategy as presented in Section 9.1 to 9.4, which assesses the possibility to stay within the given maximum freight rate. The budget which is available for producing hydrogen is given in Subsection 9.5.1, after which an elaborate overview of the costs for the hydrogen strategy is presented in Subsection 9.5.3.

### 9.5.1. Available budget

The available budget used for the liquid hydrogen production is a fraction of the operations budget as discussed in Chapter 5. The operations budget of the HUULC program was estimated at \$606.63 billion as discussed in Section 5.5. The freighter version of the Boeing 747 (Boeing 747F) is currently the largest freighter aircraft in use by commercial airlines and spends 67% of the operating costs on fuel [143]. The HUULC and the Boeing 747F differ in operating cost as the HUULC requires only partial attention from one ground controller and the Boeing 747F full attention by a full flight crew. Due to this distinction 81% of the operations budget has been made available for the HUULC program hydrogen expenses, amounting up to \$491.37 billion.

### 9.5.2. Freight rate sensitivity analysis

The budget for hydrogen production is highly dependant on the freight rate as illustrated in Figure 9.5. The hydrogen cost and budget are separated by 1.6 billion dollars contingency margin, relatively small as indicated in Figure 9.5a and 9.5. Due to the hydrogen production cost the freight rate is not allowed to be reduced as feasibility would become endangered. It should be noted however that decreasing the freight rate would enlarge the market share, however the HUULC production capacity is at the upper limit as such the market share would remain the same. Increasing the freight rate would cause stress imposed by the hydrogen costs on the operating budget to be relieved and reduce the fuel development risk. Competitiveness suffers from an increased freight rate and the market share goal would be endangered.

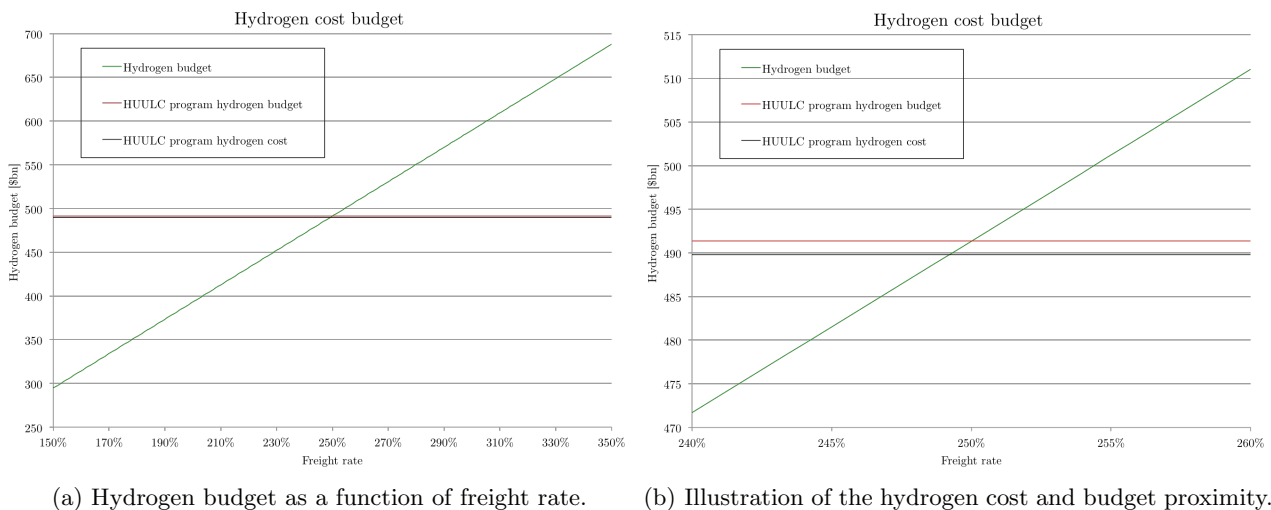


Figure 9.5.: Hydrogen budget as a function of freight rate. The red line is the HUULC program budget. The black line indicates the HUULC program hydrogen cost.

### 9.5.3. Hydrogen strategy costs overview

To obtain an estimation of the fuel cost, it was required to analyse the HUULC network. Using the route specific fuel consumption presented in Section 6.1.3 and the flight frequencies as described in Section 4.6, the maximum fuel production and storage capacity per airport has been evaluated. The initial investment cost has been determined according to the numbers listed in Table 9.2. The recurring costs such as required power and maintenance have been scaled according to the increase in the HUULCs in operation as mentioned in Section 4.2 to accommodate for the gradual increase, and eventual decrease, in operable aircraft. The amount of fuel that an airport requires has been multiplied with the energy required for electrolysis and liquefaction, 41 and 4.0  $kWh/kg$  respectively. The energy cost per airfield differs not only due to different energy demands, but also due to the various energy sources used; wind, solar and hydroelectric have a different price per kilowatt-hour. The required budget per component per airport is listed in Table 9.3 according to the cost estimates provided in Section 9.1 to 9.2. The overall HUULC liquid hydrogen price per  $kg$  is composed out of different elements; a cost breakdown is shown in Figure 9.6. The total required amount of hydrogen for the HUULC program is 593 gigatonnes costing 498.8 billion dollars resulting in a cost of \$0.826 per  $kg$  LH2. Referring to Table 9.3 and Figure 9.6 it is clear that the largest expense of the fuel cost, 97.2%, is the energy required to generate enough hydrogen to power the HUULC fleet.

Table 9.3.: Hydrogen strategy costs overview per component per airport.

Component	Te.	No.	Sh.	Du.	Me.	An.	Total	Share [%]	Budget [%]
Energy [\$bn]	119.0	105.9	105.1	69.1	41.1	35.7	475.9	97.2	96.8
Electrolysis [\$bn]	0.5	0.5	0.4	0.2	0.2	0.1	1.8	0.4	0.4
Liquefaction [\$bn]	2.7	2.9	2.4	1.2	0.9	0.8	11.0	2.2	2.2
Storage [\$bn]	0.3	0.3	0.2	0.1	0.1	0.1	1.0	0.2	0.2
Total [\$bn]	122.4	109.5	108.1	70.7	42.3	36.7	489.8	100.0	99.7
Cost share [%]	25.0	22.4	22.1	14.4	8.6	7.5	100.0		
Budget share [%]	24.9	22.3	22.0	14.4	8.6	7.5	99.7		

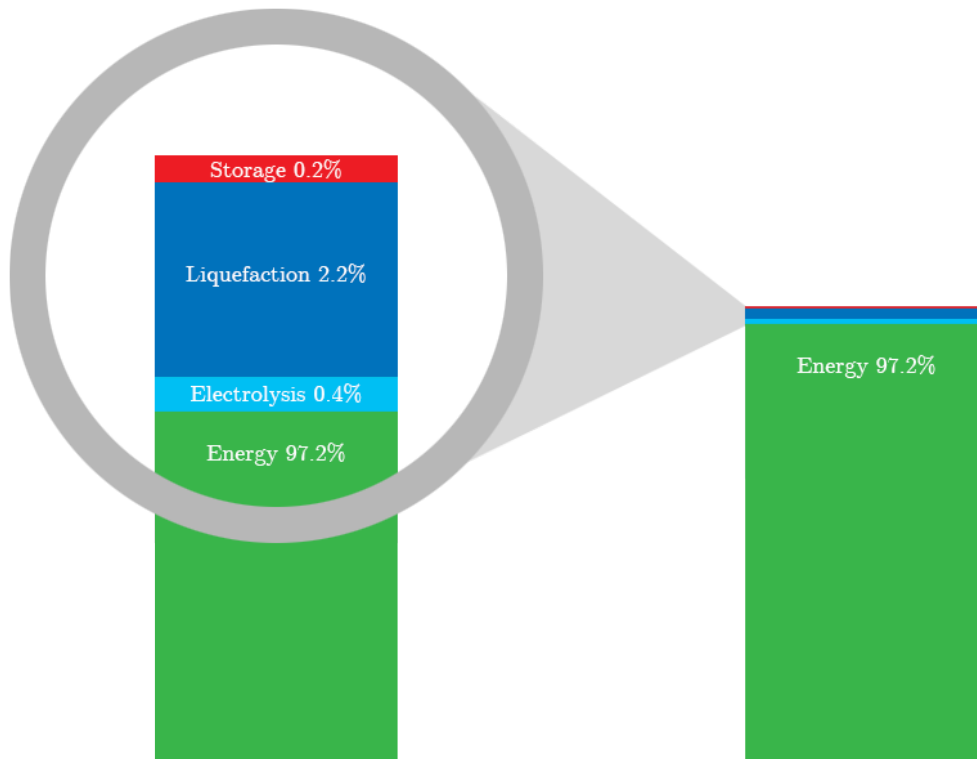


Figure 9.6.: HUULC Hydrogen cost breakdown.

## 9.6. Advantages of hydrogen fuel as compared to kerosene

Using hydrogen to power the HUULC fleet is a complicated process and it is important to assess if the increased complexity outweighs the benefits. The following section analyses the implication of liquid hydrogen as a fuel and concludes by assessing if using liquid hydrogen is advantageous for the HUULC program. Section 9.6.1 discusses the reduction in emissions after which Section 9.6.2 examines the financial implications of liquid hydrogen fuel.

### 9.6.1. Emissions

As previously mentioned combustion of liquid hydrogen has no carbon emissions but the entire life cycle of liquid hydrogen has to be assessed with regard to emissions. The analysis in this section is performed on the field of carbon emissions which have been minimised for the HUULC program. During construction of the HUULC facilities and plants, carbon emissions can not be eradicated but the production of liquid hydrogen as discussed in Section 9.1 to 9.8 has a significant impact on emissionless transport.

The carbon emission of kerosene is 3.15 kg CO<sub>2</sub> per one kg of kerosene [144]. The total amount of consumed LH<sub>2</sub> can be converted to kerosene using the energy content and the total kerosene mass can be calculated. Converting the total kerosene to carbon emissions gives the numbers in Table 9.4 where the total reduction in emissions are compared to the annual emissions of China, the US and EU in 2013 [145].

### 9.6.2. Financial aspect

As previously mentioned it is expected the price of liquid hydrogen will come down to equal the price of kerosene in 2037 [98]. The HUULC program starts operations in 2030 but does not rely on commercially produced LH<sub>2</sub> and benefits from the elimination of the fuel producer's profit margins and therefore has the advantage of producing cheaper hydrogen before the 2037 milestone. The cost of kerosene will increase as oil becomes more scarce and the associated cost of kerosene is estimated at \$0.955 per kg in 2030 [146]. The financial advantage of using liquid hydrogen is significant as the HUULC program fuel costs merely \$0.826 per kg, both values can be found in Table 9.4.

Table 9.4.: Comparison between liquid hydrogen and kerosene as fuel for the HUULC program.

Component	Hydrogen	Kerosene
Total fuel mass [Gt]	0.870	2.426
Total CO <sub>2</sub> mass [Gt]	0	7.641
Share of annual Chinese CO <sub>2</sub> emissions in 2013 [%]	-	74.0
Share of annual US&EU CO <sub>2</sub> emissions in 2013 [%]	-	84.5
Fuel cost in 2030 [\$ /kg]	0.826	0.955

## 9.7. Preliminary landscape analysis

At the peak of the HUULC program in all airports combined, 36.6 million kilograms of hydrogen have to be produced every day in order to refuel the HUULC fleet. In order to generate these amounts of hydrogen, huge amounts of energy are required, as explained in Subsection 9.5.3. These huge amounts of energy, in turn, require huge energy production facilities. In this section a first estimation is made on how much area is needed to place the energy and hydrogen production facilities on. Subsection 9.7.1 till Subsection 9.7.6 evaluate the required areas per hydrogen production and storage component and Subsection 9.7.7 summarises the combined areas for each HUULC airport.

### 9.7.1. Onshore wind facility area

To facilitate the generation of hydrogen a significant power capacity has to be realised. To estimate the required area, a reference wind turbine with 20MW is used from a report on renewable energy by W. Turkenburg et al. [136]. Using a reference capacity factor of 0.45, the turbine generates  $216 \text{ MWh/day}$  [147]. To sustain the electrolyzers and liquefiers a significant amount of wind turbines are required per airport [147], as illustrated in Table 9.5. An optimum spacing is needed to fit the wind turbines in an area as small as possible, to keep costs low, with a spacing of four rotor diameters downwind and two rotor diameters perpendicular to the wind direction [148]. The turbines have a rotor diameter of 250 meters and fitting the turbines on a square surface would result in the areas provided in Table 9.5 [136].

### 9.7.2. Solar PV facility area

At the Dubai airport site solar PV energy will be used. In order to make an estimation of the area required to meet the Dubai daily energy demand of  $179,590 \text{ MWh/day}$ , data of an appropriately similar solar park has been used: the Mohammed bin Rashid Al Maktoum solar park from Dubai [149]. The solar park datasheet used here contains information of the first phase of an ambitious plan to eventually create one gigawatt of solar PV electricity. The solar plant already was largest of its kind in the Dubai region in 2013; a title that the HUULC solar facility in Dubai will take over when it enters into service. The Mohammed bin Rashid Al Maktoum solar park generates approximately 24 million  $\text{kWh/year}$  and covers an area of  $0.238764 \text{ km}^2$ . When these amounts are scaled up to HUULC sizes, a surface area of  $550 \text{ km}^2$  is found.

### 9.7.3. Hydroelectric facility area

As mentioned in Section 9.4.1, the only airport where hydroelectric energy will be employed is the Novosibirsk airport. Here, the currently existing hydroelectric plant will be upgraded to supply enough energy to the hydrogen production facility. Therefore no further area estimations for the hydroelectric facility have been made.

### 9.7.4. Hydrogen electrolyser area

A preliminary estimate of the required area to construct the electrolysis facility is based on the NEL 50 MW hydrogen electrolyser, estimated at  $0.0072 \text{ km}^2$  [108]. By multiplying the area with the required amount of facilities results in the surface areas that can be found in Table 9.5.

### 9.7.5. Hydrogen liquefaction area

In order to make an estimation for the hydrogen liquefaction facility area per airport, the Linde Liquefier (cold box) has been used [150]. Based on the capacity and approximate required area of this liquefier the required area to fit the liquefiers has been calculated, Table 9.5 contains the necessary area per airport.

### 9.7.6. Storage facility area

Eventually, when the natural resources have been converted into liquid hydrogen fuel after going through the complete hydrogen production cycle, the liquid hydrogen has to be stored temporarily before entering one of the HUULC aircraft. According to the required hydrogen estimation made in Section 9.5.3, a total storage capacity of  $458,116 \text{ m}^3$  per day is needed. It is assumed that one HUULC should be refueled entirely by one perfectly spherical tank and a free space between every tank of  $1 \text{ m}$  is used, which results in the required area listed in Table 9.5.

### 9.7.7. Energy and hydrogen facility area per airport

From the required surface areas provided in Section 9.7.1 to Section 9.7.6, it becomes clear the power plants are most challenging to the development of the HUULC's program fuel production. The total required area per airport is provided in Table 9.5.

Table 9.5.: Total area required for liquid hydrogen production per component per airport.

Component	Terneuzen	Shanghai	Dubai	Memphis	Anchorage	Novosibirsk
Energy source	Wind	Wind	Wind	Solar	Wind	Hydroelectric
Energy [ $km^2$ ]	945.7	835.6	549.7	327.1	283.7	-
Electrolysis [ $km^2$ ]	4.43	3.91	1.95	1.53	1.33	4.73
Liquefaction [ $km^2$ ]	0.04	0.03	0.02	0.01	0.01	0.04
Storage [ $km^2$ ]	0.06	0.05	0.03	0.02	0.02	0.07
Total [ $km^2$ ]	950.21	839.63	551.73	328.63	285.06	4.83

## 9.8. Strategy execution

The first HUULC will enter into service in 2030 with a lifetime of at least 45 years. Gradually more HUULCs will be taken into service and the hydrogen production capacity will scale accordingly. As a result of the progressive increase in the hydrogen capacity required, there exists a possibility of lower LH2 production cost through the increase in maturity of technology. The hydrogen strategy presented in this chapter has been conservatively estimated with regard to projected costs and possibilities in 2030. As can be seen in Figure 4.3 of Section 4.2, hydrogen production does not reach full capacity until 2050, granting, at maximum, twenty years for technological advancements to become available for commercial usage. These scientific advancements are expected as a world largely fueled with hydrogen is currently researched and predicted to exist in 2050 [151][152][153]. As mentioned in Section 9.5 the budget required is substantial and investments of such amounts of money is a risk. The plan presented in this chapter can be executed by different parties. This section discusses the advantages and disadvantages of the possible options; an external party or execution within the HUULC program.

Multinational oil companies have experience with fuel business but lack experience in hydrogen production. As hydrogen is predicted to be the fuel of the future, experience can be gathered in this new industry and could increase interest of oil producers and gas multinationals. A price could be agreed upon with the external party and the HUULC program would not be endangered through higher hydrogen costs than predicted, and the third party would have the possibility to make a profit.

If the plan would be executed internally, potential subsidies profit the HUULC program. The hydrogen strategy presented does not account for subsidies, so external financial support directly relieves pressure on the budget. The ambitious sustainability aspect of the HUULC could benefit countries for their sustainable image as well as to meet renewable targets set by countries; e.g. the European Roadmap for 2050 [154]. Hydrogen production does not require a profit as it is executed internally but when the production cost of hydrogen decreases, extra profit or increased competitiveness are possible.

## 9.9. Feasibility conditions

To analyse the feasibility and risk of the HUULC program being powered by hydrogen, the driving parameters which influence the feasibility are defined in this section. Estimates of the process parameters have been provided in Section 9.1 to 9.8. In this section the parameters are analysed and a discussion of the limits with respect to feasibility is provided. The energy prices are discussed first in Section 9.9.1. The hydrogen price will be analysed in Section 9.9.2 and the auxiliary feasibility parameters are discussed in Section 9.9.3.

### 9.9.1. Energy price

The hydrogen production process described in Section 9.1 makes use of electricity. The cost of renewable energy per kWh are given in terms of a price range in Section 9.2. The predicted energy rates that have eventually been used in order to determine the energy costs for hydrogen production are taken from these price ranges. To ensure feasibility, it is required that the actual energy rates to be paid in the future are at least as low as the predicted energy prices. The presently predicted energy rates hence are linked to feasibility conditions, for which these predicted energy rates are valid. The current section discusses the conditions required for the energy strategy to be economically feasible.

#### 9.9.1.1. Solar PV energy feasibility

The solar energy prices mentioned in Section 9.2 assume no major technological breakthroughs and are based on conventional cost predictions. The remaining cost range is primarily dependent on cost of capital (WACC) and local solar irradiation. Due to the high accuracy of its forecasted energy yield, solar PV energy technology is considered a lower risk investment than e.g. wind or liquid gas energy [155]. This implies that the (WACC) is relatively low for large-scale PV solar power plants; only 5% [156]. WACC is a measure of the money that the energy plant will have to pay back to the financial investors in order to provide them with their predicted return on investment. When the investment technology has a low risk, the WACC will be low, and vice-versa. In the United Arab Emirates, the high solar irradiation accounts for a energy generation capacity of 1600 to 1900 kWh per year [156]. As is the case with solar energy, its costs are highly dependent on solar irradiation. More sunshine means a higher capacity factor, which results in lower costs per kWh. This concept is illustrated in Figure 9.7, where the cost range is shown. The highest cost for solar energy reflects the lowest solar irradiation. The solar energy rate used in the hydrogen strategy budget is the lowest from the range of possible solar energy prices existing in 2030. This price range is shown in Figure 9.7, and it can be seen that the lowest energy rate in 2030 is 2.38  $\$/kWh$ . This is the most optimistic solar energy cost scenario available for 2030, and has been chosen because of the highly sun-drenched location of the regarding solar farm; Dubai. However, the energy rate of 2.38  $\$/kWh$  has been used in the cost calculations for the entire HUULC lifespan, hence until the year 2095. Shown in Figure 9.7, the cost of solar energy will keep on decreasing over time. Hence during years succeeding 2030, the solar energy rate might be of a too high level used in the cost calculations. This might be far from optimistic, balancing out the most optimistic energy price picked in 2030.

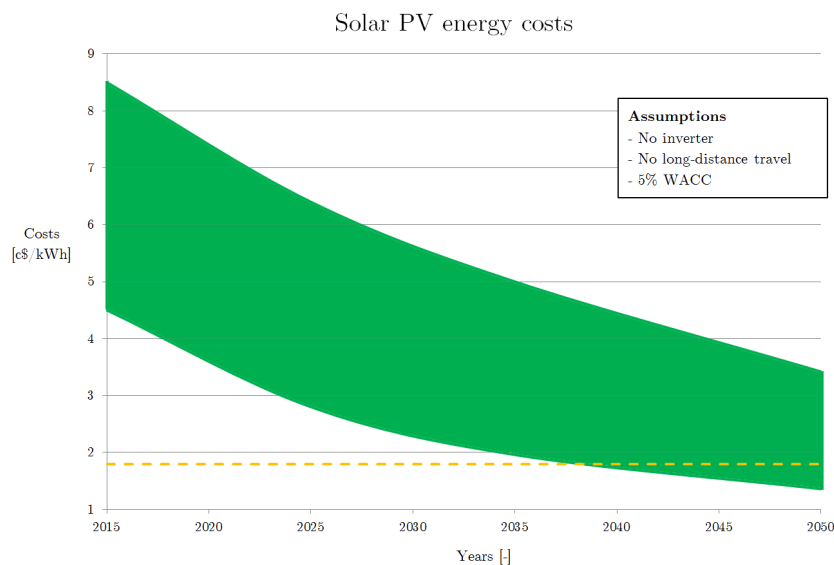


Figure 9.7.: Solar photovoltaic energy cost range scenario from 2015 to 2050. The lower and higher boundaries correspond to 1900 and 1600 kWh / kWp per year, respectively. The orange dashed line indicates the maximum energy price allowed by the available fuel budget [127][129][156].

### 9.9.1.2. Wind energy feasibility

Onshore wind energy costs are mainly dependent on local wind speed and size of the wind energy farm. Apart from that, wind energy costs are expected to become lower when time goes by. Wind energy cost hence is a function of wind speed, wind farm size and time. These dependencies result in different cost ranges for every moment in time, as shown in Figure 9.8.

All sites at which wind energy will be used in the HUULC program have been selected on their annual high wind speed available, as explained in Section 9.4. The wind resource available at all HUULC wind farms hence is characterized by the highest-speed wind category, comparable to the U.S. interior wind-speed category [131]. As clarified in Section 9.2, this category of wind speed reflects the lowest possible wind energy cost.

Concerning wind farm size, it is safe to assume that the lowest wind energy rate available (corresponding to the largest wind farms available) can be used. The smallest HUULC wind farm is the one in Anchorage; this wind farm will have a capacity of approximately 13 GW, which is more than twice as much as world's largest wind farm in 2015 [157].

According to the references on which Figure 9.8 is based, the lower limit of the wind energy cost range will decrease to 0.018  $\$/kWh$  in 2016, and not decrease further until 2050. The first HUULC aircraft will become operative in 2030, when the lowest boundary of the wind energy cost range will be 0.018  $\$/kWh$ .

It now becomes clear that, for the HUULC program, the lowest wind energy cost from the available cost range can be selected for further cost analysis. This is what has been done; a wind energy rate of 0.018  $\$/kWh$  has been used for cost calculations from 2030 onwards. This wind energy rate happens to equal the maximum energy price available from the fuel budget, indicated by the orange dashed line in Figure 9.8.

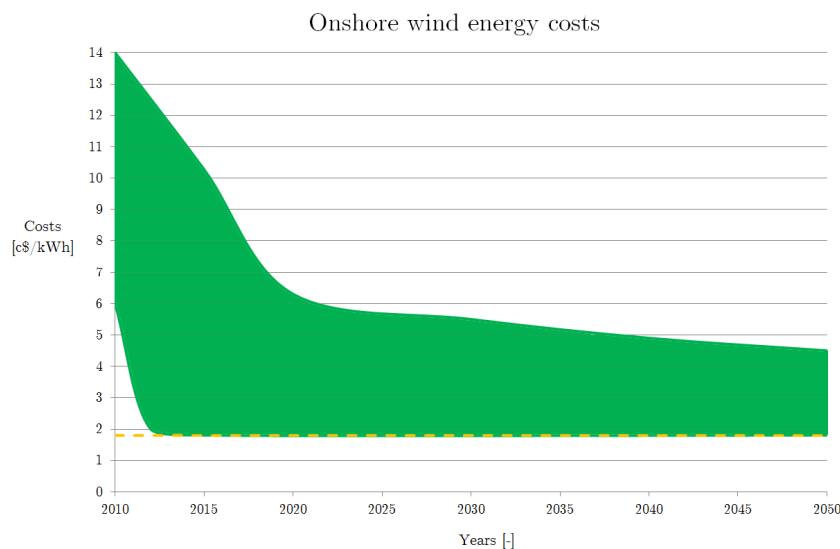


Figure 9.8.: Onshore wind energy cost range scenario from 2015 to 2050. The variance in costs is dependent on higher and lower average wind speeds and wind farm size. The orange dashed line indicates the maximum energy price allowed by the available fuel budget [131][132][158].

### 9.9.1.3. Hydroelectric feasibility

Hydroelectric energy cost is primarily dependent on plant size. The only airport that will harvest electricity using hydroelectric energy is the Novosibirsk airport. Because the Novosibirsk airport is the busiest HUULC airport, the required energy per day is the highest at this location. Due to the high capacity factor of hydroelectric energy generation as compared to solar or wind energy generation though, the required capacity is not as high as at e.g. Terneuzen airport. The required capacity in Novosibirsk is approximately the same as the capacity of the largest hydroelectric dam in the world: the Three Gorges Dam, which has a capacity of 22.5 GW [159]. The largest hydroelectric dams yield the lowest hydroelectric energy costs, and hence the lowest available hydroelectric energy rate can be used in cost calculations. Also, instead of building a completely brand-new hydroelectric facility, the currently existing dam in Novosibirsk will be upgraded, which will decrease the costs of hydroelectric power even further. As can be seen from Figure 9.9, the lowest available hydroelectric energy rate is 0.015  $\$/kWh$  from 2030 onwards. This energy rate is the lowest available energy rate and is well below the maximum energy price allowed by the available fuel budget.

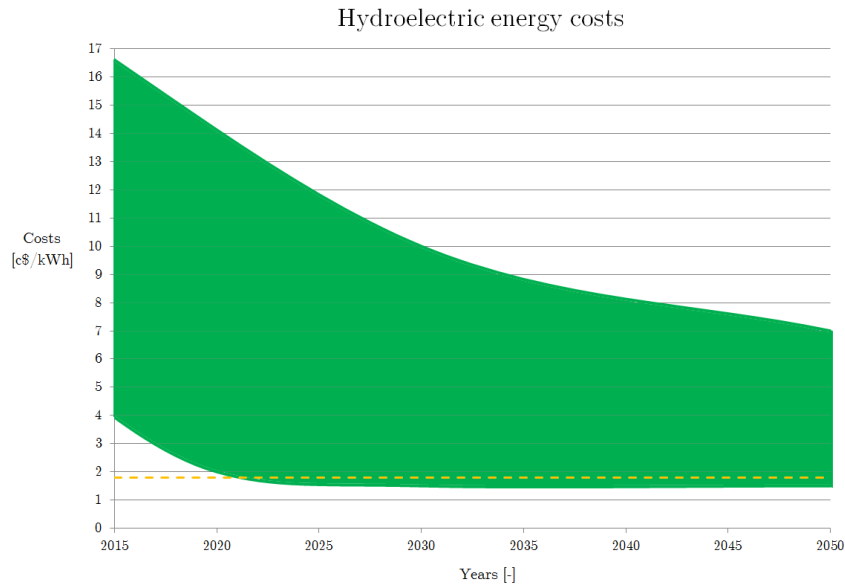


Figure 9.9.: Hydroelectric energy cost range scenario from 2015 to 2050. The variance in costs is dependent on capacity factor, plant scale and plant lifetime. The orange dashed line indicates the maximum energy price allowed by the available fuel budget [135][136][125].

## 9.9.2. Hydrogen price

The HUULC program has allocated 81% of the operations budget to the fuel budget, granting a total of \$492.9 billion to acquire 0.870 gigatonnes of liquid hydrogen. This results in the condition that the cost of one *kg* of LH2 to be produced and delivered to the HUULC can not exceed \$0.828. Hydrogen price is mainly a function of energy price, as illustrated in Figure 9.10, and feasibility of the HUULC program is highly dependent on the energy cost estimates provided in Section 9.2. The price of hydrogen as estimated in 2030 is marked in Figure 9.10, which indicates that hydrogen can be produced within budget.

The price of solar energy in 2030 as indicated in Figure 9.10 is above the feasibility price causing financial losses. The costs of solar energy are expected to decrease to the feasibility price and below after the year 2038, as can be seen in Figure 9.7. Hence all flights departing from Dubai up till 2038 are not generating profit at their final destination, because the fuel expense for those particular flights is above budget. Flights arriving in Dubai will however generate profit: these flights are refueled at wind energy - based airports. Less profit hence will be secured from HUULCs that are refueled in Dubai up till 2038, flights departing from Dubai in 2030 however will secure a higher market share for the HUULC program. Also, engaging customer relations in an early stage of the HUULC program will help to exclude future competition. Losing profit is a non-desirable situation, hence it will be considered to raise the freight rate for flights departing from Dubai, as more generally mentioned in Section 9.5.2.

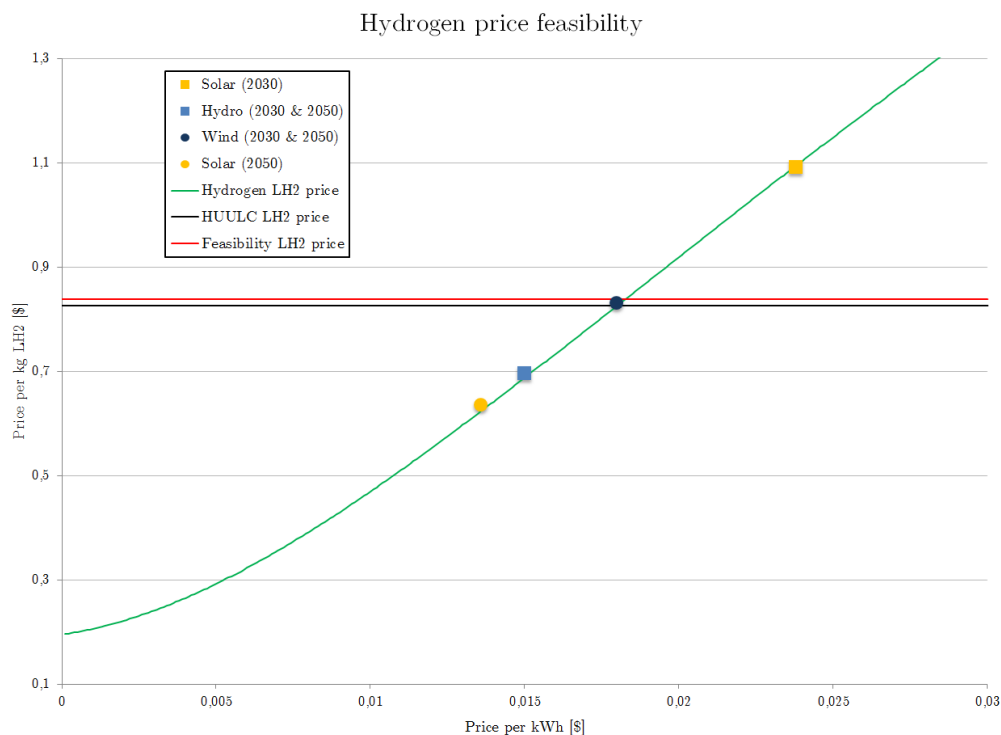


Figure 9.10.: Hydrogen price overview. Green line: Liquid hydrogen (LH2) price per kg as a function of renewable energy cost per kWh. Red line: Maximum hydrogen price with current budget. The black line indicates the HUULC program LH2 price.

## 9.9.3. Auxiliary feasibility parameters

Figure 9.10 indicates that the current budget is sufficient to produce the hydrogen; the HUULC LH2 price lies below the feasibility limit for the LH2 price. However, the hydrogen strategy presented is not risk free due to uncertainties. The parameters that can be varied to avoid setbacks due to contingency are investigated starting in Section 9.9.3.1 with the entry into service time and concludes the section with the operations and fuel budget in Section 9.9.3.2.

### 9.9.3.1. Entry into service

The HUULC program is set to start operations in 2030, and the cost projections for the hydrogen strategy are determined for 2030. If the actual prices of wind, solar and hydroelectric energy turn out to be higher than values as predicted in Section 9.2 and 9.9.1, the HUULC is not profitable which implies a development risk. Due to the high risk associated with the energy price, HUULC program feasibility is highly dependent on the technological advancements made in the energy sector which would reduce future cost in 2030. This implies

that the HUULC program is prone to delay when advancements do not progress with the predicted pace. The energy price of solar energy in 2030 is not estimated to drop below the feasibility price until 2038. After 2038, the costs of solar power are expected to become profitable as Section 9.9.1 described. With the considerations in mind as mentioned in Section 9.9.2, the possible decision could be to start servicing Dubai from 2038 onwards.

### 9.9.3.2. Operations and fuel budget

The current operations and fuel budget have high allocation percentages, 67% and 81% respectively. Reasoning behind the budget allocation can be found in Section 5.5 and 9.5.1. When hydrogen production encounters higher cost, contingency budgets of other segments of the HUULC program can be allocated to increase the operations or fuel budget.

## 9.10. Conclusion and recommendations

In this section the hydrogen strategy is concluded with a brief summary in the second paragraph and some further recommendations are given in the third paragraph.

Gaseous hydrogen will be produced using the renewable hydrogen production method of electrolysis, after which it is liquefied before it is stored on the airport. Hydrogen chemical compounds and electricity are required inputs for electrolysis. The hydrogen compounds will be supplied in the form of fresh water in Terneuzen, Novosibirsk, Anchorage and Memphis and in the form of sea water in Dubai and Shanghai. Electricity will be provided using hydroelectric energy generation in Novosibirsk, solar photovoltaic energy generation in Dubai and onshore wind energy generation in Terneuzen, Anchorage, Memphis and Shanghai. The selection of these renewables is based on local natural resource availability. The total costs for producing hydrogen for the entire HUULC fleet, for its entire lifetime, using the above-mentioned techniques are approximately \$489.8 billion. In 2030, liquid hydrogen will be produced for merely \$0.826 per kg, as compared to a rate of \$0.955 per kg for kerosene. Hence using liquid hydrogen as fuel instead of kerosene is not only more sustainable, but also financially more attractive. Energy generation has the largest share in this amount of money; 97.2%. The area required to generate hydrogen was computed for each airport of which the largest one is located in Terneuzen. The total required size for wind energy generation, electrolysis, liquefaction and storage there is estimated at  $950.21 \text{ km}^2$ .

When it comes down to recommendations for further research on the HUULC program, a few cases are to be addressed. First of all, the HUULC program on itself is a completely sustainable enterprise (apart from the process of building facilities), and hence is applicable to large amounts of different subsidies in various countries. In the cost calculations done in this report, a worst case scenario was assumed regarding subsidies; that means no subsidies were taken into account. To make more profit or to simply have broader contingency margins, one should apply for subsidies in all countries HUULC operates in. Apart from applying for government financial support, some other important potential financial benefits have been untouched. When the HUULC fleet is retiring and less and less liquid hydrogen is required to be produced, HUULC production facilities will become more and more available to produce liquid hydrogen which can be sold to third parties. It is expected that worldwide hydrogen powered transport will increase to shares of 30 to 70% by 2050 [160]. Also, when less HUULC aircraft will fly at HUULC airports, the possibility for other hydrogen-propelled aircraft to operate at HUULC airports will arise. Thus although the hydrogen strategy as presented in this report is coherent and thorough, some aspects of the HUULC program may generate lots of revenue in different ways, which are worthy to be further researched.

# 10. Cost analysis

The total budget of the HUULC program was given in Chapter 5. It was determined by working backwards from the freight rate requirement. This chapter aims to clearly estimate the actual costs incurred so far and the projected costs of the remainder of the program by working forwards, summing the costs involved in all the phases of the HUULC program lifecycle. These projected costs will then be compared to the budget to determine whether the program has, or will potentially, reach a cost overrun. Each section of this chapter deals with the costs of a different phase of the lifecycle. R&D and production are both discussed in Section 10.1. Subsequently, ground support, operations and disposal costs are reviewed in Sections 10.2 to 10.4 respectively. The projected costs are then compared to the available cost budget in Section 10.5. After the comparison has been made, the cost model for R&D and production is validated in Section 10.6. Finally, a conclusion is given along with further recommendations in Section 10.7.

## 10.1. Research & development and production costs

The research and development budget was given as \$27.16 billion in Chapter 5. The production budget of \$190.14 billion should cover all expenses ever made on manufacturing the HUULC fleet. Together, the combined R&D and production budget of \$217.30 billion determine the available funds for developing and producing 325 aircraft, or \$668.61 million per unit.

Research and development costs, or as Raymer refers to them, research, development, test and evaluation costs (RDT&E) are nonrecurring costs, independent of how many aircraft are produced. Production costs, referred to in Raymer as flyaway costs, are variable costs which are dependent on the number of units produced. Although the two are different in nature, Raymer combines them, as he states that providing a clear separation between the two proves difficult. Hence, in this report the cost analysis of the R&D and production costs for the HUULC will also be combined.

As explained in Raymer, the RAND DAPCA IV model can be used to estimate R&D and production costs, by first estimating their required hours and multiplying them by corresponding hourly rates. The cost model is given in Equation 10.1 [78].

$$RDT\&E + production = H_E R_E + H_T R_T + H_M R_M + H_Q R_Q + C_D + C_F + C_M + C_{eng} N_{eng} + C_{avionics} \quad (10.1)$$

Here,  $H_E$ ,  $H_T$ ,  $H_M$ ,  $H_Q$  refer to the required hours of engineering, tooling, manufacturing and quality control respectively, whilst  $R_E$ ,  $R_T$ ,  $R_M$ ,  $R_Q$  refer to their corresponding hourly rates.  $C_D$ ,  $C_F$ ,  $C_M$ ,  $C_{eng}$  and  $C_{avionics}$  refer to the development support costs, flight test costs, manufacturing materials costs, engine production costs and avionics costs respectively. The RAND DAPCA IV model includes a Cost Estimation Relationship (CER) for every term on the right-hand side of Equation 10.1, except for the avionics costs,  $C_{avionics}$ . For brevity, these CERs are not discussed here and can be found on pages 498-499 of Raymer [78]. Avionics costs range from approximately 5% to 25% of production cost depending upon sophistication [78]. Since this is an early-stage cost estimation and costs tend to increase over time, the most conservative scenario of 25% is assumed.

In the RAND DAPCA IV model, costs are given in constant 1986 U.S. dollars. To be able to use the results of the cost model for a new generation aircraft like the HUULC, these 1986 U.S. dollars must be adjusted for inflation. Although most HUULC aircraft will be produced from 2030 onwards, the cost model is adjusted for 2015 U.S. dollars, since the preliminary design phase began in 2015. Furthermore, adjusting for a 2030 inflation rate would be done on the basis of rough inflation estimations, which would involve a high degree of risk in the case these estimation differ heavily from reality. Therefore, 2015 U.S. dollars are used for the entire cost analysis in this report. For an initial cost estimate like the current one, converting 1986 to 2015 U.S. dollars can be done by making use of the Consumer Price Index (CPI) [78]. One 1986 U.S. dollar is worth \$2.1698 at the time of writing, in 2015, hence all outcomes of the RAND DAPCA IV model must be multiplied by a factor of 2.1698 [161][162][163].

Using Equation 10.1 under the assumption that  $C_{avionics} = 0.25 \cdot production$ , an estimated R&D and production cost of \$761.15 million per aircraft is given, or \$247.37 billion for all 325 units. This cost exceeds the R&D and production budget available, hence budgetary redistribution actions must be taken. These will be explained in Section 10.5.

## 10.2. Ground support, initial spares & purchase additions

For the ground support, initial spares and purchase additions, a budget of \$63.38 billion was allocated, as can be seen in Table 5.4.

Ground support and purchase additions may be excluded from this section of the cost analysis. Firstly, costs involved in ground support will be covered by the operations & maintenance cost analysis in Section 10.3. Furthermore, purchase additions do not exist in the HUULC program. Purchase additions are defined as additional, exclusive adjustments made to the product in order to satisfy specific consumer wishes. As the HUULC will not be sold to a third party, since the manufacturers are also the operators, no purchase additions apply. Therefore, only the cost of initial spares will be covered in this section.

For predicting the cost of initial spares, Equation 10.2 can be used. In this equation,  $QTY$  refers to the number of aircraft produced,  $W_e$  to the aircraft empty weight in pounds and  $V_{max}$  to the maximum velocity in knots. Coefficients  $C_1$  and  $C_2$  are dependent on the aircraft type; for a cargo aircraft which is not a bomber, these are 0 and 1, respectively [164].

$$C_{initialspares} = (0.0000163)QTY^{1.28}W_e^{0.974}V_{max}^{0.171}e^{-1.22C_1}e^{-2.21C_2} \quad (10.2)$$

Equation 10.2 gives the cost for initial spares in 1989 U.S. dollars. This has to be converted to 2015 U.S. dollars, for the same reasons as explained in Section 10.1, which implies multiplying by a factor of 1.9178 [161][162][163]. When Equation 10.2 is used and the dollars are converted, the estimated cost of initial spares is \$15.55 billion. An ample budget margin of \$47.83 billion thus exists for initial spares.

## 10.3. Operations & maintenance

The operations and maintenance budget was given as \$606.63 billion in Chapter 5 and is used to fund various components of the operational lifecycle of the HUULC. These include hydrogen production and storage, airport construction, personnel costs, cargo handling and asset maintenance. The costs of these elements have been evaluated in Sections 9.5.3 and 8.2. Based on these two sections, a brief summary of the operations & maintenance cost is provided in Table 10.1. As can be seen from the table, the operations budget is not used entirely; there exists a budget surplus of \$606.6 – \$605.0 = \$1.6 billion. This fiscal margin is a desirable situation and allows for some contingency.

Table 10.1.: Overview of the operations & maintenance costs.

Component	Costs [\$bn]	Share [%]	Operations budget share [%]
Energy generation	475.9	78.7	78.4
Electrolysis	1.8	0.3	0.3
Liquefaction	11.0	1.8	1.8
LH2 Storage	1.0	0.2	0.2
Airport construction	9.2	1.5	1.5
Operation & maintenance activities	106	17.5	17.5
<b>Total costs</b>	<b>605.0</b>	<b>100.0</b>	<b>99.7</b>
<b>Total operations budget</b>	<b>606.6</b>	<b>-</b>	<b>100.0</b>

## 10.4. System phase-out & disposal

For the final phase in the lifecycle of the HUULC program, the system phase-out and disposal, there has been an \$18.11 billion budget allocation, as discussed in Chapter 5.

Phase-out and disposal costs may be one of the most difficult to predict, as they heavily depend on whether or not a third party will exist at the time of retirement, who would be interested in purchasing part of, or the whole, aircraft. Traditionally, military aircraft incur a positive cost during system phase-out, as they require decommissioning, including that of armaments and classified technologies. Civil aircraft, on the other hand, may have a portion of the positive costs compensated for, by the reselling of the entire aircraft or parts of it. When it comes to the HUULC, however, one may question the demand at the disposal phase. Unlike other commercial aircraft, the HUULC cannot land on any international airport - it can only land on the six designated

airports designed as part of the HUULC program. This would mean the buyer would either have business only in those specific regions, or would be prepared to invest in the development of more similar HUULC airports in other locations around the world. Since the probability of this event is negligible, the assumption is made that the HUULC fleet will not be sold on the resale market, but that only the scrap aluminium from each aircraft will be recycled and sold. Hence the disposal costs consist of the cost to disassemble and recycle the entire fleet minus the revenue generated from selling the recycled aluminium. Even the most refined cost estimation models, like Roskam, do not provide adequate methods for the estimation of airplane disposal cost. It is suggested, however, by Roskam, to use equation 10.3 to account for the disposal costs [165].

$$C_{disp} = 0.01 \cdot LCC \quad (10.3)$$

Where  $LCC$  is defined as lifecycle cost; the total cost of ownership of the entire lifespan of the HUULC aircraft. Using equation 10.3, the total disposal costs become \$8.68 billion.

The monetary value of recyclable aluminium is now to be estimated. Each HUULC aircraft contains 400,772kg of aluminium 7075 T6 alloy, which on average is worth \$2.638 per kilogram when sold as new bulk material [166]. Thus every HUULC has a value of aluminium worth \$1.06 million and the aluminium of the entire fleet is worth \$343.60 million. Hence, the HUULC program will see a system phase-out and disposal cost of \$8.68 - \$0.34 = \$8.34 billion for the entire HUULC fleet, leaving a disposal budget surplus of \$9.77 billion.

## 10.5. Comparing the budget and cost analysis

As was discovered in Section 10.1, the R&D and production costs surpassed the allocated budget. Hence, a budget redistribution is required, from a lifecycle phase where there is an over-budget. In Section 10.2, it was discovered that the budget for ground support, initial spares & purchase additions need not be as extensive as estimated in Table 5.4, since only initial spares were accounted for in that analysis. Initially, 7% budget was allocated to this program element, whereas only 3% is actually needed. The 4% of currently unassigned budget may now be redistributed to R&D and production, to cover for the apparent cost overrun of that lifecycle phase. It was decided to enlarge the R&D and the production budget by 2% each, resulting in an available R&D and production budget of \$253.52 billion in total, or \$780.05 million per aircraft. With total R&D and production costs having been estimated as \$247.37 billion, or \$761.15 million per aircraft, the redistributed budget now completely covers the projected R&D and production costs. Table 10.2 provides the finalized budget and cost breakdown and shows the budget surplus for each lifecycle phase.

Table 10.2.: Comparison of the final budget and estimated costs.

Lifecycle phase	Final budget [\$bn]	Estimated costs [\$bn]	Budget surplus [\$bn]
R&D and production	253.5	247.4	6.2
Initial spares	27.2	15.6	11.6
Operations & maintenance	606.6	605.0	1.6
System phase-out & disposal	18.1	8.3	9.8
<b>Total</b>	<b>905.4</b>	<b>876.3</b>	<b>29.2</b>

A budget surplus of \$29.2 billion has been estimated. A large portion of this value stems from the fact that initially, \$18.1 billion was allocated to the system phase-out and disposal, whereas the team expects an expense of \$8.3 billion from recycling of parts. Secondly, the initial spares have also been over-budgeted, with a budget surplus of \$11.6 billion. It should be noted that accurate cost analyses models do not exist and predicting costs has always been something of an art. The HUULC program is no exception to this, hence these numbers are not definitive. What the results do show, however, is that the program is on track and it is believed that a budget surplus will exist, which may be used as a contingency budget.

## 10.6. Validation of the RAND DAPCA IV model

As it strengthens the legitimacy of any model, validation procedures have been performed on the RAND DAPCA IV model, which has been used for estimating the R&D and production costs in Section 10.1. Cost data of the Airbus A380-800 were used as inputs to the model. Required inputs for the model are aircraft empty weight, maximum velocity, production quantity, number of flight test aircraft, number of engines per aircraft, avionics cost and engine production cost. These parameters have been taken from references [167][168][17][169] for the Airbus A380. When the same avionics assumption and dollar conversion factor as in Section 10.1 are employed, an R&D and production cost of \$421.25 million is produced by the model.

Compared to the actual Airbus A380-800 price, which was found to be \$388.10 million [170], the model produces a result that is 8.54% more optimistic than reality, for this case. This price difference is within a 10% margin and the model is thus considered to be validated and legitimate for the current cost prediction. If the RAND DAPCA IV model would be as optimistic for the HUULC as it is for the Airbus A380-800, a slight overall budget deficit might emerge in reality. In this case some HUULC program lifecycle phases should be reconsidered to be made less expensive, or the freight rate would have to be increased.

## 10.7. Conclusion and recommendations

A cost analysis has been performed, in which R&D and production costs surpassed their initial allocated budget. After a budget redistribution, a total budget of \$905.4 billion was assumed, with an estimated total program cost of \$876.3 billion, leaving a budget surplus of \$29.2 billion. This surplus may be used as contingency funds, for example in the case that the price of hydrogen production experiences a spike, or the market for aluminium finds itself in turmoil.

As was previously stated, these cost estimations are quite crude in their nature. The large budgetary surplus could possibly turn out to be a deficit in the end, particularly with the optimism of the RAND DAPCA IV model that was found during validation. If this is the case, it is recommended to increase the freight rate, in order to cover any budget deficit.

Another recommendation, although very general and vague, would be to develop a new cost model, one that would potentially be more accurate, particularly for this program. The HUULC program is quite different from other commercial aviation programs and where analysing costs is difficult and inaccurate for those programs, analysing costs for a first-of-its-kind aircraft like the HUULC is even more difficult and inaccurate, due to a complete lack of historical data.

# 11. Sustainable development strategy

Sustainability is increasingly important and is all about designing for the short and long term at the same time, which can be quite a challenge. To ensure the HUULC has high performance regarding sustainability, a Sustainable Development Strategy (SDS) has been defined. The strategy will state clear goals to achieve a minimum environmental impact, which will consider the design phase up until the eventual disposal of the HUULC. This integrated approach covers the entire life-cycle of the HUULC and will divide the SDS into the design and operational, production and the end-of-life phase. Therefore, the strategy can be employed efficiently. The aspects to be addressed in each phase are elaborated upon in Section 11.1 to Section 11.3.

## 11.1. Design and operations

In order to make the HUULC a sustainable project, production and end-of-life are not the only phases that need to be considered. HUULC's SDS starts at the very beginning - the design process. As the design is of critical importance for operations and vice versa, the SDS will address both phases simultaneously. The design itself is made as sustainable as possible using several new technologies, including hydrogen-powered engines. Hydrogen is one of the most important fuels when considering sustainability in propulsion. Its prominence stems from the fact that it not only minimises carbon emissions, but it completely eliminates them. The burning of hydrogen has byproducts of water, hot air and hydrogen; none of which are considered harmful to the environment [171]. The drawback of many low-emission fuels is their low energy density, something which is the opposite for hydrogen. This fuel provides a higher energy density than kerosene, hydrogen provides an energy density of approximately 143 MJ/kg [172], compared to 43.5 MJ/kg [173] provided by kerosene. Its zero emission nature, coupled with its extremely high energy density, makes hydrogen a very attractive fuel. Despite the aforementioned environmental benefits of hydrogen, it is still desirable to have minimum fuel usage during operation, because producing hydrogen requires energy. During the design of the HUULC, an optimal lift to drag ratio is pursued such that a minimum amount of hydrogen fuel is used.

Although hydrogen combustion causes no direct production of harmful gasses, high temperature hydrogen combustion can cause nitrogen in the air to react with oxygen, of which the products are nitrous oxides. Nitrous oxide is considered particularly harmful to the environment, as a gram of nitrous oxide has an impact 300 times larger on the atmosphere compared to a gram of carbon dioxide [174]. With this in mind, the propulsion system is designed to operate with minimum nitrous oxide production.

As mentioned before, combustion of hydrogen produces water. Water is not typically considered environmentally unfriendly, but emission of water at an altitude will result in condensation trail (contrail) formation. Contrails insulate radiation at a higher rate than they reflect celestial radiation, which causes global warming [175]. Conventional aircraft form contrails at altitudes higher than 8000 meters [176], due to low local temperatures. Because of the high water content of the HUULC's exhaust gasses, less extreme temperatures are required for contrail formation and thus contrails may form at lower altitudes. The formation of contrails will thus be limited during operations, by flying at an altitude lower than 8000 meters.

A sustainable aircraft also needs to generate as minimal noise pollution as possible. To ensure noise pollution reduction is implemented in the design process, the trade-off between different aircraft concepts includes a criterion based on the amount of noise the HUULC produces. The aircraft with a lower level of noise pollution is preferable over an aircraft with a higher level, as it relieves impact on nearby airport communities.

The seemingly most important aspect with respect to the sustainability of the HUULC is in the propulsion aspect, which poses some opportunities, as well as difficulties. The HUULC uses hydrogen propellant and flies at low altitudes, eliminating carbon emissions and minimising contrail formation, respectively. This does not automatically result in a sustainable aircraft, as explained in the previous paragraphs. A goal has to be set with respect to harmful emissions, contrail formation and noise pollution to ensure a sustainable design. The HUULC will comply with the goals stated in Flightpath 2050 [13], a document of the Advisory Council for Aviation Research and innovation in Europe (ACARE), where a vision on sustainable aviation in Europe for the year 2050 is given.

## 11.2. Production

To have a truly sustainable operation, it is required that hydrogen is produced in an environmentally friendly manner and not shift the greenhouse gas emission to the hydrogen production process. The possibility to sustainably produce hydrogen in close proximity of the dedicated airfields is implemented. Sustainable hydrogen

production with the use of wind, solar or hydroelectric energy ensures there are no emissions during energy generation.

Since the hydrogen is produced in the airports' vicinities, less transportation of the hydrogen is needed. As transportation results in energy consumption, the hydrogen production is more efficient and requires less possible involvement of carbon emissions; for example, no or few fossil-fueled trucks are required for transportation.

The environment should be affected as little as possible during the production process. An ever-decreasing amount of in-process defects, scrap material and repairs on finished products will be pursued. Lowering the amount of in-process defects will cause the production process to be more efficient, hence overall less energy usage will be necessary to produce a certain part. Scrap material and redundant parts will be minimised to lower the required energy as well; for example, by using LEAN manufacturing. The LEAN philosophy will assure the right amount of parts are produced, hence no unnecessary and redundant parts will be made. Decreasing the amount of necessary repairs on finished products actually decreases the need for redundant parts, because less parts will have to be replaced. Also, the amount of harmful waste material will be minimised as much as possible. The use of high grade materials frequently results in advanced production processes, which require more power, time and financial resources. It can occur that certain rare materials are necessary, resulting in possible harmful extraction and transport, leading to a significant environmental impact. During the design trade-off, all materials are judged on sustainability, performance and cost to ensure a balanced choice.

### **11.3. End-Of-Life**

As, eventually, every aircraft will be taken out of service, a sustainable aircraft design needs to take end-of-life into account. Sustainable decommission of the aircraft starts in the design phase. By making use of recyclable materials and minimising usage of hazardous material, the amount of waste will be as small as possible. An environmentally friendly facility will be constructed before the expected disposal time of the HUULC fleet. To construct an environmentally friendly disposal plant, current techniques can be used as mentioned in Section 11.2. On the other hand, new technologies might also provide better solutions in the future. The facility should be able to efficiently and accurately disassemble the fleet as well, as to provide the capability to cautiously treat hazardous material and act as a recycling plant.

## 12. Design verification

To assess the quality of the design, the HUULC's performance has to be analysed to evaluate if the design complies with the requirements. The requirements have been previously stated in the Baseline report and in Chapter 3, and for an elaborate discussion of the requirements analysis and discovery process the Baseline report should be consulted [11]. The tool used for the assessment is a compliance matrix, which is provided in Section 12.1. In Section 12.2 several individual requirements are further discussed.

### 12.1. Compliance matrix

The requirements are listed in the compliance matrix Table 12.1, where the first column indicates if the requirement has been met. A tilde sign indicates the requirement can not be fully assessed at this time and in Section 12.2 these requirements will be discussed.

### 12.2. Compliance analysis

The requirements in Table 12.1 which await verification (indicated with a tilde sign) are elaborated upon in Section 12.2.1 to 12.2.4. The postponed verification is mainly caused by the assessment being part of the next design phase.

#### 12.2.1. C-Leg-1

The HUULC utilises an advanced unmanned control system, currently only employed in military aircraft. An unmanned cargo aircraft (UCA) is the next step in unmanned flight considering the opportunities such as flexibility and efficiency as described in Chapter 7. Civil unmanned aircraft encounter regulatory problems as the current regulations for unmanned aircraft do not have many degrees of freedom. The strict regulations allow small unprofessional UAV operators to operate more freely than the professional dedicated companies [81]. Revising these regulations is of great importance for full authorised operation of the HUULC. Further testing and certification are required in the following design stages to ensure the requirement will be met.

#### 12.2.2. Tr-Ops-Flight-3 and Tr-PI-4

In flight vibrations can cause an aircraft to fail or payload to be damaged and should be analysed thoroughly. Resonating frequencies should be avoided for the aircraft as well as the payload to ensure no capital is lost. Vibrational analysis is planned for the upcoming design phases where comprehensive analysis, testing and design will ensure safe and profitable operations of the HUULC, the requirements will therefore be met in future design.

#### 12.2.3. Tr-Perf-Sust-1 and Tr-Perf-Sust-2

The HUULC program has ambitious sustainability targets and noise is a key sustainability parameter. The noise levels that the HUULC produces can not be measured at this stage of the design. The HUULC does employ several noise reducing features to ensure noise levels are at a minimum. These features include for example new counter-rotating propellers which produce low noise levels and the blended wing body configuration [177][178].

#### 12.2.4. Tr-Perf-Sust-3

The HUULC transports at zero carbon emission levels which reduces the emissions to  $NO_x$  and contrails. Using engine premixing and lower cruise altitudes the  $NO_x$  levels can be reduced to a fraction of current day kerosene aircraft [14]. The emissions of the HUULC can not be quantified until a later state of the project.

Table 12.1.: Compliance matrix.

✓/x	ID	Description
✓	C-COST-1	The freight rate of container transport by HUULC shall not exceed 250% of the freight rate of standard container ships.
-	C-LEG-1	The HUULC shall meet the requirements obtained after close cooperation with certification authorities.
✓	C-RES-1	The hydrogen production shall be sustainable.
✓	C-RES-2	The HUULC hydrogen consumption shall not exceed the hydrogen production capacity available at time of operation.
✓	C-TIME-1	Refueling of the HUULC shall not exceed the turnaround time stated in requirement TR-OPS-AIRPO-2.
✓	C-TIME-2	The HUULC shall enter into service in 2030.
✓	TR-COMP-1	The HUULC shall have a combination of cruise speed, flight trajectory, freight rate, reliability and sustainability that maximizes competitiveness w.r.t. maritime transport when compared to other combinations viable at that time.
✓	TR-COMP-2	The HUULC shall have an expected lifespan of no less than 45 years.
✓	TR-CONFIG-1	The HUULC shall have a wing-lifting configuration.
✓	TR-CONFIG-2	The HUULC shall not make use of the wing-in-ground effect.
✓	TR-CONFIG-3	The HUULC shall not have a helicopter configuration.
✓	TR-CONFIG-4	The landing gear configuration shall be compatible with the pavement's strength of the selected airfields.
✓	TR-FUEL-1	The HUULC shall be propelled by cryogenic hydrogen.
✓	TR-FUEL-2	The fuel tanks shall contain the required quantity of fuel to perform the design mission.
✓	TR-FUEL-3	The fuel tanks shall allow for turnaround maintenance inspections.
✓	TR-FUEL-4	The fuel system shall distribute the fuel to the power plants.
✓	TR-FUEL-5	The fuel system shall be able to influence stability.
✓	TR-OPS-AIRPO-1	The HUULC shall be able to land on selected airports (Landing gear, pavement, gate width, runway width, runway length, etc.).
✓	TR-OPS-AIRPO-2	The turnaround time shall be less than six hours.
✓	TR-OPS-AIRPO-3	The airports shall have a cargo bay capacity for 100 TEU.
✓	TR-OPS-AIRPO-4	The airports shall be located within 25 kilometers to a renewable energy source.
✓	TR-OPS-AIRPO-MAIN-1	The HUULC shall allow access ability for repairs.
✓	TR-OPS-AIRPO-MAIN-2	The overall operational availability of the HUULC shall be at least 85%.
✓	TR-OPS-FLIGHT-1	The HUULC shall not be pressurized.
✓	TR-OPS-FLIGHT-2	The HUULC shall have no crew and no crew support systems.
-	TR-OPS-FLIGHT-3	The induced vibrations shall not cause the HUULC to lose structural integrity.
✓	TR-OPS-FLIGHT-COM-1	The HUULC shall always have contact with the control centre.
✓	TR-OPS-FLIGHT-COM-2	The communications system shall deny unauthorised control requests.
✓	TR-OPS-FLIGHT-COM-3	The HUULC shall provide communication between ATC and ground control.
✓	TR-OPS-FLIGHT-UN-1	The HUULC shall be flyable by at least one ground controller.
✓	TR-PERF-CTRL-1	The HUULC shall be controllable in such a way that it can follow the predetermined flight trajectory.
✓	TR-PERF-CTRL-2	The control system shall counteract spiral induced eigenmotions.
✓	TR-PERF-CTRL-3	The control system shall counteract phugoid induced eigenmotions.
✓	TR-PERF-MP-1	The HUULC shall have a cruise altitude of no lower than 5000 meters and no higher than 8000 meters.
✓	TR-PERF-MP-2	The HUULC shall have an operating range of more than 6000 km while carrying maximum payload.
✓	TR-PERF-STB-1	The HUULC shall be statically stable.
✓	TR-PERF-STB-2	The HUULC shall be dynamically stable for dutch roll eigenmotion.
✓	TR-PERF-STB-3	The HUULC shall be dynamically stable for short period eigenmotion.
✓	TR-PERF-STB-4	The HUULC shall be dynamically stable for aperiodic roll eigenmotion.
-	TR-PERF-SUST-1	The HUULC shall produce no more than 104.7 dB noise during take-off at distance 4400 meters.
-	TR-PERF-SUST-2	The HUULC shall produce no more than 97.1 dB noise during landing at distance 4400 meters.
-	TR-PERF-SUST-3	The HUULC shall not produce more than 0.27 grams $NO_x$ per ton kilometer.
✓	TR-PERF-SUST-4	The HUULC shall use no fossil fuels during flight.
✓	TR-PL-1	The HUULC shall be able to accommodate the contents of 100 TEU lightweight containers.
✓	TR-PL-2	The HUULC shall be able to transport a payload of 1200 metric tonnes.
✓	TR-PL-3	The HUULC shall transport the payload without inflicting payload damage.
-	TR-PL-4	The induced vibrations shall not compromise the payload integrity.
✓	TR-SF-1	The HUULC shall have a fail-safe communication system.

## 13. Post DSE Planning

After completion of the preliminary design phase the project is still in a grassroots stage. Planning is required to further develop the HUULC program until 2030, when the first HUULCs will start operations. The subsequent stages of the HUULC program are divided into research & development, prototype manufacturing, testing & certification and production & delivery. The phases will be discussed starting with research & development in Section 13.1 and concludes with production & delivery in Section 13.4. Figure 13.1 contains a logical flow of the future design and production processes and Figure 13.2 illustrates the time allocated for every phase.

### 13.1. Research & development

To acquire an accurate estimation of further development time the duration of the stages is based upon reference data from the Airbus A380 [179]. The research and development stage for the A380 started in 1994 and finished in 2002, with the start of the wing box [180]. For the HUULC the research and development stage ends in 2023, lasting for eight years. Figure 13.1 illustrates a chronological flow of the future stages of the HUULC program and Figure 13.2 is a time line indicating the duration of the stages.

### 13.2. Prototype manufacturing

Before certification can be achieved, several prototypes have to be constructed to pursue design validation. Using the reference aircraft, prototype construction has a time budget of two years, starting in 2022 and finishing in 2024 [180][181].

### 13.3. Testing & certification

As Figure 13.2 illustrate the testing and certification phase has a duration of two years [181][182][183]. The start is in 2024 and finishes in 2026. The limited flight envelope is expected to require less testing, however the unmanned aspect will need regulation alterations and as such the testing & certification phase is allocated two years.

### 13.4. Production & delivery

After certification is obtained the production process will start in 2026. Three years have been budgeted to manufacture the first five HUULCs to start operations, where the first HUULC would be finished in 2029. Three years is longer than reference aircraft required but contingency has been accounted for due to startup of the production process and difficulties due to the sheer size of the HUULC [180]. Entry into service is scheduled for 2030 which leaves one year for contingency from any of the phases described in this chapter. A more detailed view of the production & delivery process can be seen in Figure 13.1.

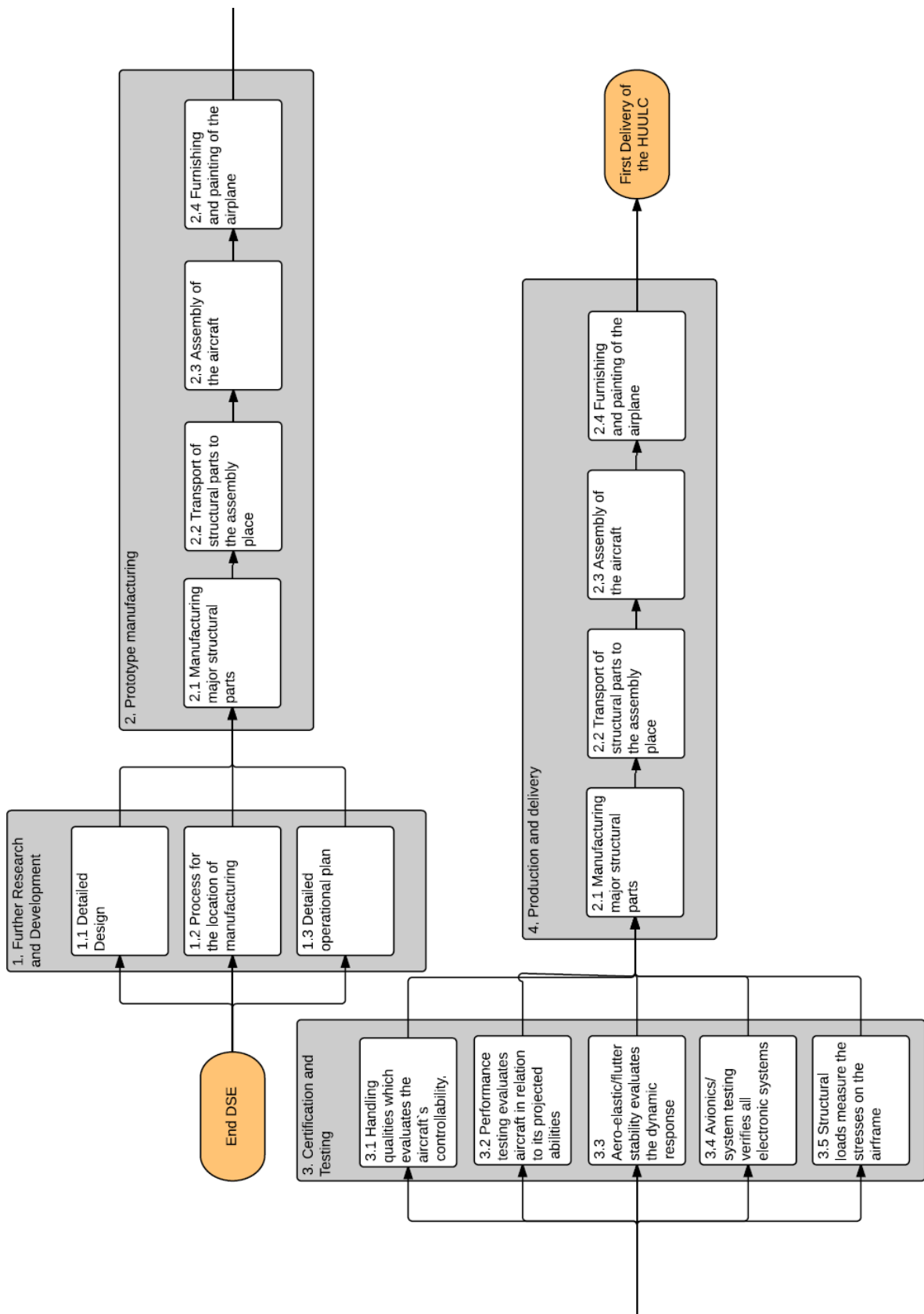


Figure 13.1.: The flowchart for after DSE.

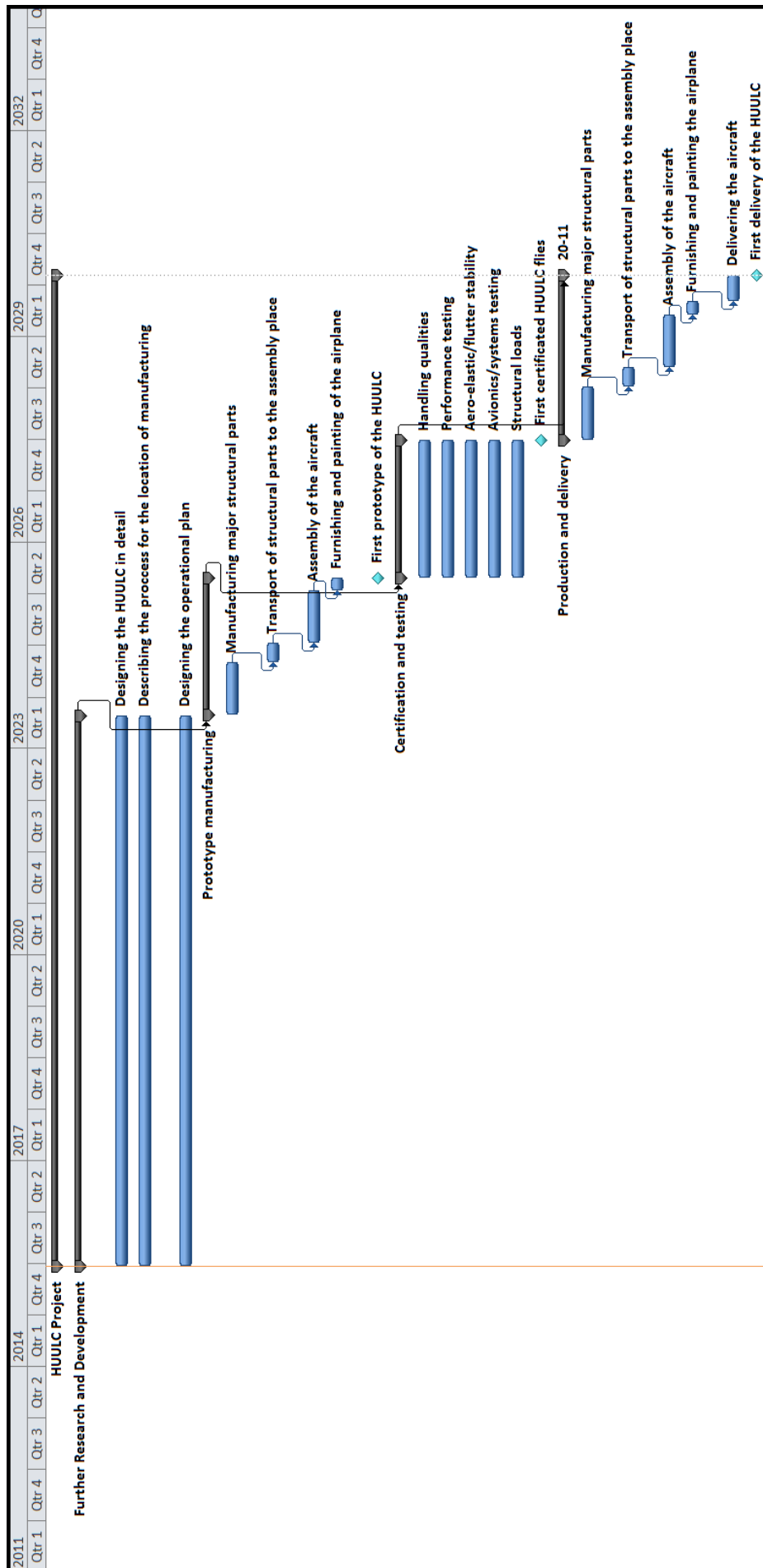


Figure 13.2.: The Gantt chart for after DSE.

## 14. Conclusion and recommendations

The task given to DSE group 9 was to design and plan the operations of a Hydrogen-powered Unmanned Ultra Large Cargo aircraft (HUULC) with a payload capacity of 1200 metric tons. The key idea behind an ultra large aircraft like the HUULC is to compete with current maritime transport by providing a freight rate of 250% compared to current shipping costs. To reach this price and capacity target, team HUULC has made key decisions on the design and operations of the HUULC. After assessing the benefits and drawbacks of different possible concepts, team HUULC has come to specific conclusions regarding the best possible solution to implement an aircraft with these size and cost requirements.

For the general layout of the HUULC, the blended wing body concept with a flat nose was chosen. With a wingspan of 200m and a lift to drag ratio of 26, the blended wing body concept allows for the shortest wingspan and also for the lowest hydrogen consumption. This was critical to meet the 250% freight rate cost target. The flat nose was chosen because it is advantageous for loading and unloading the HUULC. The flat nose doesn't have any drawbacks for the HUULC since it is flying at 483 km/h, so wave drag is not encountered.

Even though the blended wing body concept is believed to be the most efficient option when span and lift to drag ratio are considered, team HUULC has come to the conclusion that it is not possible to have a HUULC with a small enough wingspan that would at the same time be operable on existing airports and meet the required fuel consumption cost. So the only viable option is to use custom built airports.

These airports are located at regions with an important activity of import and export of goods. Furthermore, airports are needed as hub and for refuelling purposes. For these purposes airports will be built in Anchorage, Memphis, Terneuzen, Dubai, Novosibirsk and Shanghai. On this particular network, the HUULC will have 1.16% market share by volume.

The HUULC has to be a sustainable aircraft. This requirement is met by producing hydrogen with renewable energy sources. Hydrogen in Zeeland, Memphis, Anchorage and Shanghai will be produced with wind energy, the middle east will use photovoltaic panels and hydrogen in Novosibirsk will be produced from hydroelectricity. By assuming decreasing energy prices from renewable sources with an average of \$0.0189 per kW/h it is possible to meet the 250% freight rate required for the HUULC.

The HUULC is an unmanned aircraft. For large aircraft where the crew is a small fraction of the total cost the advantage of making the aircraft unmanned is reduced. However, if regulatory hurdles can be overcome it is beneficial to replace the crew with an unmanned system, even if it is only a small reduction of the total cost of operations.

Overall, from the work done by DSE group 9 the HUULC could theoretically be feasible. However the success of the HUULC is dependent on too many factors such as energy prices and market dynamics. This means that it would be challenging to find investors and a small change in external factors could make the HUULC unfeasible. In spite of the fact that the market analysis shows that there is demand for a plane such as the HUULC, communication with specific customers are necessary before more funds are invested into the HUULC project. Since no hydrogen plane has been made before, it would be more sensible to first apply this new technology on a more classic aircraft where the market is already well defined and more importantly where the upfront cost of infrastructure and design is much smaller.

## 15. Summary

Currently over 90% of long-distance goods are transported by sea, which is an inexpensive but slow solution. Air transport, on the other hand, is faster, more reliable and more flexible but is often prohibitively expensive. The best-of-both-worlds scenario - next-day delivery at a low cost - is a concept consumers may only dream of. Moreover, with increasing shipping volumes, both modes of transport contribute significantly to global environmental pollution. A breakthrough is thus required, to give consumers fast, inexpensive but environmentally-friendly transportation of their goods. Team 9 believes this breakthrough is embodied in the following mission statement:

*Team 9 will design the HUULC, a freighter aircraft that will pioneer in sustainable high capacity air transport, competitive with maritime cargo shipping from 2030 onwards.*

The HUULC aircraft will transport the content of 97 to 100 twenty-foot equivalent unit containers (TEU), making it the first aircraft to pierce the maritime container market. Its air-cargo transport time, coupled with a freight rate comparable to that of maritime transport, allow market capture from both high-value, time-sensitive goods traditionally transported by air but also low-value, less time-sensitive goods traditionally transported by ship. The HUULC will thus blur the lines between the two types of cargo.

The HUULC project is composed of two equally-sized segments: the design of the HUULC aircraft and the design of the operations surrounding the HUULC. The aircraft design efforts have culminated in a blended-wing body aircraft with a maximum take-off weight of 2.1 million kilograms. For comparison, one HUULC has the equivalent maximum take-off weight of four Airbus A380 aircraft.

In the preliminary design, a trade-off resulted in the concept based on the Burnelli blended wing body design with a total wingspan of 200 meters. The aerodynamics and planform design showed that this design is able to fly with the numbers as calculated in the preliminary design. To increase extra lift during take-off and landing, single slotted flaps will be used for the high lift devices. The propulsion of the aircraft will consist of eight leading edge mounted, contra-rotating propfan engines. The structural analysis showed that all forces, moments, flows and stresses can be designed for by including a wingbox in the HUULCs wing. The landing gear designed for HUULC consists out of a conventional set-up with 86 wheels. A weight and balance estimation showed that the centre of gravity of the aircraft lies approximately 42 meters behind the nose of the aircraft. To have an aircraft which is stable and controllable, an empennage system is designed in the form of two fuselage mounted fins and a single elevator which is placed on top of the two fins.

The operational design efforts have led to the development of six new dedicated global airports, designed to accommodate 325 units of the 200 meter wingspan aircraft. The airports used for the import and export regions are situated in the Yangtze river delta region, United Arab Emirates, Western Europe and South-East USA. Two hubs have been chosen to lower the travel distances and to gain the advantage of logistics: one in Novosibirsk (Russia) and the other in Anchorage (USA). With this network, the HUULC will be able to serve all three of the major global trading routes, which together constitute 33% of global containership traffic. With this number of HUULCs, within these regions and along these route, it is expected to obtain a market share of 1.16% by 2045.

With a total of 36.6 million kilograms of hydrogen fuel required daily, each airport will be equipped with sustainable hydrogen production facilities. Three types of renewable energy were selected to be deployed at different airports. Wind energy will be used for South-East USA, Yangtze river delta region, while solar energy will be used for United Arab Emirates and hydroelectric energy will be used for Novosibirsk.

A predicted total budget of \$905.4 billion is available for the entire HUULC program. After a preliminary cost analysis, a budget surplus of \$29.2 billion was found, which may be used as a contingency budget. Renewable energy production is an expense which requires 52.6% of the total budget, making it the largest expense in the HUULC program.

A sustainable development strategy was based on three aspects, namely the design and operation, production and end-of-life. The goal is to minimise pollution and to maximise efficiency. The main method used for SDS will be the LEAN philosophy.

# Bibliography

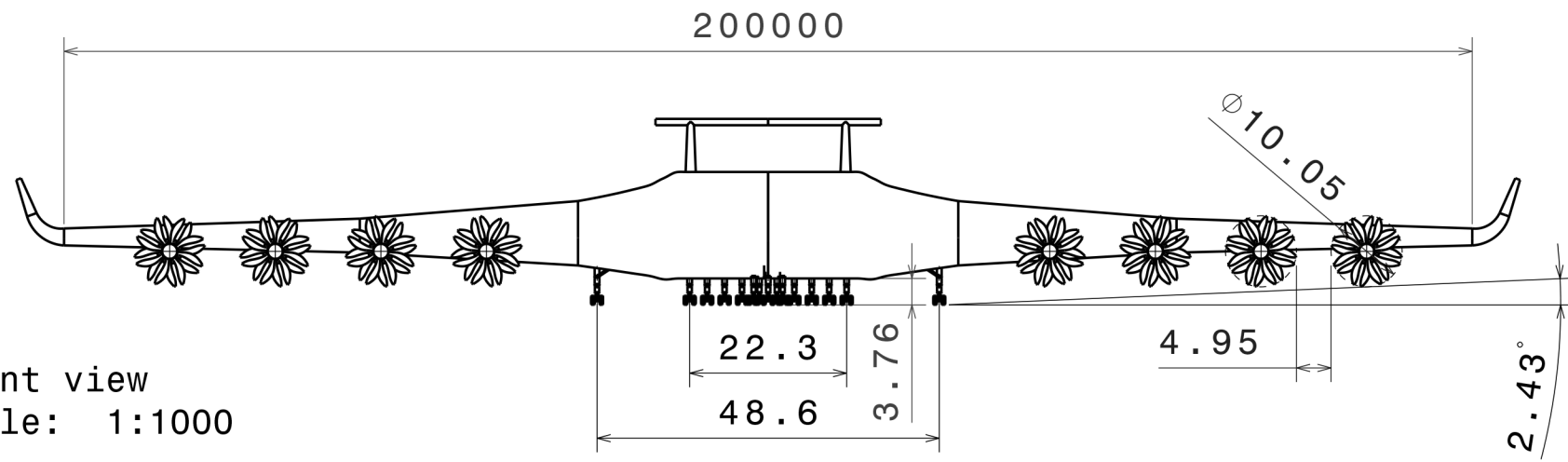
- [1] Reducing emissions from the shipping sector - European Commission. [http://ec.europa.eu/clima/policies/transport/shipping/index\\_en.htm](http://ec.europa.eu/clima/policies/transport/shipping/index_en.htm). Accessed: 2015-05-19.
- [2] Jan Dierickx, Rob Viet, Thibault Clar, Kenan Eken, Max de Feber, Myrthe Gillis, Dionisios Korovilas, Joris Neuman, Jennifer Stooft, and Rubén Suárez Millán. The HUULC - Project Plan Report. Technical report, TU Delft, Delft, 2015.
- [3] Jan Dierickx, Rob Viet, Thibault Clar, Kenan Eken, Max de Feber, Myrthe Gillis, Dionisios Korovilas, Joris Neuman, Jennifer Stooft, and Rubén Suárez Millán. The HUULC - Baseline Report. Technical report, TU Delft, Delft, 2015.
- [4] Jan Dierickx, Rob Viet, Thibault Clar, Kenan Eken, Max de Feber, Myrthe Gillis, Dionisios Korovilas, Joris Neuman, Jennifer Stooft, and Rubén Suárez Millán. The HUULC - Midterm Report. Technical report, TU Delft, Delft, 2015.
- [5] Boeing. World Air Cargo Forecast 2014 - 2015. 2014.
- [6] Airbus. Global Market Forecast, Flying on Demand, 2014 2033. 2014.
- [7] G. La Rocca. Project Guide Design Synthesis Exercise; The HUULC: Design of an Hydrogen-powered Unmanned Ultra Large Cargo aircraft. Technical report, 2015.
- [8] World Shipping Council. Trade routes. <http://www.worldshipping.org/about-the-industry/global-trade/trade-routes>.
- [9] Gesamtverband der Deutschen Versicherungswirtschaft. Container Handbook. [http://www.containerhandbuch.de/chb\\_e/scha/index.html](http://www.containerhandbuch.de/chb_e/scha/index.html), 2015.
- [10] G. La Rocca. Project Guide Design Synthesis Exercise; The HUULC: Design of an Hydrogen-powered Unmanned Ultra Large Cargo aircraft. Technical report, TU Delft, 2015.
- [11] Jan Dierickx, Rob Viet, Thibault Clar, Kenan Eken, Max de Feber, Myrthe Gillis, Dionisios Korovilas, Joris Neuman, Jennifer Stooft, and Rubén Suárez Millán. The HUULC - Baseline Report. Technical report, TU Delft, Delft, 2015.
- [12] European Conference of Ministers of Transport. Efficient Transport for Europe. OECD Publications Service, 1998.
- [13] M Dareck, C Edelstenn, and T Ender. Flightpath 2050 Europes Vision for Aviation. Office of the European, 2011.
- [14] Reinhard Faass. Flugzeuge mit Wasserstoffantrieb. Technical report, 2001.
- [15] UK Civil Aviation Authority. Noise Data for the First Three Years of Scheduled Airbus A380 Operations at London Heathrow Airport ERCD REPORT 1106 Noise Data for the First Three Years of Scheduled Airbus A380 Operations at London Heathrow Airport. (February), 2012.
- [16] Rebecca Maksel. What determines an airplanes lifespan? — Need to Know — Air & Space Magazine. <http://www.airspacemag.com/need-to-know/what-determines-an-airplanes-lifespan-29533465/?no-ist>, 2008. Accessed: 2015-06-10.
- [17] Airbus Deutschland GmbH. Airbus December 2014 Orders and Deliveries. Airbus, 2014.
- [18] Federal Aviation Administration. Flight Standards Information Management System. Federal Aviation Administration, 2009.
- [19] H.G. Visser from Delft University of Technology. AE3501 Lecture 3 Business models v4. <https://blackboard.tudelft.nl>. Accessed: 30-08-2013.
- [20] Rigas Doganis. Flying Off Course; Airline Economics and Marketing. Routledge, 4th edition, 2010.
- [21] Cornell University. Hub-and-Spoke vs Point-to-Point Networks. <http://blogs.cornell.edu/info2040/2011/09/14/hub-and-spoke-vs-point-to-point-transport-networks/>. Accessed: 2015-05-19.
- [22] Merriam-Webster. Ton-kilometer — Definition of ton-kilometer by Merriam-Webster. <http://www.merriam-webster.com/dictionary/ton-kilometer>. Accessed: 2015-06-15.
- [23] Ministry of Transport New Zealand. Freight and the transport industry : Freight volume. <http://www.transport.govt.nz/ourwork/tmif/freighttransportindustry/ft007/>, 2014. Accessed: 2015-06-15.
- [24] Fundamental Focus. Profit Margin Analysis. <http://www.aaii.com/computerizedinvesting/article/profit-margin-analysis.pdf>, 2011. Accessed: 2015-06-16.
- [25] dr. W. Verhagen Dr. R. Curran. Ae3221-i systems engineering and aerospace design; concurrent engineering & design for lifecycle, April 2015.
- [26] Helen Jiang. Key Findings on Airplane Economic Life. Technical Report March, Boeing, 2013.
- [27] Boeing. About Boeing Commercial Airplanes. <http://www.boeing.com/company/about-bca/#/prices>. Accessed: 2015-05-04.
- [28] G. La Rocca. Project Guide Design Synthesis Exercise; The HUULC: Design of an Hydrogen-powered Unmanned Ultra Large Cargo aircraft. Technical report, 2015.
- [29] Dr. Jan Roskam. Airplane Design Series Part I: Preliminary Sizing of Airplanes. DARcorporation, 1985.
- [30] Nathan Meier. Civil Turboshaft/Turboprop Specifications. <http://jet-engine.net/civtsspec.html>. Accessed: 2015-06-11.
- [31] J. van Dommelen, R. Vos. A conceptual design and analysis tool for blended wing body aircraft. Airbus, 2012.
- [32] Dieter Scholz. Flugzeugkonfiguration. 2006.
- [33] NASA. Composite Cryotank Technologies and Demonstration (CCTD). [https://gcd.larc.nasa.gov/projects/archived-projects-2/composite-cryogenic-propellant-tank/#.VvyJ00aL\\_PI](https://gcd.larc.nasa.gov/projects/archived-projects-2/composite-cryogenic-propellant-tank/#.VvyJ00aL_PI). Accessed: 2015-05-20.
- [34] G. Krainz, G. Bartlok, P. Bodner, P. Casapicola, Ch. Doeller, F. Hofmeister, E. Neubacher, and A. Zieger. DEVELOPMENT OF AUTOMOTIVE LIQUID HYDROGEN STORAGE SYSTEMS. Technical report. Accessed: 2015-05-18.
- [35] BMW Group. CRYO-COMPRESSED HYDROGEN STORAGE. [http://www.stfc.ac.uk/resources/pdf/cryogenic\\_cluster\\_day\\_kunze\\_rev1.pdf](http://www.stfc.ac.uk/resources/pdf/cryogenic_cluster_day_kunze_rev1.pdf). Accessed: 2015-05-13.
- [36] XFLR5. XFLR5 software tool. <http://www.xflr5.com/xflr5.htm>. Accessed: 27-05-2015.
- [37] Michael S. Selig and James J. Guglielmo. High-Lift Low Reynolds Number Airfoil Design. Accessed: 2015-06-4.
- [38] G. La Rocca. Aerospace Design and Systems Engineering Elements II - Wing Design Part 3. <http://blackboard.tudelft.nl>. Accessed: 12-09-2012.
- [39] A Bhowal, M.J.C Kolf, V Margos, J.I Nijssse, T.E.H Noortman, J Peeters Salazar, L.E van den Ende, M.P. van Hoorn, and institution = TU Delft mendeley-groups = HUULC pages = 21 title = The HUULC - Project Plan Report year = 2015 Wong, F.T.H. Technical report, Delft.
- [40] James L Felder, Gerald V Brown, and Hyun Dae Kim. Turboelectric distributed propulsion in a hybrid wing body aircraft. 2011.
- [41] Oliver J Murphy, Alan Cisar, and Eric Clarke. Low-cost light weight high power density pem fuel cell stack. *Electrochimica Acta*, 43(24):3829–3840, 1998.
- [42] Martin Hepperle. Electric flight–potential and limitations.
- [43] Guangsheng Zhang and Satish G Kandlikar. A critical review of cooling techniques in proton exchange membrane fuel cell stacks. *International Journal of Hydrogen Energy*, 37(3):2412–2429, 2012.
- [44] K Schoots, GJ Kramer, and BCC Van Der Zwaan. Technology learning for fuel cells: An assessment of past and potential cost reductions. *Energy Policy*, 38(6):2887–2897, 2010.
- [45] Ger. J.J. Ruijgrok. Elements of airplane performance. Delft Academic Press, Delft, 2009.

- [46] J. D. Klaus. Crs report for congress; strategic mobility innovation: Options and oversight issues. 2005.
- [47] Blades A400M. <http://www.ratier-figeac.com/?q=en/content/produitsservices/propellers/en>. Accessed: 2015-06-05.
- [48] Military Aircraft Airbus DS — A400M. <http://militaryaircraft-airbusds.com/Aircraft/A400M/A400MSpec.aspx>. Accessed: 2015-06-05.
- [49] NK12 Engine. <http://cdn-www.airliners.net/aviation-photos/photos/7/7/7/0732777.jpg>.
- [50] AN 70 picture. [http://commons.wikimedia.org/wiki/File:Antonov\\_AN-70\\_at\\_Paris\\_Air\\_Show\\_2013\\_5.jpg](http://commons.wikimedia.org/wiki/File:Antonov_AN-70_at_Paris_Air_Show_2013_5.jpg).
- [51] J S Vanderover and K D Visser. Analysis of a Contra-Rotating Propeller Driven Transport Aircraft. pages 1–11, 2000.
- [52] EU. DREAM Project (validation of Radical Engine Architecture systems). [http://ec.europa.eu/research/transport/projects/items/dream\\_en.htm](http://ec.europa.eu/research/transport/projects/items/dream_en.htm). Accessed: 2015-06-07.
- [53] EU. NACRE (New Aircraft Concepts Research) Project. [http://ec.europa.eu/research/transport/projects/items/nacre\\_en.htm](http://ec.europa.eu/research/transport/projects/items/nacre_en.htm). Accessed: 2015-06-07.
- [54] Cordis. Contra-Rotating Open Rotor (CROR) Propeller barrels. pages 2–3, 2015.
- [55] Mark Taylor and Rolls Royce. Open Rotor Engine Design and Validation. [http://aerosociety.com/Assets/Docs/GreenerbyDesign/\(6\)MarkTaylor.pdf](http://aerosociety.com/Assets/Docs/GreenerbyDesign/(6)MarkTaylor.pdf).
- [56] EPI Inc. Propeller Performance Factors. Accessed: 2015-06-18.
- [57] Dr. Jan Roskam. Airplane Design Series Part II: Preliminary Configuration Design and Integration of the Propulsion System. DARcorporation, 1985.
- [58] L.L.M. Veldhuis. Optimization of tractor propeller/wing configurations. *Journal of Aerospace Engineering*, 209(37):215–226, 1995.
- [59] b52strato. [http://www.dept.aoe.vt.edu/~mason/Mason\\_f/B52S05.pdf](http://www.dept.aoe.vt.edu/~mason/Mason_f/B52S05.pdf). Accessed: 2015-06-19.
- [60] E-THRUST - Electrical distributed propulsion system concept for lower fuel consumption, fewer emissions and less noise. [http://www.zwomp.de/wp-content/uploads/2013/06/E-Thrust\\_EN\\_V13-final.pdf](http://www.zwomp.de/wp-content/uploads/2013/06/E-Thrust_EN_V13-final.pdf). Accessed: 2015-06-18.
- [61] D. Steenhuizen. AE2111-II Aerospace Design & Systems Engineering Elements.
- [62] James Ainsworth, Craig Collier, Phil Yarrington, Ryan Lucking, and James Locke. Airframe Wingbox Preliminary Design and Weight Prediction. 69th Annual Conference, Virginia Beach, Virginia, page 41, 2010.
- [63] Dr. Jan Roskam. Airplane Design Series Part V: Component Weight Estimation. DARcorporation, 1985.
- [64] T.H.G. Megson. Aircraft Structures for Engineering Students. 2013.
- [65] ASM. ASM Aluminum 7075-T6 Data Sheet. <http://asm.matweb.com/search/SpecificMaterial.asp?bassnum=MA7075T6>. Accessed: 2015-06-15.
- [66] Wolfram Mathematica. NMinimize - Wolfram Language Documentation. <https://reference.wolfram.com/language/ref/NMinimize.html>. Accessed: 2015-06-15.
- [67] P. Horst L. U. Hansen, W. Heinze. REPRESENTATION OF STRUCTURAL SOLUTIONS IN BLENDED WING BODY PRELIMINARY DESIGN. Technical report, ICAS, 2006.
- [68] William H. Mason Joseph A. Schetz Raphael T. Haftka Leifur Thor Leifsson, Andy Ko and Bernard Grossman. Multidisciplinary Design Optimization for a Blended Wing. Technical report, Virginia Tech, 2005.
- [69] Cryogenic Liquids. [http://www.porttechnology.org/technical\\_papers/upgrading\\_to\\_automated\\_guided\\_vehicles/](http://www.porttechnology.org/technical_papers/upgrading_to_automated_guided_vehicles/).
- [70] Ahmed Abdel-Hafez. Power Generation and Distribution System for a More Electric Aircraft - A Review. <http://www.intechopen.com/books/recent-advances-in-aircraft-technology/more-electric-aircraft>. Accessed: 2015-06-10.
- [71] Gwénaëlle Renouard-Vallet, Martin Saballus, Peter Schumann, Josef Kallo, K. Andreas Friedrich, and Hans Müller-Steinhausen. Fuel cells for civil aircraft application: On-board production of power, water and inert gas. *Chemical Engineering Research and Design*, 90(1):3 – 10, 2012.
- [72] Pneumatic System. <http://www.boeing-727.com/Data/systems/infopneumat.html>. Accessed: 2015-06-22.
- [73] G. La Rocca. Aerospace Design and Systems Engineering - Lecture 4 - Design for AC longitudinal stability. <http://blackboard.tudelft.nl>. Accessed: 18-03-2013.
- [74] Rodrigo Martinez-Val and Erik Schoep. Flying wing versus conventional transport airplane: the 300 seat case.
- [75] Dr. Jan Roskam. Airplane Design Series Part III: Layout Design of Cockpit, Fuselage, Wing and Empennage Cutaways and Inboard Profiles. DARcorporation, 1985.
- [76] Mohammad H. Sadraey. Tail design. pages 265–340, 2012.
- [77] Daniel Raymer. Aircraft Design - A Conceptual Approach. American Institute of Aeronautics and Astronautics, Stanford University, fourth. edition, 2006.
- [78] Daniel P. Raymer. Aircraft Design: A Conceptual Approach. American Institute of Aeronautics, Inc., Washington DC, second pri edition, 1989.
- [79] Australian Government: Department of Defense. Technical risk assessment handbook version 1.1, 2010.
- [80] The UCA Conference: a successful second edition - Unmanned Cargo Aircraft Conference. <http://www.ucaconference.com/>. Accessed: 2015-05-31.
- [81] HansHeerkens. <http://doc.utwente.nl/85332/2/Heerkens13future.pdf>. Accessed: 2015-06-19.
- [82] Fact Sheet Pilot Flight Time, Rest, and Fatigue. [https://www.faa.gov/news/fact\\_sheets/news\\_story.cfm?newsId=6762](https://www.faa.gov/news/fact_sheets/news_story.cfm?newsId=6762). Accessed: 2015-06-19.
- [83] Jay Gundlach. Designing Unmanned Aircraft Systems: A Comprehensive Approach. page 805, 2013.
- [84] Inmarsat Remains Confident Global Xpress Will Be a Hit with U.S. Military - SpaceNews.com. <http://spacenews.com/39754inmarsat-remains-confident-global-xpress-will-be-a-hit-with-us/>. Accessed: 2015-06-22.
- [85] Our coverage - Inmarsat. <http://www.inmarsat.com/about-us/our-satellites/our-coverage/>. Accessed: 2015-06-22.
- [86] Boeing. Runway Pavement Surface Type Descriptions. [http://www.boeing.com/assets/pdf/commercial/airports/faqs/boeing\\_pavement\\_surface\\_types.pdf](http://www.boeing.com/assets/pdf/commercial/airports/faqs/boeing_pavement_surface_types.pdf). Published on: February 4th 2014.
- [87] Airbus. Airbus A350-900. <http://www.airbus.com/aircraftfamilies/passengeraircraft/a350xwbfamily/a350-900/specifications/>. Accessed: 2015-05-12.
- [88] Airbus. Airbus A380. <http://www.airbus.com/aircraftfamilies/passengeraircraft/a380family/specifications/>. Accessed: 2015-05-12.
- [89] Antonov. Antonov An-225. <http://www.antonov.com/aircraft/transport-aircraft/an-225-mriya>. Accessed: 2015-05-12.
- [90] Boeing. Boeing C-17 Globemaster III. <http://www.boeing.com/defense/c-17-globemaster-iii/>. Accessed: 2015-05-12.
- [91] Boeing. Boeing 747-8. <http://www.boeing.com/commercial/747/>. Accessed: 2015-05-12.
- [92] Boeing. Boeing 777. <http://www.boeing.com/commercial/777/>. Accessed: 2015-05-12.
- [93] Boeing. Boeing 787. <http://www.boeing.com/commercial/787/>. Accessed: 2015-05-12.
- [94] U.S. Department of Transportation: Federal Aviation Administration. Airport Pavements: Solutions for Tomorrow's Aircraft. <http://www.airporttech.tc.faa.gov/naptf/download/Airport%20Pavements%20Brochure%20April%201993.pdf>, April 1993.
- [95] Civil Engineering Dictionary. Pavements - Type of Pavements. <http://www.aboutcivil.org/types-of-pavements.html>. Accessed: 2015-05-12.
- [96] Port Technology: upgrading to automated guided vehicles. [http://www.porttechnology.org/technical\\_papers/upgrading\\_to\\_automated\\_guided\\_vehicles/](http://www.porttechnology.org/technical_papers/upgrading_to_automated_guided_vehicles/).
- [97] Carl-Jochen Winter. Hydrogen energy Abundant, efficient, clean: A debate over the energy-system-of-change. *International Journal of Hydrogen Energy*, 34:S1–S52, 2009.
- [98] Airbus Deutschland GmbH. Liquid Hydrogen Fuelled Aircraft System Analysis. Technical Report September 2003, 2003.

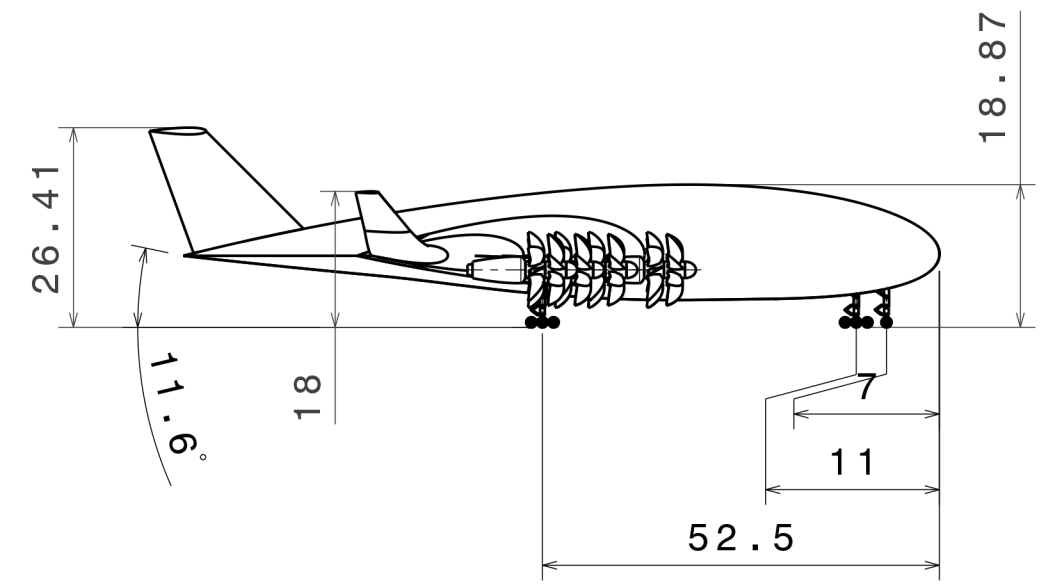
- [99] a Haryanto, S Fernando, N Murali, and S Adhikari. Current status of hydrogen production techniques by steam reforming of ethanol: A review. *Energy and Fuels*, 19(5):2098–2106, 2005.
- [100] Guido Colodi. Hydrogen Production via Steam Reforming with CO<sub>2</sub> Capture. pages 1–6, 2008.
- [101] S BAYKARA. Experimental solar water thermolysis. *International Journal of Hydrogen Energy*, 29(14):1459–1469, November 2004.
- [102] Aldo Steinfeld. Solar thermochemical production of hydrogen - A review. *Solar Energy*, 78(5):603–615, 2005.
- [103] David B. Levin, Lawrence Pitt, and Murray Love. Biohydrogen production: Prospects and limitations to practical application. *International Journal of Hydrogen Energy*, 29(2):173–185, 2004.
- [104] NEL Hydrogen AS. Efficient Electrolysers for Hydrogen Production Proud History World Class. Technical report.
- [105] Kaveh Mazloomi, Nasri B. Sulaiman, and Hossein Moayedi. Electrical efficiency of electrolytic hydrogen production. *International Journal of Electrochemical Science*, 7(4):3314–3326, 2012.
- [106] M. F. Chaplin. Electrolysis of water. <http://www1.lsbu.ac.uk/water/electrolysis.html>. Accessed: 2015-05-20.
- [107] The Hydrogen Economy: Opportunities, Costs, Barriers, and R&D Needs. The National Academies Press, 2004.
- [108] NEL Hydrogen AS. 50 MW H<sub>2</sub> Plant. Technical report, 2015.
- [109] Genevieve Saur and Todd Ramsden. Wind Electrolysis: Hydrogen Cost Optimisation. *National Renewable Energy Laboratory Publication*, Task No. H(NREL/TP-5600-50408):14, 2011.
- [110] Stephen Hodgson. FAO Legislative Study 92: Modern Water Rights - Theory and Practice. pages 1–130, 2006.
- [111] Scott Rozelle and Richard Howitt. Irrigation Water Pricing Policy in China. (February), 2007.
- [112] K Tennakone. Hydrogen from brine electrolysis: A new approach. *International Journal of Hydrogen Energy*, 14(9):681–682, 1989.
- [113] EngineeringToolbox.com. Gases - Densities. [http://www.engineeringtoolbox.com/gas-density-d\\_158.html](http://www.engineeringtoolbox.com/gas-density-d_158.html). Accessed: 2015-05-18.
- [114] Salvador M Aceves, Primary Contact, Gene Berry, Francisco Espinosa-loza, Guillaume Petitpas, Vernon Switzer, and Stan Tuholski. III. 11 LLNL / Linde 875 bar Liquid Hydrogen Pump for High Density Cryogenic Vessel Refueling. pages 51–53, 2015.
- [115] European Commission Transport Division. H<sub>2</sub>Aircraft - CRYOPLANE and the future of flight. [http://ec.europa.eu/research/transport/projects/items/h2aircraft\\_\\_cryoplane\\_and\\_the\\_future\\_of\\_flight\\_en.htm](http://ec.europa.eu/research/transport/projects/items/h2aircraft__cryoplane_and_the_future_of_flight_en.htm). Accessed: 2015-04-30.
- [116] L Schlapbach and a Züttel. Hydrogen-storage materials for mobile applications. *Nature*, 414(6861):353–358, 2001.
- [117] Satish Kumar, Hyouk Tae Kwon, Kwang Ho Choi, Jae Hyun Cho, Wonsub Lim, and Il Moon. Current status and future projections of LNG demand and supplies: A global prospective. *Energy Policy*, 39(7):4097–4104, 2011.
- [118] Songwut Krasae-in, Jacob H. Stang, and Petter Neksa. Development of large-scale hydrogen liquefaction processes from 1898 to 2009. *International Journal of Hydrogen Energy*, 35(10):4524–4533, 2010.
- [119] Christopher Yang and Joan Ogden. Determining the lowest-cost hydrogen delivery mode. *International Journal of Hydrogen Energy*, 32(2):268–286, 2007.
- [120] G D Berry and G D Rambach. Insulated pressure vessels for hydrogen on vehicles. *Contract*, 23(1):583–591, 1998.
- [121] W a Amos. Costs of Storing and Transporting Hydrogen. *Other Information*: PBD: 27 Jan 1999; PBD: 27 Jan 1999; PBD: 27 Jan 1999, (November):Medium: ED; Size: vp., 1999.
- [122] F a De Bruijn. The Hydrogen Economy Possibilities and Limitations. October, (October 2004), 2005.
- [123] Brian Thompson and Micheal Eocabacci. Maximizing hydrogen pumping speed in cryopumps without compromising safety. <http://micromagazine.fabtech.org/archive/05/03/thompson.html>, 2007. Accessed: 2015-06-17.
- [124] Alain Clément, Pat McCullen, António Falcão, Antonio Fiorentino, Fred Gardner, Karin Hammarlund, George Lemonis, Tony Lewis, Kim Nielsen, Simona Petroncini, M.-Teresa Pontes, Phillippe Schild, Bengt-Olov Sjöström, Hans Christian Sørensen, and Tom Thorpe. Wave energy in Europe: current status and perspectives. *Renewable and Sustainable Energy Reviews*, 6(5):405–431, October 2002.
- [125] EDP. Renewable energy - Myths and truths. Technical report, Energias de Portugal, 2015.
- [126] Daniel Fürstenwerth. Current and Future Cost of Photovoltaics. Long-term Scenarios for Market Development, System Prices and LCOE of Utility-Scale PV Systems. Technical report, Fraunhofer-Institute for Solar Energy Systems (ISE), Berlin, 2015.
- [127] U.S. Department of Energy. Progress Report: Advancing Solar Energy Across America. <http://energy.gov/articles/progress-report-advancing-solar-energy-across-america>, 2015. Accessed: 2015-05-20.
- [128] Architects of Energy Solar Edge. SolarEdge PV Inverters Set Record CEC Efficiency Rating. [http://www.solaredge.com/articles/solaredge\\_cec\\_20100526](http://www.solaredge.com/articles/solaredge_cec_20100526), 2010. Accessed: 2015-05-20.
- [129] Providing all global energy with wind, water, and solar power, Part II: Reliability, system and transmission costs, and policies. *Energy Policy*, 39(3):1170–1190, March 2011.
- [130] REN21. Renewables 2012 Global Status Report 2012. Technical report, 2012.
- [131] U.S. Department of Energy. Wind Vision: A New Era for Wind Power in the United States. Technical report, 2015.
- [132] RENEWABLE ENERGY TECHNOLOGIES: COST ANALYSIS SERIES. Wind Power. 2012.
- [133] Wim C Turkenburg, Jos Beurskens, André Faaij, Peter Fraenkel, Ingvar Fridleifsson, Erik Lysen, David Mills, Jose Roberto Moreira, Lars J Nilsson, Anton Schaap, and Wim C Sinke. *Renewable Energy Technologies*, pages 219–272. World energy assessment: energy and the challenge of sustainability. United Nations Development Programme, 2000.
- [134] Mark Z. Jacobson and Mark A. Delucchi. A path to Sustainable Energy by 2030. *Scientific American*, pages 58–65, November 2009.
- [135] International Renewable Energy Agency. RENEWABLE ENERGY TECHNOLOGIES: COST ANALYSIS SERIES: Hydropower. 2012.
- [136] Wim Turkenburg. Renewable energy. pages 761–900, 2004.
- [137] Elizabeth Maclin and Matt Sicchio. Dam removal success stories. Number December. 1999.
- [138] Enrico Barbier. Geothermal energy technology and current status: An overview. *Renewable and Sustainable Energy Reviews*, 6(1-2):3–65, 2002.
- [139] Rijksdienst voor Ondernemend Nederland. Sde+ 2015. 2015.
- [140] Lewis Owen. Ob River — river, Russia — Encyclopedia Britannica. <http://www.britannica.com/EBchecked/topic/423582/Ob-River#ref495574>. Accessed: 2015-05-20.
- [141] Ryan Wisser and Mark Bolinger. 2013 WIND TECHNOLOGIES MARKET REPORT. Technical Report August, U.S. Department of Energy, 2014.
- [142] 3Tier by Vaisala. Free Renewable Energy Resource Maps :: Wind Speed & Solar Irradiance. <http://www.3tier.com/en/support/resource-maps/>. Accessed: 2015-05-20.
- [143] Worldbank. Operating costs and efficiency of cargo aircraft. Technical report.
- [144] Lene Sørensen and Niels Kilde. Emission inventory guidebook. Technical report, 2006.
- [145] PBL Netherlands Environmental Assessment Agency. Trends in global CO<sub>2</sub> emissions 2013. Technical report, 2014.
- [146] California Energy Commission. TRANSPORTATION FUEL PRICE AND DEMAND FORECASTS: Inputs and Methods for the 2009. Technical Report January, 2009.
- [147] National Renewable Energy Laboratory. NREL: Energy Analysis - Utility-Scale Energy Technology Capacity Factors. [http://www.nrel.gov/analysis/tech\\_cap\\_factor.html](http://www.nrel.gov/analysis/tech_cap_factor.html). Accessed: 2015-05-21.
- [148] Department of the Environment Northern Ireland. Draft PPS 18: Renewable Energy — Annex 1 Wind Energy: Spacing of Turbines — Planning Portal. Technical report.

- [149] First Solar Inc. Phase I , Mohammed bin Rashid Al Maktoum Solar Park, Project Datasheet. Technical report, Dubai, United Arab Emirates, 2013.
- [150] Linde Kryotechnik AG. Liquefaction for Highest Density - Hydrogen Solutions Cleaner. Technical report, 2012.
- [151] Author Julia Tomei and Julia Tomei. Planning for a Transition to a Hydrogen Economy : A Review of Roadmaps UKSHEC Working Paper No . 2 Planning for a transition to a hydrogen economy : a review of roadmaps. (April):1-37, 2009.
- [152] Ulf Bossel and Baldur Eliasson. Energy and the Hydrogen Economy. 2003.
- [153] Manoj Pudukudy, Zahira Yaakob, Masita Mohammad, Binitha Narayanan, and Kamaruzzaman Sopian. Renewable hydrogen economy in Asia Opportunities and challenges: An overview. Renewable and Sustainable Energy Reviews, 30:743–757, February 2014.
- [154] European Climate Foundation. Roadmap 2050. Policy, Volume 1 -(April):1–9, 2010.
- [155] Green Rhino Energy. Economics of renewable energy power plants. <http://www.greenrhinoenergy.com/renewable/context/economics.php>, 2015. Accessed: 2015-06-03.
- [156] Daniel Fürstenwerth. AgoraEnergiewende-Current\_and-Future-Cost\_of-PV-ExcelTool\_v1, 2014.
- [157] Jonathan Watts. Winds of change blow through China as spending on renewable energy soars. <http://www.theguardian.com/world/2012/mar/19/china-windfarms-renewable-energy>, 2012. Accessed: 2015-06-11.
- [158] Samuela Bassi, Alex Bowen, and Sam Fankhauser. The case for and against onshore wind energy in the UK. Technical Report June, Grantham Research Institute, 2012.
- [159] Yue Ma. Three Gorges Dam. <http://large.stanford.edu/courses/2010/ph240/ma2/>, 2010. Accessed: 2015-06-11.
- [160] Michael Ball and Martin Wietschel. The future of hydrogen - opportunities and challenges. International Journal of Hydrogen Energy, 34(2):615–627, 2009.
- [161] U.S. Department of Labor. Inflation Calculator: Bureau of Labor Statistics. [http://www.bls.gov/data/inflation\\_calculator.htm](http://www.bls.gov/data/inflation_calculator.htm). Accessed: 2015-06-19.
- [162] US Inflation Calculator. Inflation Calculator — Find US Dollar's Value from 1913-2015. <http://www.usinflationcalculator.com/>. Accessed: 2015-06-19.
- [163] Coin News. Inflation Calculator: Money's Real Worth Over Time. <http://www.coinnews.net/tools/cpi-inflation-calculator/>. Accessed: 2015-06-19.
- [164] Daniel B Levine and Stanley A Horowitz. Predicting the cost of initial spares. Technical report, DTIC Document, 1989.
- [165] Dr. Jan Roskam. Airplane Design Series Part VIII: Airplane Cost Estimation: Design, Development, Manufacturing and Operating. DARcorporation, 2002.
- [166] Statista. Aluminum price 2003-2014 — Statistic. <http://www.statista.com/statistics/276643/aluminum-prices-since-2003/>, 2015. Accessed: 2015-06-22.
- [167] Airbus. AIRCRAFT CHARACTERISTICS AIRPORT AND MAINTENANCE PLANNING. Technical report, Airbus S.A.S., 2005.
- [168] SKYbrary Aviation Safety. AIRBUS A-380-800. <http://www.skybrary.aero/index.php/A388>. Accessed: 2015-06-20.
- [169] Flightglobal. Fixing Rolls-Royces disposable A380 engines.
- [170] S.O.L. Zijp. Development of a Life Cycle Cost Model for Conventional and Unconventional Aircraft. PhD thesis, TU Delft, 2014.
- [171] U.S. Department of Energy. Hydrogen fuel cell vehicle emissions. [http://www.afdc.energy.gov/vehicles/emissions\\_hydrogen.html](http://www.afdc.energy.gov/vehicles/emissions_hydrogen.html). Accessed: 2015-04-21.
- [172] Glenn Elert. Energy density of hydrogen. <http://hypertextbook.com/facts/2005/MichelleFung.shtml>. Accessed: 2015-04-21.
- [173] Glenn Elert. Energy density of aviation fuel. <http://hypertextbook.com/facts/2003/EvelynGofman.shtml>. Accessed: 2015-04-21.
- [174] Climate Change Division US EPA. Nitrous Oxide Emissions. <http://epa.gov/climatechange/ghgemissions/gases/n2o.html>.
- [175] Nicola Stuber, Piers Forster, Gaby Rädcl, and Keith Shine. The importance of the diurnal and annual cycle of air traffic for contrail radiative forcing. Nature, 441(7095):864–867, 2006.
- [176] Jay Madigan (NASA). Contrail Education - FAQ. <http://science-edu.larc.nasa.gov/contrail-edu/faq.php>, 2014. Accessed: 2015-04-22.
- [177] Mark Taylor and Rolls Royce. Open Rotor Engine Design and Validation. [http://aerosociety.com/Assets/Docs/GreenerbyDesign/\(6\)MarkTaylor.pdf](http://aerosociety.com/Assets/Docs/GreenerbyDesign/(6)MarkTaylor.pdf).
- [178] Russell H. Thomas, Casey L. Burley and Erik D. Olson, Casey L. Burley Russell H. Thomas, and Erik D. Olson. Hybrid Wing Body Aircraft System Noise Assessment With Propulsion Airframe Aeroacoustic Experiments. 2010.
- [179] Airbus. A380 WOW!!! timeline. <http://www.airbus.com/aircraftfamilies/passengeraircraft/a380family/a380-effect/a380-wow-timeline/>. Accessed: 2015-06-18.
- [180] Guy Norris and Mark Wagner. Airbus A380: Superjumbo of the 21st Century. Zenith Press, 2005.
- [181] Jorn Madslie. Giant plane a testimony to 'old Europe'. BBC News, 2005.
- [182] EASA. EASA Type-Certificate Data Sheet TCDS A.110 Issue 03. EASA, 2007.
- [183] FAA. FAA Type Certificate Data Sheet NO.A58NM Rev 2. FAA, 2007.

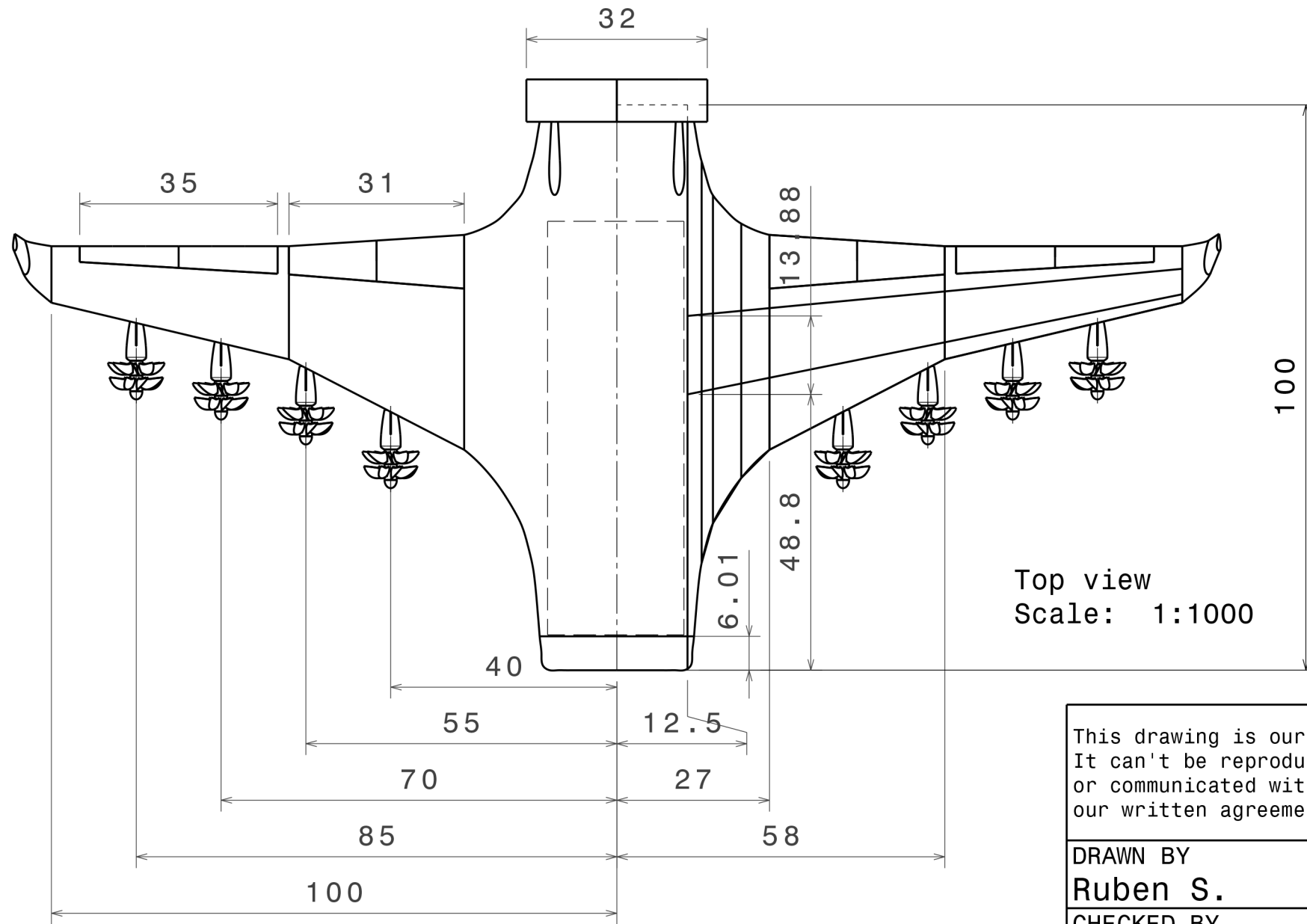
H G F E D C B A



Front view  
Scale: 1:1000



Left view  
Scale: 1:1000



Top view  
Scale: 1:1000

# APPENDIX A

## CAD Drawings

ALL DIMENSIONS IN METERS

This drawing is our property. It can't be reproduced or communicated without our written agreement.		DSE GROUP 9 - THE HUULC			
DRAWN BY <b>Ruben S.</b>		DATE 22/06/2015		DRAWING TITLE <b>General Overview</b>	
CHECKED BY <b>XXX</b>		DATE XXX		SIZE <b>A3</b>	DRAWING NUMBER <b>XXX</b>
DESIGNED BY <b>XXX</b>		DATE XXX		SCALE1: 1000	WEIGHT (kg) <b>XXX</b>
				PAGE	147

4

4

3

3

2

2

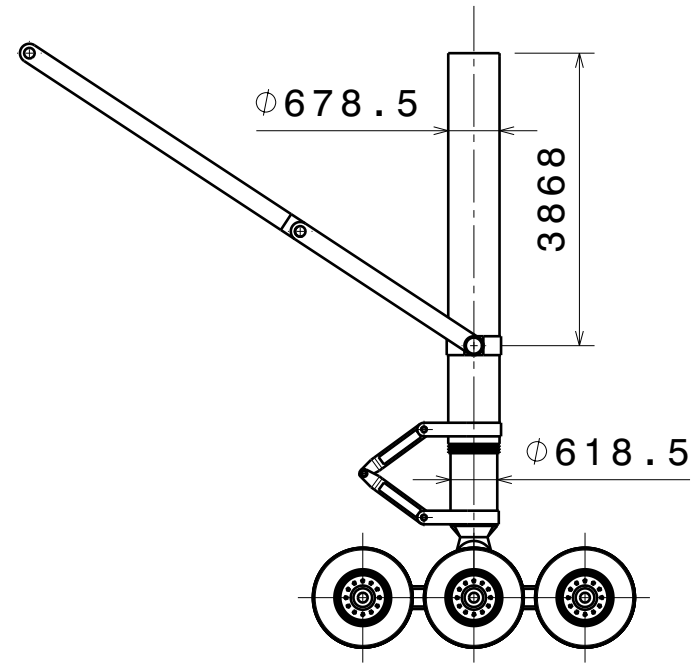
1

1

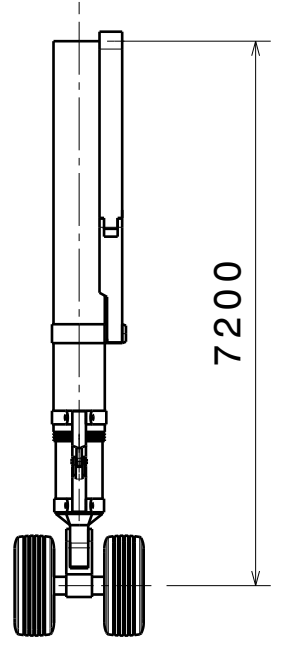
H G F E D C B A

H G F E D C B A

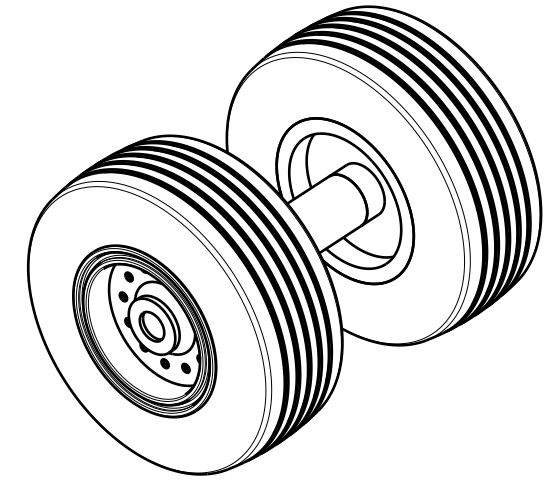
4



Front view  
Scale: 1:100

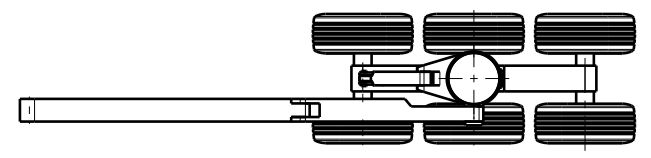


Left view  
Scale: 1:100

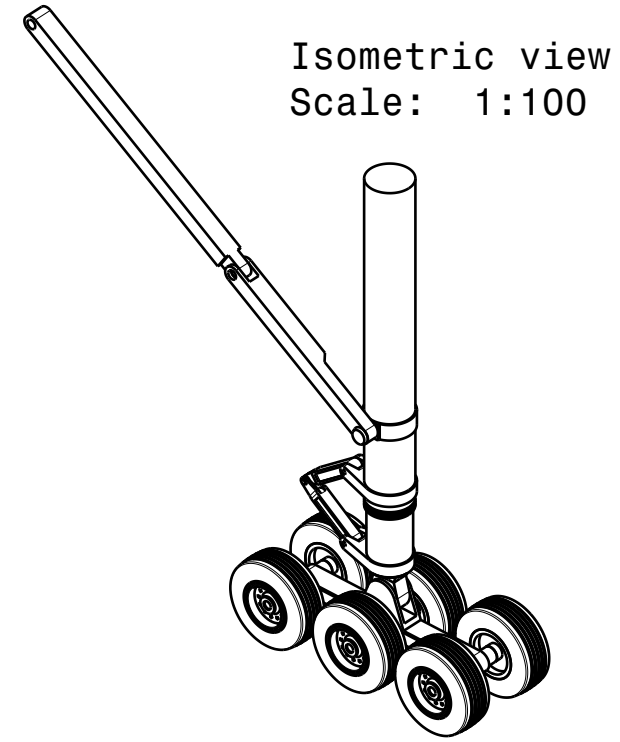


Isometric view  
Scale: 1:30

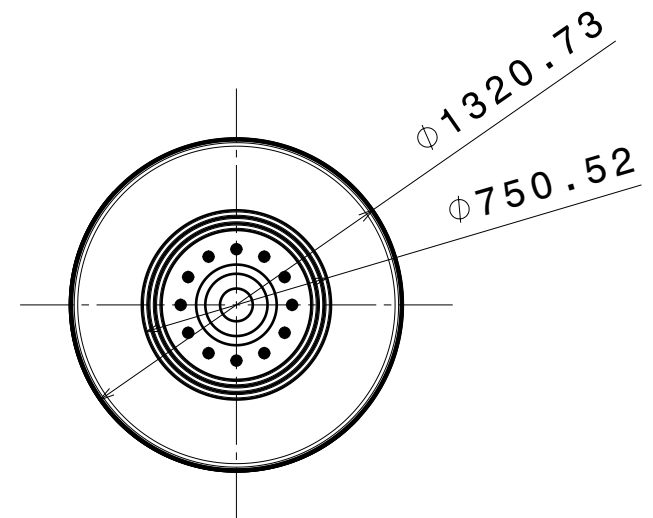
3



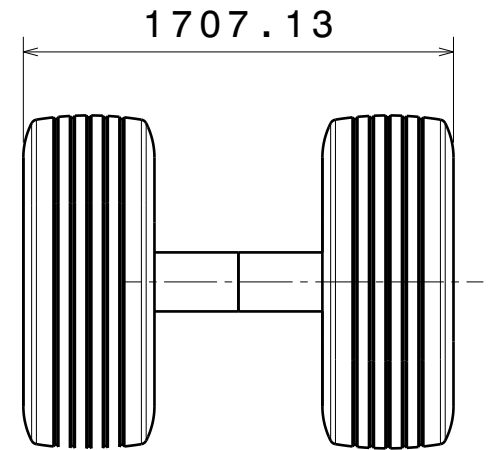
Top view  
Scale: 1:100



Isometric view  
Scale: 1:100



Front view  
Scale: 1:30



Left view  
Scale: 1:30

2

1

ALL DIMENSIONS IN MILLIMETERS

H G F E D C B A

This drawing is our property. It can't be reproduced or communicated without our written agreement.		<b>DSE GROUP 9 - THE HUULC</b>			
DRAWN BY <b>Ruben S.</b>		DATE 22/06/2015		<b>Landing Gear</b>	
CHECKED BY <b>XXX</b>		DATE XXX			
DESIGNED BY <b>XXX</b>		DATE XXX		SIZE <b>A3</b>	DRAWING NUMBER <b>XXX</b>
		SCALE 1:1000	WEIGHT (kg) <b>XXX</b>	PAGE	148
				REV <b>X</b>	

4

3

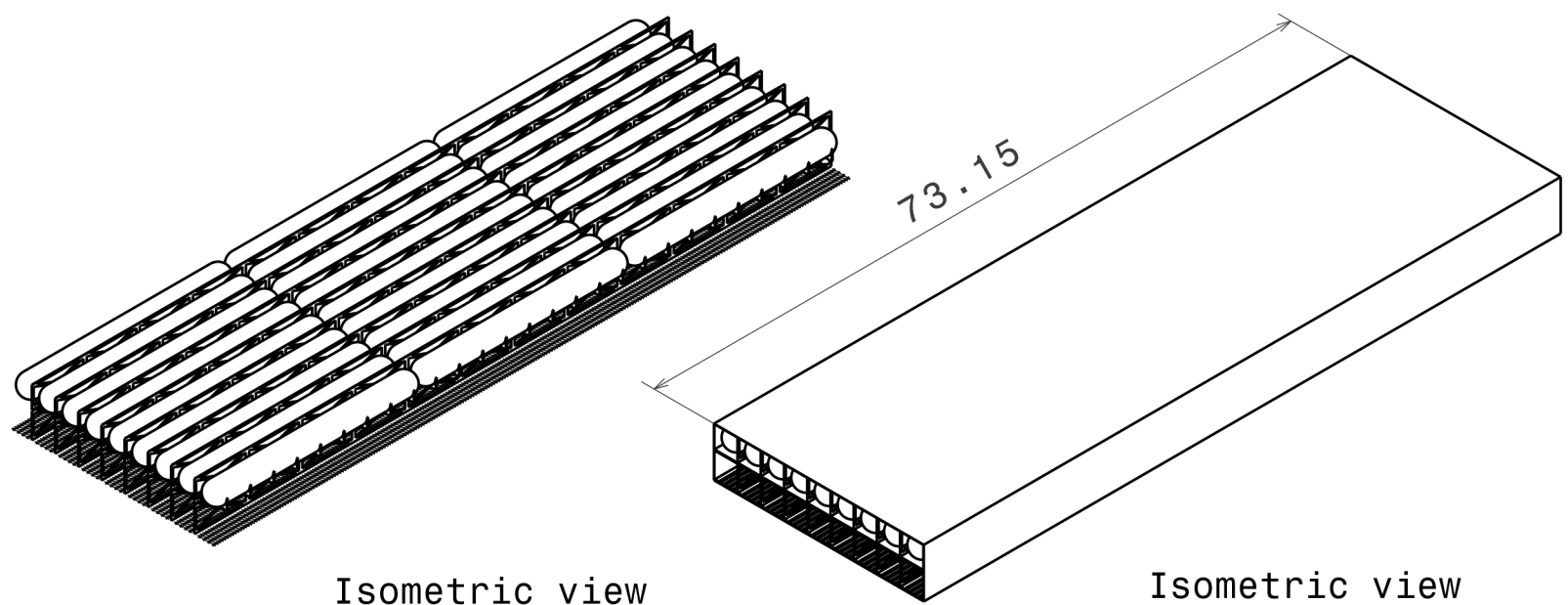
2

1

H G F E D C B A

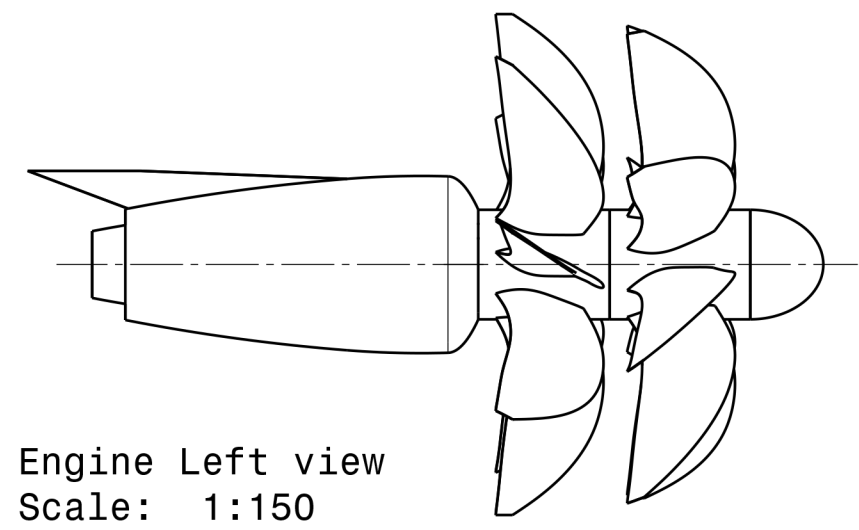
4

4



Isometric view  
Scale: 1:600

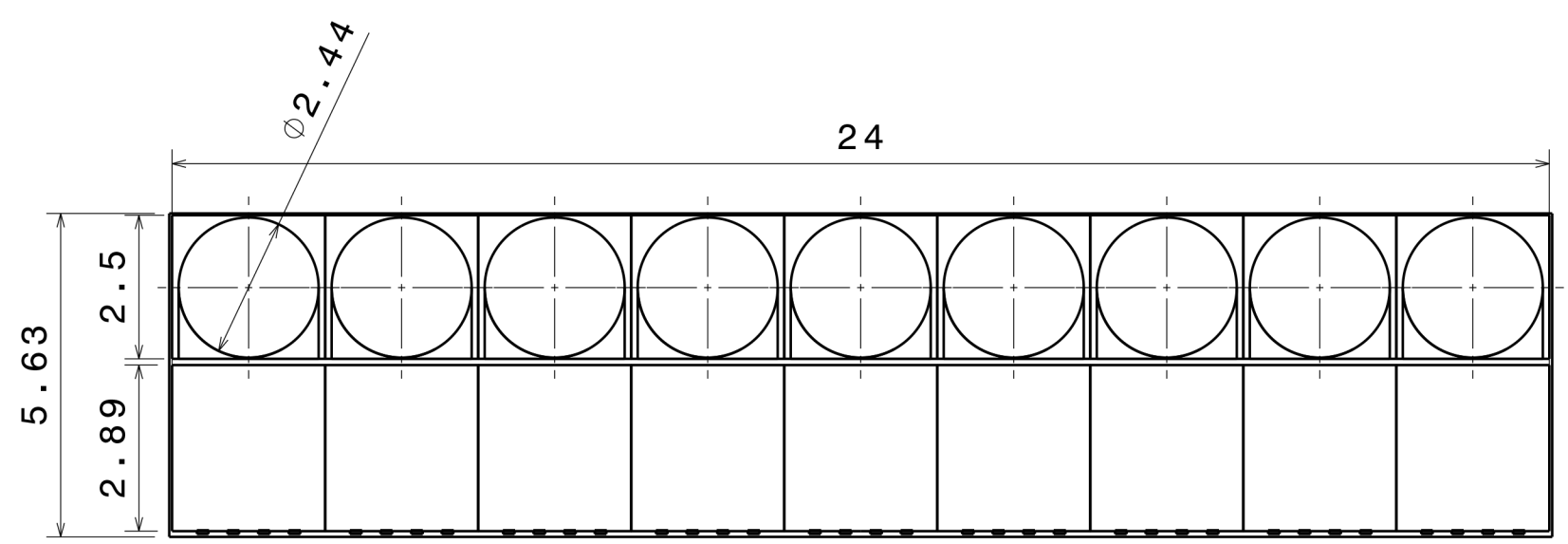
Isometric view  
Scale: 1:600



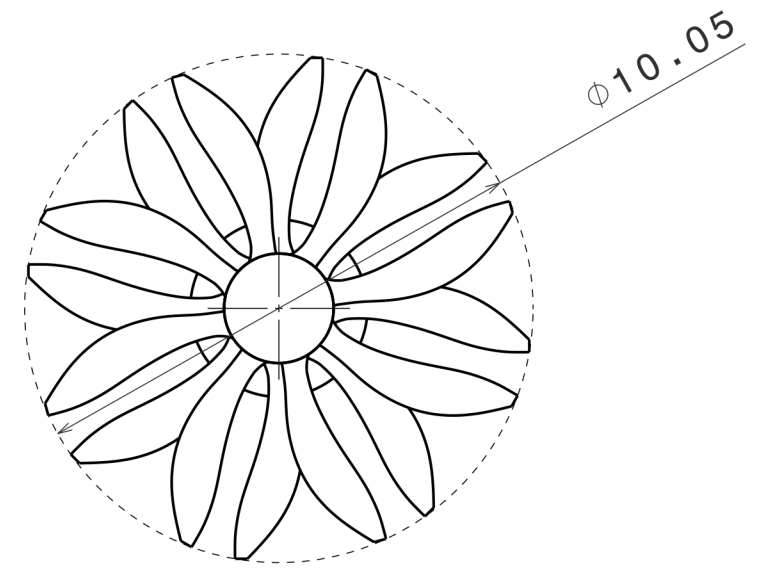
Engine Left view  
Scale: 1:150

3

3



Front view  
Scale: 1:125



Engine Front view  
Scale: 1:150

2

2

1

1

ALL DIMENSIONS IN METERS

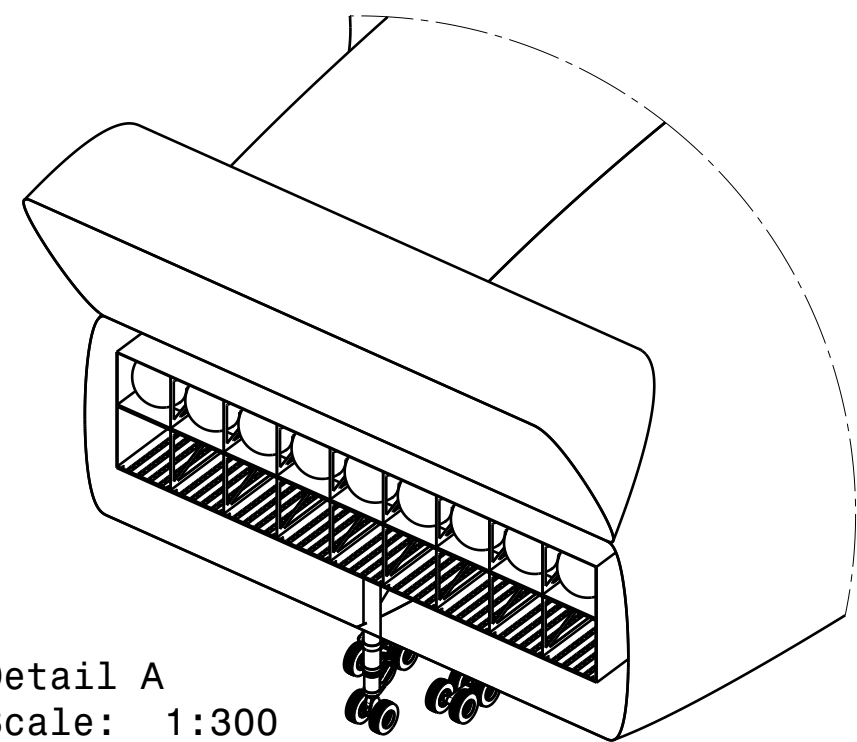
This drawing is our property. It can't be reproduced or communicated without our written agreement.		<b>DSE GROUP 9 - THE HUULC</b>			
DRAWN BY <b>Ruben S.</b>		DATE 22/06/2015		<b>Payload Bay / Engines</b>	
CHECKED BY <b>XXX</b>		DATE XXX			
DESIGNED BY <b>XXX</b>		DATE XXX		SIZE <b>A3</b>	DRAWING NUMBER <b>XXX</b>
		SCALE1 : 1000	WEIGHT (kg) <b>XXX</b>	PAGE	149

H G B A

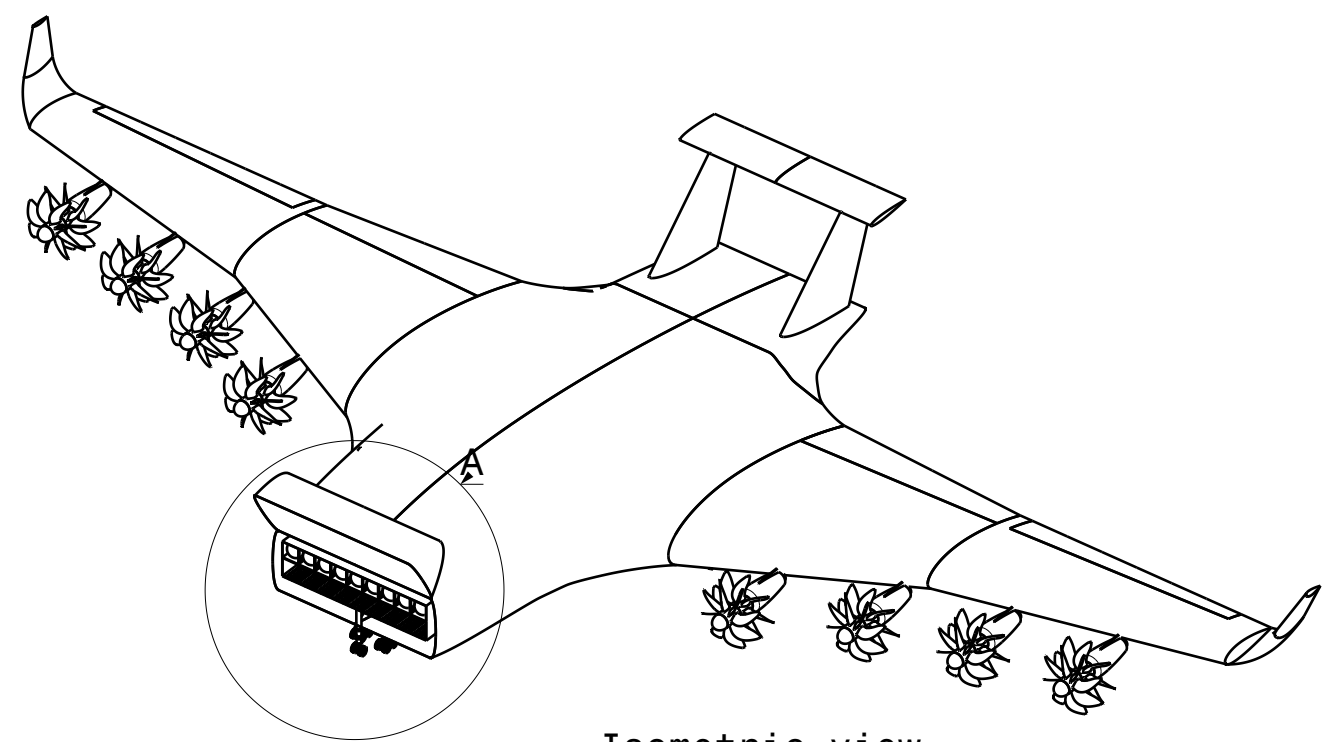
H G F E D C B A

4

4



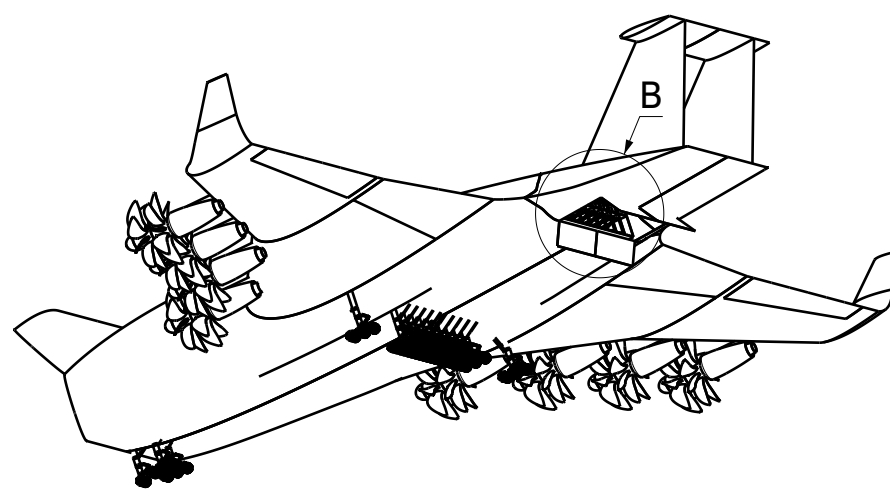
Detail A  
Scale: 1:300



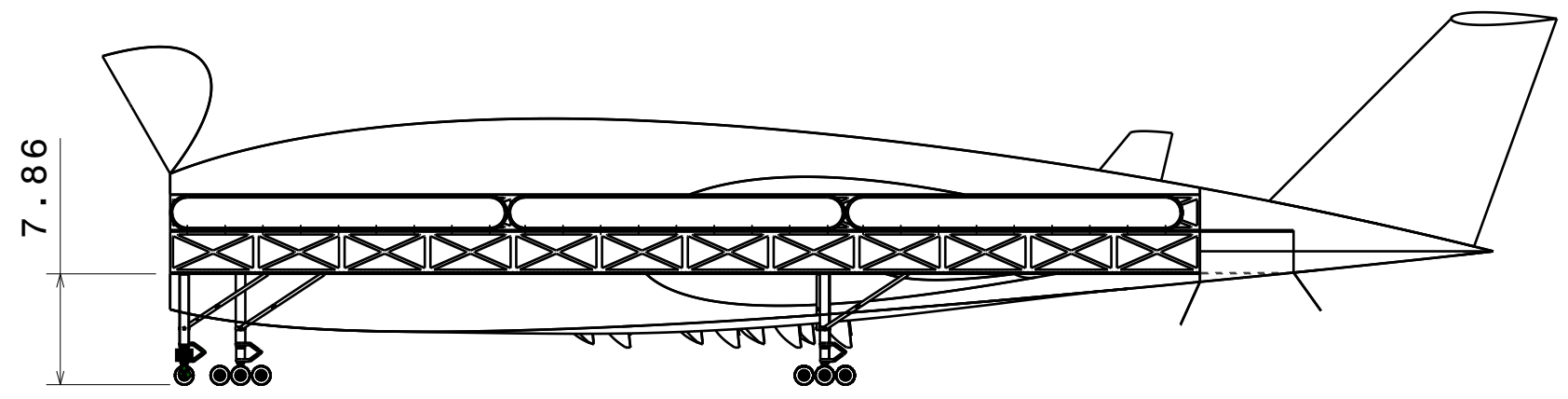
Isometric view  
Scale: 1:1000

3

3



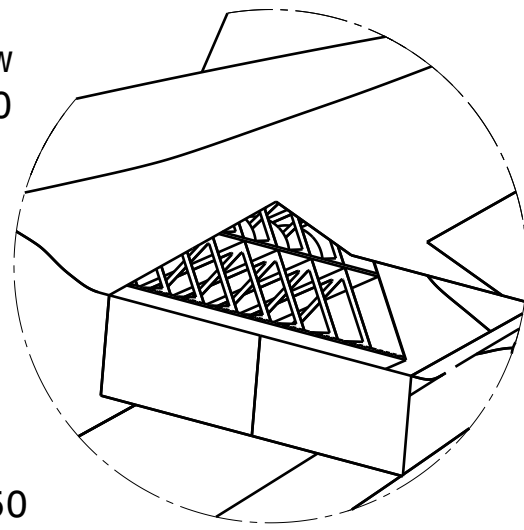
Isometric view  
Scale: 1:1000



Section view / Payload Bay  
Scale: 1:500

2

2



Detail B  
Scale: 1:250

1

1

ALL DIMENSIONS IN METERS

H G F E D C B A

This drawing is our property. It can't be reproduced or communicated without our written agreement.		<b>DSE GROUP 9 - THE HUULC</b>			
DRAWN BY <b>Ruben S.</b>		DATE 22/06/2015		DRAWING TITLE <b>Payload Bay and Doors</b>	
CHECKED BY <b>XXX</b>		DATE xxx		SIZE <b>A3</b>	DRAWING NUMBER <b>XXX</b>
DESIGNED BY <b>XXX</b>		DATE xxx		SCALE: 1:1000	WEIGHT (kg) <b>XXX</b>
				PAGE	150

1